Mouse whole embryo culture and the analysis of neural tube defects

Lucy Culshaw

Developmental Biology and Cancer Programme

University College London

A thesis submitted for the degree of Doctor of Philosophy

I, Lucy Culshaw, confirm that the work in this thesis is my own. Where information has been obtained from other sources, I confirm that it has been appropriately credited.

Abstract

Whole embryo culture enables direct observation and manipulation of organogenesis stage embryos, that would otherwise be relatively inaccessible within the maternal uterus. Rat serum is the primary medium for mouse embryo culture and can sustain growth and development comparable to that *in utero*. To enhance the “replacement, reduction and refinement” (3Rs) of animals in research, culture experiments were performed to determine whether serum-free medium can substitute for whole rat serum, or whether rat serum can be diluted, and yet still maintain high quality development *in vitro*. Of two serum-free media tested, neither could sustain development comparable to that achieved in 100% rat serum. However, dilution of rat serum 1:1 with a defined medium supported growth and development with no significant differences from 100% rat serum. Hence, rat usage can be reduced by culture in medium containing diluted serum. Neural tube defects (NTDs) are severe birth defects of the brain or spinal cord. NTDs occur in mice lacking ASPP2, a p53 agonist and tumour suppressor. Embryos with a deletion of exon 3 in the ASPP2 gene, *Trp53bp2*, were found to have a progressive NTD phenotype that worsened with gestational age. The *Trp53bp2*$^{\Delta 3/\Delta 3}$ embryonic neural tube phenotype involves ventral neuroepithelial overgrowth, ectopic lumen formation and re-opening of the neural tube. Cellular analysis revealed disruption in *Trp53bp2*$^{\Delta 3/\Delta 3}$ embryos with and without a macroscopic phenotype. These histological abnormalities included disrupted proliferation, disorganised differentiation and a reduced basal to apical migration of cells prior to mitosis. Using the open-yolk sac embryo culture method, a hypothesis based on over-proliferation in *Trp53bp2*$^{\Delta 3/\Delta 3}$ embryos was tested using the chemical inhibitor DAPT. It is proposed that deletion of ASPP2 results in an apico-basal polarity defect which increases in severity through development and results in rupture of the neural tube at variable locations along the body axis.

Impact statement

The work in this report highlights the importance and rewards of considering the 3Rs in research methods. By managing to reduce animal usage in a highly advantageous culture method in developmental research, the technique should become more appealing and cost-effective for other researchers. On a wider scale, 3Rs impacts range from policy and regulatory change to the development and uptake of new technologies and approaches.

Human NTDs are multifactorial and incredibly diverse, and controversy still remains on the origin of NTDs which arise in multiple locations along the body axis. This report provides an in-depth analysis of the spinal region of a mouse mutant with similarly variable NTDs. Reopening of the neural tube is a mechanism that possibly occurs in a subset of human NTDs, and is explored in detail here.

Acknowledgements

I would first like to thank the National Centre of the 3Rs, for funding my PhD and allowing me to explore their values in relation to developmental research. I would like to thank my primary supervisor, Professor Andrew Copp, for giving me the freedom and opportunity to explore such a complex NTD phenotype, and Dawn Savery for supporting me throughout. Thank you to Dale Moulding who helped me with image analysis and microscopy. I would like to thank my family, friends and boyfriend, Joe, for giving me positive advice and helping me through to the end.

Table of contents

Chapter 1 Introduction..... 12

1.1 Neurulation in the mammalian embryo 12

1.1.1 Primary neurulation 12

1.1.2 Secondary neurulation..... 13

1.1.3 Mechanisms involved in neurulation 14

1.2 Neurogenesis in the mammalian embryo 15

1.2.1 Structure of the neuroepithelium..... 15

1.2.2 Interkinetic nuclear migration and cell cycle kinetics 17

1.2.3 Neuronal specification and differentiation 19

1.3 Neural tube defects 21

1.3.1 Neural tube defects in humans 21

1.3.2 Neural tube defects in the mouse 25

1.4 Experimental methods used to study development and birth defects..... 28

1.5 Rodent whole embryo culture 29

1.6 Aims of the thesis 32

Chapter 2 Methods..... 33

2.1 Embryological procedures 33

2.1.1 Mouse strains and embryo collection..... 33

2.1.2 Preparation of rat serum 33

2.1.3 Preparation of serum-free culture medium..... 34

2.1.4 Embryo collection and dissection..... 35

2.1.5 Embryo culture 38

2.1.6 Administration of reagents 38

2.1.7 Morphological scoring..... 39

2.1.8 Protein content analysis..... 41

2.2 Molecular biology 42

2.2.1 ASPP2 genotyping 42

2.2.2 Synthesis of mRNA probe for in situ hybridisation 43

2.2.3 Quantitative RT-PCR..... 44

2.3 Histological procedures 45

2.3.1 Gelatine embedding and cryosectioning..... 45

2.3.2 Whole-mount in situ hybridisation 47
2.3.3 Immunostaining 49
2.4 Microscopy and imaging 52
2.5 Analysis 53
2.5.1 Immunofluorescence image analysis 53
2.5.2 Statistical analysis 58

Chapter 3 Prospects of reducing rat serum usage in mouse whole embryo culture 59

3.1 Introduction 59
3.1.1 Literature Review. 61
3.2 Results 63
3.2.1 Serum-free media fail to replicate the development of embryos cultured in rat serum 63
3.2.2 Diluted rat serum can support normal development in culture 67
3.2.3 Rat serum dilution of more than 50% results in sub optimal embryo growth in culture 72
3.2.4 Addition of glucose does not restore development in 30% rat serum-cultured embryos 75
3.3 Discussion 75

Chapter 4 Characterisation of a late-arising NTD phenotype in ASPP2 mutant mice 80

4.1 Introduction 80
4.2 Results 82
4.2.1 ASPP2 mRNA expression is strongest in the ventral neural tube and there is no difference between N- and C-terminal derived mRNA. 82
4.2.2 Trp53bp2$^{\Delta 3/\Delta 3}$ embryos have a variable NTD phenotype 86
4.2.3 Proliferation is increased in late-stage Trp53bp2$^{\Delta 3/\Delta 3}$ embryos and ectopic mitoses are increased in mutants at all gestational ages 95
4.2.4 Cell cycle exit is unchanged and neuronal differentiation is disrupted in Trp53bp2$^{\Delta 3/\Delta 3}$ embryos 105
4.3 Discussion 118
4.3.1 Trp53bp2$^{\Delta 3/\Delta 3}$ embryos exhibit a progressive phenotype leading to reopening of the neural tube 118

4.3.2 Proliferation and differentiation in Trp53bp2$^{\Delta 3/\Delta 3}$ embryos 124
4.3.3 Implications of an increase in ectopic mitotic index.....126

Chapter 5 Addressing apical polarity and interkinetic migration in ASPP2$^{\Delta exon3/\Delta exon3}$ embryos 129

5.1 Introduction 129

5.2 Results 130
5.2.1 Apical marker analysis in Trp53bp2$^{\Delta 3/\Delta 3}$ embryos.....130
5.2.2 Assessment of interkinetic nuclear migration in Trp53bp2$^{\Delta 3/\Delta 3}$ embryos 135

5.3 Discussion.....142
5.3.1 Closing in on the role of apico-basal polarity in Trp53bp2$^{\Delta 3/\Delta 3}$ embryos 142
5.3.2 Questions remain to be answered 146

Chapter 6 Targeting the phenotype in ASPP2$^{\Delta exon3/\Delta exon3}$ embryos through the use of DAPT in whole embryo culture 149

6.1 Introduction 149

6.2 Results 151
6.2.1 Macroscopic morphology of DAPT-treated embryos.....151
6.2.2 Histological morphology of DAPT-treated embryos.....157

6.3 Discussion.....161

Chapter 7 Concluding remarks 165

7.1 Overview of the research findings 165

7.2 Strengths and Weaknesses.....167

7.3 Future directions.....168

Bibliography.....171

Appendices 194

Table of tables

Table 1-1: Genetic polymorphisms associated with human NTD risk 24
Table 1-2: Examples of candidate genes associated with mouse NTDs 27
Table 2-1: Primary antibodies 51
Table 2-2: Secondary antibodies 52
Table 2-3: Staining and dyes 52
Table 2-4: Thresholds in ImageJ 55
Table 3-1: Amino acid concentrations of DMEM and GMEM + defined supplements 77
Table 4-1: NTD frequency in wild-type, heterozygous, and homozygous ASPP2 embryos 88

Table of figures

Figure 1-1: Interkinetic nuclear migration 18
Figure 1-2: Associated structures and neuronal patterning in the neural tube 20
Figure 1-3: Neural tube defects in the mouse related to closure initiation site 26
Figure 1-4: Closed and open yolk sac embryo culture methods 30
Figure 2-1: Morphological scoring parameters 40
Figure 2-2: ASPP2 genotyping 43
Figure 2-3: Post-fixation dissection and embedding of E11.5 embryos 46
Figure 2-4: Cell counting and threshold analysis 56
Figure 2-5: Tuj1 intensity analysis 57
Figure 3-1: Diagrammatic summary of literature review. 61
Figure 3-2: Comparison of whole embryo culture using rat serum or serum-free media 64
Figure 3-3: Developmental and growth parameters of embryos cultured in rat serum or serum-free media 66
Figure 3-4: Developmental and growth parameters of embryos cultured in rat serum or the four combination (diluted) media 69
Figure 3-5: Frequency of open cranial neural tube in embryos cultured in rat serum or the four combination media 71
Figure 3-6: Effect of increased dilution of rat serum on success of embryo culture 73

Figure 3-7: Developmental and growth parameters of embryos cultured in 100% rat serum or in serum diluted 30:70 with GMEM plus defined supplements 74
Figure 4-1: Whole-mount in situ hybridisation with a *Trp53bp2* mRNA probe..... 83
Figure 4-2: Transcription start sites and protein structures of ASPP2 vs ΔN-ASPP2 84
Figure 4-3: Quantitative RT-PCR results..... 85
Figure 4-4: Macroscopic appearance of *Trp53bp2*$^{\Delta 3/\Delta 3}$ embryos 90
Figure 4-5: Histological morphology of the neural tube in wild-type and *Trp53bp2*$^{\Delta 3/\Delta 3}$ embryos..... 92
Figure 4-6: Total and ectopic mitotic index analysis 96
Figure 4-7: Lumen circumference analysis..... 98
Figure 4-8: Ventral and dorsal neural tube: mitotic and ectopic mitotic index analysis 101
Figure 4-9: SOX2 threshold analysis.....103
Figure 4-10: EdU and Ki67 staining analysis.....108
Figure 4-11: TUJ1 intensity analysis within wild-type, non-macroscopically phenotypic and macroscopically phenotypic mutant E11.5 embryos.....112
Figure 4-12: TUJ1 intensity analysis between wild-type and mutant embryos.....113
Figure 4-13: NKX6.1, PAX6 and PAX3 analysis 116
Figure 4-14: Examples and model of phenotypic progression in *Trp53bp2*$^{\Delta 3/\Delta 3}$ embryos.....120
Figure 5-1: N-cadherin and F-actin staining 131
Figure 5-2: PAR3 in the ventral neural tube 134
Figure 5-3: Apical mitosis analysis.....137
Figure 5-4: 1 h EdU analysis of apical and ectopic mitoses and 2 h EdU pulse confirmatory study 139
Figure 5-5: Diagrammatic summary showing EdU analysis of apical and ectopic mitoses.....141
Figure 5-6: Final model of phenotypic progression in *Trp53bp2*$^{\Delta 3/\Delta 3}$ embryos 145
Figure 6-1: Example images of embryos pre- and post-culture in DMSO and DAPT 152
Figure 6-2: Frequency of oedema in WT/Het embryos cultured in defined concentrations of DAPT, and DMSO.....153
Figure 6-3: Macroscopic phenotype analysis of WT/Het and mutant embryos cultured in DMSO and DAPT.....155
Figure 6-4: Histological morphology of WT and mutant embryos cultured in DAPT- or DMSO-treated medium.....157

Figure 6-5: Mitotic index, % ectopic mitoses and lumen circumference of wild-type and mutant embryos treated with DMSO and DAPT 160

Chapter 1 Introduction

1.1 Neurulation in the mammalian embryo

1.1.1 Primary neurulation

Development of the vertebrate brain and spinal cord begins with primary neurulation and formation of a neural tube. The neural plate, a thickened layer of dorsal ectoderm, becomes clearly delimited then starts to bend along the midline to generate neural folds. Elevation and convergent extension of the neural folds then occurs, followed by fusion in the midline to form a closed neural tube. The process of closure occurs at distinct sites along the rostro-caudal axis, which vary in location between species.

In the mouse, closure is initiated at the level of the hindbrain/cervical boundary on embryonic day (E) 8.5 (closure 1) when the embryo has 5-6 somites. A second closure initiation point (closure 2) occurs at the forebrain/midbrain boundary, and a third at the rostral end of the future forebrain (closure 3) (Figure 1-3) (Zohn and Sarkar, 2008). Bidirectional closure or ‘zippering’ from these initiation points leads to closure of the anterior and hindbrain neuropores (open regions of neural folds), and an intact cranial neural tube. The posterior neuropore remains open for the longest period of time in primary neurulation, eventually closing at ~E10 in the mouse when somite count reaches 28-30 (Greene and Copp, 2014).

The discontinuous nature of neural tube closure is largely conserved between mammalian species. Human neurulation appears to occur in a similar manner, with two closure initiation sites that correspond to mouse closures 1 and 3 (O'Rahilly and Muller, 2002). Closure 2, however, is contested as to whether a similar event occurs as in the mouse (Nakatsu et al., 2000) or not at all (O'Rahilly and Muller, 2002). If closure 2 is absent, progression of closure in the head region simply occurs between closure 1 and the most rostral point of the neural plate (closure 3). Like the mouse, closure of the posterior neuropore, which is completed by 26-28 days post-fertilisation in the human embryo, marks the end of primary neurulation.

1.1.2 Secondary neurulation

Secondary neurulation is the process by which the neural tube forms caudal to the mid-sacral region. Undifferentiated mesenchymal cells from the primitive streak condense then undergo mesenchymal to epithelial transition to form a rod, distal to the posterior neuropore (Lew and Kothbauer, 2007). This rod then undergoes canalisation to form a neural tube lumen which is continuous with the caudal end of the primary neural tube (Zohn and Sarkar, 2008). In humans, this process leads to the formation of the most caudal spinal cord, namely the conus medullaris, cauda equina, and filum terminale (Lew and Kothbauer, 2007).

Secondary neurulation in the mammal has previously been likened to formation of the neural keel in zebrafish. The zebrafish neurectoderm first forms the neural keel, a solid rod, which goes on to form a tube with a lumen. Although initially the neural keel was thought to be a mass of mesenchymal cells (Reichenbach et al., 1990), as in secondary neurulation in the mammal, more recent studies have shown that the neuroectoderm becomes specified by members of the *SoxB1* family (Okuda et al., 2010), resulting in a pseudostratified neuro*epithelial* structure which converges to form the solid neural rod (Schmidt et al., 2013). Following this process, it has been shown that structural proteins, such as *Pard3* and *Rab11a*, localise to the midline of the neural keel during interdigitation of cells across the midline (Buckley et al., 2013). *Pard3* is then inherited into two daughter cells after localising to the mitotic cleavage furrow of mirror-symmetric divisions across the midline. It is these mirror-image polarising divisions which allow daughter cells to incorporate into opposing sides of the developing neural tube, and therefore orchestrate lumen formation in the zebrafish (Tawk et al., 2007).

A similar mechanism of lumen formation has been seen in mammalian Madin-Darby Canine kidney (MDCK) cells. Once depolarised, MDCK cells have the ability to self-organize into complex 3D structures, such as cysts, which start to express E-cadherin at cell–cell interfaces, followed by targeting of apical proteins to the future apical surface and formation of a central lumen

(Eom et al., 2013). Cavitation of the neural tube in mammalian secondary neurulation has been poorly studied, however in the mouse, it appears that the secondary neural tube forms by two mechanisms. At E9.5–10, the entire mesenchymal rod undergoes mesenchymal to epithelial transition followed by a later appearance of a lumen. Later at E11-12, only the dorsal part of the rod transitions to epithelium, forming the medullary 'plate'. Mesenchymal cells then attach to the edges of the plate, adding to the epithelium to eventually form a tube (Schoenwolf, 1984).

1.1.3 Mechanisms involved in neurulation

The complex process of neural tube closure requires tight regulation through signalling pathways and cellular mechanisms. Convergent extension is the process by which the neural plate narrows in the medio-lateral axis (convergence) and elongates in the rostro-caudal axis (extension), allowing initiation of neural tube closure. It has been found that this process depends on the planar cell polarity (PCP) pathway, a non-canonical Wnt/frizzled/dishevelled signalling cascade, involving genes such as *Vangl2* and *Celsr1* (Ybot-Gonzalez et al., 2007). Bending of the neural folds, required to appose the two sides of the neural plate to form a tube, has been shown to depend on mutually antagonistic sonic hedgehog (Shh) signalling from the notochord (Ybot-Gonzalez et al., 2002), and bone morphogenetic protein (BMP) signalling from the surface ectoderm (Ybot-Gonzalez et al., 2007, Stottmann et al., 2006). Following neural fold bending and apposition in the midline, epithelial fusion occurs via apical protrusions resembling lamellipodia and filopodia, regulated by the small GTPases Rac1 and Cdc42 (Pai et al., 2012, Rolo et al., 2016).

Maintenance of a closed, complete neural tube during rapid embryonic growth is partly controlled through regulation of cell proliferation and cell death. The importance of this growth regulation is illustrated by the finding of cranial neural tube closure defects in mouse mutants with a lack of, or excessive, apoptosis (Harris and Juriloff, 2007), and with elevated proliferation and abnormal cell cycle progression (Kim et al., 2007). Other

mouse mutants with failed neural tube closure highlight further signalling pathways that are involved in neural tube closure. For example, the c-Jun N-terminal kinase (JNK) pathway, involved in proliferation and apoptosis, was found to be implicated in neural tube closure: *JNK1/JNK2* double mutant embryos display reduced apoptosis in the hindbrain neuroepithelium and exhibit exencephaly (Sabapathy et al., 1999). The long-established association between folate status and human NTDS (1991), has led to the finding that neural tube closure also depends on the activity of both the methionine and folate cycles, specifically the generation of one-carbon units in mitochondrial folate one-carbon metabolism (Leung et al., 2017). These examples give an idea of the complexity of neurulation and exemplify how small changes in such mechanisms could result in devastating effects.

1.2 Neurogenesis in the mammalian embryo

1.2.1 Structure of the neuroepithelium

The walls of the newly formed neural tube consist of bipolar shaped neuroepithelial cells (NECs), which collectively form the pseudostratified neuroepithelium. NECs possess apical and basal processes that span the entire width of the neuroepithelium. At the basal region, or periphery, of the neural tube, NECs terminate in a flattened endfoot that contacts the basal lamina. The apical end of each cell borders the central lumen of the neural tube and typically has a single cilium (Hollyday, 2001). Initially, these cells divide in a symmetric manner, such that apical components, critically the apical plasma membrane, are equally distributed to both NE daughter cells (Gotz and Huttner, 2005). It has even been shown that the long basal processes of NECs are split equally during mitosis (Kosodo et al., 2008).

Proteins of the apical and basal domains are essential for NEC function. Adherens junctions, which contain proteins including cadherins and catenins, are situated just basal to the apical membrane, are essential for cell-to-cell adhesion, connection to the intracellular actin network, and promoting neural progenitor self-renewal via activation of β-catenin signalling (Stocker and Chenn, 2015). Polarity proteins such as Par3, Par6 and aPKC are associated

with the apical domain of NECs and have been shown to promote self-renewing cell divisions in NECs (Costa et al., 2008). The Rho family of small GTPases, such as RhoA and cdc42, also have important roles in the apical region, due to their role in maintaining adherens junctions and regulating NEC positioning and proliferation (Cappello et al., 2006, Katayama et al., 2011). Conversely, the proteins lethal giant larvae (Lgl), discs large (Dlg) and scribble (Scrib) are all expressed in the baso-lateral domain and play key roles in maintaining apico-basal polarity (Stephens et al., 2018). Cyclin D2, which is known to play a role in the transition between G1 and S phase of the cell cycle, is highly expressed in the basal endfoot of NECs, and unequal inheritance of Cyclin D2 has been demonstrated during asymmetrical NEC division (Tsunekawa et al., 2012). All of these associated proteins play a significant role in maintaining apico-basal polarity and proliferation in the neuroepithelium.

Neuroepithelial cells are able to turn into radial glial cells by downregulating Golgi-derived apical trafficking, and initiating the expression of astroglial markers such as GLAST (Paridaen and Huttner, 2014). Following asymmetric division of neuroepithelial or radial glial cells, new-born neurogenic daughter cells withdraw from the apical surface and migrate basally to differentiate. Daughter cell fate specification is induced through the expression of various region-specific transcription factors which influence the structure of the neuroepithelium. For example, expression of *Neurogenin* in neuroepithelial cells in the future dorsal telencephalon results in the generation of glutamatergic pyramidal neurons, whereas the ventral telencephalon expresses genes such as *Ascl1*, resulting in GABA-ergic basal ganglia neurons (Paridaen and Huttner, 2014). In the subventricular zone of the mammalian neocortex, there are additional types of neural progenitor cell, such as intermediate progenitors and basal radial glial cells, which remain capable of self-renewal, and therefore allow for prolonged neurogenesis and further expansion of the cortex. Wnt signalling and its downstream target N-myc have been shown to be involved in the production of these progenitors by facilitating the differentiation of apical progenitors into

intermediate progenitors during development of the neocortex (Kuwahara et al., 2010).

Considering the complex interplay of signalling pathways and proteins involved in defining neuroepithelial structure and integrity, especially in the cortex, it is not surprising that a variety of mutations can result in a wide range of cerebral cortical developmental malformations in humans. For example, microtubule proteins TUBA1A and TUBA8, involved in centrosomal positioning and nuclear transport during neuronal migration, have been implicated in lissencephaly ('smooth-brain') phenotypes (Poirier et al., 2007, Abdollahi et al., 2009). Other conditions that exhibit impaired neuronal migration include periventricular heterotopia, characterised by nodules of neurons lining the lateral ventricles, which has been shown to arise due to altered vesicle trafficking leading to impaired cell adhesion in the neuroependyma (the foetal CSF-brain barrier), due to mutations in two genes: *FLNA* or *ARFGEF2* (Ferland et al., 2009). In general, malformations of cerebral cortical development, even in the early neuron migration stages, can result in a wide range of developmental disorders that cause neurodevelopmental delay and epilepsy.

1.2.2 Interkinetic nuclear migration and cell cycle kinetics

Interkinetic nuclear migration (IKNM) is the process by which cell nuclei at distinct stages of the cell cycle occupy different positions along the apical–basal axis of the neuroepithelium (Del Bene, 2011). Typically, NEC nuclei migrate to the basal side of the neural tube during the G1 phase of the cell cycle, where they remain during DNA synthesis (S-phase). Nuclei then migrate back to the apical border during G2 phase and undergo mitosis at the apical surface of the neuroepithelium. The function of IKNM remains controversial (Del Bene, 2011), despite being first described over 80 years ago (Sauer, 1935). However, it has been proposed that IKNM contributes to determining the cell fate of NECs by moving nuclei through signalling gradients along the apico-basal axis of the neuroepithelium (Murciano et al., 2002, Baye and Link, 2007). Mechanisms controlling IKNM have also been

debated, due to the complex relationship between cytoskeletal components, stages of the cell cycle, and nuclear movement (Kosodo et al., 2008, Tsai et al., 2010, Spear and Erickson, 2012a). It is, however, generally accepted that the mechanisms that control the apical-basal movement of nuclei, differ from those that control the basal-apical movement of nuclei (Gotz and Huttner, 2005).

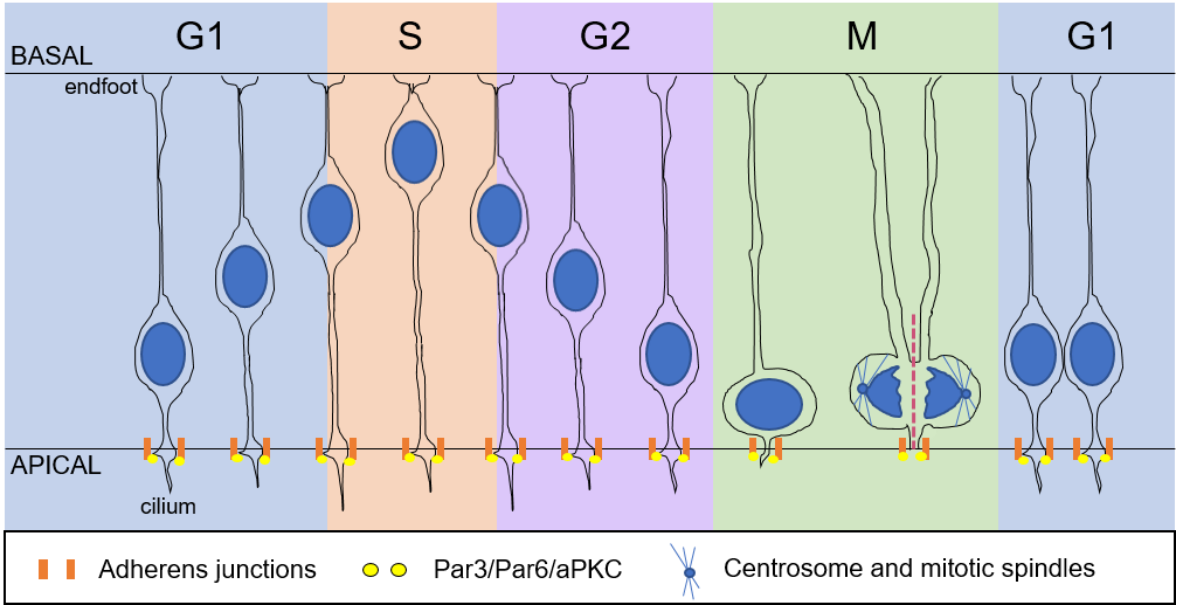

Figure 1-1: Interkinetic nuclear migration

Summary diagram illustrating the stages of interkinetic nuclear migration. Cells span the width of the neuroepithelium with a basal process ending in an endfoot, and an apical process which has a single cilium. Adherens junctions and apical polarity proteins Par3/Par6/aPKC characterise the apical domain. Nuclei move within the neuroepithelium depending on cell cycle stage. During G1, nuclei move toward the basal surface. S phase occurs at the basal surface. During G2, nuclei migrate towards the apical surface. During mitosis (M phase), mitotic cell rounding occurs followed by cell division. Symmetrical cell division causes equal partitioning of all cellular components, including the apical domain and its associated proteins, as well as the basal processes. Two neuroepithelial daughter cells are produced which resume interkinetic nuclear migration.

Cell cycle kinetics are regulated by factors other than nuclear positioning, and when altered, can determine cell fate. For example, the Cdk4/cyclinD1 active kinase complex has been shown to play a role in the length of G1. When this complex was overexpressed in neural progenitors, G1 was shortened and neurogenesis was inhibited, alongside an increase in

intermediate progenitors. When the Cdk4/cyclinD1 complex was inhibited using RNAi, neurogenesis increased, showing that lengthening of G1 is sufficient to cause neurogenesis in progenitors (Lange et al., 2009). This correlates with an earlier finding that regions of the cortex that exhibited a higher number of neurogenic divisions are characterised by progenitors with a longer G1 phase (Lukaszewicz et al., 2005). Other regulators include insulin-like growth factor-1, which has been shown to regulate neural progenitor division by reducing the length of G1 and increasing cell cycle re-entry in the ventricular zone (Hodge et al., 2004), and BM88, a neuronal protein shown to limit cell cycle progression by down-regulating cyclin D1 and induce neuronal differentiation (Politis et al., 2007, Georgopoulou et al., 2006).

1.2.3 Neuronal specification and differentiation

Neuronal specification and patterning in the dorso-ventral axis of the neural tube is controlled by ventralising signals from the notochord and floor plate, and dorsalising signals from the roof plate and surface ectoderm. Sonic hedgehog (Shh), released from the notochord, has been shown to induce activating forms of Gli proteins that induce the expression of ventral transcription factors (TFs) such as Nkx6.1, Olig2 and Nkx2.2. The dynamic dorso-ventral gradient of Gli proteins also results in the repression of dorsal TFs such as Pax3, Pax7 and Pax6 (Ericson et al., 1997, Briscoe et al., 2000, Briscoe et al., 1999). Dorsalising signals play an additional role in specifying dorsal cell fate. Important factors are BMP4 and BMP7 which are released from the epidermal ectoderm, followed by TGFβ signalling from roof-plate cells (Liem et al., 1997, Liem et al., 1995). The combinatorial expression of TFs in each domain, regulated by these signalling pathways, is sufficient to specify and generate neuronal subtypes.

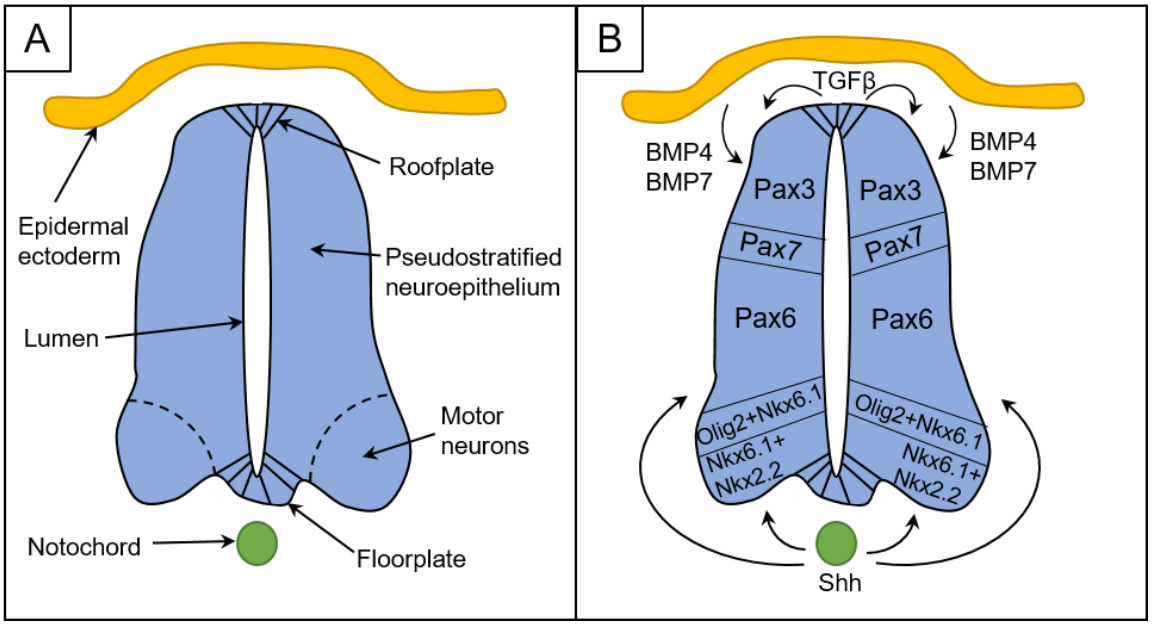

Figure 1-2: Associated structures and neuronal patterning in the neural tube

(**A**) Characteristics of the neural tube and associated structures. The roof-plate is a group of cells at the dorsal pole of the neural tube. The neuroepithelium makes up the majority of cells in the neural tube. It appears stratified due to the varying locations of nuclei between the basal and apical surfaces (IKNM). Motor neurons are located in the ventro-lateral swellings of the neural tube. The floor-plate is a group of cells at the ventral pole of the neural tube. The notochord is a mesodermal rod-like structure of cells which acts as a major signalling centre during development. The lumen is the central canal of the neural tube which contains neural tube fluid, followed by cerebrospinal fluid later in development. The epidermal, or surface, ectoderm is a single-layered epithelium which goes on to form the epidermis. (**B**) Signalling-induced neuronal specification and patterning of the neural tube. Shh is produced by the notochord which establishes a dorso-ventral signalling gradient. Ultimately, this results in TFs Nkx2.2, Nkx6.1 and Olig2 to be expressed in the ventral region of the neural tube. Low Shh levels combine with high levels of BMP4 and BMP7, released from the epidermal ectoderm, to induce expression of TFs: Pax3, Pax7 and Pax6. TGFβ is released from roof-plate cells as a secondary signal that is required for the generation of dorsal interneurons.

Motor neurons and ventral interneurons are the first mature neurons to appear in the mammalian neural tube, located in the ventro-lateral and dorso-lateral regions (Pfaff et al., 1996). At the onset of neurogenesis, NECs switch to asymmetric, neurogenic divisions at the apical border. This results in the formation of a neuroepithelial daughter cell and a neuronal daughter cell. New-born neurogenic daughter cells withdraw from the apical surface and dissociate from the apical cilium (Das and Storey, 2014), in order to migrate basally and differentiate (Paridaen and Huttner, 2014). It has been shown

that the abscission of the apical process is mediated by actin-myosin contraction, and requires the down-regulation of N-cadherin for final dissociation from the apical membrane (Das and Storey, 2014).

Notch signalling has been shown to influence neural progenitor cell activity and play a role in neural differentiation. Notch ligand, Delta-like 1, promotes neural differentiation directly, via *Cis*-inhibition of Notch receptors in the same cell. This process is blocked during delamination (the final stages prior to differentiation), by the ubiquitin ligase Mindbomb1, to allow reduction in the size of the apical process before down-regulation of apical markers and delamination (Baek et al., 2018). This ensures the integrity of the ventricular wall is preserved during neuron differentiation.

1.3 Neural tube defects

Neural tube defects (NTDs) are among the most common types of birth defects, with approximately 300,000 babies being born with NTDs each year worldwide (Zaganjor et al., 2016). These defects arise from failure of the neural folds to appose and fuse during primary neurulation, which in turn can lead to secondary abnormal development of structures associated with the neural tissue such as muscle and bone (Salih et al., 2014). By utilising NTD mouse models, researchers are able to gain an insight into the developmental processes leading to such defects in humans.

1.3.1 Neural tube defects in humans

Clinically, NTDs are classified as either ‘open’ or ‘closed’. Open NTDs are characterised by neural tissue that is exposed to the environment such as myelomeningocele or anencephaly, whereas ‘closed’ NTDs, such as spina bifida occulta, are covered by skin (Bassuk and Kibar, 2009). Anencephaly is homologous to exencephaly in the mouse, presenting at birth with absence of a skull vault over the open cranial region and degeneration of the exposed neural tissue (Detrait et al., 2005). Myelomeningocele is a form of open spina bifida where protruding neural tissue remains covered by a meningeal sac,

whereas in myelocele the neural tissue is directly exposed to the amniotic fluid (Greene and Copp, 2009).

Open NTDs in the human are proposed to result from failure of closure at an initiation site or incomplete progression of closure between sites so that a neuropore remains open. However, occasionally open human NTD types contradict this proposed mechanism, for example where multiple NTDs are seen in the same individual (Ahmad et al., 2008, Mahalik et al., 2013). It has long been debated whether open NTDs such as these arise by an alternative mechanism: rupture of the neural tube. In the 18th century it was proposed that in cases of hydrocephalus and spina bifida, the pressure of fluid from the hydrocephalic head caused neural tube rupture further caudal, in the spinal cord (Morgagni, 1769). It has also been argued that overdistention of the neural tube, resulting from an increase in hydrostatic pressure prior to neural tube rupture, could explain the many skeletal, endodermal and mesodermal abnormalities associated with NTDs (Gardner, 1980).

Closed NTDs are a less well-defined group of spinal NTDs, where open vertebral arches remain covered by skin. The spinal cord is often malformed and tethered to surrounding tissues, and there may be associated disorders such as lipoma or anorectal abnormalities (Greene and Copp, 2014).

The genetic basis of NTDs in humans is not straight forward, as most NTDs occur sporadically, with very few multigenerational family incidences. In cases where family data on recurrence risk has been documented, an oligogenic pattern of NTD risk has been suggested (Harris and Juriloff, 2010). Gene polymorphisms that have been identified in association with human NTDs are often involved in folate one-carbon metabolism or folate transport (Table 1-1). This is consistent with the epidemiological evidence that folate has a protective effect against ~70% NTDs, first established in an international randomised clinical trial (1991). Folate antagonists such as carbamazepine, trimethoprim and fumonisin, have also been shown as teratogenic agents related to NTD causation (Hernandez-Diaz et al., 2001, Missmer et al., 2006). Despite this evidence, it remains that ~30% human

NTDs are folate-resistant (1991). Combined with the variety in genetic polymorphism candidates for human NTD risk involving other, non-folate related pathways, and the questions surrounding the mechanisms of open NTDs in the human, it is clear that further investigation and understanding of NTDs is required to find new preventative measures. Utilisation of mouse models is critical to help identify candidate genes and cellular mechanisms that could enable a better understanding of the heterogeneous and multifactorial NTDs that occur in humans.

Table 1-1: Genetic polymorphisms associated with human NTD risk

Candidates for genes involved in human NTD risk		
Gene	**Protein role**	**Ref**
ADA	Purine metabolism	(Pangilinan et al., 2012)
ALDH1A2	Retinol metabolism	(Deak et al., 2005)
ARID1A	Chromatin remodelling	(Pangilinan et al., 2012)
BHMT	One-carbon metabolism	(Shaw et al., 2009)
CBS	Folate metabolism	(Shaw et al., 2009)
CELSR	PCP gene	(Juriloff and Harris, 2012)
CFL1	Actin-modulating	(Zhu et al., 2007)
DHFR	Folate metabolism	(Johnson et al., 2004)
FOLR3	Folate transport	(Findley et al., 2017)
FRβ	Folate metabolism	(Heil et al., 1999)
FZD6	Wnt signalling	(Shi et al., 2014)
GCKR	Glucose metabolism	(Fu et al., 2015)
GLUT1	Glucose metabolism	(Davidson et al., 2008)
HK1	Glucose metabolism	(Davidson et al., 2008)
LEP	Glucose metabolism	(Lupo et al., 2012)
LEPR	Glucose metabolism	(Davidson et al., 2008)
MFTC	Folate transport	(Pangilinan et al., 2012)
MS	Folate metabolism	(Morrison et al., 1998)
MTHFD1	Folate metabolism	(Minguzzi et al., 2014)
MTHFR	Folate metabolism	(Relton et al., 2004)
MTRR	One-carbon metabolism	(Doudney et al., 2009)
NOS2	Cellular signalling	(Soldano et al., 2013)
PARD3	Apico-basal polarity	(Chen et al., 2017)
PAX3	Transcription factor	(Lu et al., 2007)
PEMT	Choline metabolism	(Pangilinan et al., 2012)
SARDH	One-carbon metabolism	(Franke et al., 2009)
SCRIB	PCP gene	(Juriloff and Harris, 2012)
SHMT	Folate metabolism	(Heil et al., 1999)
SLC19A1	Folate transport	(Findley et al., 2017)
SULT1A1	Sulfate conjugation	(Wang et al., 2014)
RFC-1	Folate transport	(Shang et al., 2008)
TRDMT1	One-carbon metabolism	(Franke et al., 2009)
TYMS	Folate metabolism	(Volcik et al., 2003)
VANGL1	PCP gene	(Merello et al., 2015)
VANGL2	PCP gene	(Juriloff and Harris, 2012)

1.3.2 Neural tube defects in the mouse

NTDs in the mouse result from failure of closure at any initiation site or neuropore, with severity determined by when and where the failure occurs in the developing embryo. Failure of neural tube closure 1, results in craniorachischisis, a defect in which the hindbrain and entire spinal column remain open, leading to embryonic lethality (Figure 1-3). Examples of genetic mouse mutants that exhibit this defect include homozygotes for each PCP gene: *Vangl2*$^{Lp/Lp}$, *Scrib*$^{Crc/Crc}$ or *Celsr1*$^{Crsh/Crsh}$ (Murdoch et al., 2014). Failure to complete closures 2 or 3 results in exencephaly, where the neuroepithelium appears to protrude owing to the open cranial neural folds (Figure 1-3). This defect is the commonest NTD in mouse models, accounting for ~70% reported mouse mutants (Harris and Juriloff, 2010). Delay in closure of the posterior neuropore, caused by an impairment in spinal neurulation, can result in spina bifida aperta (open spina bifida) (Figure 1-3). More than 70 mouse models have now been identified to exhibit spina bifida, although most have co-existing exencephaly (Mohd-Zin et al., 2017).

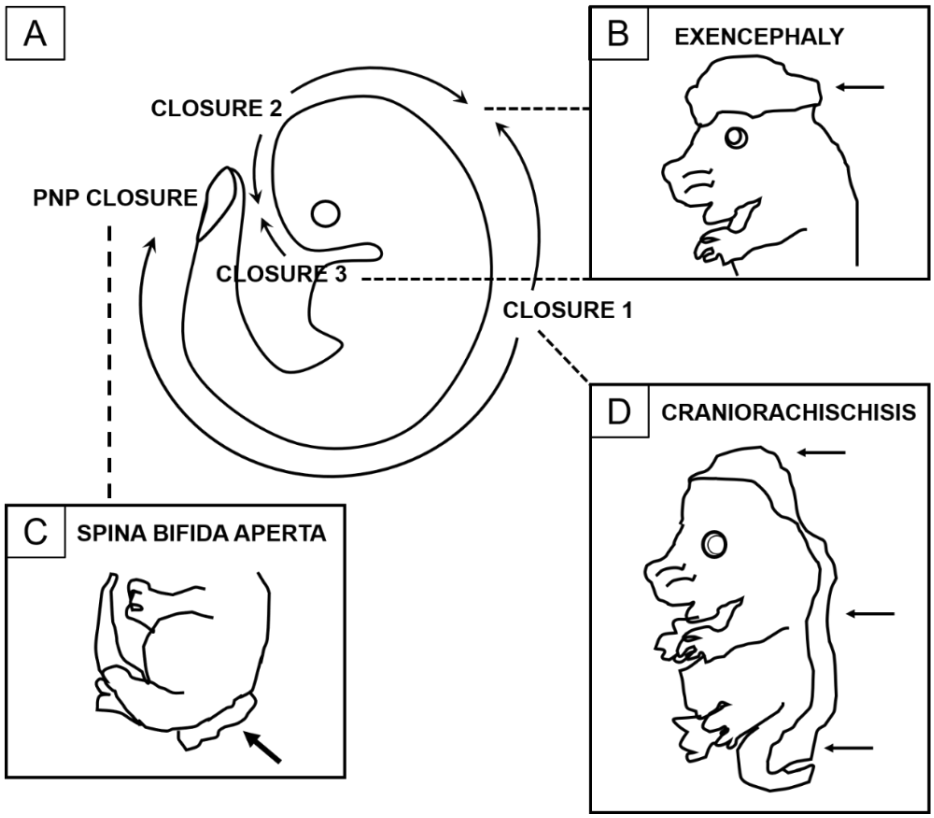

Figure 1-3: Neural tube defects in the mouse related to closure initiation site

(**A**) Diagram showing the location of each neural tube closure initiation site: closure 1 is located at the hindbrain/cervical boundary; closure 2 initiates at the forebrain/midbrain boundary; closure 3 is located at the rostral end of the developing forebrain; PNP closure occurs at the most caudal point of the neural tube. (**B**) Failure of neural tube closure at sites 2 or 3 causes exencephaly which presents as a neuroepithelial protrusion through the open cranial brain folds. (**C**) Spina bifida aperta results from failure of PNP closure, where a protrusion of neuroepithelial tissue can be seen in the caudal region, rostral to the initiation site of secondary neurulation. (**D**) Craniorachischisis occurs when embryos fail to complete closure 1. The neural tube remains open, resulting in a continuous protrusion from the hindbrain, down the entire spinal column. Modified from (Greene and Copp, 2014, Mohd-Zin et al., 2017).

The number of reported mouse genetic mutants with NTDs reached 245 in 2010, and has likely risen further in recent years (Harris and Juriloff, 2010). Craniorachischisis results from defects in genes which are only associated with non-canonical Wnt signalling: the PCP pathway (Zohn et al., 2003), however, genes involved in exencephaly and spina bifida aperta are a lot more varied in function. Table 1-2 includes just a few of the cellular mechanisms in which defective genes are associated with NTDs in the mouse.

Table 1-2: Examples of candidate genes associated with mouse NTDs

Mouse genes causing NTDs			
Function	**Gene**	**NTD type**	**Reference**
Cytoskeleton	Vinculin	Ex	(Xu et al., 1998)
	N-cofilin	Ex	(Gurniak et al., 2005)
	Palladin	Ex	(Luo et al., 2005)
	Shroom	Ex + Sba	(Hildebrand and Soriano, 1999)
Proliferation / Differentiation	Numb	Ex	(Zhong et al., 2000)
	Pax3	Ex + Sba	(Epstein et al., 1991)
	Mir-302/367	Ex	(Yang et al., 2015)
	Brd2	Ex	(Shang et al., 2009)
Chromatin dynamics	ATRX	Ex	(Berube et al., 2002)
	Brg1	Ex	(Bultman et al., 2000)
	Cecr2	Ex	(Banting et al., 2005)
Ubiquitination	Mib2	Ex	(Wu et al., 2007)
	Hectd1	Ex	(Zohn et al., 2007)
Apico-basal polarity	RhoA	Ex	(Katayama et al., 2011)
	Smad5	Ex	(Chang et al., 1999)
	Bmp2	Ex	(Castranio and Mishina, 2009)
Planar cell polarity	Vangl2	Cr	(Kibar et al., 2001)
	Scrb1	Cr	(Murdoch et al., 2003)
	Celsr1	Cr	(Curtin et al., 2003)
	Ptk7	Cr	(Lu et al., 2004)
Ex: exencephaly, Sba: spina bifida aperta, Cr: craniorachischisis			

Association studies of the human homologues of some of these mouse NTD genes have been examined, however there have been very few significant findings to date (Greene and Copp, 2009). On the other hand, NTD mouse mutants often result from complex gene-gene or gene-environmental interactions and vary depending on genetic background. For example, homozygous mutations in *Pax3,* resulting in NTDs in *splotch* mice (Epstein et al., 1991), can be exacerbated by other mutations in genes such as *grainyhead-like-3* (Estibeiro et al., 1993), as well as by environmental factors such as folate deficiency (Burren et al., 2008). Complex interactions and multifactorial aetiologies such as these may closely resemble human NTDs.

Furthermore, the similarities of neurulation at the embryonic level between the mouse and the human, ensure that mouse models continue to provide a valuable tool for the study of embryology and NTDs.

1.4 Experimental methods used to study development and birth defects

Experimental methods are required to complement purely descriptive studies, to provide a more exploratory and in-depth analysis of a developmental process or abnormality. Recent advances in *ex vivo* approaches have allowed recapitulation of developmental events that overcome the inaccessibility of the embryo during gestation. Organ culture is an example of an ex vivo approach, for example, the improvement in culture conditions has allowed the embryonic heart to remain viable for four days post-dissection (Dyer and Patterson, 2013). Gut, kidney and pancreas organoid differentiation is now possible through the use of embryonic stem cells, or iPS cells, and extrinsic factors that mimic *in vivo* signalling events (Spence et al., 2011, Takasato et al., 2015, Greggio et al., 2013). Most recently, artificial embryos created using mouse embryonic, trophoblast and extra-embryonic endoderm stem cells, are able to go through gastrulation, a significant event in early development, never before recapitulated outside of the uterus (Sozen et al., 2018).

Despite the advances in *in vitro* experimental methods, the laboratory mouse has played, and continues to play, an important role in studying embryonic growth. Unique processes in mammalian development raise questions about the use of other organisms such as fly, frog or zebrafish to model human developmental events. *In vivo* approaches in the mouse have been most widely used, for example involving intrauterine or intraperitoneal injections of reagents to assess their effect on embryonic development or implantation (Wu and Gu, 1981). These techniques have led to the modelling of human conditions during pregnancy, such as intrauterine infection through the injection of *E.coli* (Hirsch et al., 1995), and the analysis of factors important in implantation, such as αVβ3 integrin (Illera et al., 2000). Recent advances

have even allowed cell labelling of specific embryonic tissues through ultrasound-mediated microinjection (Hiriart et al., 2014). Genetic gain- and loss-of-function studies are now possible *in utero*, through using techniques such as *in utero* electroporation combined with siRNAs or plasmid DNA, which has often been used to study brain development (Nishimura et al., 2012, Ding et al., 2012).

Although often effective, these methods have their limitations, particularly in relation to the 3Rs' considerations of replacing, reducing and refining use of animals in research. To avoid inter-litter discrepancies, a large number of mice are required per study, which has both cost and ethical implications; potential harm caused by injections or manipulation of the pregnant dam could have a negative impact regarding animal welfare; considering dose-response to an injected reagent, the final concentration that reaches the developing embryos is dependent on maternal metabolism; lack of access to embryos means longitudinal assessment of development is impossible. Hence, there is a need to utilise and optimise more accessible techniques of studying embryonic development, particularly when considering a reduction in animal use.

1.5 Rodent whole embryo culture

Whole embryo culture is a technique that offers an alternative to *in vivo* studies, allowing direct manipulation and observation of developing rodent embryos. In the mid-1960s, Denis New was the first to describe an *ex utero* technique for growing postimplantation rat embryos through the stages of organogenesis (New, 1966). This work initially involved establishment of culture conditions for various 24-48 h periods between embryonic days 7.5 and 13.5 and culminated in the reporting of viable cultures continuing for as long as 5 days (Buckley et al., 1978).

Dissection methods when preparing embryos for culture vary depending on gestational age. For all embryo stages, the decidual swellings are removed from the uterus, followed by removal of the decidua and the Reichert's

membrane, to reveal the embryonic yolk sac. For culturing neurulation-stage embryos (E8.5-E9.5), the closed yolk sac method is preferential, as the yolk sac receives sufficient oxygen and nutrients from the culture medium for embryonic growth (Figure 1-4). For late-stage embryos, it becomes necessary to increase oxygen levels *in vitro* to support growth. This high oxygen pressure can have a harmful effect on the yolk sac, which loses blood circulation and ceases to function (New and Coppola, 1970). Therefore, exteriorisation of the embryo from the yolk sac and removal of the amniotic membrane are used to improve development of late-stage rodent embryos (Figure 1-4) (Martin and Cockroft, 1999). This allows the use of capillary circulation at the foetal surface for oxygen transfer, in addition to any contribution from the opened yolk sac, which remains in vascular continuity with the embryo (Cockroft, 1973).

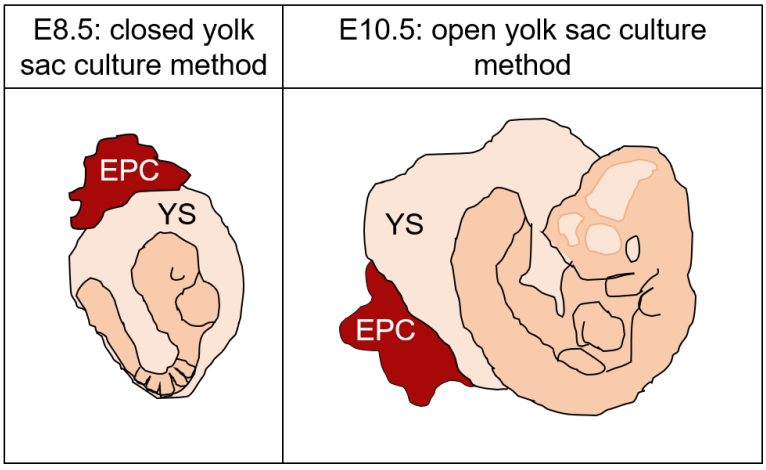

Figure 1-4: Closed and open yolk sac embryo culture methods

Diagram showing the two yolk sac culture techniques, for E8.5 and E10.5 mouse embryos. The closed yolk sac method is suitable for neurulation-stage embryos, where the yolk sac (YS) remains intact and the ectoplacental cone (EPC) is trimmed. For E10.5 embryos, an opening is made in the yolk sac and the embryo is exteriorised. The amniotic membrane is removed, and the YS and EPC remain attached via the embryonic vasculature.

The embryo culture method involves specially prepared rat serum as culture medium and specific oxygen concentrations within the gaseous environment, depending on embryo stage. Following termination of the culture, embryo development is scored, based on yolk sac circulation and diameter, somite number, degree of axial rotation and protein content of the embryos and their

membranes. Brown and Fabro devised an objective scoring system whereby developmental stages of 17 morphological features could be assessed to provide a precise index of embryonic development, and to detect retardation or dysmorphogenesis of specific embryonic features (Brown and Fabro, 1981).

Rat serum was selected as the primary medium for use in embryo culture, due to embryonic development showing comparability to that of *in utero* growth when quantified using the aforementioned scoring systems (New et al., 1976a). This was true when using both rat embryos (New, 1978), and mouse embryos (Sadler, 1979). It was shown to be irrelevant whether rat serum was obtained from male rats, pregnant females or non-pregnant females (New, 1966). Immediate centrifugation and heat inactivation of the serum was demonstrated to improve embryonic development even further (New et al., 1976a). Rat serum, therefore, became the standard medium for use in rodent whole embryo culture until the present day (Ellis-Hutchings and Carney, 2010).

Whole embryo culture has enabled investigations into normal embryonic development (Wilson and Beddington, 1996, Fleming et al., 1997), as well as a plethora of research on teratogenesis and birth defects (Piersma, 1993, Cockroft and Coppola, 1977, Ellis-Hutchings and Carney, 2010). The method is increasingly being incorporated into preclinical drug testing for teratogenicity by the pharmaceutical industry (Flick and Klug, 2006). Additional to its experimental advantages, whole embryo culture also provides a refinement and reduction of animals used per experiment: it allows multiple treatments to be applied to the same litter from a single pregnant dam, ensuring a lower number of dams are exposed to harmful procedures or sacrificed. However, in utilising rat serum as the primary growth medium, limitations remain in regards to animal usage, and progress towards use of a non-serum-based medium would be beneficial for the 3Rs.

1.6 Aims of the thesis

The present thesis represents a combination of *in vitro* and *in vivo* analyses, with NTDs as the primary developmental outcome under study. In Chapter 3, an initial study of mouse whole embryo culture is described in which the aim was to replace or reduce rat serum in the culture medium. Extensive developmental assessment of neurulation stage embryos, comparing serum-free or reduced serum-cultured embryos with 100% rat serum controls, was carried out post-culture to meet this aim. In Chapter 4, the aim was to carry out thorough analysis of ASPP2 mutant mouse embryos which exhibit a complex NTD phenotype. This was achieved through macroscopic phenotype analysis, in situ hybridisation, cell cycle exit analysis and immunofluorescence studies. The aim of Chapter 5 was to address apical polarity and interkinetic nuclear migration in the neuroepithelium of the ASPP2 mutants. Hypothesis-driven analysis of nuclear movement was assessed through the use of EdU labelling, a thymidine analogue. In Chapter 6, the aim was to rescue a specific characteristic of the NTD phenotype in ASPP2 mutant embryos, using an anti-proliferative reagent in whole embryo culture with the open yolk sac method.

Chapter 2 Methods

2.1 Embryological procedures

2.1.1 Mouse strains and embryo collection

Random-bred CD1 mice were used in the rat serum replacement culture experiments (Chapter 3). *ASPP2*$^{+/-}$ mice (Chapter 4-6) were on a mixed (C57BL/6J x 129SvJ) genetic background. Female mice were paired with males in the evenings and checked for vaginal plugs the following morning. If positive, embryos were counted as E0.5 days post coitum (dpc) at 12:00 on the day of plug detection. Litters were then collected on the appropriate embryonic day by euthanizing the pregnant mice by cervical dislocation, followed by decapitation to ensure death and removal of the pregnant uterus into DMEM containing 10% fetal bovine serum (FBS).

2.1.2 Preparation of rat serum

Blood used in rat serum preparation was collected from pathogen-free male Sprague-Dawley rats. For anaesthesia, gaseous 2.5-4.0% isoflurane was applied to the rats in an inhalation box for 10 min (2.0-3.5 L/min). Anaesthesia was confirmed by checking for the loss of the response to stimulation on the paws with forceps. To deeply anesthetize the rats during blood collection, the same concentration and flow of anaesthetic was administered through a mask covering the nose of the rats.

70% ethanol was used to disinfect the skin and avoid contamination. Using a pair of forceps and scissors, the skin and abdominal wall were cut simultaneously toward the thorax region to expose the internal organs, and toward the hind limbs to further expose the posterior abdominal region. The gut and fat of the abdominal region was reflected. Visceral fat was split to expose the abdominal aorta and its bifurcation. A 21 G needle connected to a 20 ml syringe was then inserted immediately cranial to the bifurcation of the aorta. The syringe was pulled up slowly to extract ~15 ml of blood from a male rat. Once removed, the blood was poured into 10-ml sterile test tubes.

The collected blood was centrifuged for 5 min at 1,200 x g and then left at room temperature (RT) for at least 20 mins. A fibrin clot formed in the upper (plasma) layer, which owing to centrifugation was entirely free of red cells. Once formed, the fibrin clot was squeezed using a pair of sterile, curved forceps, ensuring the red cell pellet in the base of the tube remained undisturbed. The tubes were then centrifuged for 5 min at 1,200 x g at 4˚C to collapse the fibrin clot onto the upper surface of the red cell pellet. This left clear serum in the upper layer which was decanted into 15 ml sterile tubes using a sterile pipette. These tubes were centrifuged for 5 min at 1,200 x g and RT to remove any remaining red cells. Serum was decanted into new 15 ml sterile tubes using a sterile pipette, avoiding contamination by residual red cells at the bottom of the tube. To inactivate the complement system, serum was incubated in a water bath at 56 °C for 30 min. Tubes were then cooled to RT and aliquoted. Serum aliquots were stored at -20˚. Aliquots were thawed at 37˚C and filtered through a 0.45 µm pore size filter before immediate use.

2.1.3 Preparation of serum-free culture medium

Serum-free media (100%).

To make KnockOut serum-free culture medium, as described (Moore-Scott et al., 2003), 2% Bovine Serum Albumin (Sigma A9418-50G) was first added to KnockOut DMEM (Gibco 10829-018) then filtered through a 0.45 µm pore size filter. All other media components were added, including 10% KnockOut Serum Replacement (KSR) (Gibco 10828010), 1X N-2 Supplement (100X stock, Gibco, 17502-048) and 25 U/ml of Penicillin-Streptomycin (Gibco, 15140-122). The final solution was mixed thoroughly and filtered once more through a 0.22 µm pore size filter. Aliquots of KSR and N-2 were made in a sterile culture hood and stored at -20˚ to avoid repeated thawing and refreezing. All other media components were stored at 4˚C.

N2B27 serum-free culture medium was made using 25% low glucose DMEM without phenol red (Invitrogen, 11880-028), 25% Ham's F-12 Nutrient Mix with GlutaMAX (Invitrogen, 31765), 50% Neurobasal-A Medium without

Phenol Red (Gibco, 12349-015), 2X N2 Supplement (100X stock, Gibco, 17502-048), 2X B27 Supplement (50X stock, Gibco, 17504-044), 25 U/ml of Penicillin-Streptomycin (Gibco, 15140-122) and 0.1 mM β-Mercaptoethanol (Sigma, M3148). Aliquots of N-2 and B27 supplement were made in a sterile culture hood and stored at -20˚ to avoid repeated thawing and refreezing. All other media components were stored at 4°C.

Serum-free media for 50% dilution. These were as follows:

DMEM: DMEM with phenol red, +4.5 glucose, +L-glutamine, +HEPES, –Sodium Pyruvate (ThermoFisher, 42430-025)

GMEM and defined supplements: Glasgow Minimum Essential Medium (Sigma, G5154) was combined with 1% Non-Essential Amino Acids (NEAA) (Life Technologies, 11140050), 2 mM L-glutamine (HyClone™ SFM4CHO-Utility media (liquid) with L-glutamine) (Fisher Scientific, SH30549.01), 1 mM Sodium Pyruvate Solution (Fisher Scientific, SH30239.01) and 25 U/ml of Penicillin-Streptomycin (Gibco, 15140-122). GMEM with defined supplements was also tested at 70% of the culture medium (30% rat serum), and an additional experiment explored the effect of adding glucose to the medium (Glucose (D-(+)-Glucose SigmaUltra ≥99.5% GC) (Sigma, G7528).

Once made, all serum-free media with multiple components were stored at 4˚C and used within 2 days. All media were warmed to 37˚C and gassed with 5% O2 and 5% CO2 before the embryos were added.

2.1.4 Embryo collection and dissection

Removal of the uterus

The abdominal area was cleaned using 70% ethanol. The skin in the abdominal region was then lifted using forceps and cut to expose the abdomen using large U-shaped longitudinal incisions up to the thoracic level. To expose the uterus, the intestine was moved, one end of the uterus was then lifted using forceps and cut away from the ovary. Further cutting of the

fat around the uterus to the end of the other uterine horn, allowed complete extrication of the uterus. The uterus was transferred to DMEM + 10% FBS (previously warmed to 37˚C).

E8.5 embryo dissection

Embryos were dissected in warm DMEM + 10% FBS using fine forceps. To start dissection, fat and muscles were trimmed away from the mesometrial surface of the uterine wall. The uterus was then opened from the mesometrial surface, at each implantation site. The opening in the uterine wall was gently expanded using forceps until the decidual swelling protruded outwards. The decidua could then be squeezed out of the opening through gentle compression on the neighbouring section of uterus. To open each decidua, forceps were used to prize apart the anti-mesometrial end to expose the ectoplacental cone and trophoblast layer. Gradual removal of the decidual debris revealed the entire mural trophoblast covering the embryo yolk sac. Forceps were then used to pinch up and gently remove the trophoblast and underlying Reichert's membrane, which came off together in one sheet. Reichert's membrane was then trimmed up to the ectoplacental cone.

All embryos were dissected to the same stage in each step for comparable time points. Embryos were transferred to fresh warm DMEM + FBS 3 times during dissection to improve visibility and maintain 37˚C temperatures.

E10.5 ASPP2 embryo dissection

For ASPP2 experiments, the 'open yolk sac' culture method was used (Martin and Cockroft, 1999). Embryos were dissected using the conditions mentioned above with modifications appropriate for the later stage in gestation. E10.5 embryos have a much larger and tauter yolk sac than at E8.5, with a reduced decidual proportion in each implantation site. This meant that increased care had to be taken to prevent internal pressure build-up which could cause the embryo to 'pop out' from its extraembryonic

membranes. A larger ectoplacental cone meant further trimming was required. Following trimming of the Reichert membrane and ectoplacental cone, a small opening was made in the yolk sac with a pair of fine forceps, adjacent to the head region of the embryo and avoiding major blood vessels. The hole was then enlarged to a size wide enough to fit the embryonic head. The amniotic membrane surrounding the head was then pinched away from the embryo using forceps, and pulled through the hole to gently exteriorise the embryo head first through the yolk sac, while maintaining the integrity of the embryonic vasculature and its connection with that of the yolk sac. Any embryo with damaged vasculature was not used for culture. The open yolk sac technique described here has proved superior to intact yolk sac methods when culturing E10.5 embryos (Kalaskar and Lauderdale, 2014).

E8.5 embryo culture preparation

Once dissected, embryos were ranked according to size (rough estimation) and distributed alternately to provide two groups balanced for developmental stage. Somite number or morphological scoring was not involved in staging embryos at this point, as this would postpone time to culture. The two groups of embryos were then transferred into the prepared separate culture media. Care was taken to minimise the amount of DMEM + FBS entering the culture medium during embryo transfer.

E10.5 ASPP2 embryo culture preparation

Following dissection, any macroscopic morphological abnormalities were noted prior to culture. Head length was measured using a micrometer eyepiece as described below (see Morphological scoring), and photographs were taken for pre- and post-culture comparisons. Each embryo was put in a separate culture bottle due to its large size at this late stage in gestation. Coculture of embryos in the same culture bottle has been shown to result in a significantly worse developmental outcome at this time point (Kalaskar and Lauderdale, 2014).

2.1.5 Embryo culture

The sealed roller-bottle technique was used to culture mouse embryos for 24 h. Sterile 50ml free-standing centrifuge tubes were used as culture bottles, sealed with high vacuum grease (Dow Corning). Culture bottles were placed on a digital tube roller (Stuart) which was installed in an incubator to allow culture at 37˚C. For E8.5 embryo cultures, 5% O2 and 5% CO2 were added via a sterile pipette 3 x over the 24 h period. For the pilot study with ASPP2 embryos which assessed the effect of DAPT treatment, E10.5 embryos were gassed with 95% O2 and 5% CO2, 3 x over 24 h period. Across all culture experiments, 0.5-1 ml rat serum or serum-free medium was allowed per embryo except for the volume experiment (Section 3.2.2), in which volumes were reduced to 0.3 ml per embryo. To ensure blinding, as encouraged by the NC3Rs ARRIVE guidelines, labels were covered and culture tubes relabelled by a second party to ensure lack of bias when embryos were scored after the 24 h culture period.

2.1.6 Administration of reagents

In vivo administration of EdU

50mg EdU (Click-iT ThermoFisher) was dissolved in 10 ml 1 X phosphate buffer solution (PBS), aliquoted and stored at -20˚C. 15 minutes before use, EdU solution was defrosted and vortexed to ensure it was fully dissolved. The solution was then injected intraperitoneally into the pregnant dam at 50 mg/kg. Strict time-keeping for injections and subsequent collections was essential to ensure accuracy in time-pulse analysis.

In vitro administration of DAPT

DAPT (Calbiochem) stock solution was made up to 25 mM in DMSO, aliquoted and stored at -20°C. 15 minutes before use, DAPT solution was defrosted and vortexed to ensure it was fully dissolved. At 15-30 minutes post embryo explantation into culture bottles, DAPT solution was added at no more than 1:250 (DAPT solution volume: rat serum volume) at all tested

concentrations, to avoid DMSO toxicity. An equal volume of DMSO was added to at least one culture bottle per experiment to provide an accurate control.

2.1.7 Morphological scoring

E8.5 culture medium experiments

After 24 h in culture, embryos were transferred to 2 separate dishes containing FBS + DMEM (1:9) for evaluation. Without removing external embryonic membranes, yolk sac circulation was scored immediately, based on the Brown and Fabro scoring system (Brown and Fabro, 1981): 0 - no visible blood islands and no obvious blood movement, slow or infrequent heartbeat; 1 – evidence of blood islands but slow/very little blood movement; 2 – evidence of developed yolk sac vasculature and steady frequent heartbeat; 3 – full yolk sac plexus of vessels with rapid blood movement. Extent of axial rotation was then scored: 1 – ventrally convex (unturned); 2 – mid-axial rotation in progress but not complete (turning); 3 – dorsally convex (fully turned). Yolk sac diameter was measured from the base of the ectoplacental cone to the furthest yolk sac perimeter using a micrometer eyepiece.

An incision was then made in the yolk sac in the head region of the embryo, near the ectoplacental cone. The yolk sac and amnion were inverted over the head and rump of the embryo, and completely removed by an incision through the allantoic insertion.

Head length was measured from the superior to inferior aspect of the head using the micrometer eyepiece of a stereomicroscope. Each embryo was photographed for a dorsal length measurement using ImageJ: a freehand line was drawn from the inferior aspect of the head, round over the crown continuing along the entire dorsal aspect of the embryo to the tail tip. This measurement was designed to remove discrepancies in the traditional crown-rump length measurement which is not appropriate for ventrally flexed embryos. Somite number was then recorded by counting in a caudal to

rostral direction and notes were taken on any developmental abnormalities such as an open cranial neural tube. Examples of how each of these scoring parameters were measured are shown in Figure 2-1.

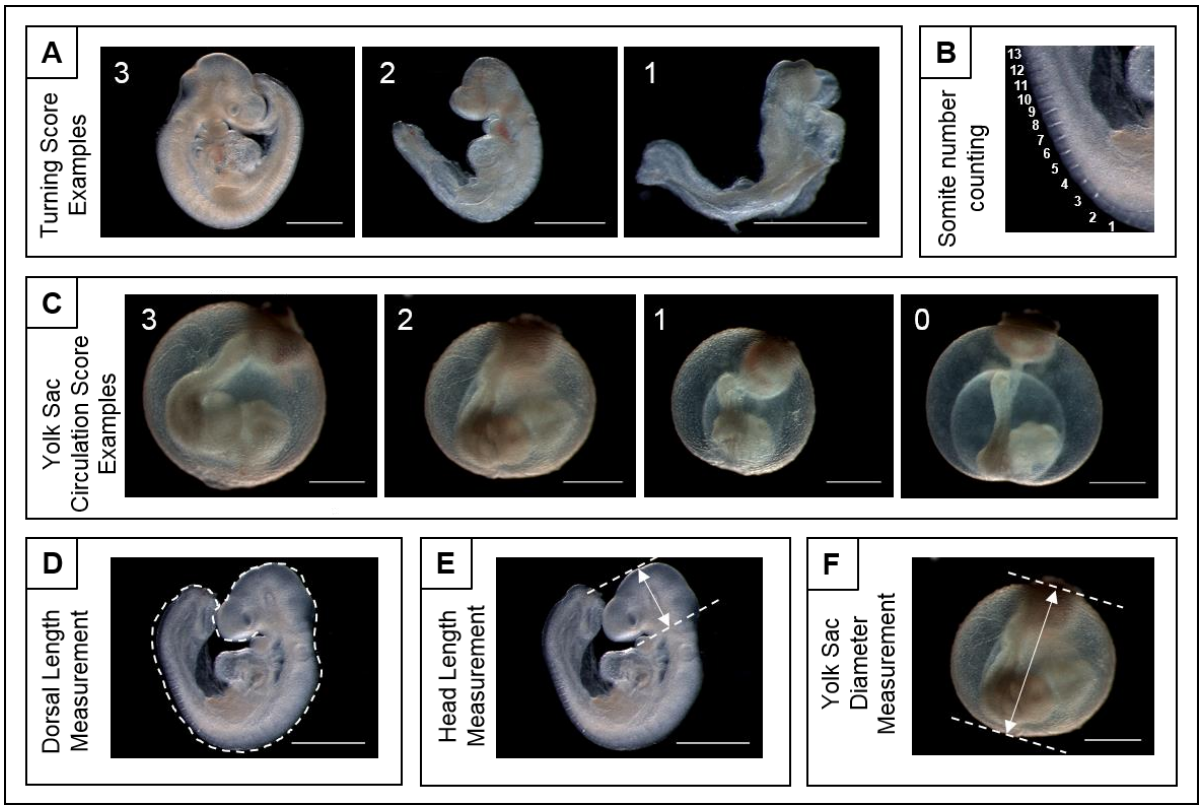

Figure 2-1: Morphological scoring parameters

(**A**) 'Turning' (i.e. axial rotation) scores: 3 - embryo with full turning, exhibiting an entirely convex dorsal surface; 2 - embryo with incomplete turning, where the caudal part of the body axis remains dorsally concave and is not positioned beside the head; 1 - embryo with no turning, where the dorsal surface is entirely concave. (**B**) Somite number counting, performed in a rostral to caudal direction along the dorsal length of the embryo. (**C**) Yolk sac circulation scores: 3 - full yolk sac plexus of vessels with rapid heartbeat and rapid, pulsatile blood flow; 2 - developed yolk sac vasculature and steady heartbeat but slow or intermittent blood movement; 1 - blood islands and/or minimal blood movement; 0 - no visible blood islands and no blood movement, with slow or infrequent heartbeat. (**D**) Dorsal length, as measured along the entire dorsal aspect of the embryo, from the ventral surface of the forebrain where it abuts the first branchial arch, to the caudal extremity of the body axis. Line measurement was determined using ImageJ. (**E**) Head length, measured between parallel lines tangential to the crown of the head, and to the ventral forebrain surface. (**F**) Yolk sac diameter, measured from the base of the ectoplacental cone to the furthest perimeter. Scale bars: 1 mm.

E10.5 ASPP2 culture experiments

ASPP2 embryos were transferred to pre-warmed FBS + DMEM (1:9) after 24 h in culture. Head length was measured as described above. Other morphological factors that had been noted as *Trp53bp2*$^{\Delta 3/\Delta 3}$ hallmarks, were also analysed as follows. Eye pigmentation: absent - no coloration visible; present – any amount of coloration (usually black / brown) visible in either developing eye. Oedema (presence of a fluid filled cavity): absent; present – location of oedema noted. Abnormal face morphology: absent; present – visible abnormalities in facial structure, noted if oedema in the head region was likely the cause. Neural tube status was classed as either closed or open in the forebrain / midbrain / hindbrain / upper neural tube or lower neural tube regions. Embryos also scored as either positive or negative for a contorted neural tube. Photographs were taken post-culture to measure dorsal length using ImageJ, as described above.

2.1.8 Protein content analysis

Reagents:

Radio-Immunoprecipitation Assay (RIPA): RIPA lysis buffer (stock) was made using: 1.5 ml sodium chloride (5 M stock), 0.5 µl NP-40 (1%) (Fluka), 0.25 g sodium deoxycholate (0.5%) (Sigma), 0.05 g sodium dodecyl sulfate (0.1%), 2.5 ml Tris-Cl (1 M, pH 7.4) and 5 protease inhibitor cocktail tablets (1x) (Complete). All reagents were mixed and made up to a final volume of 50 ml with milli-Q water. Aliquots were stored at -20˚C.

Bovine serum albumin (BSA; for standards) stock solution was prepared by dissolving 0.05 g BSA in 50 ml distilled water (1 mg/ml). To ensure complete dissolution, the stock solution was mixed on a digital tube roller (Stuart) for 0.5-1 h. Dilutions of this 1 mg/ml solution were used to make standard concentrations of: 1, 0.5, 0.2, 0.1, 0.05, 0.02 and 0.01 mg/ml. An additional concentration of 0 was made using RIPA buffer only. These standards were made up fresh for each protein sample collection to ensure a fair comparison against the standard graph.

The Bicinchoninic Acid (BCA) assay was chosen due to its high sensitivity and low protein-to-protein variation (Smith et al., 1985). BCA was prepared as per manufacturer's (Pierce) protocol: a 1:50 solution of reagents B:A.

Lysate preparation and concentration measurement

After post-culture morphological scoring, embryos were washed in PBS and snap-frozen on dry ice. 100 µl of previously prepared RIPA lysis buffer was added to each embryo. Embryos were then immediately homogenised via sonication (High Intensity Ultrasonic Processor, SONICS VIBRA CELL). 5 x 1-second pulses at 40% amplitude were sufficient to completely homogenise each embryo in RIPA lysis buffer. Embryos were immediately put on wet ice. The samples were then clarified by centrifugation at 10,000 g for 20 min at 4˚C, and 1 µl of each protein lysate and each BSA standard were added to 20 µl of previously prepared BCA solution. Samples were then incubated at 37˚C for 45 min. Absorbance levels were measured using a NanoDrop 1000 Spectrophotometer (ThermoFisher). Average absorbance results were assumed accurate if BSA standards formed an appropriate trend line with an R^2 value close to 1.

2.2 Molecular biology

2.2.1 ASPP2 genotyping

Trp53bp2$^{\Delta exon3/\Delta exon3}$ mice were first described in (Vives et al., 2006), where targeted disruption of the ASPP2 gene, *Trp53bp2*, was achieved by replacing exon 3 with a neomycin-resistance gene cassette (neo). 3X genotyping primers were designed to bind within exon 3 (a), downstream of exon 3 (b) as well as in the neo cassette itself (c) (Figure 2-2). This allowed differentiation of a wild-type band (~1.2kb), a double heterozygote band, and a homozygote/mutant band (~1.7kb).

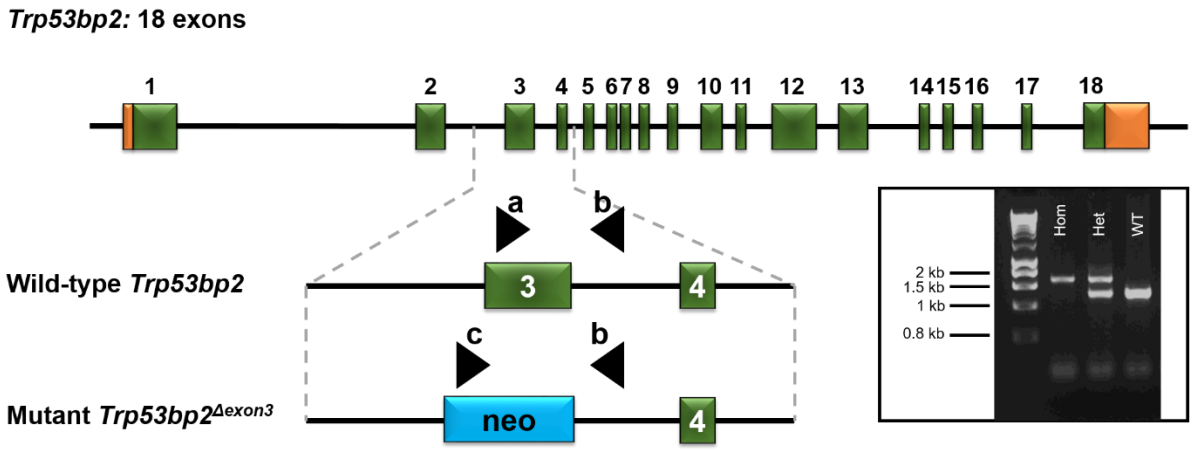

Figure 2-2: ASPP2 genotyping

Diagram showing the structure of *Trp53bp2*, primer-binding locations and an example of an embryo genotyping gel. *Trp53bp2* has 18 exons. *Trp53bp2*$^{\Delta exon3/\Delta exon3}$ mice, first described in (Vives et al., 2006), were created by using a targeting vector in which exon 3 was replaced by a neomycin-resistance gene cassette (neo). Forward primer **a** binds within exon 3. Reverse primer **b** binds downstream of exon 3. Forward primer **c** binds within the neo cassette. In wild-type embryo DNA, primers **a** and **b** bind to *Trp53bp2* to give a ~1.2kb PCR product (WT). In homozygote *Trp53bp2*$^{\Delta exon3/\Delta exon3}$ embryo DNA, primers **c** and **b** bind to mutant *Trp53bp2* to give a ~1.7kb PCR product (Hom). Heterozygotes result in a double band, due to primer binding to exon 3 on one allele, and to neo on the other (Het).

To collect tissue for genotyping, the tail tip of embryos was removed and immediately put in a 0.2 ml PCR tube on ice. 24 µl DNA lysis buffer + 1 µl proteinase K was then added to each tube and left at 56°C overnight. The reaction was then incubated at 85°C to deactivate proteinase K for 45 min. A PCR reaction was set up according to the number of samples and the resulting PCR product was run on a 2 % agarose gel at 130 V for 30 min.

2.2.2 Synthesis of mRNA probe for *in situ* hybridisation

Primer pairs for a *Trp53bp2* mRNA probe were designed using Primer-BLAST, ensuring ~50% GC content, similar melting temperatures, a self-complementarity of <5, a product length between 300-650 bp, and ~20 bp length for each primer. A selection of primer pairs were designed, and the pair that showed the clearest band when running a gel to check for an insert, was selected. After running the PCR product of these primers against wild-type mouse cDNA, the PCR product was cleaned using a QIAquick gel

extraction kit (Qiagen), and the nucleic acid content was measured using a Nanodrop spectrophotometer 1000 (ThermoFisher). Cloning PCR products through ligation and transformation, was completed using the pGEM-T easy vector protocol (Promega). Following colony selection, cells were allowed to grow overnight then harvested by centrifugation and removal of the supernatant. Plasmid DNA purification was then completed, using the QIAprep Spin Miniprep Kit (Qiagen). Nucleic acid content of the miniprep was measured using a Nanodrop (ThermoFisher). A restriction digest with restriction enzyme EcoR1 was used to ensure double restriction of the plasmid. Large cultures were grown up in LB broth overnight, centrifuged, then supernatant was removed to expose the pellet. A maxiprep was then completed, following the Hispeed Plasmid Purification handbook (Qiagen). Nucleic acid content was measured using the Nanodrop (ThermoFisher), and a sample was sent off for sequencing. Linearisation was then achieved with the plasmid DNA from the maxiprep, using the Nco1 restriction enzyme for SP6 polymerase, in a restriction digest reaction. The linearised plasmid was then cleaned using the QIAquick PCR purification kit (Qiagen). Once again, nucleic acid content was measured using the Nanodrop (ThermoFisher). The probe was transcribed using 1 µg linearised DNA, Digoxigenin (DIG) RNA labelling mix, transcription buffer, RNase inhibitor and SP6 polymerase (all Merck). DNase 1 was used to break down any excess DNA, followed by centrifugation and elution steps using CHROMA SPIN columns and collection tubes (ClonTech), to clean the probe. A Nanodrop reading determined the final quantity of RNA. Finally, ultra-pure formamide and RNase inhibitor were added to the probe solution for preservation.

2.2.3 Quantitative RT-PCR

Primer pairs for quantitative RT-PCR (qPCR) were designed within the same parameters as stated above, using Primer-BLAST. Primers were tested on cDNA from wild-type mice within the ASPP2 colony, using a standard Taq PCR, to assess whether band size corresponded to expected product size. For RNA extraction, in separate eppendorf tubes, E11.5 embryos were homogenised in Trizol using a pipette. Chloroform was added to each

embryo, followed by centrifugation to cause phase separation. The upper phase of the aqueous solution was transferred to a fresh eppendorf, isopropanol was added and the solution was mixed gently by inverting the tubes, followed by incubation on ice for 10 minutes. A second centrifugation step ensured RNA precipitation. After removing the supernatant, the pellet was washed with 75% ethanol. Centrifugation and supernatant removal was repeated, followed by air-drying of the remaining pellet for 10 minutes.

The RNA was resuspended in RNase free water and heated at 55°C for 10 minutes before returning to ice. RNA concentration was measured using a Nanodrop (ThermoFisher). To remove any traces of DNA in the solution, DNase 1 buffer and rDNase 1 (Ambion) were added to the RNA and incubated at 37°C for 20-30 min. DNase inactivation reagent (Ambion) was added, followed by centrifugation and transfer of the RNA supernatant to a fresh eppendorf. RNA concentration was measured once again. Based on these values, cDNA was synthesised from RNA using the VILO superscript kit (Invitrogen), and VILO thermocycler programme. cDNA samples were stored at -20°C. To run the qPCR, selected primers, GAPDH control primers and cDNA were all diluted in RNase/DNase free water. SYBR Green master mix (ThermoFisher) was combined with the forward and reverse primers in each pair, and with water. This solution was added to wells in a 96 well plate following a pre-designed layout. cDNA was added to the wells, excluding 3 x negative control wells per primer pair, in which Milli-Q water (Merck) was added instead of cDNA. The qPCR programme was run on a Bio-Rad real-time PCR system.

2.3 Histological procedures

2.3.1 Gelatine embedding and cryosectioning

Reagents

Paraformaldehyde (PFA): 4% PFA was made up in 1X PBS. To ensure full dissolution the solution was incubated at 65˚ and shaken every 10 minutes throughout a 2 h period. Stock PFA was stored at -20˚C.

Sucrose: 30% sucrose was dissolved in PBS. Aliquots were stored at 4˚C. Sucrose was used to equilibrate and protect the embryo before cryo-embedding.

Gelatine: Gelatine from bovine serum was dissolved to 7.5% in sucrose solution (see above) and stored at -20˚C.

Fixation and embedding

Embryos were fixed in 4% PFA overnight at 4˚C, then washed twice in 1x PBS. PBS was replaced with sucrose solution and embryos were incubated between 1 h and overnight, depending on gestational age, with slow shaking on wet ice. Ensuring the embryo had sunk to the base of the incubation tube, the sucrose solution was replaced with melted gelatine.

Each embryo, within the melted gelatine, was then transferred to a dish lined with pre-set gelatine and orientated to ensure transverse sections could be taken when mounted. Embryos that were E9.5 or older, were divided into three parts prior to this step to ensure transverse sections could be obtained throughout the body axis (Figure 2-3). After the gelatine had set and been cut, the gelatine block was then snap-frozen in isopentane, and chilled to -65˚ using dry ice. Gelatine blocks were stored at -80˚C.

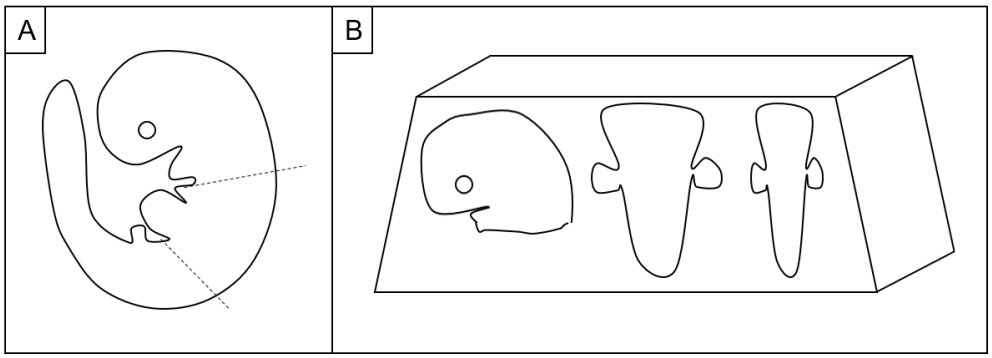

Figure 2-3: Post-fixation dissection and embedding of E11.5 embryos

(**A**) Diagram showing dissection lines of an E11.5 embryo before embedding. (**B**) Arrangement of embryo parts within a gelatine block to ensure consequent sectioning was in a transverse plane.

Cryosectioning

For sectioning embedded embryos, the cryostat (Leica) was set to a temperature of -21/-22°C for both stage and chamber. Transverse sections of thickness 10 µm were taken, then mounted on *Superfrost* slides (Thermo Scientific) and stored at -20˚ (short term) or -80˚ (long term).

2.3.2 Whole-mount *in situ* hybridisation

Reagents

DEPC solutions: DEPC-H_2O: 1 ml diethylpyrocarbonate (DEPC) dissolved in 1 L Milli-Q (Merck). PBS-DEPC: 1 ml DEPC dissolved in 1 L PBS. PBT-DEPC: 1 ml Tween-20 (Merck) dissolved in 1L PBS-DEPC. All DEPC solutions were stirred at room temperature (RT) and autoclaved before use.

Hybridisation mix: 50% formamide, 5X SSC pH 4.5 (87.7g NaCl and 44.1g sodium citrate tribasic dihydrate dissolved in 500 ml DEPC-H_2O), 50 µg/ml yeast RNA, 1% SDS (prepared in Milli-Q), 50 µg/ml heparin and DEPC-H_2O. Stored at -20°C.

10X TBS: 80g NaCl, 2g KCl and 250 ml 1M Tris HCL, made up to 1 L Milli-Q. For TBST, 4 ml Tween-20 and 0.192g tetramisole, were added to 40 ml TBS, made up to 1 L H_2O.

NTMT solution: 100 mM NaCl, 100 mM Tris HCL pH 9.5, 50 mM $MgCl_2$, 1% Tween-20, 0.024 g tetramisole, dissolved in H_2O.

Developing solution: 4.5 µl/ml 4-nitroblue tetrazolium (NBT) and 3.5 µl/ml 5-bromo-4-chloro-3-inodyl-phosphate (BCIP), dissolved in NTMT.

Preparation of embryos

Embryos were fixed in 4% PFA at 4°C overnight. The following day, they were washed in PBT, then MeOH in PBS-DEPC at concentrations of 25% to 100%, for 20 – 30 min per concentration, depending on gestational age. Embryos were stored at -20°C.

Experimental procedure (4-day protocol)

Day 1 - Embryos were rehydrated by washing in 75%, 50% and 25% MeOH in PBT, shaking on ice for 15 min each, then washed 2 X in PBT. Embryos were bleached using 6% hydrogen peroxide in PBT for 1 h. Following 3 X PBT wash, embryos were incubated in proteinase K at RT for 2-8 min, depending on gestational age. They were then washed in 2 mg/ml glycine in PBT for 5 min, followed by a PBT wash. Embryos were fixed in 0.2% glutaraldehyde in 4% PFA in PBS for 20 min at RT, while hybridisation mix was pre-heated to 70°C. Embryos were incubated in hybridisation mix for at least 2 h at 70°C. 1 µl/ml DIG-labelling probe (see Synthesis of mRNA probe for *in situ* hybridisation), was used to incubate embryos overnight at 70°C.

Day 2 – Hybridisation mix was removed and embryos were washed with a solution consisting of 50% formamide, 5X SSC, 1% SDS and DEPC-H_2O, 2X 30 min at 70°C. This was then replaced with a similar solution, this time 2X SSC, and incubated 2X 30 min at 65°C. Blocking solution (10% sheep serum in TBST) was then added to embryos. Blocking solution was replaced with 0.05% anti-DIG-AP antibody (Merck), 1% sheep serum in TBST and left on shaker overnight at 4°C.

Day 3 – Embryos were washed 3X 5 min in TBST, followed by 5X 1 h in TBST. Left on shaker overnight at 4°C.

Day 4 – Embryos were washed 3X 10 min with NTMT, then incubated in developing solution at RT, protected from light. Signal development was checked every 15 min. Once the signal had sufficiently developed, the reaction was stopped by washing embryos 3X 5 min in PBT at RT. Embryos were then re-fixed in 4% PFA at RT for 2 h, and stored in PBT at 4°C.

Vibratome sectioning – Embryos were fixed in 4% PFA for at least 2 h at RT, followed by 3X PBS washes. PBS was removed and replaced with a gelatine/albumin mix and left overnight at 4°C. Fresh gelatine/albumin mix was put in a vibratome mould the following day, with 10% glutaraldehyde. The embryo was quickly placed and orientated within the mould before setting occurred. Gelatine/albumin blocks were dried and washed 1X PBS before sectioning on the vibratome (50 µM sections). Sections were mounted on slides with 50% glycerol in dH_2O, and sealed with nail polish.

2.3.3 Immunostaining

Reagents

PBT: 0.1% Triton X100 (Merck) in 1X PBS.

Blocking solution: 0.1% Triton X100, 2 mg/ml bovine serum albumin, 0.15% glycine and 10% or 1% heat inactivated sheep serum (HISS) in 1X PBS.

Immunostaining (2-day protocol)

Day 1 - Embryo sections were thawed and rehydrated for 30 min at RT in 1X PBS. They were then fixed with 4% PFA for 10 min and washed in PBT. Samples were blocked in blocking solution (10% HISS) for 1 h, then incubated in primary antibody (see Table 2-1: Primary antibodies), diluted in blocking solution (1% HISS) overnight at 4°C.

Day 2 - Samples were washed 3X PBT. Secondary antibody (see Table 2-2: Secondary antibodies), and/or phalloidin (see Table 2-3: Staining and dyes) was applied in blocking solution (1% HISS) for 1 h, RT, followed by 3X PBT washes. Slides were incubated in DAPI (see Table 2-3: Staining and dyes) in 1X PBS for 2 mins then washed in 1X PBS. Fluorescent immunolabelled slides were mounted using Hydromount (National Diagnostics) and stored at 4°C, protected from light.

EdU immunostaining

Day 1 protocol as above (same as for PHH3 / Ki67 primary antibodies).

Day 2 – 3X PBT wash followed by 30 min incubation in ClickiT EdU Alexa Fluor 488 Imaging Kit reaction cocktail (ThermoFisher): ClickiT reaction buffer, $CuSO_4$, Alexa Fluor azide (see Table 2-3: Staining and dyes) and reaction buffer additive. This was followed by 3X PBT wash, protected from light, to stop the reaction. Secondary antibody was applied in blocking solution (1% HISS) for 1 h, RT, followed by 3X PBT wash. Slides were incubated in Hoescht (see Table 2-3: Staining and dyes) for 30 min then washed in 1X PBS. Slides were mounted using Hydromount (National Diagnostics) and stored at 4°C, protected from light.

Table 2-1: Primary antibodies

Antibody	Species	Manufacturer	Concentration
SOX2	Goat	Immune systems (GT15098)	1:250
PAR3	Rabbit	Merck (07-330)	1:100
Ki67	Rabbit	Abcam (ab16667)	1:250
PHH3	Rabbit	Merck (06-570)	1:200
TUJ1	Rabbit	BioLegend (PRB-435P)	1:200
N-cadherin	Rabbit	Santa Cruz (SC-7939)	1:100
PAX3	Mouse	R&D Systems (MAB2457)	1:200
PAX6	Rabbit	BioLegend (PRB-278P)	1:200
NKX6.1	Mouse	DSHB (F55A12)	1:5

Table 2-2: Secondary antibodies

Antibody	Species	Manufacturer	Concentration	Absorbance
Anti-rabbit	Goat	Alexa Fluor	1:250	488
Anti-rabbit	Goat	Alex Fluor	1:250	568
Anti-goat	Donkey	Alexa Fluor	1:250	568
Anti-mouse	Goat	Alexa Fluor	1:250	488

Table 2-3: Staining and dyes

Name	Manufacturer	Concentration	Absorbance
Phalloidin	Alexa Fluor	1:250	568
Alexa Fluor azide	Alexa Fluor	1:400	488
DAPI	Severn Biotech	1:10,000	405
Hoechst	ThermoFisher (33342)	1:2000	460

2.4 Microscopy and imaging

A dissection stereo-microscope (Zeiss SV11) was used to photograph pre- and post-culture embryos and whole-mount *in situ* hybridisation embryos. An upright Leica fluorescence compound microscope was used to analyse and photograph all fluorescent immunolabelled sections. Sections were imaged within a day of completing an immunofluorescence assay, to avoid degradation of the signal.

2.5 Analysis

2.5.1 Immunofluorescence image analysis

ImageJ v1.52c was used for all image analysis of immunofluorescence-stained sections. For image analysis involving an automatic macro plugin, at least 3X section images per embryo were cross-checked with the original image to ensure accuracy in counting or threshold analysis.

Cell counting analysis

Nuclear counting was the first step in all analyses, apart from when measuring lumen circumference or quantifying Tuj1 staining. A region of interest (ROI) was drawn around the perimeter of the neural tube and the remainder of the image was cleared. A macro was designed to automatically count positively stained nuclei (Figure 2-4, D). Median and maximum filter editing, followed by the 'find maxima' function was sufficient for both DAPI and Hoescht nuclei staining. The same macro was used for PHH3+ cells in 1 h EdU pulse / PHH3 experiments, with the exception of a higher noise tolerance in the find maxima function.

PHH3 staining analysis

To analyse cells positive for PHH3, nuclear counting markers, generated by the macro (see above), were overlaid on to the PHH3 channel. Apical and ectopic mitoses were then counted manually, where markers corresponded to a positively stained cell. Apical mitoses were counted as between 0-3 nuclear widths away from the lumenal surface. Ectopic mitoses were counted as all other positively labelled markers >3 nuclei away from the lumenal surface within the neuroepithelium. For ventral and dorsal region separation, images were orientated to ensure the dorsal aspect of the neural tube was vertically above the ventral part. A line was then drawn through the midline of the lumen, equidistant from the dorsal roof-plate and the ventral floor-plate. A horizontal line was then drawn perpendicular to the midpoint of this line. This

reference line was then used to draw 2 new ROIs for cell counting in the dorsal and ventral halves of the neural tube.

1 h EdU pulse/PHH3 staining analysis

This analysis followed a similar method to the one described above, with the following changes: PHH3+ cell counting was automated, using the macro described in ‘Cell counting analysis’. Apical and ectopic mitoses were differentiated as described above. Cell markers were then overlaid on to the EdU channel and counted as positive or negative for EdU.

Threshold analysis

The auto threshold plugin in ImageJ was the basis for EdU, Ki67, PAX3, PAX6, NKX6.1 and SOX2 analysis. Threshold function is designed to identify pixels above or below a particular threshold value in any given image. To account for the area of the neural tube stained positive for a particular staining, an auto threshold was chosen that best represented the staining in 3 or more section images per embryo. Automated thresholds are global (applied to every pixel in the image), histogram-derived thresholds, that were developed to avoid manual thresholds which lead to bias. IsoData, Moments, Shanbhag and Yen thresholds were used here (Calvard, 1978, Tsai, 1985, Shanbhag, 1994, Yen et al., 1995). The threshold chosen for each antibody stain, and the experiment combination they were used with, are presented in Table 2-4.

Table 2-4: Thresholds in ImageJ

Antibody/EdU pulse	Threshold in ImageJ	Experiment combination
24h and 6h EdU pulse	IsoData	DAPI cell counting and Ki67 threshold analysis
1h EdU pulse	Moments	DAPI cell counting
Ki67	Moments	DAPI cell counting and EdU threshold analysis
Sox2	Shanbhag	DAPI cell counting
Nkx6.1	Moments	DAPI cell counting
Pax3	Shanbhag	DAPI cell counting
Pax6	Yen	DAPI cell counting

Where automated cell counting was combined with auto threshold analysis in a specifically designed macro, a percentage of markers positive/negative for a specific staining was calculated (Figure 2-4).

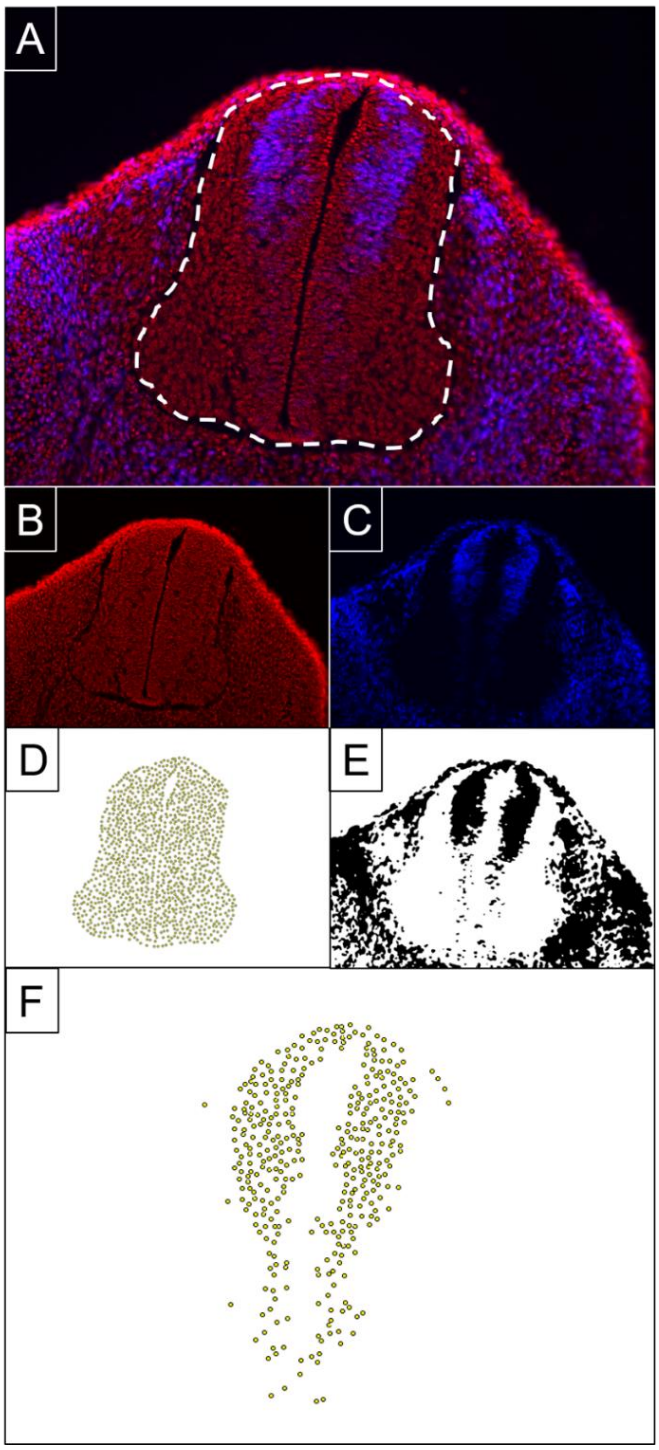

Figure 2-4: Cell counting and threshold analysis

DAPI and EdU labelled section examples of cell counting and threshold image analysis. (**A**) Original composite image. White dashed line highlights neural tube boundary. DAPI (red) and 1 h EdU pulse staining (blue). (**B**) DAPI nuclear staining. (**C**) 1h EdU pulse staining. Cells in S-phase labelled upon EdU injection. (**D**) Automated cell counting markers for DAPI-labelled nuclei. (**E**) 'Moments' auto threshold for EdU staining. (**F**) Cell markers positive for EdU after automatic cross-referencing between nuclear cell count and EdU threshold.

Tuj1 intensity analysis

Tuj1 staining of E11.5 embryo sections was analysed using pixel intensity values. To ensure analysis was representative of the entire neural tube, a dorsal, middle, and ventral percentage band was analysed per section as follows. Neural tube images were orientated with the dorsal roof-plate aligned on the right, in a horizontal plane with the ventral floor-plate on the left. Using the line function in ImageJ, width was modified to encompass both basal surfaces of the neural tube at the midpoint between dorsal and ventral aspects. This line was then converted to a defined area and the selected region was cropped to form a new image. An automatic macro plugin was designed to process this image: the rectangular area was automatically divided into 10 equal sections from left to right (i.e. ventral to dorsal), and an intensity value for every pixel in the 2nd, 5th and 8th section (each representing 10% of the image), running from left to right/ventral to dorsal was calculated (see Figure 2-5: Tuj1 intensity analysis). From this, line graphs were generated in ImageJ and pixel intensity values were transferred to Excel for further analysis.

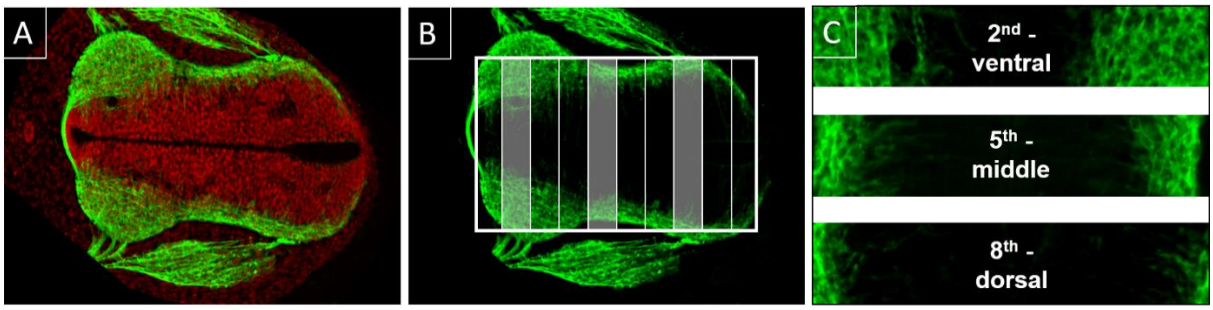

Figure 2-5: Tuj1 intensity analysis

DAPI and Tuj1 labelled section, as an example of the Tuj1 intensity analysis method. (**A**) Original composite image. DAPI (red), Tuj1 (green). (**B**) Diagrammatic interpretation of intensity analysis. Area drawn manually to include both left and right basal surfaces of the neural tube. Translucent filled areas represent 2nd, 5th and 8th 10-percentile sections analysed (automated). (**C**) Example 10-percentile section images from which pixel intensity would be measured. 2nd section represents ventral intensity, 5th section represents middle intensity and 8th section represents dorsal intensity.

Lumen and neural tube circumference and area measurements

Lumen and neural tube circumference and area measurements were made in ImageJ using the freehand line tool. A line was drawn around the lumenal circumference or neural tube circumference in each section image. Measurements were set to include both the perimeter and the area within the ROI. In cases of a neural tube with multiple lumens, a sum of all lumenal circumferences and areas was calculated. All measurements were in pixel number to alleviate discrepancies between image magnifications.

2.5.2 Statistical analysis

One–way analysis of variance (ANOVA) was used to test for overall significance in parametric growth measurement data: yolk sac diameter, dorsal length, head length, somite number and protein content. Where significant, post-hoc pair-wise Student's t-tests were then performed in comparisons of serum-free or diluted media versus rat serum controls. Chi-square tests were used to test for overall significance in yolk sac circulation score frequencies (3x4) and axial rotation score frequencies (3x3). Where significant, post-hoc pairwise Chi-square tests (2x4 and 2x3) were then performed to compare serum-free or diluted media versus rat serum controls. For statistical analysis of ASPP2 embryo section images, one–way ANOVA was used to test for overall significance in counting, measurement or intensity value data sets. Where significant, post-hoc pair-wise Student's t-tests were then performed in comparisons of wild-type, mutants without a phenotype and mutants with a phenotype. Contingency table chi-square tests (3X3) were used to analyse genotype ratio and phenotype frequency in ASPP2 embryos. Pairwise Chi-square tests (2X2) were used to assess phenotype frequency in cultured ASPP2 embryos.

Chapter 3 Prospects of reducing rat serum usage in mouse whole embryo culture

3.1 Introduction

Whole embryo culture is a technique that has been used for many years as an alternative to *in vivo* studies. The method allows direct observation and manipulation of developing rodent embryos outside the confines of the maternal uterus. Denis New, the first person to describe this *ex utero* technique, found that the use of rat serum as the primary growth medium allowed rodent development comparable to that *in utero*.

Since these pioneering studies, however, many different sera and media have been tested with the aim of finding a simple, cheap alternative to rat serum (Figure 3-1). Despite its significant advantages in terms of supporting optimum embryonic growth, rat serum is expensive, time consuming to collect, has an ill-defined make-up, and requires high animal usage. Early work evaluated Waymouth's medium, Tyrode's solution, new-born calf serum and fetal calf serum as alternatives, but all proved inadequate for supporting normal growth (Sadler and New, 1981). Sera from humans, monkeys, cows and dogs were also tested, but none proved as effective as rat serum (Chatot et al., 1980, Chambers et al., 1995, Coelho et al., 1989, Flynn et al., 1987).

A handful of recent attempts have been made to identify a serum-free medium for use in mouse embryo culture. KnockOut DMEM and KnockOut Serum Replacement were the main medium constituents in two studies of embryo culture beginning at embryonic day (E)10.5 (Kalaskar and Lauderdale, 2014, Moore-Scott et al., 2003). One described embryos cultured for 24 h as being 'morphologically similar' to freshly dissected E11.5 embryos (Moore-Scott et al., 2003), while the other reported 'intermediate development' in 28% of embryos (Kalaskar and Lauderdale, 2014). Neither study compared serum-free embryo culture with rat serum controls. Another serum-free medium named 'N2B27' was used for 24 h and 48 h cultures of E5.5 mouse embryos, which were then compared to a previously established

in utero scoring system. These authors describe 100% of embryos reaching 'various gastrulation stages' (Drakou and Georgiades, 2015). In addition, a few groups have used diluted rat serum as culture medium: for example, Huang et al diluted rat serum 1:1 with a GMEM-based medium for studies involving cellular grafting and electroporation of mouse embryos (Huang et al., 2015). This article, like many others, reports the use of diluted serum for manipulative techniques or histological comparisons between treated and untreated embryos, without assessing development itself (Kesby, 2000, Ambroso and Harris, 1993, Hardy and New, 1991, Fisher and Martinez de Villarreal, 1982).

Without a formal comparison with embryos cultured in undiluted rat serum or developed *in vivo*, it is impossible to evaluate the effectiveness of serum-free media or diluted serum in terms of developmental potential. Hence, while the history of rodent whole embryo culture has shown major advances in terms of methods for manipulating and imaging mammalian development (Takahashi et al., 2014, Calegari et al., 2004, Massarwa and Niswander, 2013), there are still no successful alternatives to the use of rat serum as the primary culture medium.

The present study was designed to assess the effect of replacing or reducing rat serum on the success of whole mouse embryo culture, by comparison with littermate embryos developing in 100% rat serum. The period of development from E8.5 to E9.5 was chosen for several reasons. Firstly, the two serum-free media previously mentioned were used to culture E10.5 (i.e. post-neurulation) and E5.5 (pre-neurulation) embryos, leaving open the question of their efficacy for culture during the intervening developmental time period. Secondly, the E8.5-E9.5 period of organogenesis is known to be critical for the origin of developmental anomalies that lead to clinically important birth defects; hence, embryo culture is of particular importance in enabling experimental studies at this stage. Thirdly, the E8.5-E9.5 culture period has been used previously as a teratogen screening tool (Webster et al., 1997), and so advances in culture methodology would be beneficial for this purpose.

3.1.1 Literature Review

A literature review was conducted to fully assess the history of culture medium used in rodent whole embryo culture, and to clarify where advancements could be made. Figure 3-1 summarizes the main findings of the review. The search term: ‘Postimplantation rodent embryo culture medium’ was used to search in PubMed, and relevant Denis New publications were added if not identified in the PubMed search. Review articles and studies using embryos younger than embryonic day 5, were excluded. This resulted in a total publication number of 64 to be carefully reviewed. The full table with publication references can be found in Appendices.

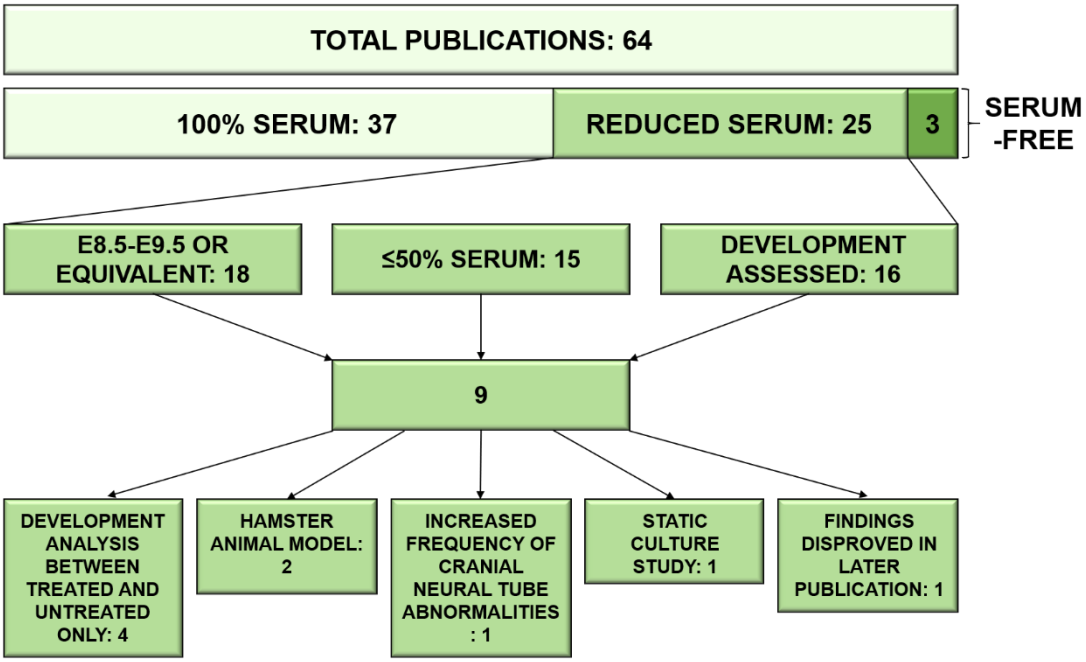

Figure 3-1: Diagrammatic summary of literature review.

Literature review focused on media used for whole embryo culture. This was based on the search term: 'Postimplantation rodent embryo culture medium’ in PubMed, combined with relevant Denis New publications (no restriction on year published). Numbers indicate the number of articles that included embryo culture methods within each category.

It was found that 37/64 publications had used 100% serum in all embryo culture experiments and 25/64 had used media with a reduced serum component (< 100%). Only 3/64 publications had used 100% serum-free

medium, and these are detailed above (KnockOut and N2B27 media) (Kalaskar and Lauderdale, 2014, Moore-Scott et al., 2003, Drakou and Georgiades, 2015). Of the 25 publications which used a reduced serum component, 18 had assessed the gestational time point (E8.5-E9.5) which was to be addressed in this study, 15 had used equal to or less than 50% serum and 16 had assessed embryonic development post-culture. Only 9 publications combined all 3 of these prerequisites. Of these, 4 had assessed development between untreated and treated embryos only (both sets cultured in reduced serum), with no comparison to 100% rat serum or *in vivo* controls (Kesby, 2000, Ambroso and Harris, 1993, Hardy and New, 1991, Fisher and Martinez de Villarreal, 1982). This allowed conclusions to be drawn on toxicity of a test reagent, but not on the appropriateness of the reduced-serum media in supporting 'normal' development. 2/9 publications used hamster embryos as the rodent animal model (Wlodarczyk et al., 2001, Ebron-McCoy et al., 1988). Although hamster embryos bear similarities to mouse and rat embryos, they have a shorter period of gestation and their use is limited amongst developmental biologists. 1 publication found comparable development between 50:50 rat serum:DMEM, and 100% rat serum-cultured embryos (Sadler and New, 1981). However, the incidence of open cranial neural tube was increased, a developmental biomarker which would lead to exencephaly. 1 publication used a reduced-serum medium to grow embryos in static culture (Jones et al., 2002), where developmental assessment was limited to somite number counting and degree of axial rotation (see 2.1.7). The final publication found development to be improved in embryos cultured in 20:80 rat serum: Waymouth's MB 752/1 medium, compared with rat serum controls (Clarkson et al., 1969). However, these findings were later challenged when insufficient development was seen in embryos cultured in 50% rat serum diluted with the same medium (Sadler and New, 1981).

Hence, detailed assessment of the literature has clarified that, although a number of attempts have been made to replace or reduce rat serum in rodent whole embryo culture, there have been no systematic comparisons between serum-free, or reduced serum cultures and those in 100% rat serum. Therefore, the following aims of this project, utilising the whole embryo

culture method to support embryonic development from E8.5 to E9.5, were as follows:

- Investigate the possibility of complete replacement of rat serum with two serum-free media that ‘performed well’ in previous assessments.

- Test a variety of diluents at 50:50 with rat serum, for their efficacy in supporting development.

- If possible, optimise serum reduction further through increased rat serum dilution or supplementation of the media.

3.2 Results

3.2.1 Serum-free media fail to replicate the development of embryos cultured in rat serum

Embryonic development was evaluated by measuring yolk sac circulation and diameter, degree of axial rotation, dorsal and head length, somite number (see Figure 2-1: Morphological scoring parameters), and total protein content.

Yolk sac circulation was scored first to assess the state of embryo health (Pinter et al., 1986). Embryos cultured in KnockOut serum-free medium showed very poor yolk sac circulation. Blood islands were occasionally present but there was little evidence of circulation and no maturely developed blood vessels, in contrast to embryos cultured in rat serum (Figure 3-2, B). The majority of KnockOut serum-free embryos had a yolk sac score of 0 (69%), whereas 76% of their littermates that were cultured in rat serum achieved a maximum score of 3. Similarly, among embryos cultured in serum-free N2B27, 73% scored 0 with most showing no evidence of blood islands, and 100% embryos scored ≤1. Both serum-free media were found to give a significantly lower yolk sac circulation score than rat serum controls (Figure 3-3, A). In contrast, yolk sac diameter showed no significant difference across the three culture conditions (Figure 3-3, C).

Axial rotation, the third scoring parameter, is a vital developmental process which embryos should have initiated or completed, when cultured from the headfold stage (Matsuda and Yasutomi, 1995). Following this expectation, 24% of embryos grown in rat serum had fully turned (score of 3) and 68% were in the process of turning (score of 2) at the end of the 24 h culture (Figure 3-3, B). In contrast, no embryo cultured in either serum-free medium had fully turned. Only 31% of embryos cultured in KnockOut medium achieved a score of 2 (turning) and 69% were entirely unturned. In N2B27 medium, 18% embryos were partially turned and 82% were unturned (Figure 3-3, B). These results for serum-free media were significantly different from rat serum-cultured embryos.

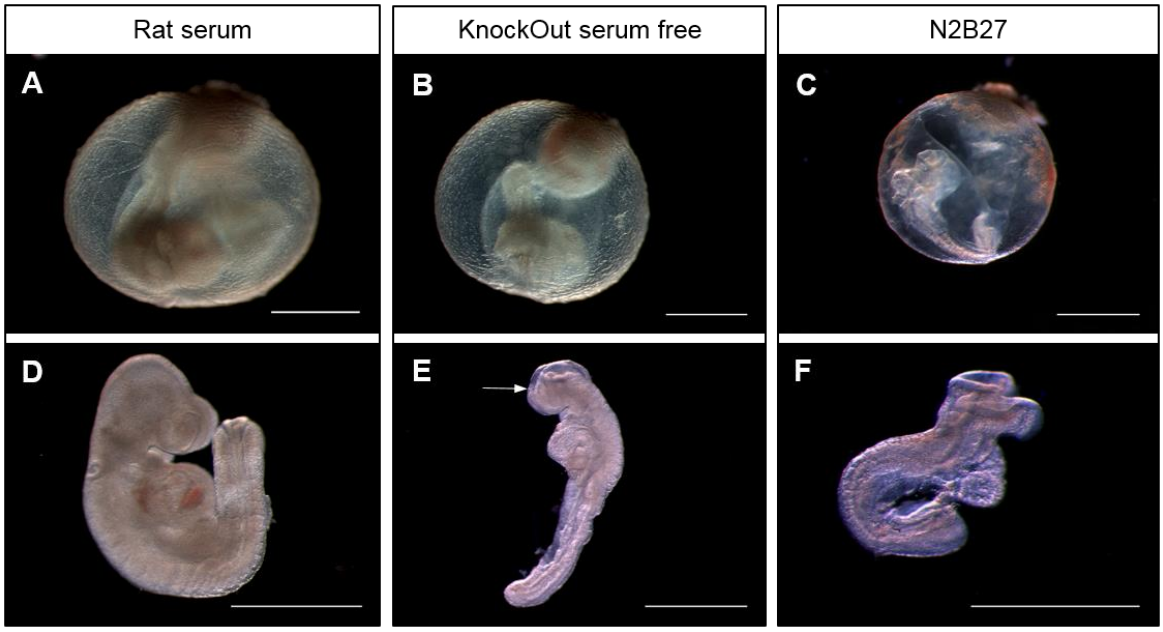

Figure 3-2: Comparison of whole embryo culture using rat serum or serum-free media

Representative images of yolk sac-containing (A-C) and isolated embryos (D-F) following 24 h culture from E8.5 in rat serum (A,D), KnockOut serum-free medium (B,E) or N2B27 serum-free medium (C,F). (**A,D**) Rat serum culture was generally associated with extensive vasculature and rapid blood movement in the yolk sac (e.g. score of 3 shown in A) together with fully turned embryos that exhibited a mostly normal appearance for this developmental stage. (**B,E**) KnockOut serum-free culture produced conceptuses with evidence of yolk sac blood islands but little blood movement (score of 1 shown in B) and embryos that were growth retarded, incompletely turned, and with an open cranial neural tube (arrow in E). (**C,F**) N2B27 serum-free culture yielded conceptuses with no evidence of yolk sac circulation (score of 0 shown in C) together with embryos that were unturned, growth retarded and with open cranial neural tube. Note that the embryo in C was completely unturned although it secondarily developed a convex dorsal surface following removal from the yolk sac (in F). Scale bars: 1 mm.

Dorsal length and head length were measured following removal of the embryos from their extraembryonic membranes. Both growth parameters were significantly reduced in serum-free media compared with rat serum cultures. Mean (± SEM) dorsal length in rat serum culture was 6.02 ± 0.22 mm, whereas embryos in serum-free medium had values of 4.41 ± 0.22 mm (KnockOut medium) and 3.63 ± 0.43 mm (N2B27). Head length was 0.73 ± 0.03 mm in rat serum, compared with 0.49 ± 0.03 mm, and 0.40 ± 0.06 mm in KnockOut medium and N2B27 medium respectively (Figure 3-3, C)

Somite number is used as a measure of developmental progression in embryo culture, as there is a linear increase with time between E8.5 and E9.5, with a new somite pair added approximately every 2 h (Kalaskar and Lauderdale, 2014). E8.5 CD-1 embryos typically had 3-6 somites prior to culture (data not shown), suggesting that these embryos should exhibit 15-19 somites after 24 h culture. Mean somite number in rat serum-cultured embryos (16.3 ± 0.39) fell within this expected range, whereas somite number in embryos cultured in serum-free media fell short. KnockOut serum-free cultures (14.9 ± 0.71), however, did not differ significantly from rat serum controls, whereas culture in N2B27 yielded a significantly lower mean somite number (13.1 ± 0.64) (Figure 3-3, D).

Exencephaly, a NTD that commonly affects the midbrain and hindbrain of mouse embryos, results from failure of cranial neural tube closure. Open cranial neural tube frequency was assessed as follows: 2/25 (open/total) in rat serum, 7/16 in KnockOut medium and 9/11 in N2B27 medium. However, it is important to consider the mid/hindbrain of most mouse strains remains open until the 16 somite stage (van Maele-Fabry et al., 1992), so exencephaly can only be considered to be present in embryos with 17 somites or more. While 12/25 embryos cultured in rat serum had 17 or more somites, only one embryo in KnockOut medium and no embryos in N2B27 had 17 or more somites. Therefore, the higher apparent frequency of cranial closure failure in serum-free media culture compared to rat serum, may be

related to the developmental retardation of these embryos, rather than the specific requirement for rat serum in successful cranial neurulation.

Protein content was measured following embryo lysate preparation, to assess total embryonic growth. Embryos cultured in rat serum had a mean (± SEM) protein content of 45.2 ± 3.53 µg whereas embryos in serum-free media contained significantly less protein: 29.6 ± 3.50 µg (KnockOut) and 21.5 ± 4.38 µg (N2B27) (Figure 3-3, E).

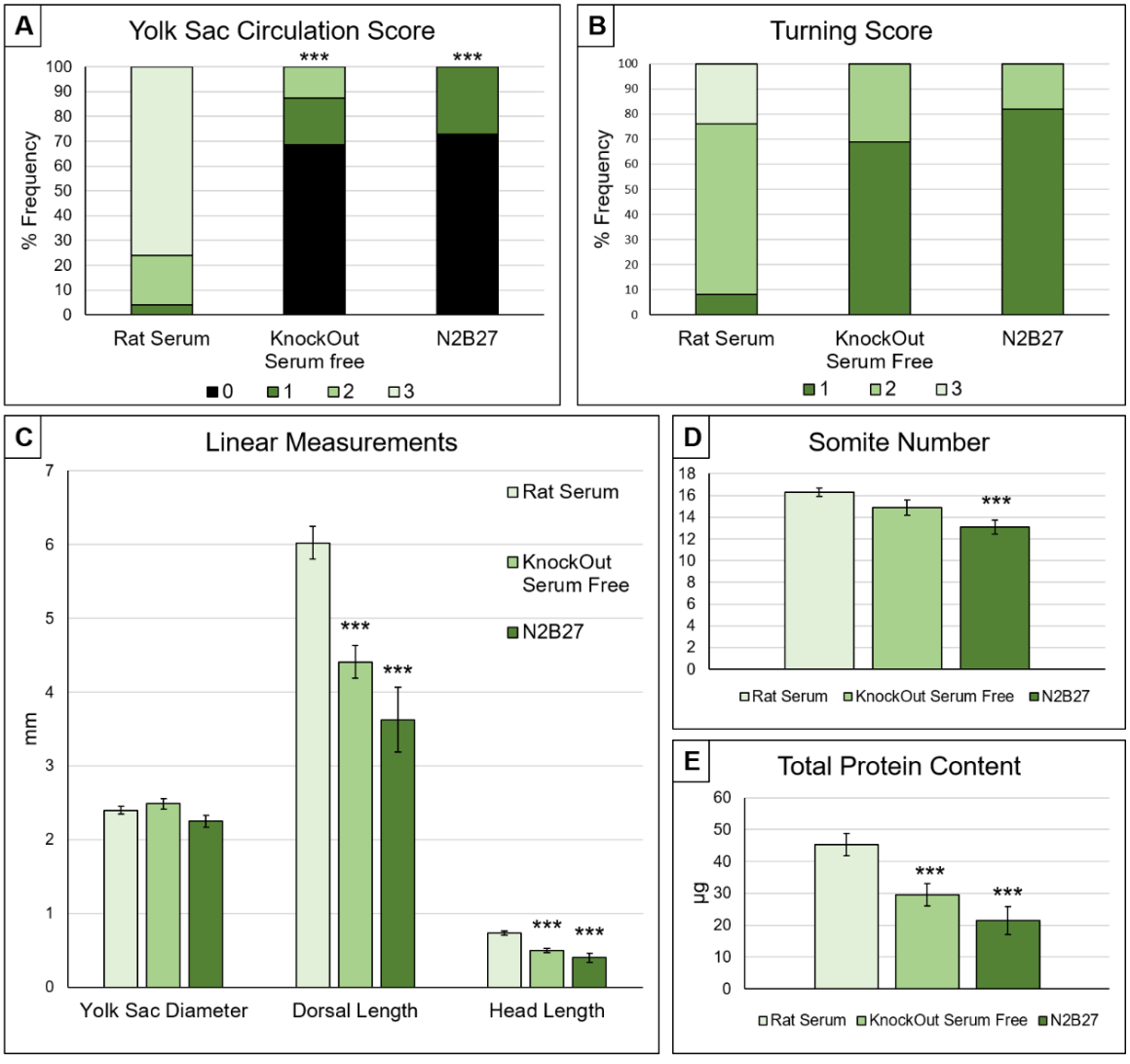

Figure 3-3: Developmental and growth parameters of embryos cultured in rat serum or serum-free media

(A) Yolk sac circulation scores. KnockOut serum-free medium and N2B27 produce significantly lower scores than culture in rat serum. **(B)** Turning scores. KnockOut serum-free medium and N2B27 embryos have significantly lower scores than rat serum-cultured embryos. **(C)** Yolk sac and embryo size measurements (mean ± SEM). Rat serum and

serum-free media do not differ significantly in yolk sac diameter, whereas both dorsal length and head length are significantly reduced in embryos cultured in serum-free media compared with rat serum. **(D)** Somite numbers. Embryos cultured in KnockOut serum-free medium show no significant difference compared with rat serum controls, whereas embryos cultured in N2B27 have significantly fewer somites than those grown in rat serum. **(E)** Total protein content. Embryos from both serum-free media cultures have significantly reduced total protein content compared with rat serum-cultured embryos. **Statistical analysis**: (A,B) Chi-square tests comparing all score categories across the 3 culture media are significant for both yolk sac circulation and turning ($p \leq 0.001$). Post-hoc tests of serum-free media versus rat serum: *** $p \leq 0.001$; 2x4 Chi-square test for yolk sac circulation and 2x3 Chi-square test for turning score. (C-E) One-way ANOVA shows significant variation in each measurement between the 3 culture media ($p \leq 0.01$), with the exception of yolk sac diameter. Post-hoc tests of serum-free media versus rat serum: *** $p \leq 0.001$, Student's t-tests. Rat serum: n = 25; KnockOut serum-free medium: n = 16; N2B27 serum-free medium: n = 11.

In conclusion, when all developmental parameters are considered, neither serum-free medium can support embryonic development in a comparable way to 100% rat serum.

3.2.2 Diluted rat serum can support normal development in culture

Four different serum-free media were tested as diluents for rat serum, to assess the potential of reducing serum usage in embryo culture. KnockOut serum-free medium, N2B27 medium, DMEM, and GMEM + defined supplements were each used to dilute rat serum 2-fold, with quantification of development after 24 h culture.

Yolk sac circulation achieved the maximum score of 3 in the majority of embryos cultured in 100% rat serum and in all the diluted serum-containing media, with the exception of N2B27 medium (Figure 3-4, A). All diluted media, however, gave markedly higher yolk sac scores (2-3) than the two 100% serum-free media. Embryos cultured in N2B27-diluted rat serum had a significantly lower proportion (38%) of embryos with a yolk sac score of 3 than undiluted rat serum (66%), whereas dilution with DMEM gave a significantly higher proportion (95%) of embryos with a score of 3. In contrast, axial rotation scores in all combination media, did not differ significantly from undiluted rat (Figure 3-4, B).

Yolk sac diameter was significantly reduced in DMEM-diluted rat serum, whereas other combination media did not differ significantly from undiluted rat serum (Figure 3-4, C).

Embryonic growth measurements showed more discrepancy between diluted rat serum and controls. Dorsal and head length were both reduced in all combination media, compared to rat serum controls, excluding the GMEM + defined supplement-diluted rat serum cultures, where embryonic growth measurements were very similar to 100% rat serum-cultured embryos (Figure 3-4, C).

Somite number did not vary significantly from rat serum controls across any of the combined media (Figure 3-4, D). Somite numbers ranged between 17.2 ± 0.8 and 18.3 ± 0.5 somites, well within the expected frequency following 24 h culture from the headfold stage (Kalaskar and Lauderdale, 2014).

Total protein content did not differ between embryos cultured in undiluted rat serum and any of the diluted media. The apparent increase in protein content following culture in GMEM + defined supplements (Figure 3-4, E) was not significantly different from rat serum controls.

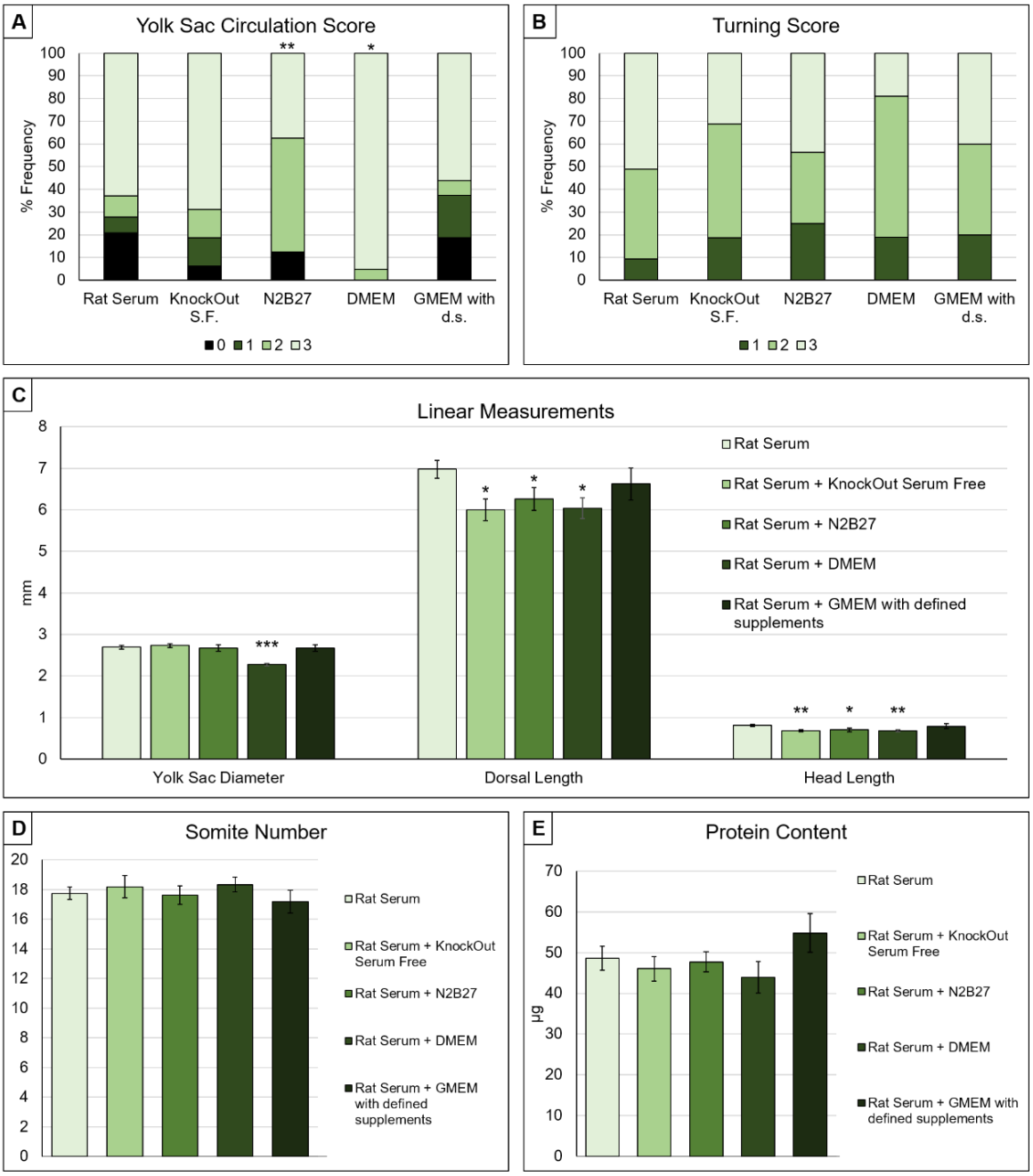

Figure 3-4: Developmental and growth parameters of embryos cultured in rat serum or the four combination (diluted) media

(A) Yolk sac circulation scores. Rat serum diluted with N2B27 supports significantly diminished yolk sac circulation compared with 100% rat serum, whereas dilution with DMEM produces significantly enhanced scores. Dilution with KnockOut serum-free medium or GMEM + defined supplements show no significant difference from 100% rat serum controls. **(B)** Turning score. No significant differences are observed between 100% rat serum and the four combination media. **(C)** Yolk sac diameter is significantly reduced when DMEM is the diluent, whereas other media do not differ from the rat serum control. Dorsal length and head length are both significantly reduced in all combination media cultures except GMEM + defined supplements, which does not differ from 100% rat serum. **(D)** Somite number. No significant differences are observed between undiluted rat serum and the four diluted media. **(E)** Total protein content. No difference in total protein content were found for any of the combination media compared with 100% rat serum controls. **Statistical analysis**: (A,B) Chi-

square tests comparing all score categories across the 5 culture media are significant for yolk sac circulation ($p \leq 0.001$) but not for turning ($p > 0.05$). Post-hoc tests of combination media versus rat serum: ** $p \leq 0.01$ and * $p \leq 0.05$; 2x4 Chi-square tests for yolk sac circulation. (C-E) One-way ANOVA shows significant variation in linear measurements between the 5 culture media ($p \leq 0.05$). Post-hoc tests of combination media versus rat serum: *** $p \leq 0.001$, ** $p \leq 0.01$, * $p \leq 0.05$; Student's t-tests. Rat serum: n = 43. Other diluents: KnockOut serum-free medium: n = 16; N2B27 serum-free medium: n = 16; DMEM: n = 21; GMEM + defined supplements: n = 16.

Open midbrain frequency, in relation to somite number, was recorded for all 5 media. An open midbrain neural tube was present in only 2/33 embryos with ≥17 somites cultured in 100% rat serum (Figure 3-5, D), and the brain in both of these embryos appeared almost closed (Figure 3-5, B). Similarly, only a minority (2/10) of embryos with ≥17 somites cultured in serum diluted with GMEM + defined supplements had open midbrain: not significantly different from rat serum controls. In contrast, rat serum dilution with KnockOut medium, N2B27 and DMEM diluents all produced a significantly higher proportion of open midbrain in embryos with 17 somites or more, compared with undiluted rat serum, and 50 – 100% of these embryos exhibited neural folds that were widely separated (Figure 3-5, C, D).

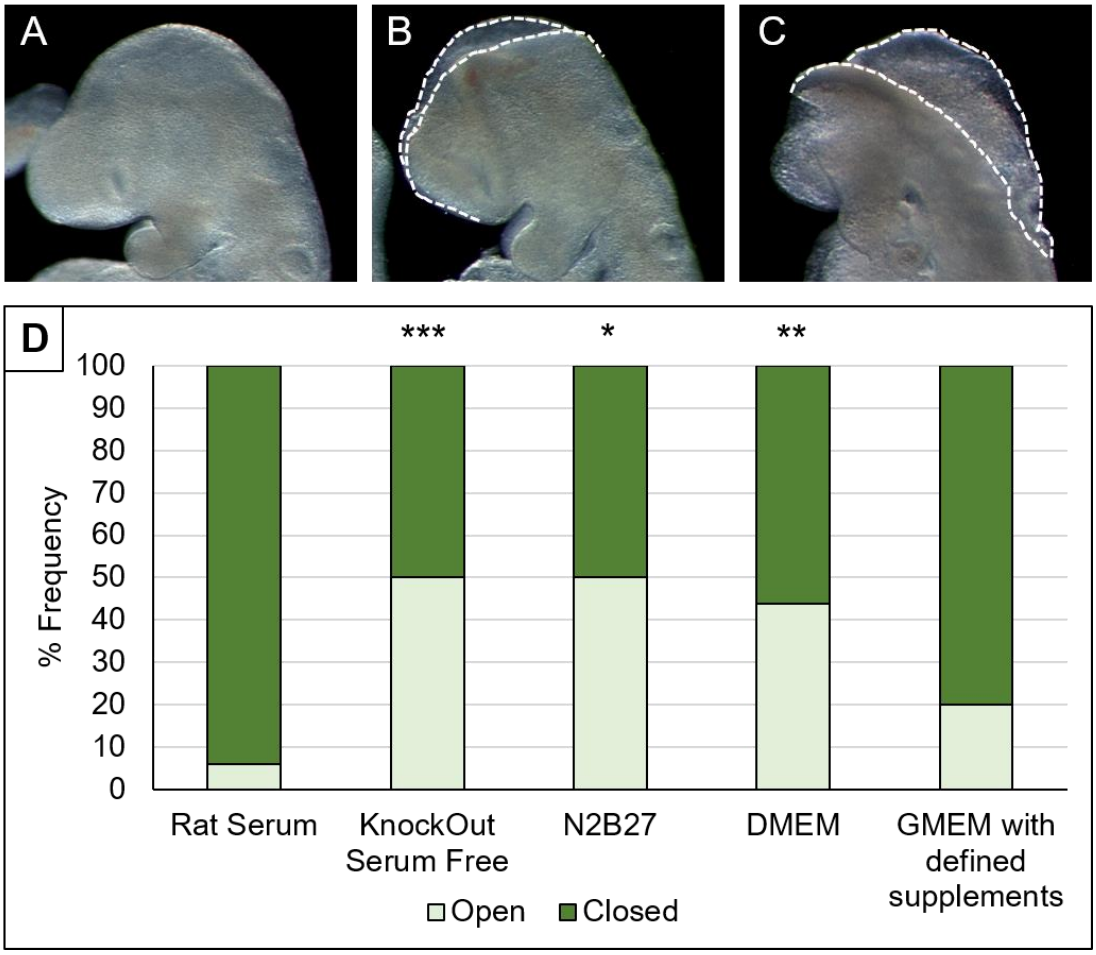

Figure 3-5: Frequency of open cranial neural tube in embryos cultured in rat serum or the four combination media

(A-C) Sample images to demonstrate extent of cranial neural tube closure. (A) Closed cranial neural tube. (B) Open cranial neural tube but with fully elevated neural folds which are likely to complete closure. (C) Open cranial neural tube with neural folds that are widely 'splayed apart'. Embryos with this appearance are unlikely to complete cranial neural tube closure. **(D)** Dilution of rat serum with KnockOut Serum-Free medium, N2B27 medium and DMEM are all associated with a significant increase in the proportion of embryos with ≥17 somites that have an open cranial neural tube. GMEM + defined supplements shows no significant difference, compared with 100% rat serum. **Statistical analysis**: Chi-square test comparing frequency of open cranial neural tube across the 5 culture media is significant ($p \leq 0.05$). Post-hoc tests of combination media versus rat serum: *** $p \leq 0.001$, ** $p \leq 0.01$, * $p \leq 0.05$; 2x2 Chi-square tests. Rat serum embryos with ≥17 somites: n = 33. Other diluents: KnockOut serum-free medium: n = 12; N2B27 serum-free medium: n = 12; DMEM: n = 17; GMEM + defined supplements: n = 10.

Throughout these dilution experiments, a volume of 0.5-1 ml of medium was used per embryo in all treatment groups. However, typical mouse culture studies often include three embryos per ml of medium from E8.5 to E9.5. To

assess whether a smaller volume of medium might compromise any of the developmental parameters, five embryos were cultured in 1.5 ml of rat serum diluted with GMEM + defined supplements. No significant changes were seen in any of the growth or developmental parameters compared with the larger volume cultures (data not shown).

Overall, GMEM + defined supplements is the only diluent that shows no statistically significant difference in any growth or developmental parameter, when compared with 100% rat serum (Figure 3-4, Figure 3-5). All other diluents show statistically significant reductions in one or more of the parameters, showing they support sub-optimal growth or development.

In summary, it is possible to reproduce embryonic growth and development of the quality of 100% rat serum using GMEM + defined supplements as a 50% diluent. Although this is a significant advancement in terms of the 3Rs, further dilution of rat serum using GMEM with defined supplements is an important avenue to investigate.

3.2.3 Rat serum dilution of more than 50% results in sub optimal embryo growth in culture

Greater dilution of rat serum to 30% of total medium volume, would represent a further saving in rat usage for embryo culture. Embryos were cultured in rat serum diluted 30:70 with GMEM + defined supplements as the diluent, by comparison with 100% rat serum controls. Embryo health appeared unchanged in the 30:70 diluted medium: 10/11 embryos achieved a yolk sac score of 3, indicating extensive vasculature and rapid blood circulation were observed in most cases (Figure 3-6, C). This proportion did not differ significantly from parallel rat serum control cultures (5/7 with yolk sac score of 3), nor from the rat serum controls in the 50% culture experiments. In terms of neural tube development, 2/3 embryos with ≥ 17 somites in the 30:70 diluted medium exhibited an open cranial neural tube (Figure 3-6, F), in comparison to only 1/4 embryos with ≥ 17 somites in 100% rat serum controls, where the brain appeared almost closed (as in Figure 3-5, B).

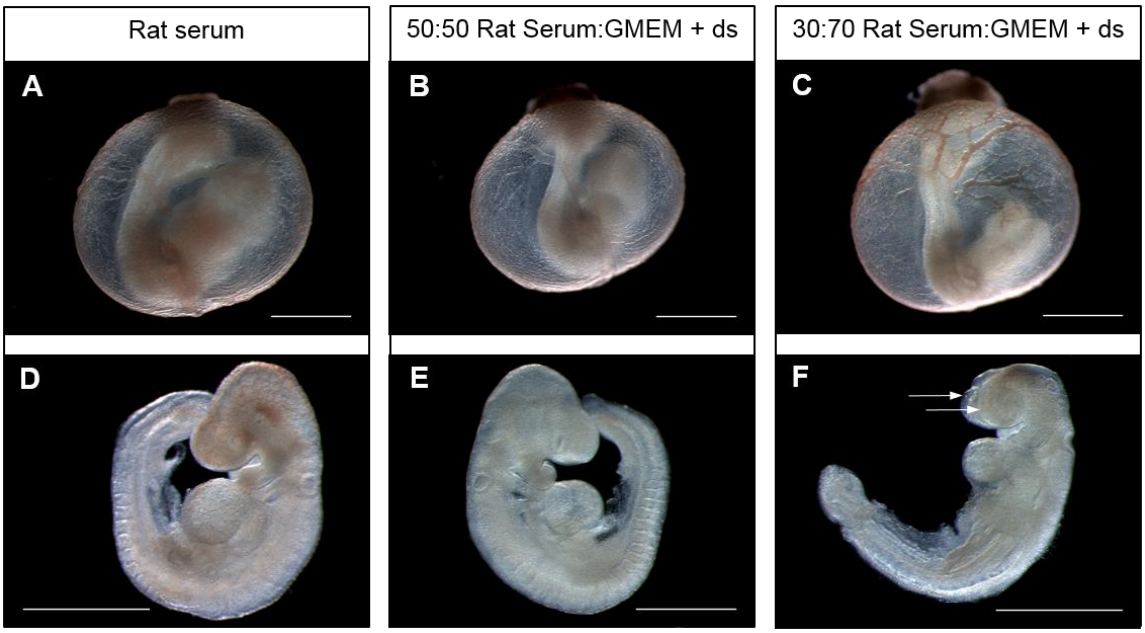

Figure 3-6: Effect of increased dilution of rat serum on success of embryo culture

Representative images of yolk sacs (A-C) and isolated embryos (D-F) cultured in 100% rat serum (A,D), or in rat serum diluted 50:50 (B,E) or 30:70 (C,F) with GMEM plus defined supplements (ds). (**A-C**) Yolk sac development is closely comparable in 100% rat serum and in both dilutions with GMEM + ds. All three examples (A-C) scored a maximum of 3 on the yolk sac circulation scale. (**D-F**) Morphological appearance of embryos is closely similar in 100% rat serum (D) and in serum diluted 50:50 with GMEM + ds (E). Embryos are fully turned, of similar size, and with no obvious abnormalities. In contrast, embryos cultured in rat serum diluted 30:70 with GMEM + ds (F) exhibit reduction in growth parameters (e.g. small head) and more often have an open cranial neural tube (arrows). Scale bars: 1 mm.

Axial rotation score did not differ between groups (data not shown), and with regard to yolk sac diameter and somite number (Figure 3-7, A, B), both showed no significant differences between the 30:70 diluted medium and the control media.

In contrast, growth parameters were adversely affected by culture in the 30:70 serum dilution. Mean dorsal length and head length were both significantly reduced in 30:70 diluted medium compared with 100% rat serum (Figure 3-7, A). Mean head length differed between 0.68 ± 0.02 (rat serum) and 0.53 ± 0.04 (30:70 serum dilution). Mean dorsal length in 100% rat serum was 6.01 ± 0.14, compared to 4.77 ± 0.35 in diluted serum cultures.

These measurements were also significantly lower than the 50% rat serum controls shown previously (p≤0.001, Student's t Test) (data not shown).

Total protein content replicated the reduction in embryo size seen in dorsal and head length results: there was a significant reduction in total protein content in the 30:70 serum dilution cultures compared to controls (Figure 3-7, C).

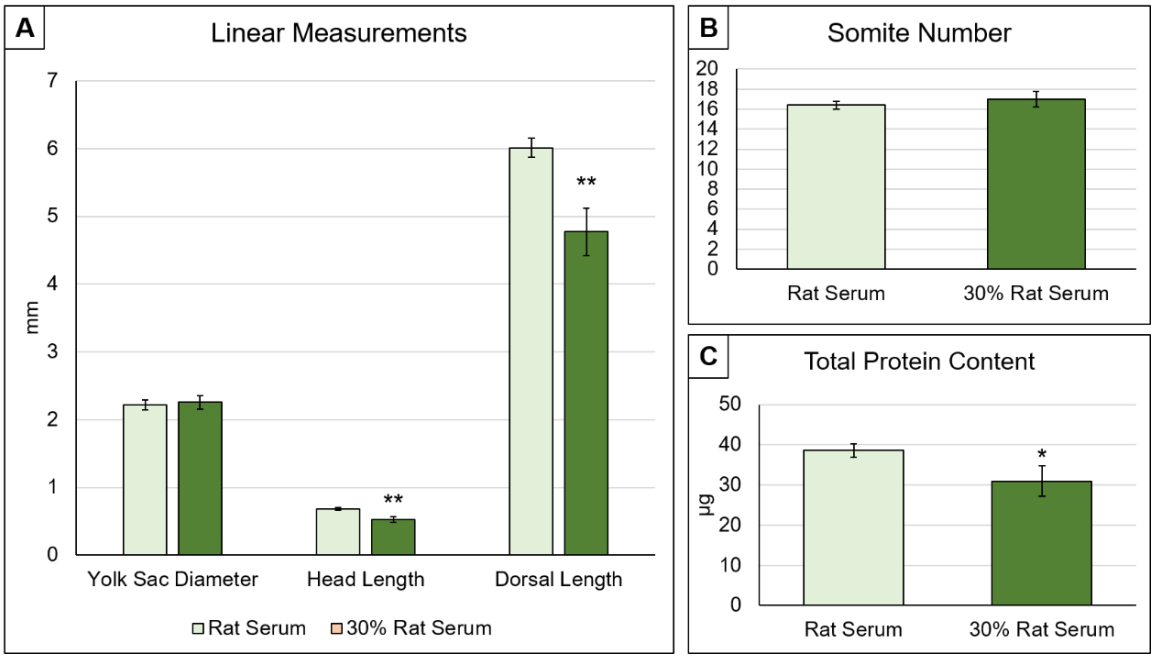

Figure 3-7: Developmental and growth parameters of embryos cultured in 100% rat serum or in serum diluted 30:70 with GMEM plus defined supplements

(A) Yolk sac diameter shows no difference between 100% and diluted rat serum cultures, whereas dorsal length and head length are both significantly diminished in the 30% rat serum cultures. **(B)** Somite number does not differ significantly in embryos cultured in 100% or 30% rat serum. **(C)** Total protein content shows a trend towards reduction in 30% rat serum cultures, although there is no significant difference from 100% rat serum controls. **Statistical analysis**: ** p ≤ 0.01, * p ≤ 0.05; Student's t-tests. Rat serum: n = 7, 30% rat serum: n = 11.

In summary, 70% dilution of rat serum by GMEM + defined supplements is not able to replicate embryonic growth in 100% rat serum culture. Although embryo health and developmental progression are comparable, there is a significant adverse effect on embryonic growth parameters and there

appears to be a higher incidence of cranial neural tube closure delay or failure. This finding would preclude the use of rat serum diluted by more than 50% for experimental studies in the E8.5-E9.5 embryonic period.

3.2.4 Addition of glucose does not restore development in 30% rat serum-cultured embryos

Previous studies of rat embryos undergoing organogenesis *in vitro* found that addition of glucose could restore embryo growth in a minimal medium (Cockroft, 1979). To investigate a possible beneficial effect of glucose addition in the current study, E8.5 embryos were cultured for 24 h in the 30:70 dilution of rat serum by GMEM + defined supplements, with the addition of 2 mg/ml glucose. All aforementioned parameters were assessed. Although some improvement in growth parameters was seen, yolk sac diameter ($p \leq 0.01$) and head length ($p \leq 0.05$) both showed significant reductions compared with 100% rat serum cultures (data not shown). Hence, the addition of glucose is unable to rescue the compromised growth of mouse embryos cultured in rat serum diluted 70% with serum-free medium.

3.3 Discussion

This study is the first to compare developmental progression and growth of embryos cultured in serum-free media compared with rat serum littermate controls, using the original optimised method of whole embryo culture (Sadler and New, 1981). In some of the earliest studies with rodent embryos, it was found that approximately parallel progression of embryo development *in utero* can be obtained *in vitro* using rat serum (New, 1978, New et al., 1976a). As summarised in Figure 3-1, previous serum replacement or reduction studies have been insufficient in drawing conclusions on the developmental viability of embryos grown in defined medium, compared to littermate controls in 100% rat serum. Here it was demonstrated that, although rat serum cannot be replaced entirely with serum-free medium due to significant loss in embryo quality, it is possible to dilute rat serum by 50%, with GMEM + defined supplements, while still achieving excellent embryonic growth and development.

This leads to the question: which components in GMEM + defined supplements make it a more suitable medium for embryo growth, compared with the other mediums. Amino acids have been shown to be essential for embryo development. In pre-implantation embryos, non-essential amino acids and L-glutamine have been shown to reduce the time of cleavage divisions to the eight-cell stage in zygotes and enhance blastocyst formation and hatching, and essential amino acid transport supports development of more viable embryos (Lane and Gardner, 1997, Van Winkle, 2001). In post-implantation embryos, there is evidence that nonessential amino acids and glutamine also support the highest implantation and embryo development rates, with the highest implantation rate observed when all 20 amino acids (11 non-essential + 9 essential) were in the culture medium (Lane and Gardner, 1994). The evident need for the non-essential amino acid glutamine, is perhaps the reason why KnockOut Serum-Free medium, mainly composed of L-glutamine-free basal medium (KnockOut DMEM) and N2B27, composed of 50% L-glutamine-free Neurobasal medium, were unable to support optimal embryo growth.

The difference between GMEM + defined supplements and DMEM was determined in more detail to assess the differences in amino acid content. GMEM + defined supplements contains half the concentration of amino acids compared to DMEM, with the exception of additional non-essential amino acids: proline, asparagine, aspartic acid and alanine, and an increased concentration of L-glutamine through supplementation (Table 3-1).

Table 3-1: Amino acid concentrations of DMEM and GMEM + defined supplements

	DMEM	GMEM + defined supplements
Essential amino acids	**mg/L**	**mg/L**
L-Histidine hydrochloride-H2O	42	21
L-Isoleucine	105	52.4
L-Leucine	105	52.4
L-Lysine hydrochloride	146	73.1
L-Methionine	30	15
L-Phenylalanine	66	33
L-Threonine	95	47.6
L-Tryptophan	16	8
L-Valine	94	46.8
Non-essential amino acids		
Glycine	30.0	15
L-Arginine hydrochloride	84.0	42
L-Cystine 2HCl	63	31.3
L-Glutamine	580	712
L-Serine	42	21
L-Tyrosine	72	36
L-Proline	-	11.5
L-Asparagine	-	13.2
L-Aspartic acid	-	13.3
L-Alanine	-	8.5

This suggests that, as shown in implantation rates (Lane and Gardner, 1994), embryo growth and development could also be reliant on nearly all 20 amino acids (essential and non-essential) being present in the medium, and the lower doses in GMEM + defined supplements (half DMEM) are sufficient for this point in gestation. Additionally, the increased concentration of L-glutamine could be the key factor, its importance demonstrated in early studies (Lane and Gardner, 1997, Van Winkle, 2001).

Rat serum reduction by 50% represents a significant step towards realising the goals of the National Centre for the 3Rs (NC3Rs) which aims to replace, reduce and refine animal use in research (Burden et al., 2015). Whole embryo culture, as it stands, provides a refinement of developmental studies on rodent embryos: it allows multiple treatments and conditions to be applied to the same litter from a single pregnant dam, ensuring a lower number of dams are exposed to harmful procedures or sacrificed. However, the culture

medium used in whole embryo culture studies remains to be improved. Based on the literature search detailed in (3.1.1) and Appendices, 73% publications used rat serum as the main medium component in rodent whole embryo cultures. A PubMed search identified 118 papers that used whole embryo culture in the period 2013 to 2018. Based on the work in our lab, each study may have cultured ~ 200 embryos. If, on average, 1 ml of serum is used per embryo and an adult male rat produces 6 ml serum, this approximates to > 550 rats that are used per year purely for serum production in embryo culture.

The diluted rat serum medium identified here, provides a means towards significantly reducing the number of rats used for whole embryo culture experiments. Preparation of rat serum to the specifications demanded by embryo culture is expensive and technically demanding (Takahashi et al., 2014). By reducing the requirement for rat serum in the culture medium, whole embryo culture could become a more attractive experimental method for developmental biologists and reproductive toxicologists. As a result, this has the potential to lead to a further reduction in mouse experimental usage, as *in vitro* culture gradually replaces *in vivo* treatment of pregnant dams.

GMEM + defined supplements, as a diluent, has provided a significant optimisation for culture of E8.5-E9.5 mouse embryos, yet further experimentation could define exactly how useful this medium could be in reducing rat serum usage. For example, it is conceivable that the culture period could be extended beyond 24 h, perhaps with regular replenishment of the combined medium, to allow further progression in embryo development. It has been shown that mouse embryos with 2-4 somites can be cultured for at least 48 h in 100% rat serum without any deterioration in development, using a single serum replenishment and a gas phase change (Sadler, 1979). Other embryonic stage starting points could also be investigated. Postimplantation embryos have been cultured as early as E5.5 (pre-gastrulation stage) and as late as E10.5 (Rivera-Perez et al., 2010). If the proposed combination medium in this study could be used for longer culture periods, and for cultures starting at multiple gestational ages, this

would further improve the versatility of whole embryo culture. It is also possible that rat serum proportions could be reduced further for less sensitive developmental time points or for shorter cultures.

Further experimentation to determine the constituents of rat serum which become limiting at 70% dilution, leading to sub-optimal growth, would also be interesting. Rat serum is relatively uncharacterised in terms of the factors that contribute to rodent embryonic development. Early experiments studying the components of rat serum that change over the culture period found the most significant decrease was in glucose concentration, whose exhaustion coincided with embryonic death (Sanyal, 1980). It was also shown in experiments with dialysed serum, that the addition of glucose as an energy source, restored growth to control levels (Cockroft, 1979). For these reasons, the addition of glucose to the 70% diluted rat serum medium was tested in an attempt to re-establish normal growth, but this was unsuccessful: yolk sac diameter and head length were significantly impaired, compared with control embryos cultured in 100% rat serum. Vitamins including pantothenic acid, riboflavin and inositol are essential constituents of rat serum as a culture medium, at certain concentrations (Cockroft, 1979). All three of these vitamins are also components of GMEM and DMEM, yet the low relative concentrations may be the reason behind unsuccessful development. Therefore, further experiments involving these vitamins and perhaps other growth factors could potentially enable the rat serum component of embryo culture medium to be reduced below 50%.

In conclusion, the present study describes an optimisation of whole embryo culture in relation to the 3Rs, enabling reduced costs and a potential extension of the use of embryo culture as a key tool in developmental and toxicological analysis of mouse embryo development.

Chapter 4 Characterisation of a late-arising NTD phenotype in ASPP2 mutant mice

4.1 Introduction

ASPP2 (apoptosis-stimulating protein of p53, 2) belongs to the ASPP family of proteins, characterized by ankyrin repeats, an SH3 domain, and a proline-rich region in the C-terminal (Sullivan and Lu, 2007). The best-known function of ASPP2 is as a haplo-insufficient tumour suppressor, related to its positive regulation of p53-dependent apoptosis through enhancing DNA binding and transactivation of pro-apoptotic genes (Bergamaschi et al., 2004, Samuels-Lev et al., 2001). As a result, the role of ASPP2 has been most thoroughly explored in relation to cancer, with findings of ASPP2 dysregulation in colorectal cancer (Yin et al., 2018), downregulation in pancreatic cancer (Song et al., 2015), and association with pituitary adenomas (Turnquist et al., 2014).

Investigations into the relevance of ASPP2 in embryology and development have been far fewer. Interestingly, however, one such investigation shed light on the importance of ASPP2 during development, through creation of an ASPP2 mutant mouse model (Vives et al., 2006). Exon 3 of *Trp53bp2*, the mouse gene that encodes ASPP2, was deleted and replaced with a neomycin resistant cassette in order to produce a 'null' mutant. This was found to cause significant perinatal death in a proportion of homozygous *Trp53bp2*$^{\Delta 3/\Delta 3}$ fetuses, whereas hydrocephalus was observed in those *Trp53bp2*$^{\Delta 3/\Delta 3}$ mice that survived beyond birth (Vives et al., 2006).

Trp53bp2 consists of 18 exons and codes for three separate mRNA species and three protein isoforms. Exon 1 contains the translation start site for ASPP2, the longest protein of 1128 amino acids. BBP, sometimes referred to as 53BP2, is a shorter isoform (1005 amino acids), which has a reduced but similar function to ASPP2 (Van Hook et al., 2017) and has its translation start site in exon 6. The open reading frame of ASPP2 is interrupted by a stop codon located in exon 3, and it has been shown that exon 3 is transcribed in

BBP mRNA (hence the more downstream translation start site), but not ASPP2 mRNA species (Takahashi et al., 2004). The third and most recently discovered isoform is named ΔN-ASPP2, which arises from a separate transcription start site in intron 6 (Van Hook et al., 2017). Deletion of exon 3, as in *Trp53bp2*$^{\Delta 3/\Delta 3}$ mice, has been shown to result in deletion of the ASPP2 protein, detected using an N-terminal targeted antibody (Vives et al., 2006). This suggests that the translational machinery is disrupted, resulting in knockout of ASPP2 as well as BBP. Neither mRNA quantity or ΔN-ASPP2 protein have been assessed in *Trp53bp2*$^{\Delta 3/\Delta 3}$ mice.

Trp53bp2$^{\Delta 3/\Delta 3}$ mice were later used in a study to further assess the reason for perinatal death in homozygotes (Sottocornola et al., 2010). Dilation of the brain ventricles (correlated with 100% hydrocephalus in homozygotes), loss of cellular organisation in the neuroepithelium, and bilateral retinal dysplasia were all observed in *Trp53bp2*$^{\Delta 3/\Delta 3}$ fetuses (Sottocornola et al., 2010). Although this study highlighted many neural-related consequences of a homozygous exon 3 deletion in ASPP2, it did not study regions outside of the cranial region, nor did it examine mutant embryos at neurulation stages. More recently, a variety of NTD lesions were observed in *Trp53bp2*$^{\Delta 3/\Delta 3}$ mouse embryos (Zak et al., 2016), although the developmental origin of these defects was not investigated. The conclusion of these previous studies is that *ASPP2* mutation, on a mixed genetic background, produces partially penetrant NTDs, together with ~30% of *Trp53bp2*$^{\Delta 3/\Delta 3}$ embryos surviving postnatally, when hydrocephalus arises and leads to premature death (Sottocornola et al., 2010).

Further work in our lab (Copp et al, unpublished) has demonstrated that the NTDs in *Trp53bp2*$^{\Delta 3/\Delta 3}$ embryos arise by re-opening of a closed neural tube, in contrast to failure of primary neurulation (neural tube closure) as is seen in most mouse mutants with NTDs. Moreover, it was found that folic acid, which can reduce the risk of NTDs in humans and in some mouse strains, actually has an exacerbating effect on NTDs in *Trp53bp2*$^{\Delta 3/\Delta 3}$ embryos. In contrast, maternal folate deficiency reduced the NTD frequency. Hence, the NTDs in

the *Trp53bp2*$^{\Delta 3}$ strain are unusual among mouse models and deserving of more detailed analysis.

The present work was designed to further characterise the phenotype seen in *Trp53bp2*$^{\Delta 3/\Delta 3}$ embryos, largely concentrating on the spinal region. An important question is why only a proportion of homozygous embryos develop NTDs whereas the remainder lack this overt phenotype, despite having the same genetic defect. Hence, a key element of the approach in the present study was to perform a 3-way comparison between wild-type (*Trp53bp2*$^{+/+)}$ embryos, *Trp53bp2*$^{\Delta 3/\Delta 3}$ non-macroscopically phenotypic (NMP) embryos and *Trp53bp2*$^{\Delta 3/\Delta 3}$ macroscopically phenotypic (MP) embryos. Specific aims of this chapter are to:

- Visualise and quantify ASPP2 mRNA expression in the mouse embryo

- Assess the variability of the NTD phenotype seen in *Trp53bp2*$^{\Delta 3/\Delta 3}$ mouse embryos

- Assess cell proliferation in the spinal neuroepithelium of *Trp53bp2*$^{\Delta 3/\Delta 3}$ embryos

- Address cell cycle exit and neuronal differentiation in the spinal neuroepithelium of *Trp53bp2*$^{\Delta 3/\Delta 3}$ embryos

4.2 Results

4.2.1 ASPP2 mRNA expression is strongest in the ventral neural tube and there is no difference between N- and C-terminal derived mRNA

It has been shown previously that ASPP2 is expressed in the brain, spinal cord and optic cup of wild-type embryos from E9.5 onwards (Sottocornola et al., 2010). To confirm these findings and extend the analysis to include a *Trp53bp2*$^{\Delta 3/\Delta 3}$ embryo, whole-mount *in situ* hybridisation was used on E9-9.5 embryos: one wild-type and one non-macroscopically phenotypic mutant

were compared using a *Trp53bp2* mRNA probe (see details in 2.2.2 and 2.3.2).

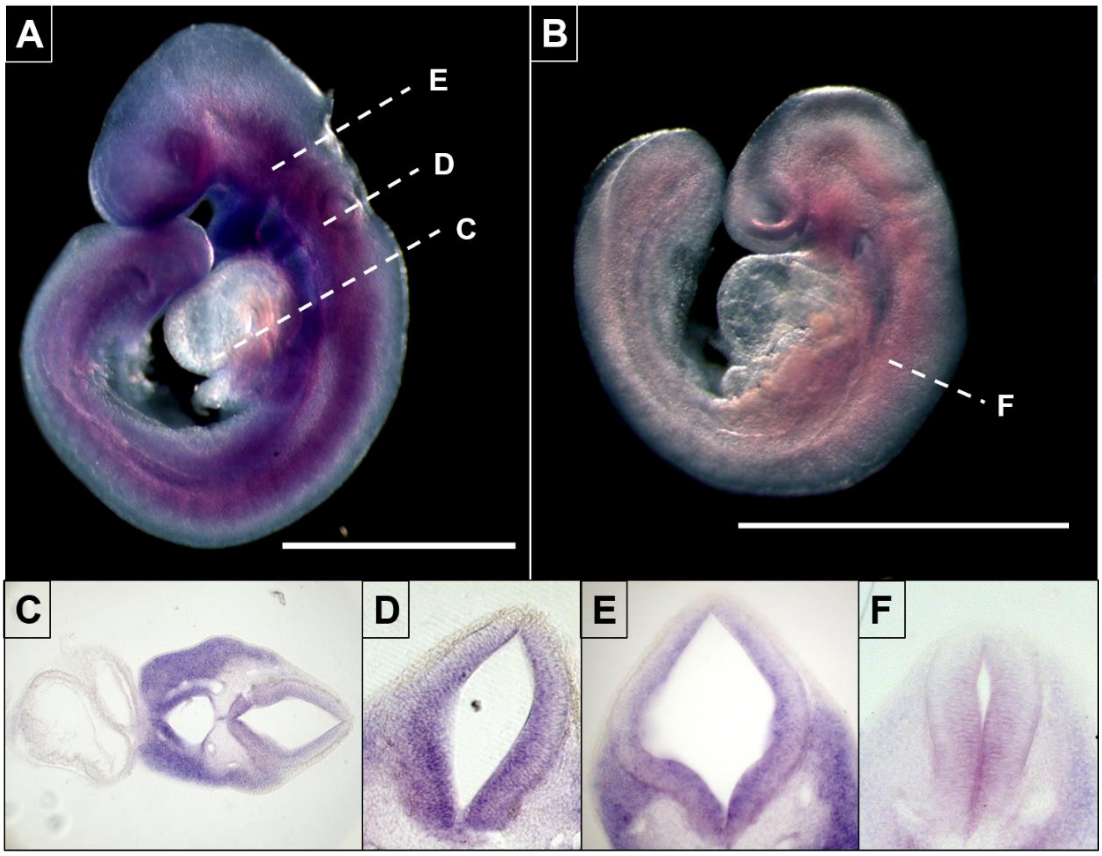

Figure 4-1: Whole-mount in situ hybridisation with a *Trp53bp2* mRNA probe

(A) E9.5 wild-type embryo from ASPP2 litter hybridised with *Trp53bp2* mRNA probe. Expression can be seen in the first 2 branchial arches, the ventral neural tube and the developing eye. Dashed lines refer to the section images C-E. (**B**) E9 *Trp53bp2*$^{\Delta 3/\Delta 3}$ embryo probed with the same mRNA probe, for an equal amount of time as the embryo in (**A**). Weaker but similar expression pattern seen as in (**A**). Dashed line refers to section image **F**. (**C-F**) Vibratome sections taken from embryos in (**A**) and (**B**), showing strongest expression of ASPP2 mRNA in the ventral neural tube, particularly the apical surface (**C-F**), and branchial arches (**C**). The *Trp53bp2*$^{\Delta 3/\Delta 3}$ embryo section (**F**) shows much less intense expression than in the wild-type. Scale bars 1mm.

The *Trp53bp2* mRNA probe revealed expression in the ventral neural tube, the first two branchial arches and the developing eye (Figure 4-1). Expression in the ASPP2 mutant embryo was in a similar distribution to that of the wild-type, although the signal appeared weaker (Figure 4-1, B, F), despite probe development for the same time, in the same experiment. If the

Trp53bp2$^{\Delta 3}$ allele is a null, then there should be no detectable ASPP2 expression in homozygous embryos. This issue was therefore explored further through mRNA quantification.

Quantitative RT-PCR was used to measure *Trp53bp2* mRNA in wild-type (WT), heterozygous *Trp53bp2*$^{\Delta 3/+}$ (Het) and homozygous *Trp53bp2*$^{\Delta 3/\Delta 3}$ (Hom) embryos. ΔN-ASPP2 arises due to a *transcriptional* rather than *translational* alternative start site, beyond the N-terminus in intron 6 (Figure 4-2). Therefore, it became relevant to study both N- and C-terminal derived mRNA expression. As a result, primer pairs used to generate site-specific mRNAs for qPCR, were designed to bind exons 1-3 (to confirm exon 3 deletion in *Trp53bp2*$^{\Delta 3}$), exons 1-2 (N-terminal; excluded from *ΔN-ASPP2* mRNA but included in both *Trp53bp2* and *BBP* mRNA), and exon 13 (C-terminal; present in *ΔN-ASPP2*, *Trp53bp2* and *BBP* mRNA).

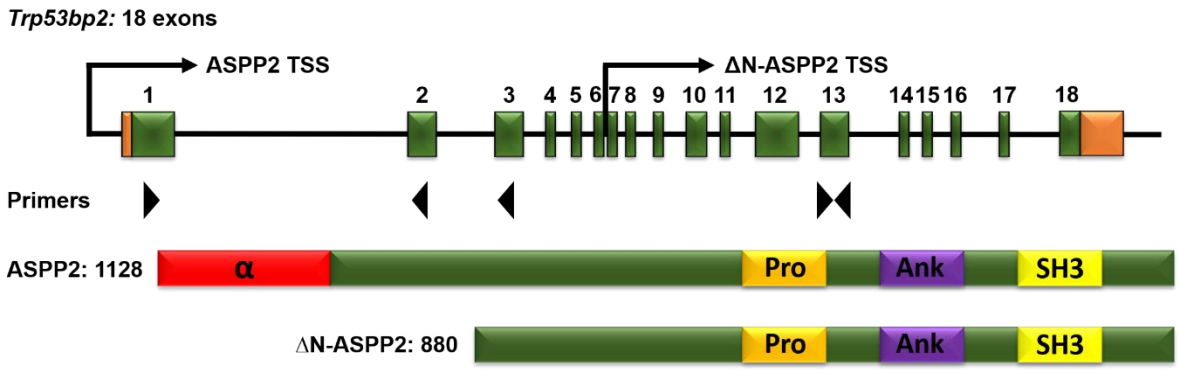

Figure 4-2: Transcription start sites and protein structures of ASPP2 vs ΔN-ASPP2

The transcription start site (TSS) of full-length ASPP2 protein is upstream of exon 1. The TSS of ΔN-ASPP2 is in intron 6. Following translation, this results in the creation of a 1128 amino acid (aa) ASPP2 protein and a 880 aa ΔN-ASPP2 protein. Both proteins contain the proline domain, ankyrin repeats and SH3 domain which characterise the C-terminal. Only the full-length ASPP2 protein has an N-terminus which contains an alpha-helical domain. Primers for qPCR included a forward primer in exon 1, reverse primers in exon 2 and 3, and a primer pair within exon 13.

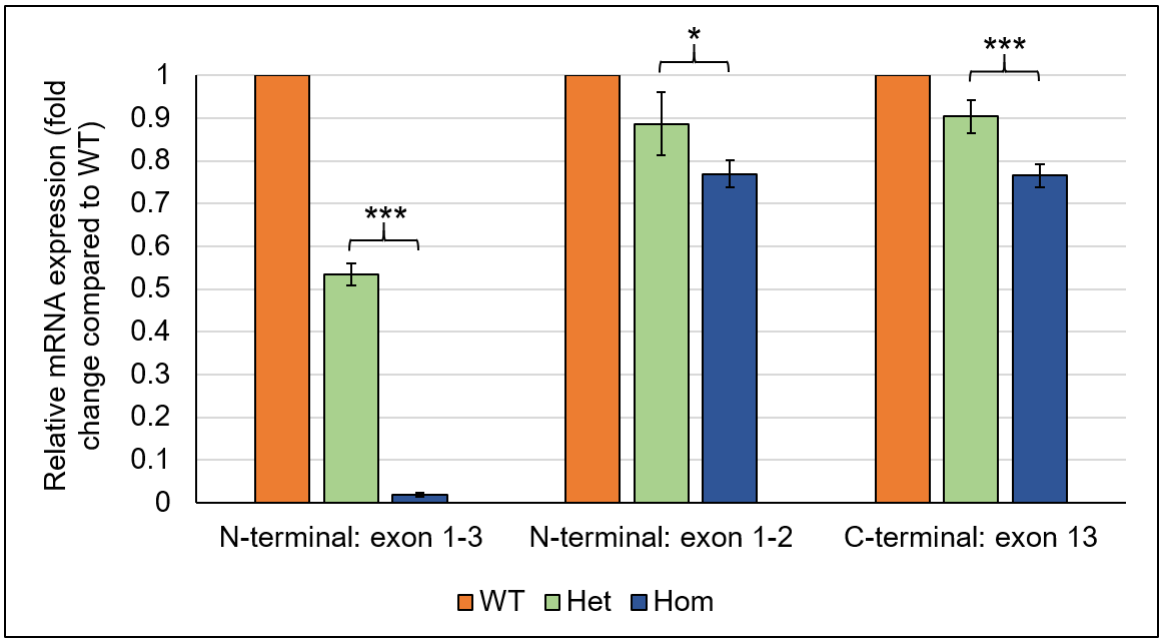

Figure 4-3: Quantitative RT-PCR results

Amplification of N- and C-terminally-derived mRNAs in WT, Het and Hom embryos. Y-axis values represent relative mRNA expression: i.e. fold change compared with WT, which is assumed to represent total *Trp53bp2* mRNA and assigned a value of 1.0. **N-terminal: exons 1-3:** mRNA expression in Het embryos: ~0.53 (53%) mRNA, Hom embryos: ~0.02 (2%) mRNA compared to WT embryo mRNA. **N-terminal, exons 1-2:** Het embryos: ~0.89 (89%) mRNA, Hom embryos: ~0.77 (77%) mRNA compared to WT embryo mRNA. **C-terminal: exon 13:** Het embryos: ~0.9 (90%) mRNA, Hom embryos: ~0.76 (76%) mRNA compared to WT embryo mRNA. One-way ANOVA showed significant variation in Het and Hom mRNA fold change (compared to WT mRNA) ($p \leq 0.05$). Post-hoc pair-wise tests of Het mRNA fold change / Hom mRNA fold change: *** $p \leq 0.001$, * $p \leq 0.05$; Student's t-tests. No significant difference between Het or Hom mRNA fold change between N-terminal: exon 1-2, and C-terminal: exon 13. Error bars: standard error. WT / Het / Hom: n = 3 embryos per genotype. Number of replications: 2.

The quantitative RT-PCR results were analysed by measuring mRNA expression fold-change in Het and Hom embryos, compared to WT embryo mRNA. When primers were used to amplify a region between exons 1-3, a ~50% reduction in mRNA in Het embryos and almost a complete loss of mRNA in Hom embryos was observed (Figure 4-3). Since exon 3 is deleted in one (Het) or both (Hom) alleles at the *Trp53bp2* $^{\Delta 3}$ locus, the percentage fold changes were as expected. Interestingly, there was no difference in the mRNA expression between WT, Het and Hom embryos for either of the N-terminal (exons 1-2) or C-terminal (exon 13) targeted primer pairs. In both regions, Het embryos showed ~90% mRNA expression, and Hom embryos

showed ~77% mRNA expression, compared to total mRNA expression in the wild-type (Figure 4-3). Slight reduction in mRNA expression in Het embryos, and further reduction in Hom embryos, reflected the weaker mRNA expression seen in the *Trp53bp2*$^{\Delta 3/\Delta 3}$ embryo following *in situ* hybridisation. Despite persistent mRNA expression in homozygous mutants, ASPP2 protein knockdown has been confirmed previously as a result of a frame-shift induced by deletion of exon 3 (Vives et al., 2006).

To summarise, mRNA expression of *Trp53bp2* is strongest in the ventral neural tube, the branchial arches, and in the developing eye. Both *in situ* hybridisation and RT-PCR showed that mRNA expression is reduced in heterozygotes and homozygotes, due to exon 3 knockout via insertion of a neomycin cassette. Complete protein knock-down has already been confirmed (Vives et al., 2006).

4.2.2 *Trp53bp2*$^{\Delta 3/\Delta 3}$ embryos have a variable NTD phenotype

To analyse the phenotype of *Trp53bp2*$^{\Delta 3/\Delta 3}$ embryos, three gestational ages were assessed: E9.5, E11.5 and E13.5. These stages were chosen as it is apparent that *ASPP2* is not expressed at E8.5 (Sottocornola et al., 2010), and that complex NTDs can be observed at E14.5 or earlier (Zak et al., 2016). Therefore, it was reasoned that a potential temporal progression of the phenotype could best be assessed between E9.5 and E13.5.

Table 4-1 shows the total number of embryos assessed and the frequency of embryos with: (i) a closed and normal neural tube; (ii) an open neural tube; (iii) a deflated or undulated head region at E9.5; (iv) an overgrown head region at E11.5 or E13.5. Cranial defects were often first to arise, therefore embryos were categorised based on this region initially; however, spinal regions were also affected, most notably in the later embryonic stages (E11.5 and E13.5). Appearance of closed cranial defects changed with developmental stage: from a deflated or undulating brain at E9.5 to an appearance of tissue overgrowth at E11.5 and E13.5. The final column in Table 4-1 shows the proportion of embryos, where sectioning was performed,

that were found to have histological abnormalities within the spinal region. WT, Het and Hom embryos were analysed. Homozygous embryos were separated into ‘non-macroscopically phenotypic’ (NMP), with wild-type appearance, and ‘macroscopically phenotypic’, where there was any evidence of a macroscopic phenotype (MP).

Table 4-1: NTD frequency in wild-type, heterozygous, and homozygous ASPP2 embryos

	Total Number	Closed and normal	Open	Deflated/undulated brain	Histological abnormality
E9.5	**34**				
WT	12 (35.3%)	12 (100%)	0	0	0/3 analysed
Het	13 (38.2%)	13 (100%)	0	0	Not analysed
Hom-NMP	3 (8.8%)	3 (100%)	0	0	1/3 analysed
Hom-MP	6 (17.6%)	0	2 (33.3%)	4 (66.7%)	3/3 analysed
E11.5	**46**			**Overgrown cranial region**	
WT	9 (19.6%)	9 (100%)	0	0	0/3 analysed
Het	22 (47.8%)	21 (95.4%)	1 (4.5%)	0	Not analysed
Hom-NMP	6 (13%)	6 (100%)	0	0	3/3 analysed
Hom-MP	9 (19.6%)	0	4 (44.4%)	5 (55.6%)	3/3 analysed
E13.5	**27**			**Overgrown cranial region**	
WT	7 (25.9%)	7 (100%)	0	0	0/3 analysed
Het	13 (48.1%)	13 (100%)	0	0	Not analysed
Hom-NMP	3 (11.1%)	3 (100%)	0	0	3/3 analysed
Hom-MP	4 (14.8%)	0	3 (75%)	1 (25%)	3/3 analysed

To generate all three genotypes (WT/Het/Hom), heterozygous females were crossed with heterozygous males (*Trp53bp2*$^{\Delta 3/+}$ x *Trp53bp2*$^{\Delta 3/+}$). Therefore the expected ratio would be 1:2:1 WT:Het:Hom. This was largely true at each age group, with E13.5 embryos following the expected frequency almost exactly: 26% WT, 48% Het, and 26% Hom (Hom-NMP and Hom-MP combined) (Table 4-1). The genotypic ratio did not differ significantly between the 3 age groups (3X3 Chi-square contingency table, data not shown). This suggests embryonic lethality is not a contributing factor to genotype ratio within these gestational time points.

In all cases, WT and Het embryos were normal, bar one *Trp53bp2*$^{\Delta 3/+}$ embryo at E11.5 which had a small opening in the forebrain region (see Table 4-1). This is not sufficient evidence to suggest heterozygosity for *Trp53bp2*$^{\Delta 3}$ increases NTD risk.

The ratio of homozygotes scored as ‘closed and normal’ (Hom-NMP) compared to either open or deflated/undulated/overgrown (Hom-MP), did not differ significantly between the three gestational ages (3X3 Chi-square test, data not shown). Despite this, within Hom+ embryos, there does appear to be a trend towards increased open neural tube frequency with increased age: 33% E9.5 Hom+ embryos, compared to 75% E13.5 Hom+ embryos (Table 4-1), as well as a decreasing trend of closed defects with age, from 67% E9.5 embryos to 25% E13.5 embryos. However, statistically, the three phenotypic categories do not change in proportion with stage.

Histological abnormality was classified as any cellular disruption of the neural tube, compared to wild-type, in transverse embryo cryosections (see 2.3.1). 3 WT, 3 Hom-NMP and 3 Hom-MP embryos were sectioned per stage, in a way that ensured the whole-body axis was represented (see 2.3.1). Only 1/3 E9.5 non-macroscopically phenotypic homozygous (Hom-NMP) embryos exhibited an abnormal neural tube histologically, whereas 100% of Hom-MP embryos that were analysed at E11.5 and E13.5 exhibited histological overgrowth or abnormality (see Table 4-1). This suggests that a ‘normal’ exterior does not always equate to a ‘normal’ interior in *Trp53bp2*$^{\Delta 3/\Delta 3}$

embryos. 100% macroscopically phenotypic (Hom-MP) embryos at each stage also had histological abnormalities.

Figure 4-4 and Figure 4-5 provide examples of the macroscopic and histological abnormalities seen in *Trp53bp2*$^{\Delta 3/\Delta 3}$ embryos.

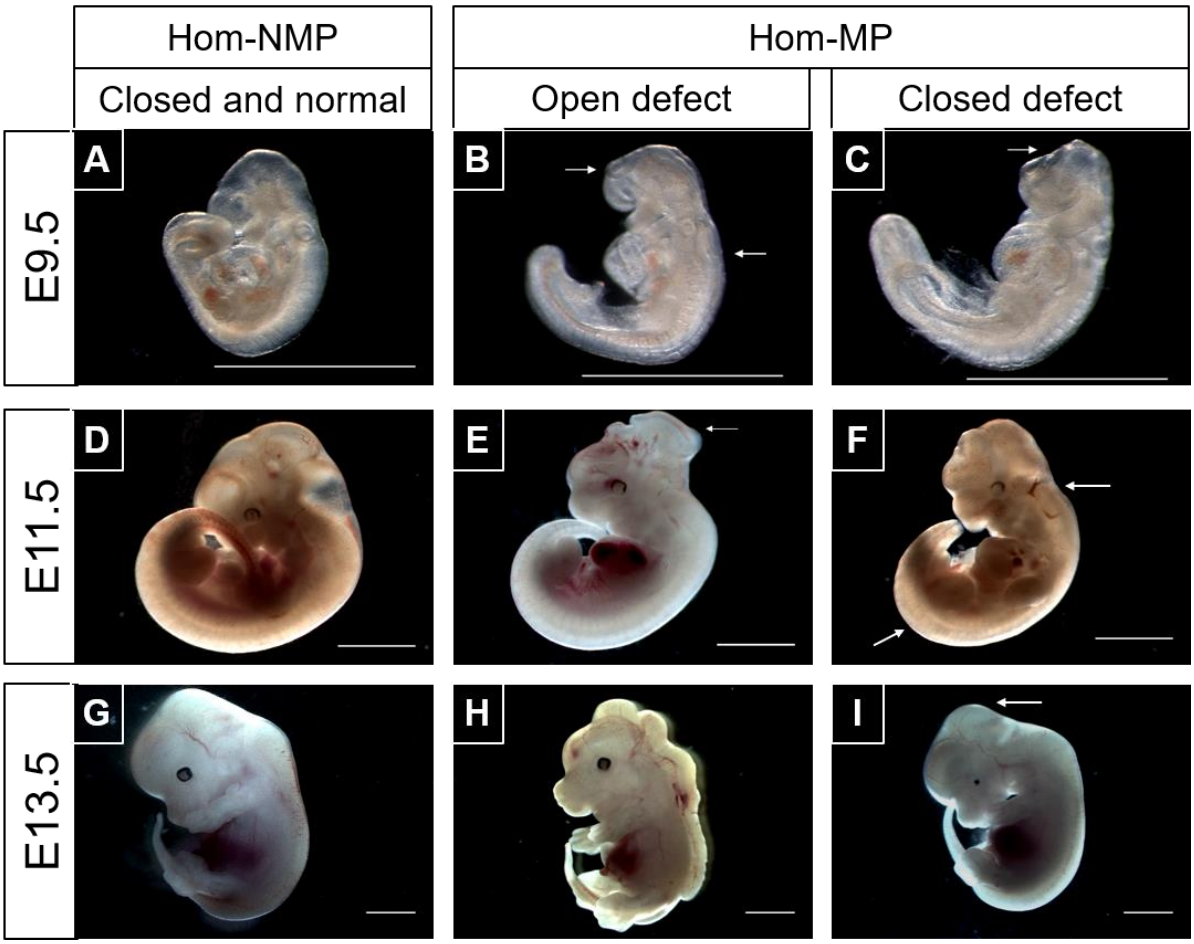

Figure 4-4: Macroscopic appearance of *Trp53bp2*$^{\Delta 3/\Delta 3}$ embryos

Representative images of homozygous *Trp53bp2*$^{\Delta 3/\Delta 3}$ embryos: non-macroscopically phenotypic (Hom-NMP) (closed and normal), and macroscopically phenotypic (Hom-MP) (open and closed defects). (**A**) Normal E9.5 embryo with domed, smooth head and closed neural tube, excluding the PNP (**B**) E9.5 embryo with open neural tube region between the midbrain and upper neural tube (see arrows). (**C**) E9.5 embryo with a misshapen, deflated cranial region. (**D**) Closed and normal E11.5 homozygote. (**E**) E11.5 embryo with wide open cranial neural folds and intracranial haemorrhage. (**F**) E11.5 embryo with a closed defect. Cranial region is expanded and misshapen, with facial abnormalities. Neural tube is overgrown to the level of the hindlimb bud (see arrows). (**G**) Normal E13.5 homozygote. (**H**) E13.5 embryo with craniorachischisis. Plaque of tissue seen protruding through the neural tube opening along the body axis. (**I**) E13.5 embryo with slight overgrowth of the hindbrain (see arrow) and a unilateral eye abnormality. Scale bars 1mm.

Macroscopically, the severity of open NTDs in *Trp53bp2*$^{\Delta 3/\Delta 3}$ embryos increased with gestational age, from an open region spanning the cranial and upper NT regions only (see arrows in Figure 4-4, B), to craniorachischisis (almost entirely open neural tube) in some E13.5 embryos (see Figure 4-4, H). E9.5 and E11.5 open defects mostly appeared as open cranial neural folds (Figure 4-4, B, E), whereas at E13.5 a plaque of tissue could often be seen protruding through the neural tube opening, overlying the dorsal aspect of the entire spinal region (Figure 4-4, H).

Closed defects were highly variable and did not appear to progress as clearly through gestational age points compared to open defects. At E9.5 the newly closed cranial neural folds were often misshapen and asymmetrical (Figure 4-4, C), whereas E11.5 and E13.5 embryos showed a variety of facial abnormalities, uni/bi-lateral eye abnormalities/agenesis, and overgrowth of the cranial and spinal regions (Figure 4-4, F, I). These abnormalities have been previously reported (Zak et al., 2016), as well as histological structural changes of the retina (Sottocornola et al., 2010). For the purpose of this study on NTDs, the analysis of histological structural changes was limited to the neural tube.

Figure 4-5 shows the variation of disruption in neural tube architecture observed in sections at the three developmental ages, in mutant (*Trp53bp2*$^{\Delta 3/\Delta 3}$) embryos with and without a macroscopic phenotype, in comparison to wild-type embryos.

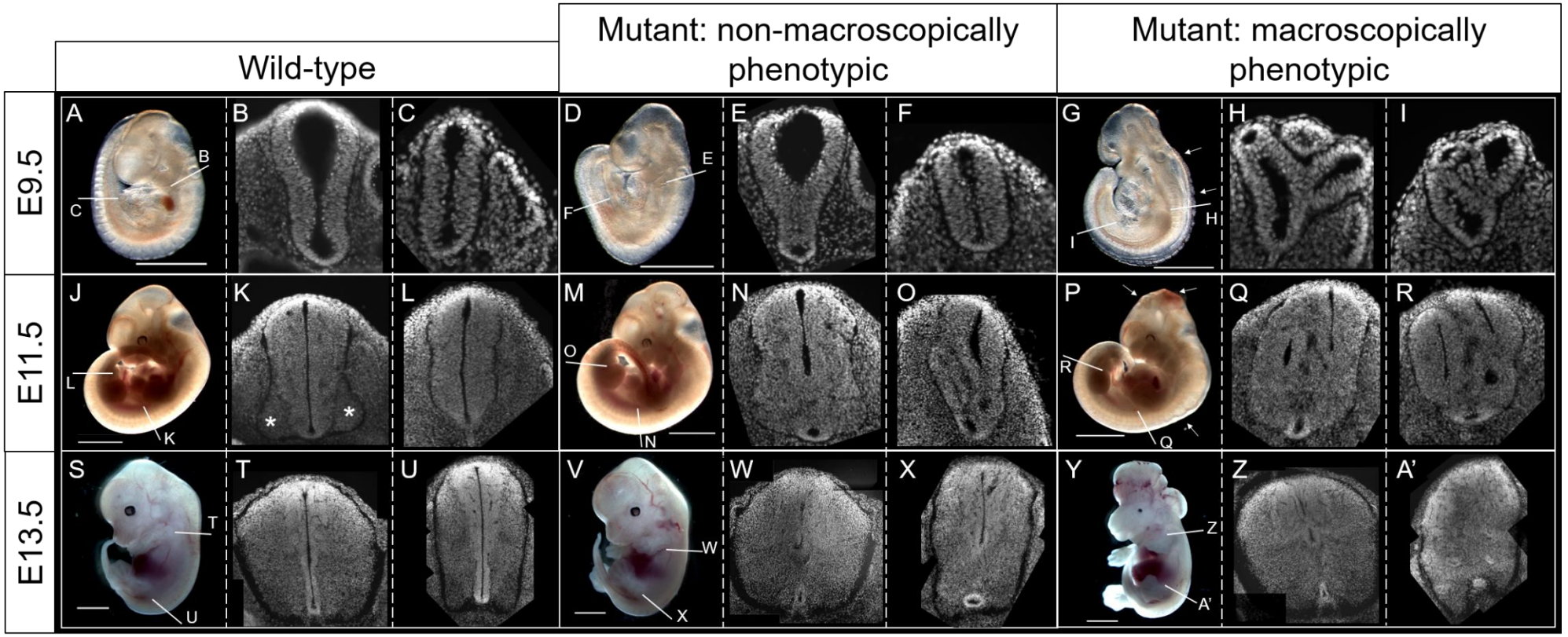

Figure 4-5: Histological morphology of the neural tube in wild-type and *Trp53bp2*$^{\Delta 3/\Delta 3}$ embryos

Example images of wild-type, non-macroscopically phenotypic mutant and macroscopically phenotypic mutant embryos, at each of E9.5, E11.5 and E13.5, with corresponding section images depicting their histological morphology. Dorsal is upwards and ventral is downwards for all section images. (**A**) Wild-type E9.5 embryo with two section lines relating to images B and C. (**B**) Neural tube with single lumen spanning the majority of the midline neuroepithelium in the dorso-ventral axis. Otic vesicle can be seen on the right-hand side (RHS). (**C**) Neural tube further caudal to B with single lumen. (**D**) Non-macroscopically phenotypic mutant E9.5 embryo with two section lines relating to images E and F. (**E**) Neural tube with 2 lumens separated by an apparent 'bridge' of neuroepithelium that crosses the midline. Otic vesicle on RHS. (**F**) Neural tube further caudal to E, with single lumen spanning dorsal to ventral aspects. (**G**)

Macroscopically phenotypic mutant embryo with a small, deformed cranial region and an open neural tube in the region between the arrows. Two section lines relate to images H and I. (**H**) Neural tube section with 3 lumens and an undefined mass of cells in the dorsal region, inferior to the surface ectoderm. (**I**) Neural tube section further caudal to H, showing 3 lumens surrounding central cell cluster containing a possible 4th lumen. (**J**) Wild-type E11.5 embryo with two section lines corresponding to images K and L. (**K**) Neural tube with single lumen spanning the dorsal-ventral axis in the midline. Asterisks show the regions of motor neuron differentiation in the ventro-lateral swellings of the neural tube. (**L**) Neural tube further caudal to K, with single continuous lumen and lack of motor neuron swellings. (**M**) Non-macroscopically phenotypic E11.5 embryo with two section lines relating to images N and O. (**N**) Neural tube with 2 lumens separated by a bridge of neuroepithelium crossing the midline. Small circular lumen retained just above the floor-plate. (**O**) Neural tube section further caudal to O, with 3 clear lumens and 3 lesion-like openings. (**P**) Macroscopically phenotypic mutant E11.5 embryo with craniofacial abnormalities, intracranial haemorrhage and a contorted, overgrown neural tube (see arrows). Section lines relate to images Q and R. (**Q**) Neural tube with 3 lumens and potential midline lesions. Small circular lumen retained just above the floor-plate. (**R**) Caudal neural tube with 2 slit-like lumens, 1 circular lumen and a flattened disc-shaped lumen immediately above the floor-plate. (**S**) Wild-type E13.5 embryo with two section lines corresponding to images T and U. (**T**) Neural tube section showing a circular, symmetrical neural tube with a lumen spanning the midline in the dorso-ventral axis. (**U**) Similar neural tube architecture as in T, but slightly more elongated. (**V**) Non-macroscopically phenotypic mutant E13.5 embryo with section lines corresponding to W and X. (**W**) Neural tube of a similar proportion and shape as in T, but with 3 separate lumens located along the midline. (**X**) Similarly shaped neural tube as in U, with 2 lumens separated by a bridge of neuroepithelium. A clearly distinct circular lumen lies just above the floor-plate. (**Y**) Macroscopically phenotypic E13.5 embryo with exencephalic-like protrusions extending to the hindbrain and upper neural tube, and eye abnormalities (also exhibited uni-lateral eye agenesis, not seen in this image). Section lines correspond to Z and A' (**Z**) Neural tube of embryo in Y, with 3 slit-like lumens situated along the midline (**A'**) Neural tube further caudal to Z, with no apparent lumen. Cell clusters appear in the neuroepithelium, the most distinct being just above the floor-plate. Scale bars 1mm.

The histological appearance of wild-type embryos at all three gestational ages was of a symmetrical neural tube containing a single midline lumen, extending from roof-plate to floor-plate. At E9.5, the lumen was bordered by a pseudostratified neuroepithelium of relatively uniform appearance except at the dorsal and ventral poles where it was extremely thin (Figure 4-5, B, C). At E11.5, ventro-lateral thickenings of the neuroepithelium corresponded to motor neuron differentiation in these regions, whereas the proliferative neuroepithelium occupied most of the wall thickness of the neural tube more dorsally (Figure 4-5, K). By E13.5 the proliferative neuroepithelium had reduced to a thin ventricular zone, bordering the lumen along the entire dorso-ventral axis, while the majority of the neural tube more laterally (the 'mantle zone') contained differentiated neurons.

The histological architecture of the neural tube in E9.5 non-macroscopically phenotypic *Trp53bp2*$^{\Delta 3/\Delta 3}$ embryos (Hom-NMP) appeared normal in 2/3 embryos compared to the wild-type (Table 4-1). However, in 1/3 non-macroscopically phenotypic embryos, disruption could be seen in certain regions where apparent overgrowth of the neuroepithelium resulted in lumen obliteration. This mainly affected the ventral portion of the neural tube, whereas the dorsal region showed a relatively normal structure (Figure 4-5, E). The histological architecture of macroscopically phenotypic E9.5 *Trp53bp2*$^{\Delta 3/\Delta 3}$ embryos appeared chaotic, with multiple lumens and abnormal neuroepithelial organisation (Figure 4-5, H-I). At E11.5, the neural tube of non-macroscopically phenotypic embryos tended to vary depending on location along the body axis. More rostral regions were often similar to wild-type, with the exception of a neuroepithelial tissue bridge that crossed the midline, separating the dorsoventrally-aligned lumen into two parts (Figure 4-5 N). In macroscopically phenotypic cases, multiple lumens were visible within the neural tube, often with a highly complex folded structure (Figure 4-5 Q-R). At E13.5, the *Trp53bp2*$^{\Delta 3/\Delta 3}$ embryonic spinal cord varied histologically, based on whether the region of neural tube in the section was open or closed. Where open, an extensive plaque lay over the affected region, appearing histologically as a mass of tissue over a small lumen retained just superior to the floor-plate (not shown). Sections of closed neural

tube regions at E13.5 often exhibited chaotic neuroepithelial cells and intersected midline lumens (Figure 4-5, W-X, Z-A'). Occasionally cell clusters or rosettes could be seen dispersed throughout the neuroepithelium (Figure 4-5, A'). A small lumen above the floor-plate was retained in the majority of sections in E11.5 and E13.5 *Trp53bp2*$^{\Delta 3/\Delta 3}$ embryos, which was a striking finding given the otherwise highly variable appearance of the overgrowth phenotype.

In conclusion, while many *Trp53bp2*$^{\Delta 3/\Delta 3}$ embryos appear 'normal' by macroscopic morphology (Hom-NMP), leading to the idea that the ASPP2 phenotype is partially penetrant, the histological architecture of these embryos suggests otherwise, and tissue-level abnormalities are present in almost all cases from E11.5 onwards. This raises the possibility that all mutants have defects at the cellular level, but that this is only sufficient to produce a macroscopically visible phenotype in a proportion of homozygotes.

4.2.3 Proliferation is increased in late-stage *Trp53bp2*$^{\Delta 3/\Delta 3}$ embryos and ectopic mitoses are increased in mutants at all gestational ages

To understand the cellular mechanisms leading to the complex phenotype in *Trp53bp2*$^{\Delta 3/\Delta 3}$ embryos, which involves apparent overgrowth of the ventral neuroepithelium by E11.5, proliferation was the first cellular process to be assessed. Although it was now clear that mutant embryos lacking a macroscopic phenotype exhibit histological abnormalities, the distinction between non-macroscopically phenotypic and macroscopically phenotypic homozygous mutants was maintained to assess the progression of the phenotype within the same gestational age group. Therefore, for all future immunofluorescence assessment, a 3-way comparison between *Trp53bp2*$^{+/+}$ (wild-type) embryos, *Trp53bp2*$^{\Delta 3/\Delta 3}$ (mutant) non-macroscopically phenotypic (NMP) embryos and *Trp53bp2*$^{\Delta 3/\Delta 3}$ macroscopically phenotypic (MP) embryos was used (phenotypic classed as any macroscopic sign of abnormality).

Phospho-histone H3 (PHH3) was used to label cells going through mitosis at the time embryos were fixed. Mitosis normally occurs at the apical/lumenal border of the neural tube in mouse embryos. However, a previous study found an increase of mitotic cells away from the lumenal border in the brains of ASPP2 mutant embryos (Sottocornola et al., 2010). Hence, two quantifications were made: total mitotic index was calculated as: (no. PHH3+ cells / DAPI+ cells) x 100, and ectopic mitotic index (mitoses away from the lumenal border) was calculated as: (no. ectopic PHH3+ cells / no. total PHH3+ cells) x 100. Mitoses were considered as ectopic if they occurred >3 nuclear diameters away from the lumenal surface within the neuroepithelium (see 2.5.1).

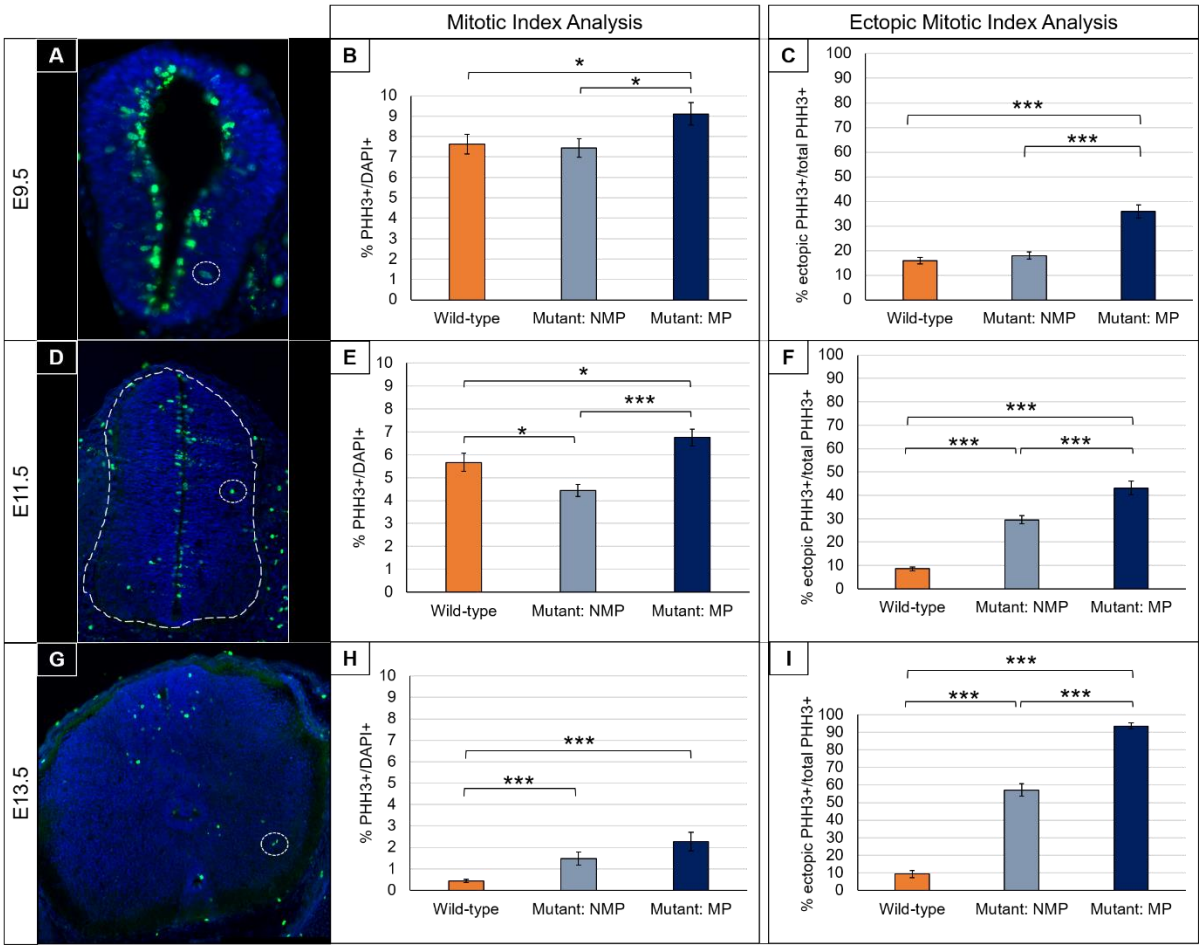

Figure 4-6: Total and ectopic mitotic index analysis

(**A,D,G**) Transverse sections of E9.5, E11.5 and E13.5 neural tubes, with PHH3-labelled mitoses in green, DAPI-labelled nuclei in blue, and dotted circles around examples of ectopic mitoses. Dashed line highlights neural tube border. (**B,E,H**) % PHH3+ cells / DAPI+ cells (y-axis max. 10%) in E9.5 (B), E11.5 (E), and E13.5 (H) embryos. Macroscopically phenotypic

mutant embryos (mutant: MP) have a significantly higher proportion of mitoses (PHH3) out of total cell count (DAPI), compared to wild-type embryos at all stages, and compared to non-macroscopically phenotypic embryos (mutant: NMP) at E9.5 and E11.5. NMP mutant embryos have a significantly different mitotic index compared to wild-types at E11.5 and E13.5. (**C,F,I**) % ectopic PHH3+ cells / total PHH3+ cells in E9.5 (C), E11.5 (F) and E13.5 (I) embryos. MP mutants have a significantly higher proportion of ectopic mitoses compared to wild-type and NMP mutant embryos at all 3 stages. NMP mutants have a significantly higher proportion of ectopic mitoses compared to wild-type embryos at E11.5 and E13.5. **Statistical analysis**: One-way ANOVA showed significant variation in mitotic index and % ectopic mitoses measurements between the 3 genotype/phenotype combinations in all analyses ($p \leq 0.05$). Post-hoc pair-wise tests of NMP mutant / MP mutant / wild-type embryos: *** $p \leq 0.001$, * $p \leq 0.05$; Student's t-tests. Error bars: standard error. n = 3 embryos per genotype/phenotype group, 3-4 slides per embryo, 4-5 sections per slide. Total mitoses/ectopic mitoses counted: E9.5: wild-type: 1580/262. Mutant: NHM: 1650/308. Mutant: MP: 2223/845. E11.5: wild-type: 2707/241. Mutant: NHM: 3082/947. Mutant: MP: 4202/1954. E13.5: wild-type: 403/53. Mutant: NHM: 931/530. Mutant: MP: 2668/2560.

Initial observations of PHH3-labelled mutant embryo sections highlighted an apparent increase in mitotic cells away from the apical border (ectopic mitoses), compared to wild-type sections (see Figure 4-6, A, D, G). To explore this in more detail, both overall mitotic index and % ectopic mitoses were determined in wild-type and mutant embryos.

An indication of total proliferative rate was obtained by calculating % PHH3+ cells / DAPI+ cells. This showed that total mitotic index is increased in MP mutants at all gestational ages studied, compared to wild-type embryos and also significantly increased compared to non-macroscopically phenotypic embryos at both E9.5 and E11.5. Interestingly, total mitotic index was reduced in the NMP mutant embryos compared with wild-type at E11.5, yet was significantly increased at E13.5 (Figure 4-6, B, E, H).

Quantification of ectopic PHH3+ cells / total PHH3+ cells revealed that macroscopically phenotypic mutant embryos had a significantly higher proportion of ectopic mitoses than both wild-type and non-macroscopically phenotypic embryos at each gestational age. NMP mutant embryos also had a significantly higher proportion of ectopic mitoses compared to wild-type at E11.5 and E13.5. Hence, not only are non-macroscopically phenotypic *Trp53bp2*$^{\Delta 3/\Delta 3}$ embryos disrupted histologically, the apical localisation of mitosis is also affected.

It was noted that ectopic mitoses often correlate with the presence of a smaller apical border / lumenal surface (Figure 4-6, G). On the other hand, even when the neural tube appeared of normal structure, ectopic mitoses were still numerous in mutant embryos (Figure 4-6, D). To investigate this question in more detail, it was decided to explore the relationship between lumenal circumference (and therefore total length of the apical border), and frequency of ectopic mitoses (Figure 4-7).

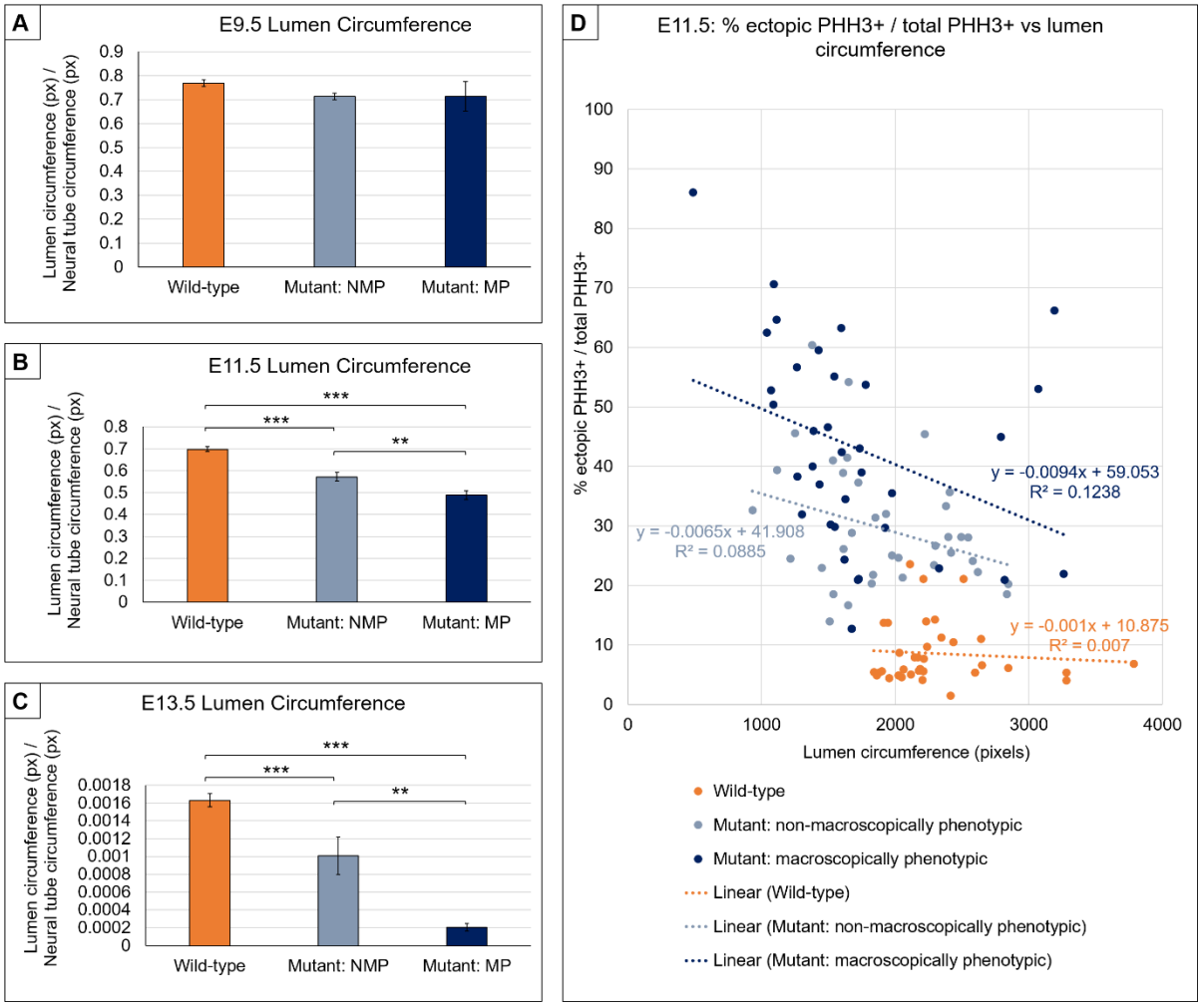

Figure 4-7: Lumen circumference analysis

(**A-C**) Lumen circumference in pixels (px) normalised to neural tube circumference (px) for wild-type, non-macroscopically phenotypic (Mutant: NMP) and macroscopically phenotypic mutant embryos (Mutant: MP). (**A**) Total lumen circumference did not differ significantly compared to wild-type embryos in either E9.5 mutant type. (**B,C**) Both MP and NMP mutants had a significantly smaller total lumen circumference compared to wild-type embryos at E11.5 (B) and E13.5 (C). MP mutants had a significantly smaller lumen circumference compared to NMP mutants at both stages. (**D**) % ectopic PHH3+ / total PHH3+ (y-axis) plotted against lumen circumference (x-axis) (E11.5 only). The proportion of ectopic mitoses stays low (around ~10%), regardless of lumen circumference, in wild-type embryos, whereas

large variation is seen in both MP and NMP mutants. Linear regression lines show a trend towards a decrease in % ectopic mitoses when lumen circumference increases. (Wild-type: $y=-0.001x+10.875$, $R^2=0.007$, mutant: NMP: $y=-0.0065x+41.908$, $R^2=0.0885$, mutant: MP $y=-0.0094x+59.053$, $R^2=0.1238$. Linear regression for total data points: $y=-0.0159x+58.452$, $R^2=0.2485$ (not shown). **Statistical analysis**: One-way ANOVA showed significant variation in lumen circumference between the 3 genotype / phenotype combinations in E11.5 and E13.5 analysis ($p \leq 0.05$). No significant variation was found in E9.5 analysis. Post-hoc pair-wise tests of NMP mutant / MP mutant / wild-type E11.5 and E13.5 embryos: *** $p \leq 0.001$, ** $p \leq 0.01$; Student's t-tests. Error bars: standard error. n = 3 embryos per genotype/phenotype group, 3-4 slides per embryo, 4-5 sections per slide. Number of lumens measured: E9.5: wild-type: 35. Mutant: NHM: 37. Mutant: MP: 35. E11.5: wild-type: 30. Mutant: NHM: 35. Mutant: MP: 34. E13.5: wild-type: 25. Mutant: NHM: 19. Mutant: MP: 19.

Firstly, total lumen circumference (sum of all present lumens in the neural tube) in each embryo group was measured. To alleviate discrepancies of neural tube size between sections, lumen circumference was normalised to neural tube circumference (both measured in pixels). In E9.5 embryos there proved to be no significant difference in lumen circumference in either mutant type, compared to wild-type embryos (Figure 4-7, A). E11.5 and E13.5 embryos, however, showed a reduction in lumenal circumference (i.e. normalised length of apical border) in both the macroscopically phenotypic and non-macroscopically phenotypic mutants compared to the wild-type, with the largest reduction in lumen circumference seen in MP mutants at both gestational ages (Figure 4-7, B, C). Hence, with increasing occurrence of multiple lumens within the neuroepithelium, the proportion of lumenal circumference to neural tube circumference reduces.

It was hypothesised that the significant increase in % ectopic mitoses in E11.5 and E13.5 mutants (Figure 4-6, F, I) may result from the reduction in apical border (lumenal circumference) at these stages. To visualise the relationship between lumen circumference and ectopic mitosis, % ectopic PHH3+ cells / total PHH3+ cells was plotted against lumen circumference (px), using E11.5 embryo data. The expectation, assuming there is a direct correlation between the two factors, would be: when lumen circumference is decreased, ectopic mitoses are increased (less apical border = fewer apical mitoses and more ectopic mitoses). Figure 4-7, D, shows that in E11.5 wild-type embryos the proportion of ectopic mitoses remained at a low level despite variations in lumen circumference. In the mutant situation, however,

where the proportion of ectopic mitoses is higher and lumen circumference more varied, linear regression lines suggest a more negative correlation between lumen circumference and ectopic mitotic index (Figure 4-7, D).

Importantly, however, Figure 4-7D shows that for a given lumenal circumference (e.g. 2000-2500 pixels), mutants show a 3-4 times higher % ectopic mitoses than wild-type embryos. This argues that ectopic mitosis is a feature specific to loss of ASPP2 function, and not simply a result of reduced apical neuroepithelial border.

To further investigate the location of proliferating cells within the neuroepithelium, E11.5 embryos were used to analyse mitosis in the ventral and dorsal halves of the neural tube. E9.5 embryos had a more variable and less established neural tube structure and a large proportion of E13.5 MP *Trp53bp2*$^{\Delta 3/\Delta 3}$ embryos were open with an extensive plaque, whereas E11.5 embryos, even when macroscopically phenotypic, provided an appropriate basis to differentiate between the ventral/dorsal regions. Using the images taken for complete neural tube PHH3 analysis, a midline was drawn between the dorsal and ventral regions of the neural tube in E11.5 sections, and PHH3+ counting was repeated (see 2.5.1).

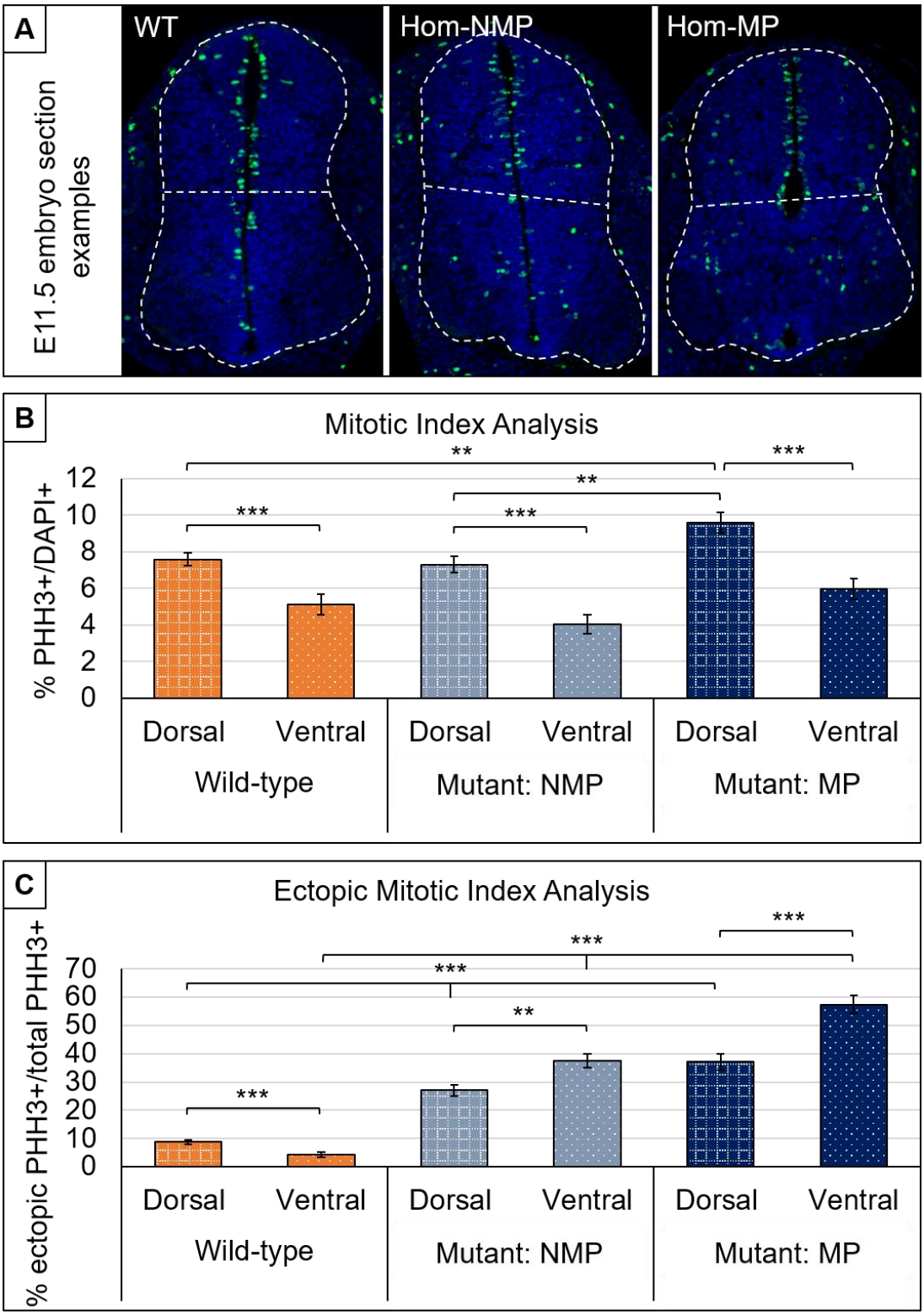

Figure 4-8: Ventral and dorsal neural tube: mitotic and ectopic mitotic index analysis

(**A**) Section examples of E11.5 wild-type (WT), mutant: non-macroscopically phenotypic (Hom-NMP), and mutant: macroscopically phenotypic (Hom-MP) embryos. Dashed lines represent neural tube border and half-way section line separates ventral and dorsal regions. (**B-C**) Dorsal vs ventral analysis of E11.5 WT, mutant: non-macroscopically phenotypic

(NMP), and mutant: macroscopically phenotypic embryos (MP). (**B**) Mitotic index analysis (% PHH3+ cells / DAPI+ cells). All 3 genotype / phenotype combinations had a significantly lower proportion of mitoses in the ventral half compared to the dorsal half. MP mutant embryos had a significantly higher mitotic index in the dorsal region compared to both wild-type and NMP mutant dorsal regions. (**C**) Ectopic proliferation analysis (% ectopic PHH3+ cells / total PHH3+ cells). WT embryos had significantly fewer ectopic mitoses in the ventral portion compared to the dorsal region. In both NMP and MP mutants there was a significantly higher proportion of ectopic mitoses in the ventral half compared to the dorsal half. MP mutant embryos had significantly more ectopic mitoses in both the ventral and dorsal halves compared to the corresponding half in NMP mutants and wild-types. NMP mutants had significantly more ectopic mitoses in both halves compared to the wild-type. **Statistical analysis**: One-way ANOVA showed significant variation in dorsal half mitotic index and both dorsal and ventral half ectopic mitotic index between the 3 genotype / phenotype combinations ($p \leq 0.05$). No significant variation was found in ventral half mitotic index analysis. Post-hoc pair-wise tests of NMP mutant / MP mutant / wild-type: *** $p \leq 0.001$, ** $p \leq 0.01$; Student's t-tests. Tests of dorsal vs ventral regions for each embryo set: *** $p \leq 0.001$, ** $p \leq 0.01$; Student's t-tests. Error bars: standard error. n = 3 embryos per genotype/phenotype group, 3-4 slides per embryo, 4-5 sections per slide. Number of total mitoses/ectopic mitoses counted: Wild-type dorsal: 1075/98, wild-type ventral: 665/35. Mutant: NHM dorsal: 1226/339, mutant: NHM ventral: 713/273. Mutant: MP dorsal: 1809/701, mutant: MP ventral: 1061/612.

Total mitotic index analysis showed that within the wild-type and both mutant types, the proportion of PHH3+ / DAPI+ cells was reduced in the ventral half of the neural tube, compared to the dorsal region of the same section (Figure 4-8, B). This was unsurprising due to the presence of post-mitotic, differentiating motor neurons in the ventro-lateral regions of the neural tube at this time point (see asterisks in Figure 4-5, K). When comparing the 3 embryo sets, mitosis was increased in the dorsal region of macroscopically phenotypic mutants compared to the dorsal region of wild-type embryos (Figure 4-8, B), whereas no significant difference was found between ventral regions. This suggests it is the dorsal region only, that corresponds to the total increase in mitoses in MP mutants seen previously (Figure 4-6, E).

Ectopic proliferation analysis showed significantly reduced ectopic PHH3+ / total PHH3+ cells in the ventral region of wild-type embryos compared to the corresponding dorsal region (Figure 4-8, C). This was reversed in both mutants with and without a phenotype, where the ventral region had a higher proportion of ectopic mitoses compared to the dorsal region (Figure 4-8, C). When comparing between embryo sets, a significant increase in ectopic mitoses in both dorsal and ventral regions was found in macroscopically phenotypic and non-macroscopically phenotypic mutants compared to the

corresponding region in wild-type embryos, with the largest increase seen in MP mutants. Therefore, the significant increase in the overall proportion of ectopic mitoses reported earlier (Figure 4-6, F), was not restricted to either dorsal or ventral regions of the neural tube.

To expand proliferation analysis further, a SOX2 antibody was used to assess the proportion of progenitor cells in the neuroepithelium of E11.5 ASPP2 embryos. For this, image analysis was based on a staining threshold combined with automated cell counting (see 2.5.1, Table 2-4, Figure 2-4).

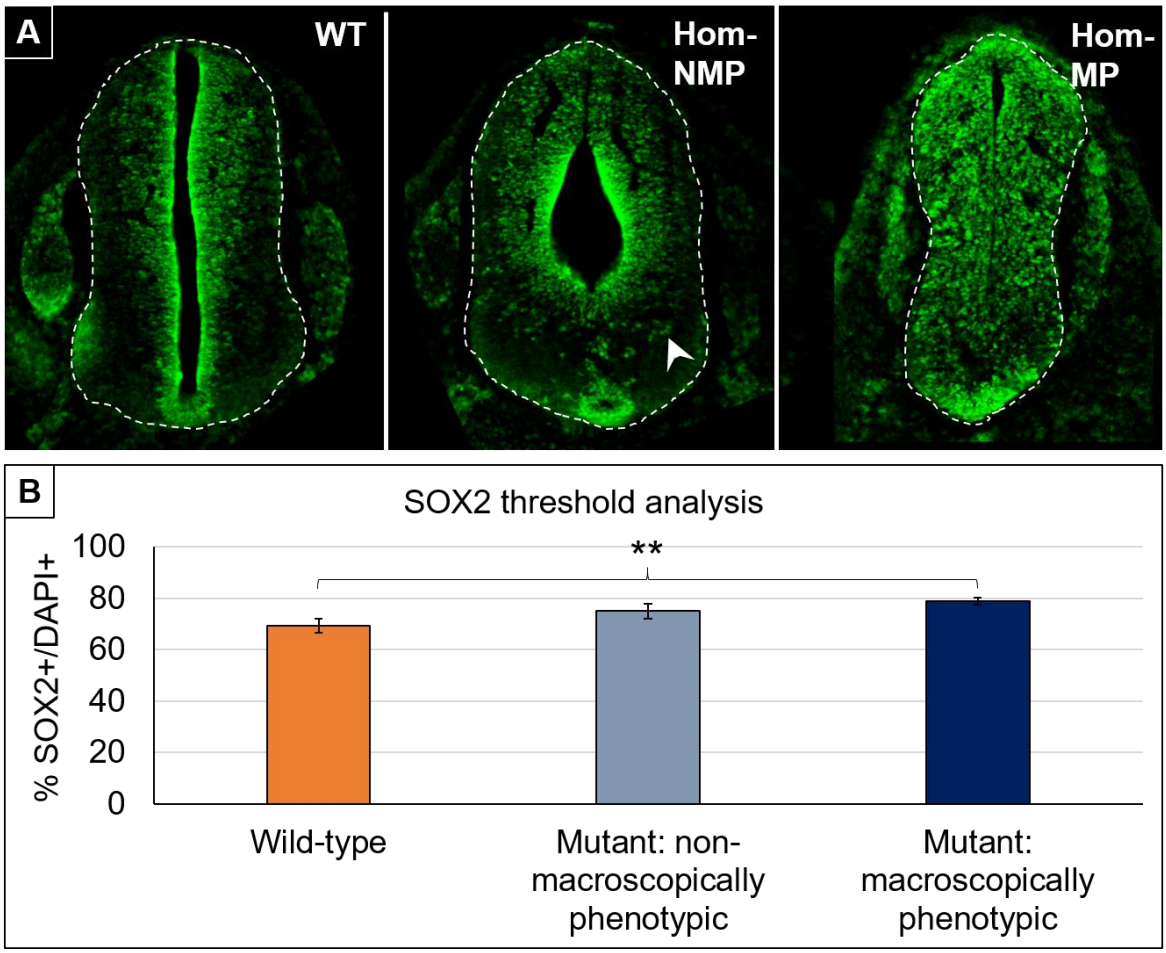

Figure 4-9: SOX2 threshold analysis

(**A**) Example images of E11.5 wild-type (WT), non-macroscopically phenotypic mutant (Hom-NMP) and macroscopically phenotypic mutant (Hom-MP) embryos immunostained for SOX2 (DAPI staining channel removed in these images). White dashed line demarcates neural tube border. SOX2 staining in the WT appeared strongest around the lumen, with little staining found laterally. SOX2 staining in Hom-NMP embryos remained strong around the lumen(s) yet had a more scattered appearance with positive cells appearing in ventro-lateral positions (see arrow head in Hom-NMP image). SOX2 staining in MP mutants appeared

more widespread throughout the neuroepithelium. (**B**) SOX2 staining quantification using threshold analysis combined with cell counting analysis. %SOX2+ cells / DAPI+ cells did not differ significantly between wild-type and non-macroscopically phenotypic mutants. Macroscopically phenotypic mutants had a significantly higher proportion of SOX2+ cells compared to wild-type embryos. There was no difference between MP and NMP mutants. **Statistical analysis**: One-way ANOVA showed significant variation in SOX2 staining between the 3 genotype / phenotype combinations ($p \leq 0.05$). Post-hoc pair-wise tests of NMP mutant / MP mutant / wild-type: ** $p \leq 0.01$; Student's t-tests. Error bars: standard error. n = 3 embryos per genotype/phenotype group, 3-4 slides per embryo, 4-5 sections per slide. Nuclei count/SOX2+ count: wild-type: 21948/14640, mutant: NHM: 21008/15373, mutant: MP: 21424/16841.

SOX2 is a transcription factor, known to be expressed in neural progenitor populations within the central nervous system (Hutton and Pevny, 2011). It was used here to assess a wider population of proliferating, immature cells within the neuroepithelium. Observations of wild-type embryos showed densely populated SOX2 positive cells lining the border of the lumen. In the dorsal region of the neural tube, positive cells reached more laterally within the neuroepithelium but were rarely found at the basal border (Figure 4-9, A, WT). In non-macroscopically phenotypic mutant embryos, although SOX2 staining remained strongest around the apical border, it also appeared more disordered and scattered throughout the neuroepithelium. Positive cells were even found in ventro-lateral positions where motor neuron differentiation is normally occurring (see arrowhead in Figure 4-9, A, Hom-NMP). SOX2 staining in macroscopically phenotypic mutants appeared to be present across the entire mid-lateral width of the neural tube in dorsal and middle regions. Staining was not strongest around the lumen border, as in the wild-type, but instead was equally spread out over a wide proportion of the neuroepithelium (Figure 4-9, A, Hom+).

To quantify these observations, Shanbhag threshold analysis of SOX2 staining was combined with automated cell counting of DAPI staining, to give % SOX2+ cells / DAPI+ cells (see 2.5.1). It was found that there was no significant difference between NMP mutant SOX2 staining compared to the wild-type, nor between mutants. However, there was a significantly higher proportion of SOX2 positive cells (~79%) within the neuroepithelium of MP mutants, compared to wild-type embryos (~69%) (Figure 4-9, B).

In conclusion, cell proliferation and progenitor cell population assessment suggested considerable disruption in *Trp53bp2*$^{\Delta 3/\Delta 3}$ embryo neuroepithelial cells, both quantitatively, and qualitatively (distribution of mitoses and progenitor cells). Mitotic index of the neural tube was shown to be significantly increased in macroscopically phenotypic mutants at all 3 gestational ages, as well as in NMP E13.5 embryos (Figure 4-6, B, E, H), and the most striking change in both MP and NMP ASPP2 mutant embryos was the increase in ectopic mitoses, at least partially irrespective of lumen circumference (Figure 4-7). The next investigation followed what became of cells in *Trp53bp2*$^{\Delta 3/\Delta 3}$ embryos when they left the cell cycle and started to differentiate.

4.2.4 Cell cycle exit is unchanged and neuronal differentiation is disrupted in *Trp53bp2*$^{\Delta 3/\Delta 3}$ embryos

Cell cycle exit occurs when cells stop dividing and begin to differentiate. To assess this process, EdU, a modified thymidine analogue, can be combined with Ki67 staining to calculate the proportion of cells leaving the cell cycle, as follows: EdU, when injected intraperitoneally into a pregnant dam, is incorporated into cells during DNA synthesis (S-phase) within the embryo (the ‘pulse’); after a pre-determined period of time (the ‘chase’), embryos from the injected pregnant dam are collected, fixed, and stained for Ki67, a marker that labels cells in any phase of the cell cycle; cells originally labelled with EdU (therefore within the cell cycle upon the point of injection) can now be assessed as to whether they, and their progeny, have remained in the cell cycle up to the time of collection. This technique has been used in many studies previously: e.g. to assess cell cycle exit in the developing cerebral cortex, using an alternative thymidine analogue, BrdU (Woodhead et al., 2006).

E11.5 embryo sections stained for EdU / Ki67 / DAPI were analysed, firstly, for % EdU+ cells / DAPI+ cells, to assess the proportion of cells in S phase at the point of injection, and secondly, for % Ki67+ & EdU+ cells / EdU+ cells, to assess the proportion of cells that re-enter and remain in the cell cycle during

the time period prior to embryo collection. For both analyses, 2 different time points were assessed: 6 and 24 h after EdU injection. Both sets were collected at the same time on embryonic day 11.5, to ensure matching of gestational ages at the end-point for observational comparisons.

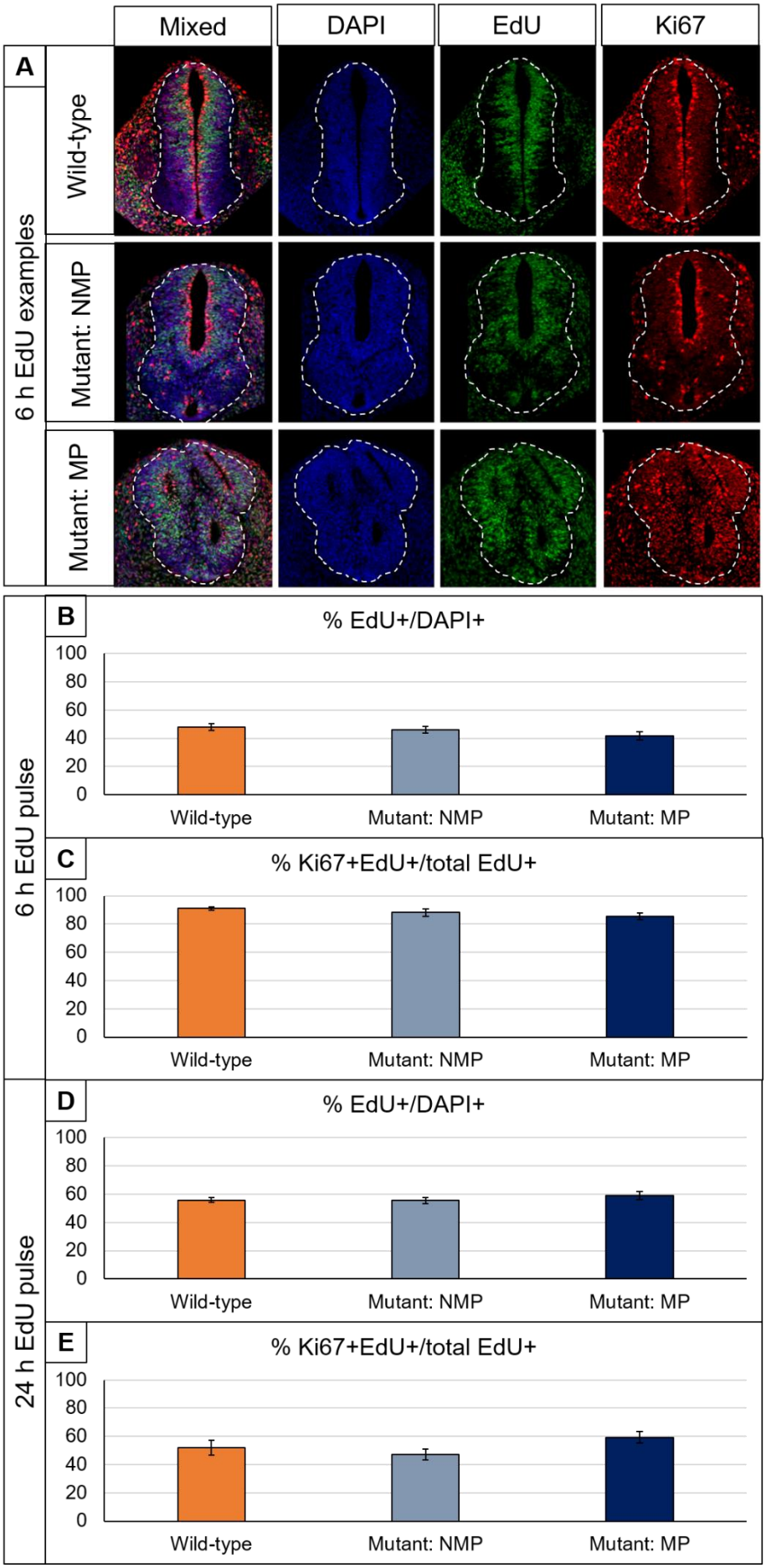
A
6 h EdU examples
Mixed
DAPI
EdU
Ki67
Wild-type
Mutant: NMP
Mutant: MP
6 h EdU pulse
B
% EdU+/DAPI+
C
% Ki67+EdU+/total EdU+
24 h EdU pulse
D
% EdU+/DAPI+
E
% Ki67+EdU+/total EdU+
100
80
60
40
20
0
Wild-type
Mutant: NMP
Mutant: MP

Figure 4-10: EdU and Ki67 staining analysis

(**A**) Example image panel of 6 h EdU and Ki67-stained sections from E11.5 wild-type, non-macroscopically phenotypic (Mutant: NMP) and macroscopically phenotypic mutant embryos (Mutant: MP). Mixed = composite image. Blue = DAPI. Green = EdU. Red = Ki67. Note: Ki67 staining intensities vary depending on cell cycle stage, e.g. mitotic cells are brightest but not exclusively labelled. White dashed line demarcates neural tube border. On first observations, EdU staining appears more disorganised in both mutants compared to the wild-type. Ki67 appears to closely match the EdU staining in all 3 embryos sets. (**B**) 6 h EdU pulse: % EdU+ cells / DAPI+ cells. No significant difference was found in the proportion of EdU positive cells between the three embryo sets. % EdU+ cells ranged ~40-50%. (**C**) 6 h EdU pulse: % Ki67+EdU+ cells / total EdU+ cells. No significant difference was found in the proportion of double-labelled cells (out of total EdU positive cells) between either mutant group and wild-types. % Ki67+EdU+ cells ranged ~85-90% total EdU+ cells. (**D**) 24 h EdU pulse: % EdU+ cells / DAPI+ cells. No significant difference was found in the proportion of total cells that were EdU positive between any embryo group type. % EdU+ cells ranged ~50-60%. (**E**) 24 h EdU pulse: % Ki67+EdU+ cells / total EdU+ cells. No significant difference was found in the proportion of double-labelled cells (out of EdU positive cells) between either mutant group and wild-types. % Ki67+EdU+ cells ranged ~45-60% total EdU+ cells. **Statistical analysis**: One-way ANOVA showed no significant variation in % EdU or % Ki67+EdU staining between the 3 genotype / phenotype combinations. Error bars: standard error. n = 3 embryos per genotype/phenotype group. Number of sections analysed: wild-type: 6h: 35, 24h: 23. Mutant: NMP: 6h: 41, 24h: 22. Mutant: MP: 6h: 37, 24h: 25.

Figure 4-10, A, shows example images of E11.5 embryo sections following a 6 h time chase, between EdU injection and embryo collection. EdU staining in wild-type showed positive cells around the lumenal border and covering ~1/2 - 2/3 of the neuroepithelium in the dorsal and mid regions. Non-macroscopically phenotypic mutants had a more disorganised and scattered EdU staining. Macroscopically phenotypic mutants had a variable staining which was harder to analyse by eye due to the chaotic neural tube architecture. Ki67 staining is known to be variable in its distribution within the cell depending on cell cycle stage (Galea et al., 2013). Although Ki67 staining intensity was strongest in the mitotic cells, positively labelled cells were found to cover similar areas of the neural tube as the EdU staining, at 6 h. Embryos collected following a 24 h chase period (images not shown), appeared to have a slightly higher coverage of EdU staining in the neuroepithelium, reaching the lateral borders of the neural tube. The staining intensity had reduced compared to 6 h pulse embryos, likely due to EdU dilution with cell divisions.

Quantification was achieved through double threshold analysis for EdU and Ki67 staining, combined with automated DAPI cell counting (see 2.5.1, Figure 2-4). The proportion of EdU+ cells / DAPI+ cells was calculated to assess the percentage of cells at 6 h or 24 h that were the mitotic descendants of cells originally labelled with EdU. No significant difference was seen after a 6 h EdU chase, or a 24 h EdU chase, across the three embryo sets (Figure 4-10, B, D). Between the two time points, the % EdU+ cells increased by ~10% (~40-50% after 6h pulse, ~50-60% after 24h pulse). Furthermore, there was no significant difference found between wild-type, macroscopically phenotypic and non-macroscopically phenotypic mutants in the proportion of cells that had stayed within the cell cycle between point of EdU injection and embryo collection (% Ki67+ EdU+ / EdU+). Following the 6 h EdU pulse, % double-labelled cells ranged between ~85-90% of EdU+ cells and after the 24 h pulse, ~45-60% EdU+ cells were also Ki67+. This reduction in double-labelled cells from 6 h to 24 h was expected due to increased cell cycle exit over time.

The lack of a significant difference in cell cycle exit between wild-type and mutant E11.5 ASPP2 embryos was surprising, considering the previous finding that both proliferation (total PHH3 staining), and progenitor cell populations (SOX2 staining) are increased in macroscopically phenotypic mutants (0). It was proposed that if cell cycle exit remains unchanged, perhaps cell differentiation is also disrupted in the neuroepithelium of *Trp53bp2*$^{\Delta 3/\Delta 3}$ embryos. To explore this theory, neuronal differentiation was assessed in E11.5 embryos, by immunostaining for the neuron-specific class III β-tubulin, TUJ1. E11.5 embryos only were assessed for TUJ1, due to little / no neuron differentiation seen in E9.5 embryos, and almost entire differentiation of the neural tube by E13.5 (data not shown).

TUJ1 analysis was based on pixel intensity levels throughout the neural tube, using a macro in ImageJ to calculate intensity values for dorsal, middle, and ventral percentile bands (see 2.5.1, Figure 2-5). Data values for each band were then divided into three sets: two basal and one apical portion for each percentile measured (Figure 4-11). This allowed TUJ1 intensity of 6 distinct

neural tube regions (basal regions combined) to be compared both within and between wild-type and mutant ASPP2 embryo sets.

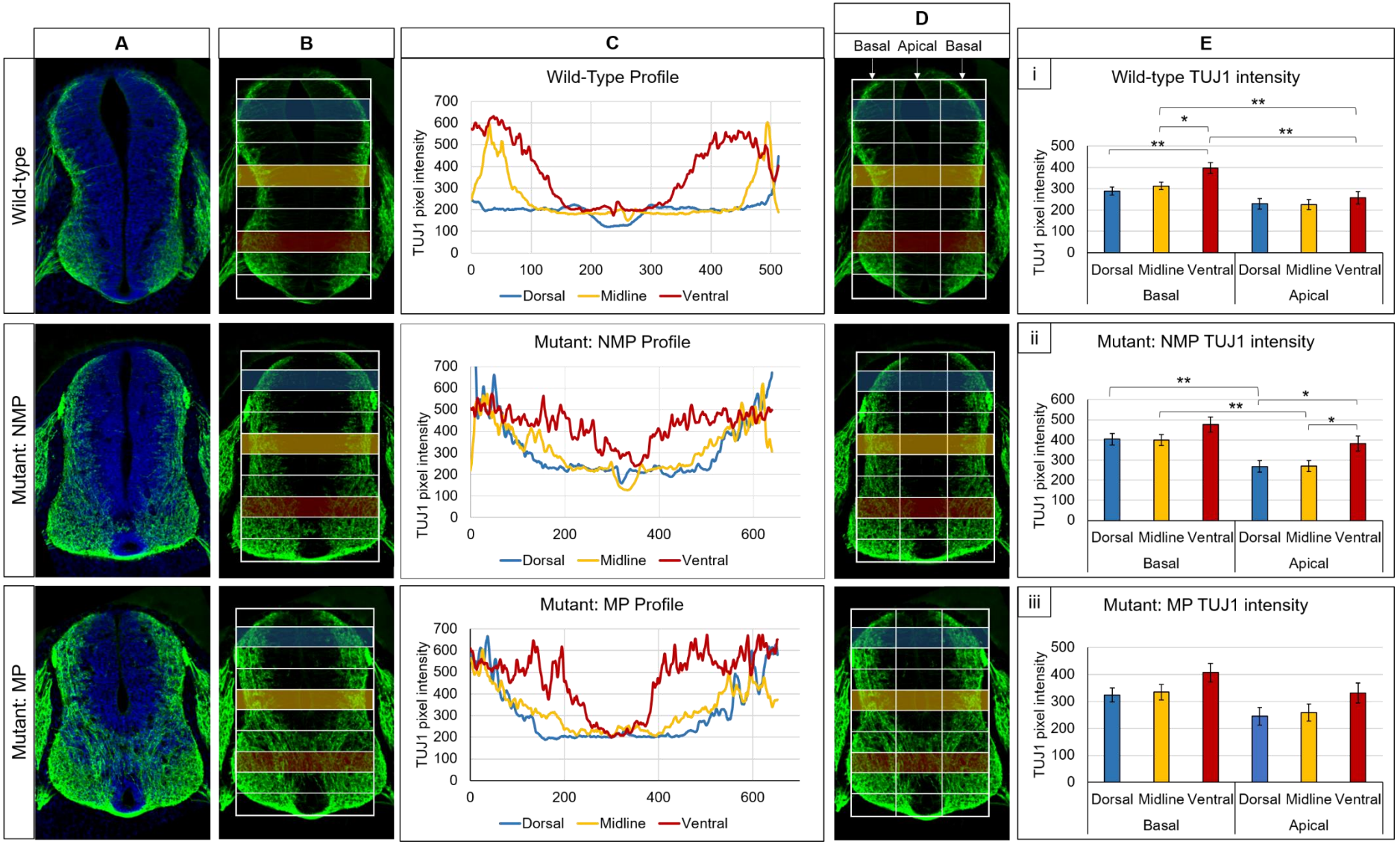
A
B
C
D
E
Wild-type
Mutant: NMP
Mutant: MP
Basal Apical Basal
Wild-Type Profile
Mutant: NMP Profile
Mutant: MP Profile
TUJ1 pixel intensity
Dorsal
Midline
Ventral
i
Wild-type TUJ1 intensity
ii
Mutant: NMP TUJ1 intensity
iii
Mutant: MP TUJ1 intensity
Basal
Apical

Figure 4-11: TUJ1 intensity analysis within wild-type, non-macroscopically phenotypic and macroscopically phenotypic mutant E11.5 embryos

(**A**) Wild-type, non-macroscopically phenotypic and macroscopically phenotypic mutant examples of TUJ1 staining in the neural tube. TUJ1 = green. DAPI = blue. TUJ1 staining appears more apically in ventral regions and less confined to the ventro-lateral aspects in both mutants compared to the wild-type. (**B**) Examples of percentile bands analysed for TUJ1 staining intensity. Dorsal percentile = blue. Midline percentile = yellow. Ventral percentile = red. (**C**) Intensity profiles for adjacent images in B. Dorsal percentile profile = blue. Midline percentile profile = yellow. Ventral percentile profile = red. X-axis is distance (pixels) across width of the neural tube, from one lateral aspect of the custom ROI, to the other. Y-axis is TUJ1 pixel intensity values. All 3 profiles show a decreased expression close to the middle of the plotted profile and raised intensities at either extreme of the pixel distance measured. The ventral TUJ1 profile reaches high intensity for the furthest distance across the neural tube, compared to dorsal and midline bands, in all 3 embryo examples. In both mutant examples, the intensity profile is more variable across the ROI, and the ventral intensity profile appears to reach more medially, in relation to the neural tube, compared to the wild-type profile. (**D**) Diagrammatic examples of percentile bands with further divisions into 2X basal and 1x apical portion for average intensity analysis (actual portion dividing was completed using intensity data values, not original image). (**E**) Comparisons between basal and apical portion TUJ1 intensity values within the dorsal, midline and ventral percentile bands. (**i**) Wild-type. TUJ1 intensity in the basal portions of the ventral band was significantly increased in comparison to the basal portions of the midline and dorsal bands. There was no significant difference between apical portions. Midline and ventral basal intensities were significantly higher than in the corresponding apical portions. (**ii**) Mutant: NMP. There was no significant difference between basal portions. TUJ1 intensity in the apical portions of the ventral band was significantly increased in comparison to the apical portions of the midline and dorsal bands. Dorsal and midline basal intensities were significantly higher than in the corresponding apical portion. (**iii**) Mutant: MP. There was no significant difference between basal portions or between apical portions. No significant difference between apical and basal portions within the same percentile bands. **Statistical analysis**: One-way ANOVA showed significant variation in wild-type basal portions, total wild-type values, NMP mutant apical portions, NMP total intensity values and MP mutant total intensity values. Post-hoc tests of dorsal vs midline vs ventral (basal / apical portions), and basal vs apical (dorsal, midline and ventral portions) within embryo subsets. ** $p \leq 0.01$, * $p \leq 0.05$; Student's t-tests. Error bars: standard error. n = 3 embryos per genotype/phenotype group. Number of sections analysed for pixel intensity per portion: wild-type: 17, mutant: NMP: 17. mutant: MP: 16.

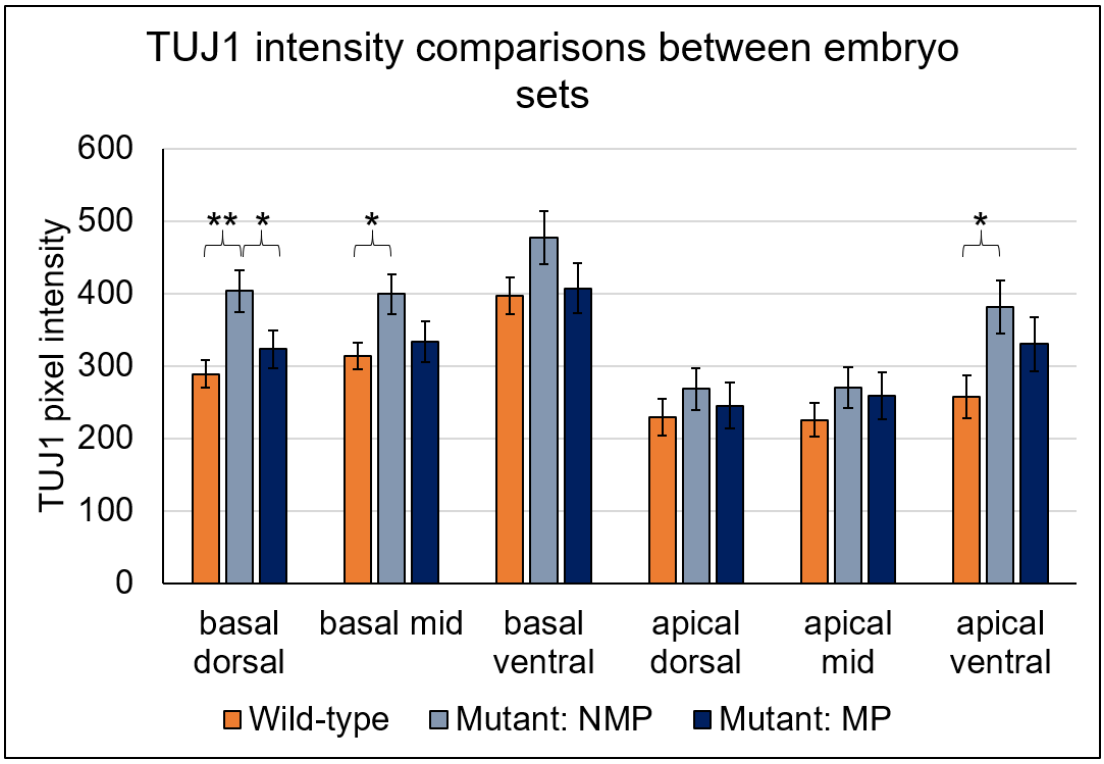

Figure 4-12: TUJ1 intensity analysis between wild-type and mutant embryos

Graph showing TUJ1 intensity in each embryo set: wild-type, mutant: non-macroscopically phenotypic (NMP) and mutant: macroscopically phenotypic (MP), for each region analysed: basal dorsal / mid / ventral, apical dorsal / mid / ventral. Mutant: NMP TUJ1 intensity was significantly increased in basal dorsal, basal mid and apical ventral regions, compared to the wild-type. **Statistical analysis**: One-way ANOVA showed significant variation in basal dorsal, basal mid and apical ventral regions between total wild-type, mutant: NMP and MP TUJ1 intensity values. Post-hoc pair-wise tests of NMP mutant / MP mutant / wild-type: ** $p \leq 0.01$, * $p \leq 0.05$; Student's t-tests. Error bars: standard error. n = 3 embryos per genotype/phenotype group. Number of sections analysed for pixel intensity per portion: wild-type: 17, mutant: NMP: 17. mutant: MP: 16.

Firstly, it was important to assess regional neuronal differentiation in the neural tube within each embryo subset. TUJ1 is present in newly generated post-mitotic neurons as well as in fully differentiated neurons. Initial observations showed, as expected, only basally-located differentiation in dorsal and mid neural tube regions, and the most extensive differentiation in the ventro-lateral / basal regions of the wild-type neural tube (Figure 4-11, A), where motor neuron differentiation is occurring (see asterisks, Figure 4-5, K). The immediately apparent difference in mutant *Trp53bp2*$^{\Delta 3/\Delta 3}$ embryos (as shown in the two representative images, Figure 4-11, A) was the increase in

TUJ1 staining in the ventro-apical region, often where the lumen was no longer present.

To assess the differentiation profile across the neural tube, a dorsal, mid, and ventral percentile band was assessed (Figure 4-11, B). Intensity profiles showed a dip in TUJ1 intensity in the centre of the neural tube width measured, corresponding to the vertical dorso-ventral line where the lumen was often situated. A rise in intensity was seen at either end of the profile, corresponding to the basal differentiation in the neural tube. The ventral TUJ1 profile tended to reach the highest intensities, and the intensity was sustained across a wider proportion of the neural tube compared to the dorsal and mid percentile bands, in all 3 embryo subsets (Figure 4-11, C). The most obvious difference observed between wild-type and mutant profiles was the increase in variation and a more jagged linear profile for every percentile in both non-macroscopically phenotypic and macroscopically phenotypic mutant profiles compared to the wild-type. The ventral percentile profile in mutant embryos also appeared to stay in the high intensities further towards the centre of the neural tube width, compared to wild-type profiles (Figure 4-11,C), emulating the increase in TUJ1 staining seen in the ventro-apical region of the mutant neural tube (Figure 4-11, A).

To quantify these observations, average intensity values were taken by equally dividing the data into three sections. This allowed the percentile bands to be ‘split’ into two basal, and one apical portion (visualised in Figure 4-11, D). In wild-type embryos, there was a significantly higher average TUJ1 intensity in mid and ventral percentile basal portions compared to the corresponding apical portions. Between the percentiles in the basal portions, the ventral band was significantly increased compared to both mid and dorsal regions (Figure 4-11, E, i). Again, this supports the observation of increased differentiation in the motor neuron regions. There was no difference between apical percentile regions in the wild-type. In non-macroscopically phenotypic mutant embryos, dorsal and mid basal portions were significantly higher than the corresponding apical percentile region, however, ventral basal regions were no longer significantly higher than ventral apical regions. Furthermore,

within the apical regions, the ventral percentile showed a significant increase in TUJ1 intensity compared to mid and dorsal percentiles (Figure 4-11, E, ii). This reflects the increase in ventro-apical TUJ1 staining seen in the non-macroscopically phenotypic mutant neural tube (Figure 4-11, A). Macroscopically phenotypic mutant embryos showed overall significance in total intensity data analysis (one-way ANOVA) but interestingly did not prove significantly different following pair-wise comparisons between apical and basal portions within the same percentile or percentile comparisons between apical / basal regions (Figure 4-11, E, iii).

Following histological comparisons within each embryo subset, the regional TUJ1 intensity values were compared across wild-type, non-macroscopically phenotypic and macroscopically phenotypic mutants. NMP mutants were shown to have a significantly higher average TUJ1 intensity, compared to both wild-type and MP embryos, in the basal dorsal region. Basal mid and apical ventral regions were also significantly increased in comparison to wild-type embryos only. There was no significant difference seen in MP mutants compared to wild-type (Figure 4-12). This is likely due to the variable neuroepithelial architecture of MP mutants, for example ectopic lumens and altered neural tube shape, being less well suited to the percentile model used here.

Neuronal subtypes originate from an undifferentiated neuroepithelium that is progressively divided into dorso-ventral progenitor domains by transcription factors such as PAX3, PAX6 and NKX6.1. Given the progressive loss of normal neuroepithelial architecture in ASPP2 mutant embryos, it was important to determine whether this was accompanied by alterations in dorso-ventral neural tube specification. To investigate this, neural tube sections were immuno-stained for each of the aforementioned transcription factors (Figure 4-13).

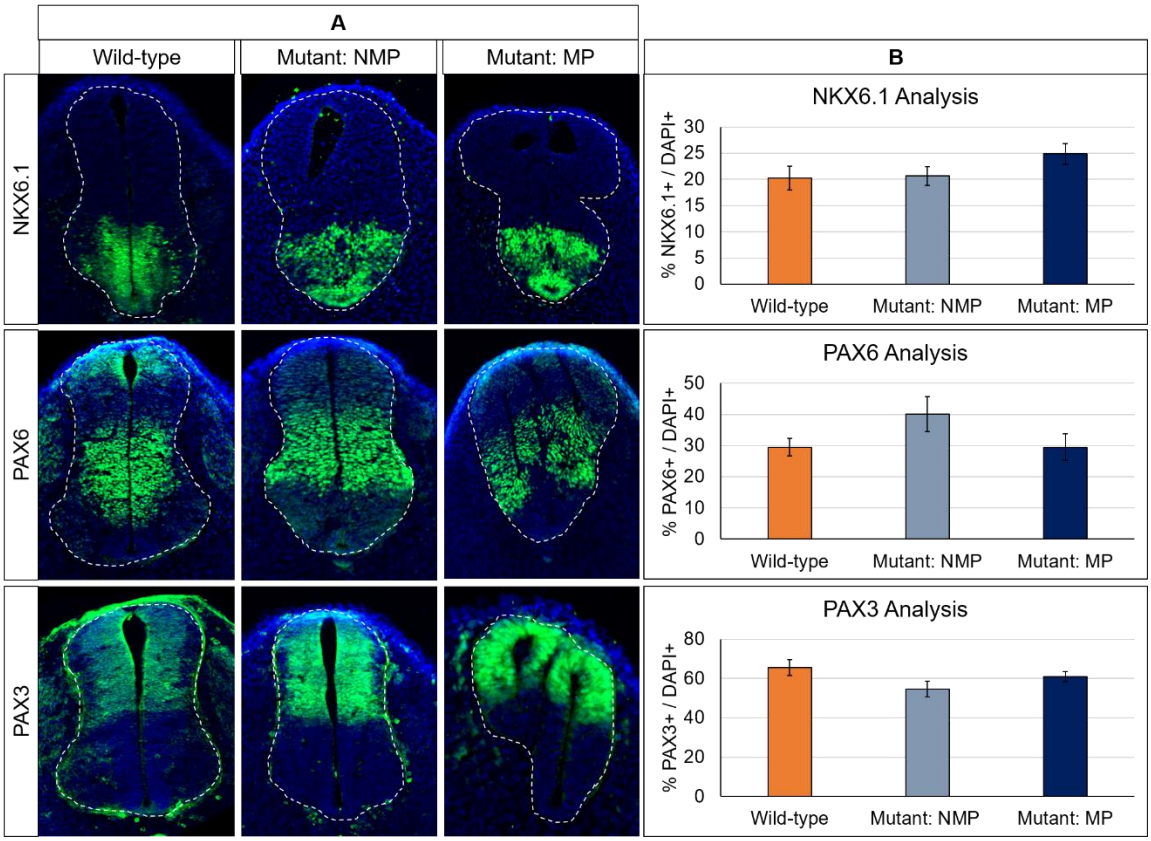

Figure 4-13: NKX6.1, PAX6 and PAX3 analysis

(**A**) Example images of wild-type, and mutant (non-macroscopically phenotypic (NMP) and macroscopically phenotypic (MP)) embryos, immunostained for NKX6.1, PAX6 and PAX3. NKX6.1 is restricted to the ventral portion of the neural tube in all embryo subsets. A more disordered appearance of NKX6.1 staining is seen in both mutants compared to wild-type. PAX6 staining shows positive cells that span the mid-portion of the dorso-ventral axis in all embryo subsets. PAX6+ cells reach further basally / laterally within the neuroepithelium of both mutant types compared to wild-type. PAX3 labels the dorsal region of the neural tube in all embryo sets. (**B**) Quantification of NKX6.1, PAX6 and PAX3 staining using threshold analysis combined with automated DAPI cell counting. No significant difference was found between wild-type, NMP and MP mutant embryos in % NKX6.1, PAX6 or PAX3 positive cells out of total cells in neural tube (DAPI). **Statistical analysis**: One-way ANOVA showed no significant variation in % NKX6.1 / PAX6 / PAX3 staining between the 3 genotype / phenotype combinations. Error bars: standard error. n = 3 embryos per genotype/phenotype group, 3-4 slides per embryo, 4-5 sections per slide. Total nuclei/NKX6.1+ count: wild-type: 22247/4377, mutant: NMP: 15919/2974, mutant: MP: 19846/3963. Total nuclei/PAX6+ count: wild-type: 11778/3302, mutant: NMP: 6588/2347, mutant: MP: 11709/3178. Total nuclei/PAX3+ count: wild-type: 11417/7574, mutant: NMP: 6401/3592, mutant: MP: 16318/9969.

The transcription factor analysis revealed that there is striking preservation of dorso-ventral expression domains despite the radical alterations in neuroepithelial structure in the mutant embryos. NKX6.1 is expressed by progenitor cells in the ventral neural tube (Sander et al., 2000). This was

shown to be true in both wild-type embryos as well as *Trp53bp2*$^{\Delta 3/\Delta 3}$ embryos (Figure 4-13, A). Interestingly, NKX6.1 positive cells in both mutant embryo types appeared more disordered, particularly in the apical region, where gaps in the staining often occurred. PAX6 is known to be expressed in the intermediate neural tube (Timmer et al., 2002), and PAX6 protein was similarly located within the mid-portion of the neural tube of wild-type and mutant embryos. Strikingly, this occurred even within neural tubes that contained multiple lumens (Figure 4-13, A, mutant: MP image). Slight differences were seen in the apical-basal distribution of PAX6: positive cells appeared to reach the basal aspects of the neural tube in both mutants, compared to the wild-type, where few cells reached the lateral borders (Figure 4-13, A). The expression of PAX3 is predominantly in the dorsal spinal cord (Mansouri and Gruss, 1998), as was seen in both wild-type and *Trp53bp2*$^{\Delta 3/\Delta 3}$ embryos, even where multiple lumens occurred.

All 3 neuronal progenitor marker expression patterns were quantified using a threshold analysis combined with automated cell counting using DAPI staining (2.5.1, Table 2-4). No statistically significant difference was found in the percentage values for NKX6.1, PAX6 or PAX3 out of total cell count, between wild-type, non-macroscopically phenotypic mutants or macroscopically phenotypic mutant embryos (Figure 4-13, B).

In summary, there was no change in the proportion of S-phase cells or cell cycle exit in *Trp53bp2*$^{\Delta 3/\Delta 3}$ embryos (Figure 4-10), and no quantifiable disruption in pre-determined neuronal transcription factor expression throughout the neural tube (Figure 4-13). Despite this, neuron differentiation was disrupted in specific areas of the neural tube, predominantly the ventral apical region, where neurons appeared to cross the midline (Figure 4-11).

4.3 Discussion

4.3.1 *Trp53bp2*$^{\Delta 3/\Delta 3}$ embryos exhibit a progressive phenotype leading to reopening of the neural tube

The aim of this chapter was to thoroughly investigate neural tube development in *ASPP2* mutant embryos, focusing on the spinal region. The complex phenotype seen in *Trp53bp2*$^{\Delta 3/\Delta 3}$ embryos develops with gestational age. Both *Trp53bp2*$^{\Delta 3/\Delta 3}$ embryos with *and without* a macroscopic phenotype have histological abnormalities of varying severity. Together, this suggests that the mutation in question is both fully penetrant, despite macroscopic appearances, and results in a progressive phenotype which culminates in neural tube reopening.

Worsening of the macroscopic phenotype

Open neural tube frequency increased by 42% in macroscopically phenotypic mutants between stages E9.5 and E13.5, paralleled by a decrease in closed NTDs (Table 4-1). Severity of the open NTDs also worsened, from an open cranial region and upper NT in E9.5 embryos, to craniorachischisis in several E13.5 embryos (Figure 4-4, B, H). Most mouse mutants with NTDs help to identify genes required for neural tube closure (Harris and Juriloff, 2010), however, ASPP2 is not expressed at E8.5 (Sottocornola et al., 2010), the time point at which closure of the neural tube is initiated. Therefore, the increased open neural tube frequency with gestational age seen in *Trp53bp2*$^{\Delta 3/\Delta 3}$ embryos is instead indicative of neural tube re-opening. Surgical re-opening of the neural tube has been shown to lead to NTDs in the rostro-caudal axis (Campbell and Sohal, 1990), and cytotoxic agents have been shown to cause reopening in embryo culture, or following maternal exposure (Schmid et al., 1985, Padmanabhan, 1990, Padmanabhan, 1984). However, only one previously reported genetic alteration in mice has been shown to cause small post-neurulation openings in the midbrain (Zhu et al., 2015). *Trp53bp2*$^{\Delta 3/\Delta 3}$ embryos, therefore, are unique in their variable and severe NTD phenotype as a result of neural tube re-opening.

In humans, multiple NTDs are occasionally seen in the same individual (Ahmad et al., 2008, Mahalik et al., 2013), a phenotype similar to E13.5 *Trp53bp2*$^{\Delta 3/\Delta 3}$ embryos, and hard to explain by failure of neural tube closure at a particular initiation site or neuropore. Furthermore, re-opening has been proposed as a possible mechanism for NTDs in the parietal region of human embryos (Smith et al., 1993). Due to the many unknowns surrounding the mechanistic origins of NTDs, it may be that *Trp53bp2*$^{\Delta 3/\Delta 3}$ embryos could provide an alternative model to be investigated further in relation to the origin of a subset of human NTDs.

Worsening of the histological phenotype

Given that a significant proportion (40-50%) of homozygotes at all 3 stages did not exhibit a macroscopic phenotype, it was decided to include both 'non-macroscopically phenotypic' (NMP) and 'macroscopically phenotypic' (MP) mutants in analysis of the histological architecture of the neural tube, and immuno-staining of specific cell types. Histological abnormalities were found in 1/3 NMP E9.5 and 3/3 NMP E11.5 and E13.5 mutant embryos. Furthermore, cellular analysis showed that the neural tubes of NMP embryos were significantly different, in comparison to wild-types, in the proportion of mitoses and ectopic mitoses (Figure 4-6), lumen circumference (Figure 4-7), and distribution of neural differentiation (Figure 4-12). This discounted the possibility of partial penetrance and instead suggested NMP mutants are less severely affected than MP mutants, and perhaps are simply at an earlier stage of phenotypic progression. Cellular characteristics in mutant embryos with a macroscopic phenotype were even more disrupted, showing significant differences in the proportion of mitoses and ectopic mitoses (Figure 4-6) and lumen circumference (Figure 4-7), compared to NMP embryos, further supporting the progressive phenotype theory.

Architecturally, worsening severity can be seen in the neural tubes of E11.5 and E13.5 embryos. Even within a single mutant embryo, changes can be seen in neural tube organisation in different sections taken from its dorsal axis. Figure 4-14 represents a model of phenotypic progression starting from

a neural tube with a single lumen spanning the majority of the midline neuroepithelium in the dorso-ventral axis (E11.5), which gradually gets occluded by the neuroepithelium crossing the midline. Multiple lumens arise, perhaps to compensate for loss of the midline lumen. Eventually neural tube reopening occurs, perhaps due to increased hydrostatic pressure or opening of a dorsally-situated lumen (as in Figure 4-14, vii).

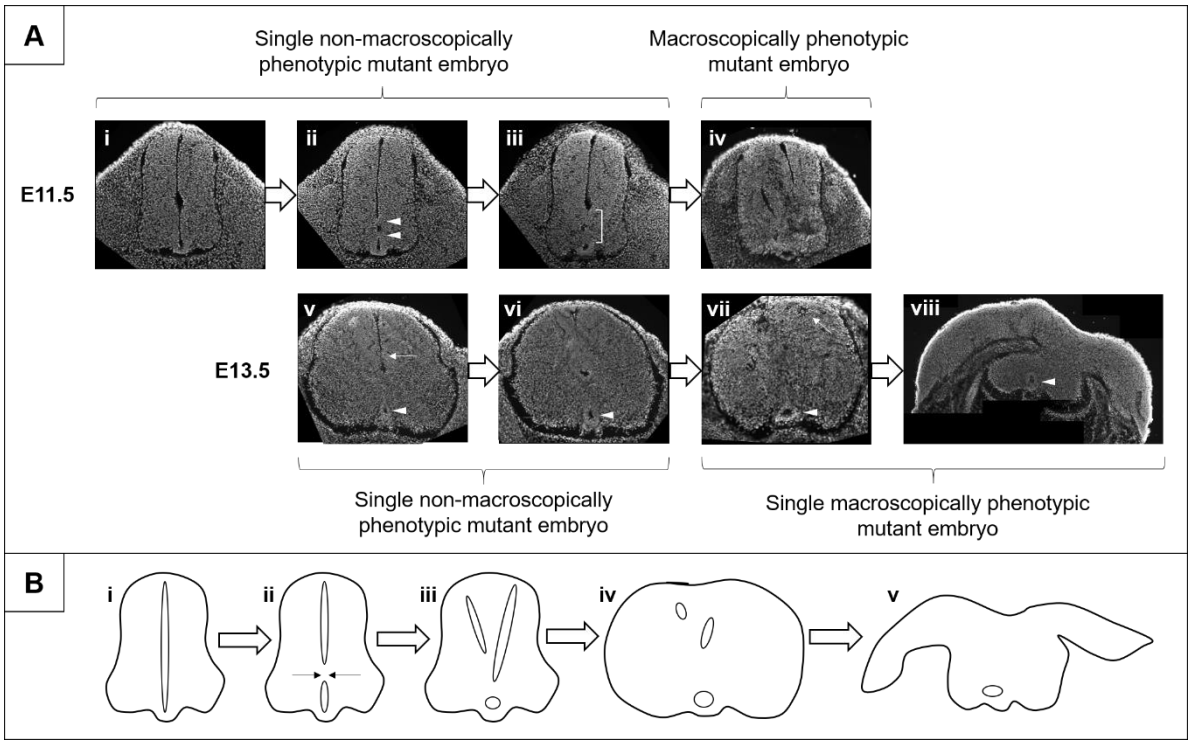

Figure 4-14: Examples and model of phenotypic progression in *Trp53bp2*$^{\Delta 3/\Delta 3}$ embryos

A) E11.5 and E13.5 embryo sections illustrating how the phenotype progresses in mutant embryos. (**i-iv**) Sections taken from E11.5 non-macroscopically phenotypic and macroscopically phenotypic mutant embryos. (**i-iii**) Sections taken from a single NMP mutant embryo showing progression (along the body) from a neural tube with a single lumen (**i**), to neuroepithelial outgrowths in the ventral portion of the neural tube forming 2 'bridges' across the ventral lumen (arrow heads in **ii**), leading to complete midline obliteration of the ventral lumen by neuroepithelium, with the exception of a retained circular lumen just superior to the floor-plate (**iii**). (**iv**) MP mutant embryo showing further disruption in the neuroepithelium, exhibiting 3 distinct lumens. (**v-viii**) Sections taken from E13.5 NMP and MP mutant embryos. Arrowheads show the small circular lumen above the floor-plate that persists in the majority of mutants (**v-vi**) Sections taken from a single NMP mutant embryo: (**v**) neural tube with 2 lumens that already separated by an intersection of neuroepithelium in the ventral half of the neural tube. The dorsal lumen is being occluded by an outgrowth of neuroepithelium (see arrow), (**vi**) neural tube with 3 lumens (ventral, middle, dorsal) separated by large intersections of neuroepithelium crossing the midline. (**vii-viii**) Closed and open sections within the same MP mutant embryo. (**vii**) Closed neural tube with a single lumen located above the floor-plate. A rosette with a small lumen at its centre can be seen in the dorsal neural tube to the right of the midline (see arrow). (**viii**) Open region of the neural tube, displaying a retained lumen above the floor-plate and a large plaque of tissue covering the

dorsal exterior of the embryo. (**B**) Panel showing proposed stages of phenotypic progression in *Trp53bp2*$^{\Delta 3/\Delta 3}$ embryos. (**i**) In the early stages of the phenotype at E11.5, the neural tube resembles the wild-type embryo, with a single lumen lining the majority of the midline neural tube in the dorso-ventral axis. Outgrowth of the neuroepithelium then starts to occur, interrupting the lumen in the ventral half of the neural tube (**ii**). Further disruption and obliteration of the midline lumen by neuroepithelial outgrowths, can result in new lumens forming away from the dorso-ventral midline (**iii**). As development progresses, disorganisation of the neuroepithelium is increased and new lumens appear away from the midline (**iv**). Eventually the neural tube reopens, due to accumulation of disruption in the neuroepithelium (**v**).

The least severe histological defect, proposed as being the first in the sequence of phenotype progression in *Trp53bp2*$^{\Delta 3/\Delta 3}$ mutants at E11.5, is overgrowth in the ventral neuroepithelium, resulting in an intersection or 'bridge' that crosses the midline and divides the original lumen into two parts. This initial ventral location of overgrowth coincides with the strong expression of *Trp53bp2* mRNA in the ventral neuroepithelium (Figure 4-1). Although it was first hypothesised that increased mitosis may lead to this phenomenon, the mitotic index in ventral regions was in fact unchanged between wild-type and mutant embryos. However, the proportion of ectopic mitoses in the ventral region of *Trp53bp2*$^{\Delta 3/\Delta 3}$ embryos, outnumbered that of the dorsal region (Figure 4-8, C) which is the reverse of the wild-type situation. This indicates that (i) ASPP2 is necessary for correct localisation of mitoses at the apical border in the ventral region of the neural tube, (ii) ectopic mitoses predate an increase in total mitosis in the first stages of phenotypic progression (further supported by the rise in ectopic mitoses in E9.5 mutant embryos, where no change in the mitotic index is seen), (iii) overgrowth is not necessarily a result of increased proliferation in the affected region.

Neuroepithelial overgrowth has been seen in other animal models such as the *TSC2* mouse mutant (Rennebeck et al., 1998), '*fog*' spontaneous autosomal recessive mouse mutant (Harris et al., 1997), and overexpression of *FoxG1* in the chick (Ahlgren et al., 2003). In the latter, overgrowth was not always associated with increased mitotic index (Ahlgren et al., 2003). There has also been speculation that neural tube reopening may result from overgrowth and increased ventricular pressure in human NTDs (Smith et al., 1993).

A reduction in lumen circumference, seen in both NMP and MP E11.5 and E13.5 mutants (Figure 4-7), may support the idea of increased ventricular pressure leading to neural tube reopening. The positive pressure of embryonic CSF (eCSF) has been seen to create an expansive force inside the brain ventricles of the chick embryo, allowing brain expansion during development (Desmond and Jacobson, 1977). Furthermore, it has been hypothesised that intracerebral chondroitin sulfate in the eCSF plays a relevant role in the regulation of the expansive process of the brain anlage of rat embryos, due to its special osmotic properties leading to water retention in the brain cavities (Alonso et al., 1999). Aside from its mechanical properties, eCSF has been shown to be required for neuroepithelial precursors to undergo normal rates of cell survival, replication and neurogenesis (Martin et al., 2009). A reduction in lumen circumference, as seen here, infers a reduction in lumenal volume, and therefore a potential increase in hydrostatic pressure within the neural tube. It could also suggest that a reduced number of neuroepithelial cells are coming into contact with eCSF, potentially disrupting their normal cellular behaviours. Taken together, the decrease in lumen circumference may be responsible for worsening of the phenotype, eventually leading to neural tube reopening.

Despite the reduction in total lumen circumference, multiple lumens were often seen in *Trp53bp2*$^{\Delta 3/\Delta 3}$ embryos as the phenotype progressed. Progenitor labelling was able to shed light on the development of these histological abnormalities. The MP mutant examples in Figure 4-13 exhibited multiple lumens, however neural progenitor patterning in the dorso-ventral axis, shown by transcription factors NKX6.1, PAX6 and PAX3, appeared largely unchanged compared to the wild-type (Figure 4-13). This suggests that ectopic lumens in *Trp53bp2*$^{\Delta 3/\Delta 3}$ embryos do not represent entire new neural tubes, as in *Tbx6* mouse mutants (Chapman and Papaioannou, 1998), *Gcm1* ectopic expression mutants (Nait-Oumesmar et al., 2002), and *Shp2* mouse mutants (Saxton and Pawson, 1999). Instead, the phenotype more closely adheres to a polarity-based defect such as in the *par6γb* zebrafish mutant, where disruption of the *Par6* gene exhibits defects in epithelial tissue

development as well as multiple lumens in the neural tube (Munson et al., 2008).

The open neural tube covered by a plaque of tissue, shown in the last stage of (Figure 4-14), could be a result of either gradual exteriorisation of cells through a small opening, or complete rupture of the neural tube. However, even in late stage *Trp53bp2*$^{\Delta 3/\Delta 3}$ embryos, neural tube regions were either closed or open, with no 'mid-way' features to suggest a gradual progression between the two. This suggests that neural tube rupture is the most likely cause of the plaque seen in open neural tube regions, perhaps resulting from reduced lumen circumference leading to increased ventricular pressure, as discussed previously.

The final feature which was continuous throughout, even when a plaque was present, was the small circular lumen retained just superior to the floor plate in mutants (arrow heads in Figure 4-14, A, v-viii). This lumen was typically formed in the earliest stages of phenotypic progression, due to neuroepithelial cells crossing the midline in the ventral neural tube (Figure 4-14, A, ii). Despite continued disruption of the neuroepithelium, this ventral lumen remained open. Floor-plate cells are directly in contact with the notochord at E8.5, and remain influenced by Shh released from the notochord following notochord regression and throughout development (Figure 1-2) (Chamberlain et al., 2008). This may mean that Shh is able to provide a protective mechanism, whereby the ventral lumen is closed off in the early stages, and retained due to continued Shh signalling. Supporting this idea, the notochord was not seen to be malformed or misplaced in mutants (not shown). The early onset of Shh signalling also determines why neural progenitor patterning remained unchanged in *Trp53bp2*$^{\Delta 3/\Delta 3}$ embryos. Shh-dependent patterning is initiated as early as E8.5 (Chamberlain et al., 2008), before the effects of ASPP2 knockdown were observed. Therefore, even in the instance of multiple lumens arising in the neuroepithelium, progenitor patterning is pre-established and therefore unaffected.

In conclusion, the worsening histological neural tube abnormalities, and increased severity of macroscopic abnormalities that have been quantitatively and qualitatively assessed, shed light on the mechanistic processes involved in phenotype progression in *Trp53bp2*$^{\Delta 3/\Delta 3}$ mutants.

4.3.2 Proliferation and differentiation in *Trp53bp2*$^{\Delta 3/\Delta 3}$ embryos

Mitotic index of the neural tube was shown to be significantly increased in macroscopically phenotypic mutants at all 3 gestational ages, as well as in NMP E13.5 embryos (Figure 4-6, B, E, H). This leads to the question of the involvement of ASPP2 in proliferation. ASPP2 is best known for its role in enhancing the DNA binding and transactivation function of p53 on the promoters of pro-apoptotic genes (Samuels-Lev et al., 2001). However, it has been previously shown that the excessive growth of neural progenitors observed in *Trp53bp2*$^{\Delta 3/\Delta 3}$ embryos is not caused by a lack of apoptosis (Sottocornola et al., 2010). ΔN-ASPP2, the recently discovered ASPP2 isoform, is reported to have the opposite effect on p53 compared to full-length ASPP2: it inhibits p53 transcriptional activity and reduces damage-induced apoptosis (Van Hook et al., 2017). It was also found to enhance cell proliferation and survival in human osteosarcoma cell lines (Van Hook et al., 2017). N-ASPP2 has an entirely separate transcription start site to ASPP2, and therefore should be unaffected by the exon 3 deletion (Figure 4-2). Here it was shown that N- and C-terminally derived mRNAs were not differentially disrupted due to the lack of exon 3: in both cases, mRNA quantities were decreased by ~10% in heterozygotes and ~23% in homozygotes (Figure 4-3). Hence, while the frame-shift caused by deletion of exon 3 (Vives et al., 2006) results in full-length ASPP2 mRNA degradation, we cannot rule out the production of ΔN-ASPP2 in *Trp53bp2*$^{\Delta 3/\Delta 3}$ embryos. Protein level analysis would be required to identify ΔN-ASPP2, and further explore its relation to increased mitotic index in ASPP2 mutant mice.

SOX2 is known to be expressed in proliferating CNS progenitors, such as ventricular zone cells of the neural tube, whereas it is excluded from regions of differentiation (Graham et al., 2003). Here, it was shown that SOX2

expression was strongest around the apical border of the neural tube in both wild-type and NMP mutant embryos, yet largely dispersed across the entire neuroepithelium in MP mutants. Threshold analysis confirmed an increase in SOX2 positive cells in MP mutant embryos compared to wild-type (Figure 4-9). Constitutive expression of SOX2 has been shown to inhibit neuronal differentiation and result in the maintenance of progenitor characteristics (Graham et al., 2003). Perhaps increased or sustained SOX2 expression in the neuroepithelium of MP mutants is therefore contributing to the increased proliferation index seen in MP *Trp53bp2*$^{\Delta 3/\Delta 3}$ embryos.

It was important to understand the effect of ASPP2 knockdown on other stages of the cell cycle. Interestingly, there was no significant difference in the number of cells in S phase (% EdU / total cells), between mutant and wild-type embryos after a 6 or 24 h EdU pulse (Figure 4-10). This implies that the cell cycle is being differentially affected between S and M phase. BBP, a splice variant of ASPP2 has been shown to impede cell cycle progression at G2/M (Naumovski and Cleary, 1996). This splice variant is formed due to a stop codon in exon 3 (Takahashi et al., 2004), and would therefore be disrupted following exon 3 deletion. Perhaps, following depletion of this protein, the progression of cells from G2 into M phase is accelerated, resulting in an imbalance of cells in M phase vs S phase.

To examine whether the increase in SOX2 progenitors (Figure 4-9), and in the proportion of mitoses (Figure 4-6) results from a shift in the fraction of progenitors that remain progenitors instead of differentiating, cell cycle exit was analysed. Analysis showed no significant change in the number of cells retained within the cell cycle (% Ki67+EdU / EdU labelled cells) between mutant and wild-type embryos after a 6 or 24 h EdU pulse (Figure 4-10). This suggests ASPP2 does not influence the decision of neural precursors to either re-enter the cell cycle or differentiate.

There are many possible modes of interaction between cell cycle exit, cell cycle lengthening and neural progenitor differentiation (Hardwick et al., 2015). Therefore, although cell cycle exit remained unchanged, it was

important to assess the patterning of neural differentiation in *Trp53bp2*$^{\Delta 3/\Delta 3}$ embryos. The most striking change in mutant embryos was the presence of TUJ1 staining in the apical ventral region, often between 2 midline lumens (Figure 4-11). Quantitatively, NMP mutant embryos were shown to have significantly increased TUJ1 staining in apical ventral regions compared to the wild-type, and to the corresponding dorsal and mid regions within the same neural tube (Figure 4-12) (Figure 4-11, E, ii). This implies that the neuroepithelial 'bridge' that appears in the initial stages of phenotypic progression, is formed by invasion of early neurons. Furthermore, in both mutants, the differentiated neuron intensity in ventral basal regions, where motor neuron differentiation occurs, was no longer significantly higher than the other basal regions in the neural tube. This suggests that neuroepithelial disruption in the ventral region not only occurs in the midline, but also at the basal extremities. Despite this, it is unlikely that motor neuron differentiation is disrupted as this is induced by signals from the notochord and floor-plate (Yamada et al., 1993), similar to Shh-determined neural progenitor patterning, which appears unaffected by ASPP2 knockdown (Figure 4-13)(Figure 1-2).

Overall, proliferation and differentiation are disrupted in *Trp53bp2*$^{\Delta 3/\Delta 3}$ embryos, but perhaps as a secondary effect of neuroepithelial disruption.

4.3.3 Implications of an increase in ectopic mitotic index

The most striking change in both MP and NMP ASPP2 mutant embryos was the increase in ectopic mitoses. Ectopic mitoses could arise because of faulty IKNM (Figure 1-1), or because apical attachment of cells is disrupted due to a reduced apical border. To explore the latter, lumen circumference was measured and normalised to neural tube circumference. A significant reduction in lumen border length was seen in mutants compared to the wild-type at E11.5 and E13.5, and in the mutant situation, linear regression lines showed a general decrease in ectopic mitoses when lumen circumference was increased (Figure 4-7). However, despite a significant increase in % ectopic mitoses in E9.5 mutants (Figure 4-6, C) there was no change in

lumen circumference (Figure 4-7, A), demonstrating that lumen circumference cannot be the only contributing factor to the appearance of ectopic mitoses. At least in the early stages, ectopic mitosis is independent of apical border length.

The apparent relationship between lumen circumference and ectopic mitoses in E11.5 and E13.5 embryos could perhaps be explained in a converse manner, as it has been shown that the 'rounding up' of mitotic cells causes apico-basal contraction of epithelial cells which can mechanically contribute to expansion of the lumen (Hoijman et al., 2015). Furthermore, orientation of progenitor cell division determines lumenogenesis in the zebrafish neural keel (Zigman et al., 2011). Perhaps ectopic mitoses start to arise in E9.5 embryos, which leads to the gradual loss of apical mitoses in later stages, meaning retention of the lumen can no longer be sustained and lumen circumference is reduced by E11.5.

Considering that increased ectopic mitoses precede changes in lumen circumference, their derivation could instead be explained by a disruption in IKNM, caused by an imbalance in apico-basal polarity. To support this idea, apical polarity-related mutations in other models have shown close similarities to ASPP2 mutants. For example, it was found that in the zebrafish, loss of Pard6γb (a member of the Par3/Par6/aPKC polarity complex), results in multiple lumens forming in the neuroepithelium (Munson et al., 2008). Deficiencies in small GTPases such as RhoA and cdc42, which are involved in maintaining adherens junctions, have been associated with hyperproliferation in the neuroepithelium, mislocalised mitosis at the basal surface and exencephaly-like protrusions in the mouse (Katayama et al., 2011). Conditional deletion of N-cadherin in the mouse has been shown to cause mitoses to be scattered throughout the cortex (Kadowaki et al., 2007). Finally, disruption of atypical Protein Kinase C proteins (aPKCλ/ι and aPKCζ) was shown to result in abundant ectopic mitoses and abnormal post-mitotic cell migration in the zebrafish neural retina (Cui et al., 2007).

In conclusion, *Trp53bp2*$^{\Delta 3/\Delta 3}$ embryos, regardless of whether they exhibit a macroscopic phenotype, have a highly complex histological phenotype. The gradual unravelling of this phenotype has shown signs of an apico-basal polarity – associated defect, due to the general disorganisation of the neuroepithelium and similarities with previously reported polarity-related mutations (Munson et al., 2008, Katayama et al., 2011, Kadowaki et al., 2007, Cappello et al., 2006, Cui et al., 2007). To explore the basis of this progressive phenotype, it was important to look further into the origin of increased ectopic mitoses, the phenotype seen in the earliest of stages assessed (Figure 4-6), in both the ventral and dorsal halves of the neural tube (Figure 4-8). The next questions to answer were as follows:

- Are apical markers expressed 'normally' in *Trp53bp2*$^{\Delta 3/\Delta 3}$ embryos?

- Where do ectopic mitoses come from in *Trp53bp2*$^{\Delta 3/\Delta 3}$ embryos?

- What possible binding partners of ASPP2 could explain a polarity-associated phenotype?

Chapter 5 Addressing apical polarity and interkinetic migration in ASPP2$^{\Delta exon3/\Delta exon3}$ embryos

5.1 Introduction

Epithelial cell membranes exhibit apical and baso-lateral compartments which are separated by tight junctions and adherens junctions (Margolis and Borg, 2005). Polarity protein complexes facilitate this separation such as the tight junction-associated PAR-complex (PAR3, PAR6 and atypical protein kinase C (aPKC)), a more apically located Crumbs complex, and baso-lateral proteins such as Scribble (Eom et al., 2013). The adherens junctions, immediately subjacent to tight junctions of epithelial cells and made up of cadherins, interact with apical actin and are critical for cell adhesion and for the ability of epithelial cells to form three-dimensional tissue structures (Harris and Tepass, 2010). One such structure is the neural tube. Basal retention of cell nuclei together with apical actomyosin contraction in the neural plate causes apical constriction ('wedge-shaped' cells) and the formation of the median hinge points during closure of the neural tube (Eom et al., 2013). Apico-basal thickening of the neural plate and the formation of dorso-lateral hinge points (McShane et al., 2015), combined with apico-basal shortening at the median hinge point, are also vital processes in NTC.

In both the open and closed neural tube, apico-basal polarity is also important for the process of interkinetic nuclear migration (IKNM), in which cell nuclei at distinct stages of the cell cycle occupy different positions along the apical–basal axis of the neuroepithelium (Figure 1-1). Not only has the function of IKNM remained controversial (Del Bene, 2011), but the mechanisms controlling this process have also been debated. It has been suggested that cell cycle phase is the driving factor of IKNM (mediated by the microtubule-associated protein Tpx2), in that the basal to apical movement of cells is an active process dependent on cells transitioning from S phase to G2 phase, whereas apical to basal movement of cells is a passive process, dependent on the cells moving in the opposite direction (Kosodo et al., 2011). Conversely, a biomechanical explanation of IKNM suggests dynein is

responsible for the basal to apical movement of cells and KIF1A (a kinesin) is required for basally directed nuclear movement (Tsai et al., 2010). Other proteins such as actin and Rho Kinase have also been implicated in the process of IKNM, through regulating mitotic cell rounding and recruitment of the nucleus to the apical border (Spear and Erickson, 2012a).

To better understand the role of apico-basal polarity in *Trp53bp2*$^{\Delta 3/\Delta 3}$ embryos, sections were stained for proteins associated with the neural tube apical border: N-cadherin, F-actin and PAR3, a binding partner of ASPP2 (Miyamoto et al., 2015, Morita et al., 2010, Eom et al., 2013, Sottocornola et al., 2010). It was also important to understand the origin of the ectopic mitoses in mutant embryos: i.e. whether they resulted from disruption in the apical to basal, or basal to apical, migration of cells during IKNM. 1 h EdU pulse staining was combined with PHH3 labelling to track cells discriminated by their neuroepithelial location: apical or ectopic.

5.2 Results

5.2.1 Apical marker analysis in *Trp53bp2*$^{\Delta 3/\Delta 3}$ embryos

N-cadherin contributes to cell-cell adhesion in neural progenitor cells through its role in forming adherens junctions together with α-catenin, β-catenin, and actin fibres (Miyamoto et al., 2015). N-cadherin is broadly expressed in neuroepithelial cells, although this protein is most highly concentrated at the sub-apical region, where the adherens junctions develop (Miyamoto et al., 2015). F-actin plays a crucial role in stabilizing adherens junctional structure and tightening the epithelial barrier (Ivanov, 2008). Similarly, to N-cadherin, there is accumulation of apical F-actin in the neuroepithelium (Morita et al., 2010). For these reasons, an antibody against N-cadherin and phalloidin staining for F-actin were used in E11.5 wild-type and *Trp53bp2*$^{\Delta 3/\Delta 3}$ embryos, to assess whether the distribution of apical-associated proteins had been disrupted as a result of ASPP2 knockout.

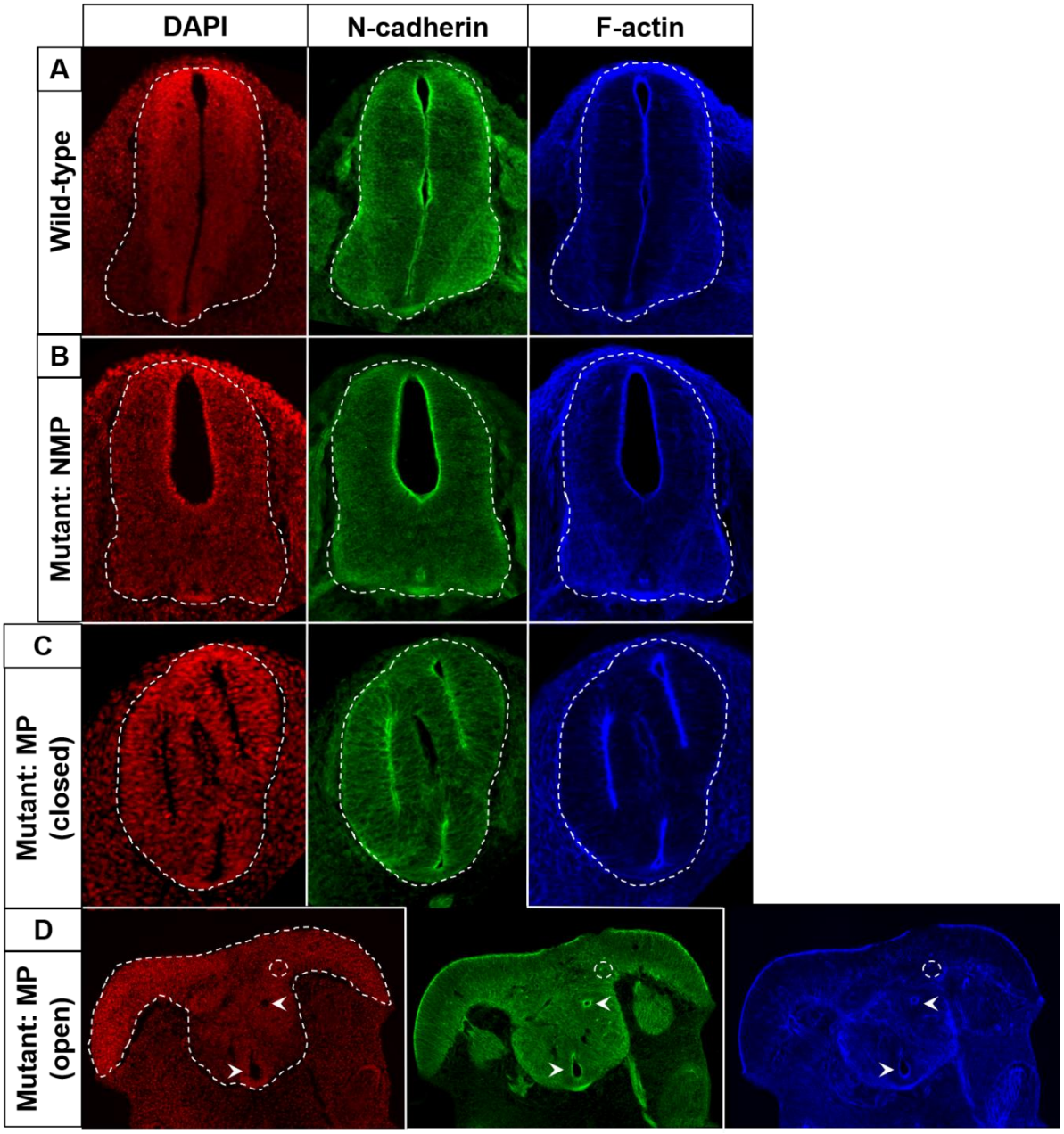

Figure 5-1: N-cadherin and F-actin staining

Wild-type, non-macroscopically phenotypic (NMP) and macroscopically phenotypic (MP) (both open and closed examples) mutant ASPP2 embryos, stained with DAPI (red), an antibody against N-cadherin (green), and phalloidin (F-actin stain) (blue). White dashed line represents neural tube border. (**A**) Wild-type: N-cadherin is globally expressed throughout the neuroepithelium, with enrichment of staining lining the lumenal border. F-actin is expressed in ventro-lateral motor neuron regions, with strongest expression lining the lumenal border. (**B**) Mutant: NMP: N-cadherin remains globally expressed throughout the neuroepithelium, with strongest expression seen lining the borders of the large dorsal lumen and small ventral lumen, in this example. F-actin is expressed in ventro-lateral motor neuron regions, and strongly at the lumenal borders. Actin filament orientation around the ventral aspect of the larger lumen forms a fan-shaped distribution, and staining appears to spread medially in the ventral region. (**C**) Mutant: MP (closed): both N-cadherin and F-actin staining is enriched at the lumenal border of all 3 lumens present in this example. (**D**) Mutant: MP (open): N-cadherin is globally expressed throughout the neuroepithelium, with enrichment of staining lining the lumenal borders, including a small lumen within the centre of a rosette

(see arrows). Bright staining of N-cadherin appears in puncta, spotted around the neuroepithelium. One such punctum appears in the location of a rosette (see small dotted circle in DAPI and N-cadherin images). Strong N-cadherin staining also appears along the dorsal edge of the open NT region (plaque). F-actin appears highly disrupted and is no longer strongly expressed in ventro-lateral regions. Staining appears to correspond to N-cadherin expression in most instances, with the strongest signal seen at the lumenal borders, in puncta throughout the neuroepithelium, and along the dorsal edge of the open region. Images representative of observational analyses: WT / Mutant: NMP / Mutant: MP: n = 3 embryos.

In the wild-type situation, N-cadherin was expressed throughout the neuroepithelium, yet most highly concentrated at the lumenal border (Figure 5-1, A). F-actin, stained with phalloidin, showed similarly, high expression along the apical border of the neural tube. Otherwise, strongest expression of F-actin appeared in the ventro-lateral (motor neuron) regions. Horizontal (apical-basal) linear pattern staining was seen in the remainder of the neuroepithelium (Figure 5-1, A). In sections of *Trp53bp2*$^{\Delta 3/\Delta 3}$ neural tubes with 2 lumens in the dorso-ventral axis, separated by an overgrowth of ventral neuroepithelium (such as the NMP mutant example in Figure 5-1, B), N-cadherin and F-actin remained most strongly expressed around both lumen borders. Conversely, F-actin appeared slightly more spread out in these embryos compared to the wild-type, reaching across the medio-ventral intersection of neuroepithelium. The horizontal linear patterning of actin seen in the wild-type was also seen in the dorsal region of such neural tubes. However, towards the ventral portion of the superior lumen, actin appeared in a ‘fan’ formation, extending out radially from the curved ventral end of the lumen.

Both open and closed regions are shown as examples of macroscopically phenotypic mutant embryos (Figure 5-1, C, D). In the closed section, N-cadherin and F-actin showed the strongest expression along the three lumenal borders, with little / no expression around a central blood vessel (see red cells in the DAPI image), which could otherwise have been mistaken as a fourth lumen (Figure 5-1, C). The section through an open region shows 2 small lumens: one above the floor-plate, as seen before (Figure 4-14, A) and another away from the midline in the centre of a rosette, both positive for N-

cadherin at their apical borders (arrowheads Figure 5-1, D). Bright puncta of N-cadherin staining were seen, seemingly randomly distributed within the neuroepithelium. One such punctum was located in the centre of a smaller rosette identified in the DAPI image channel (see dotted circle Figure 5-1, D). Strong expression of N-cadherin was also seen along the dorsal aspect of the open plaque, with radial projections crossing the near-horizontal neuroepithelium. F-actin staining of the same mutant was seen to closely match that of the N-cadherin staining. Other areas of strong F-actin staining included the ventral aspect of the open plaque, and diagonally across the midline of the neural tube, a seemingly disorganised distribution. Strong expression of both N-cadherin and F-actin along the dorsal aspect of the open 'plaque', supports the idea that neural tube rupture occurs, causing separation of the neural tube walls to expose the once apical border to the exterior of the embryo.

The partition defective (PAR) complex, consisting of PAR3, PAR6 and atypical protein kinase C (aPKC), is known to be localised to the apical domain of neuroepithelial cells (Miyamoto et al., 2015). Moreover, PAR3 has been shown to interact directly with ASPP2 (Sottocornola et al., 2010, Cong et al., 2010). PAR3 was localised by immunostaining within the neuroepithelium of *Trp53bp2*$^{\Delta 3/\Delta 3}$ embryos in comparison to wild-type controls. Whole-neural tube observations showed that, similar to N-cadherin and F-actin, PAR3 appeared strongest around the lumenal border in both wild-type and mutant embryos (data not shown). A more detailed assessment was performed on the ventral portion of the neural tube, as this region had thus far appeared to be the first location of disruption and overgrowth in E11.5 embryos. Ventral regions of NMP mutants with a maximum of two lumens in the dorso-ventral axis were therefore compared with the equivalent portion of wild-type neural tubes in an observational study.

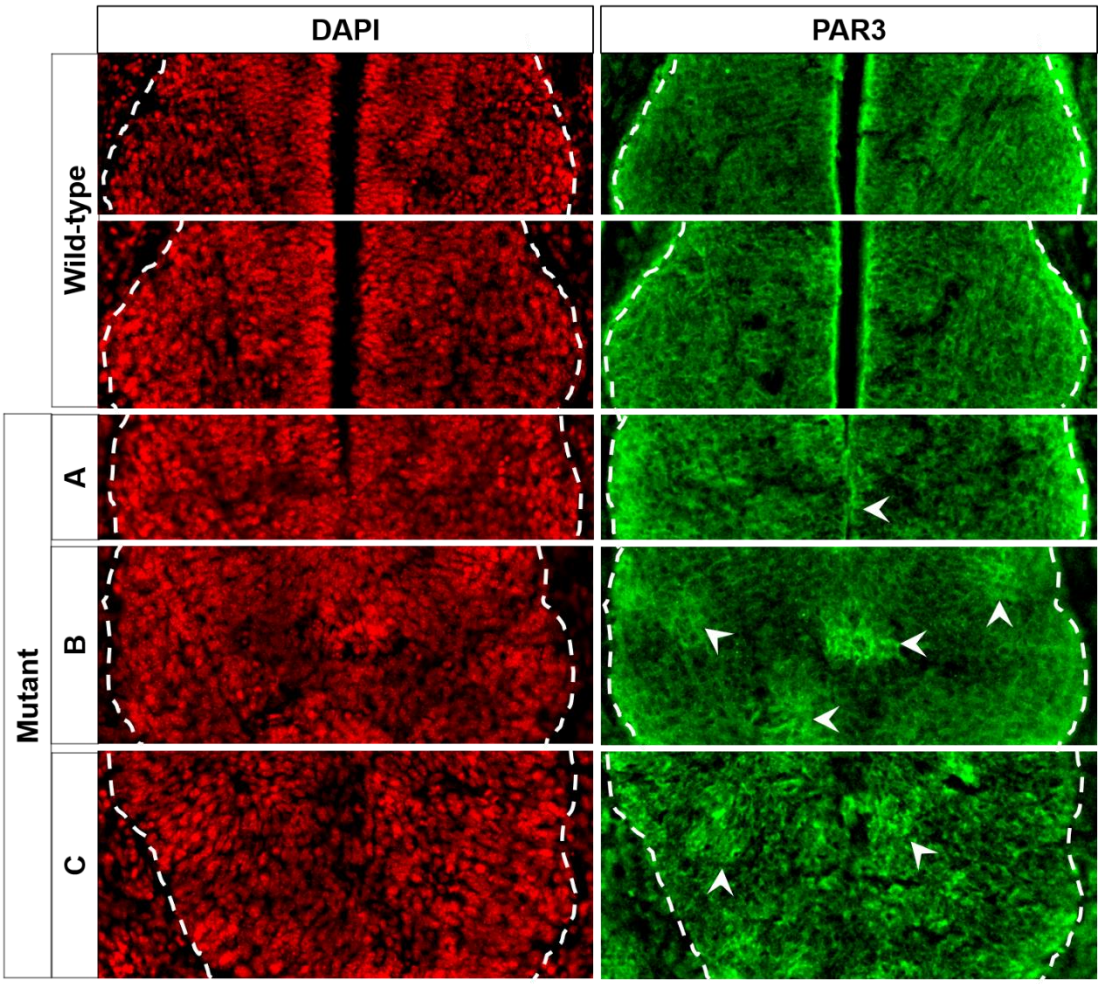

Figure 5-2: PAR3 in the ventral neural tube

Wild-type and mutant example images showing DAPI (red) and PAR3 (green) staining in the ventral neural tube. White dashed line represents neural tube border. Images show the portion of the neural tube immediately dorsal to the floor-plate and ventral to the upper lumen in mutants. PAR3 staining shows strongest expression along the lumenal border with reduced, uniform staining throughout the remainder of the neuroepithelial tissue. ASPP2 mutant (**A**) shows a portion of the neural tube with the ventral aspect of the upper lumen within view. PAR3 in this region appears to be less strongly expressed in the midline, compared to wild-type, and more strongly expressed on one side of the midline than the other (see arrow showing stronger expression on right side of the embryo). ASPP2 mutant (**B**) has a complete absence of a lumen in this region. PAR3 expression appears in clusters of high expression (see arrows). The strongest expression is seen in a large cluster of cells in the midline. ASPP2 mutant (**C**) has a disorganised structural appearance and no lumen is present in the region assessed. PAR3 expression pattern is disorganised with apparently random clusters of high expressing cells (see arrows). Images representative of observational analyses: WT / Mutant: non-macroscopically phenotypic: n = 3 embryos.

To compare the ventral region of the neural tube, between wild-type and mutant embryos, a portion of neural tube was defined by: the area immediately dorsal to the floor-plate / small lumen retained above the floor-

plate, and immediately ventral to the upper lumen in mutants, assumed level with the dorsal extremity of motor neuron horns in wild-type embryos, (see Figure 5-2 for examples). In wild-type embryos the ventral region was bisected in the midline by the lumen and flanked by the motor neuron horns either side. PAR3 expression appeared most strongly expressed along the apical border of the neural tube, lining the lumen, with less intense, relatively uniform PAR3 staining in the remainder of the neuroepithelium. PAR3 expression in the mutant (non-macroscopically phenotypic) embryos was more variable. For example, in Figure 5-2, A, where the lumen appeared to have recently been closed off, PAR3 was still most strongly expressed in the apical region, yet less strongly than in the wild-type. PAR3 also appeared to be more spread out from the midline, and less equally distributed either side of the pre-existing lumenal border (see arrowhead in mutant A, Figure 5-2). In more 'advanced' phenotypes, where the ventral region above the floor-plate was largely disorganised and without a lumen, PAR3 appeared in clusters of high expression, apparently randomly distributed within the neuroepithelium (see arrow heads in mutants B and C, Figure 5-2).

In conclusion, although apical markers show some signs of disruption in *Trp53bp2*$^{\Delta 3/\Delta 3}$ embryos, each one seems to remain most strongly expressed at apical lumenal borders, regardless of whether these are established lumens or in the centre of rosettes (Figure 5-1). PAR3 appeared perhaps the most disorganised in ventral regions of E11.5 embryos, out of the three markers assessed. However, it is not clear whether apical marker disruption is causative or consequential to the first stages of an NTD. Therefore, it was essential to assess the mechanistic origin of the first notable change in *Trp53bp2*$^{\Delta 3/\Delta 3}$ embryos: ectopic mitoses.

5.2.2 Assessment of interkinetic nuclear migration in *Trp53bp2*$^{\Delta 3/\Delta 3}$ embryos

Previous assessment of mitotic cells in the neuroepithelium showed a marked increase in ectopic mitoses in E9.5 macroscopically phenotypic mutant embryos and in both mutant types at E11.5 and E13.5, compared to

wild-type (Figure 4-6). Furthermore, lumen circumference was not significantly changed in E9.5 mutant embryos, demonstrating that the occurrence of ectopic mitoses, at least in the early stages, was independent to apical border length (Figure 4-7). This suggests a possible intrinsic defect in IKNM in ASPP2 mutant embryos, which was investigated here.

First, the PHH3 data were further analysed to assess the balance between ectopic and apical mitoses. Apical mitoses were quantified by subtracting the number of ectopic cells from total mitotic cells and finding the proportion of this number out of total cell count. Ectopic mitoses were quantified by the same method, enabling a direct comparison with apical mitoses.

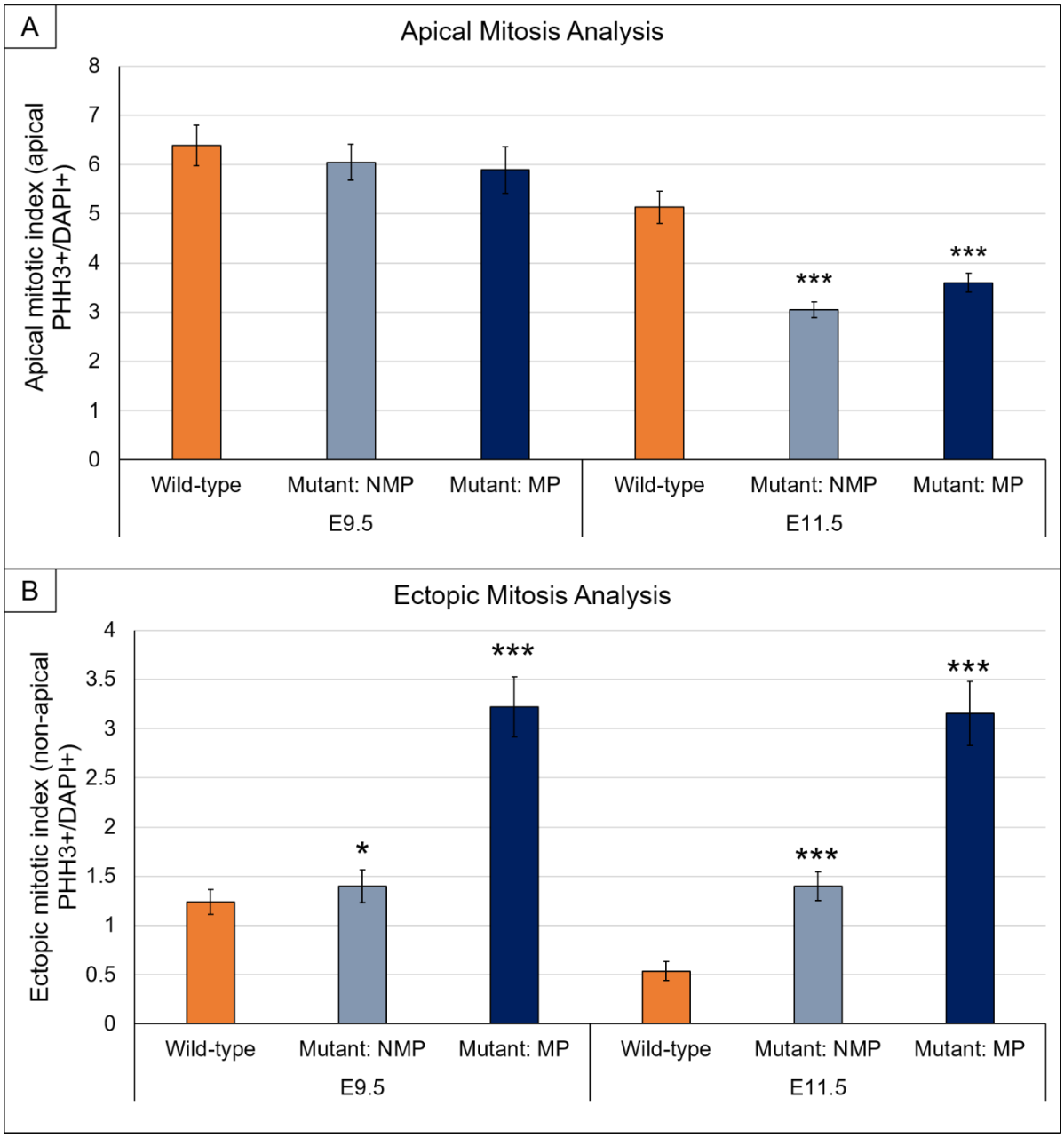

Figure 5-3: Apical mitosis analysis

(**A**) Apical mitotic index in the neuroepithelium, calculated by subtracting ectopic mitoses from total mitoses and dividing by total cell number (DAPI+). No difference is seen between mutant, either non-macroscopically phenotypic (NMP) or macroscopically phenotypic (MP) and wild-type embryos at E9.5. At E11.5, both mutant types have a significantly reduced apical mitotic index compared with wild-type embryos. (**B**) Ectopic mitotic index: number of non-apical PHH3+ mitoses divided by total cells in the neuroepithelium (DAPI+). Both mutants have a significantly increased ectopic mitotic index compared to wild-type at E9.5 and E11.5. **Statistical analysis**: One-way ANOVA showed no significant variation in apical mitotic index in E9.5 embryos, but significant variation between the E11.5 embryo groups. Ectopic mitotic index values showed significant variation between embryo groups at both E9.5 and E11.5. Post-hoc tests of mutant (NMP and MP) vs wild-type: *** $p \leq 0.001$, * $p \leq 0.05$; Student's t-tests. Error bars: standard error. WT / Mutant: NMP / Mutant: MP: n = 3 embryos, 3-4 slides per embryo, 4-5 sections per slide. Total nuclei/apical mitoses/ectopic mitoses counted: E9.5: wild-type: 21580/1580/262. Mutant: NHM: 22685/1650/308. Mutant:

MP: 27283/2223/845. E11.5: wild-type: 52652/2707/241. Mutant: NHM: 72717/3082/947. Mutant: MP: 65449/4202/1954.

Interestingly, in E9.5 embryos, there was no significant difference in the proportion of apical mitosis in mutant embryos, compared to wild-type (Figure 5-3, A), despite a significantly increased ectopic mitotic index in both mutants (Figure 5-3, B). At E11.5, however, apical mitotic cells were significantly reduced in both macroscopically phenotypic and non-macroscopically phenotypic mutants compared to the wild-type (Figure 5-3, A). This suggests that at E9.5, ectopic mitoses are additional to the apical mitoses, whereas by E11.5, new mitoses are arising in ectopic locations and replacing mitoses at the apical border. This phenomenon is strongly suggestive of an interkinetic nuclear migration defect, therefore mutant E11.5 embryos were explored further in relation to this process.

It was important to compare ectopic mitoses with apical mitoses within the same neural tube, to assess the point at which IKNM was being disrupted. By using EdU as a tracking signal (since EdU labelling occurs in S-phase nuclei which are located at the basal border of the neural tube), the proportion of mitotic cells that were EdU positive could be separated into whether the cells were apical or ectopic at the point of fixation. Through combining a short EdU chase period (1 h) with PHH3 staining after fixation, this was achieved. A 2 h EdU pulse chase experiment within a single embryo was used as a follow-up confirmatory study. Due to the histological analytical nature of this experiment (comparing apical and ectopic mitoses), only E11.5 non-macroscopically phenotypic mutant embryos were analysed, as a relatively normal appearing neural tube was required to assess IKNM.

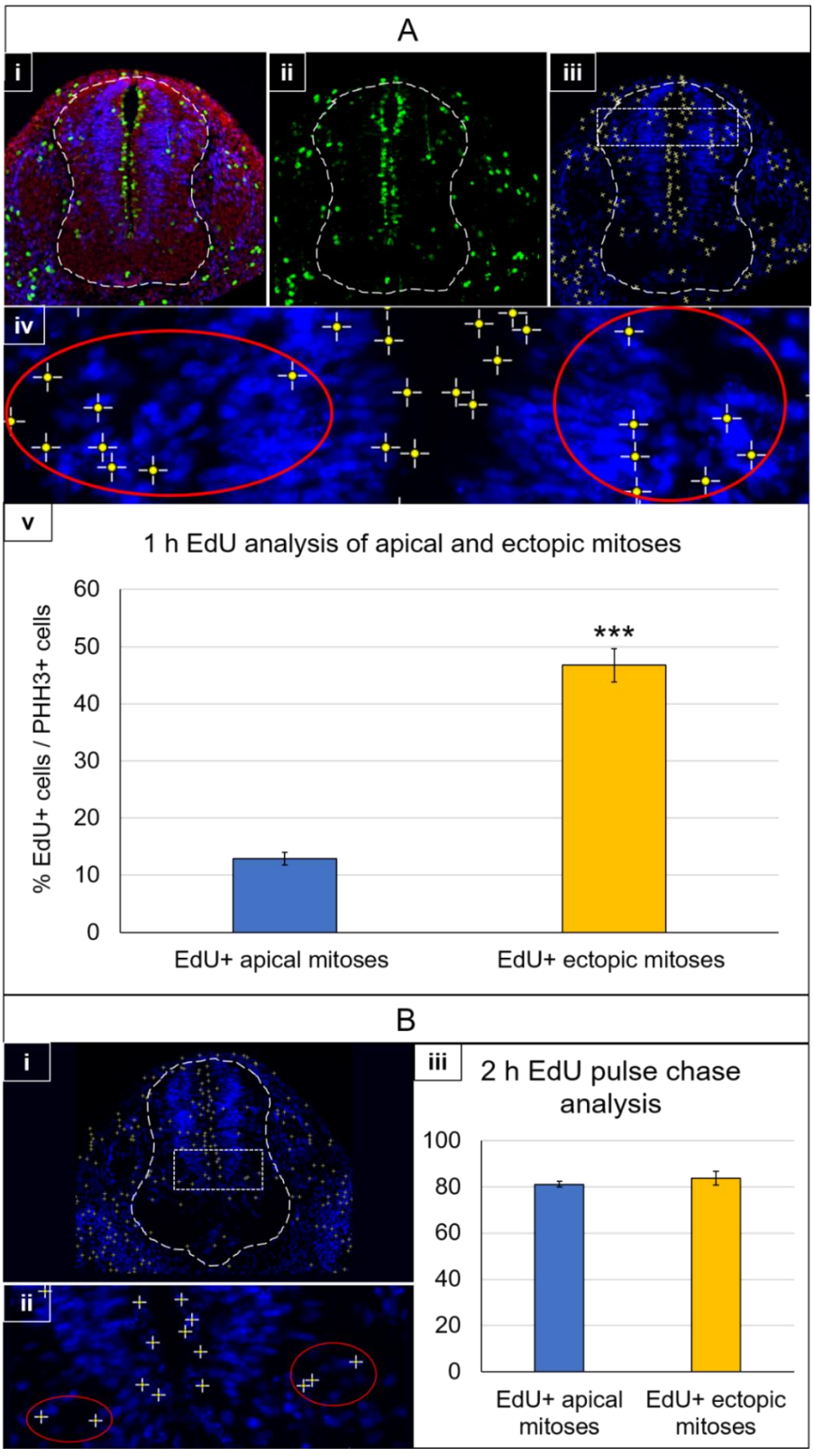

Figure 5-4: 1 h EdU analysis of apical and ectopic mitoses and 2 h EdU pulse confirmatory study

(**A**) 1 h EdU pulse chase analysis of apical and ectopic mitotic cells in E11.5 non-macroscopically phenotypic mutant embryos. (**i-iii**) White dashed line represents neural tube border. (**i**) Example composite image showing DAPI (red), PHH3 (green) and EdU (blue). (**ii**)

PHH3 channel from image in (i) showing both apical and ectopic mitoses within the neuroepithelium. Automated counting was performed on this channel. (**iii**) EdU staining following 1 h chase, overlaid with counting markers from PHH3 channel in (ii). Rectangular area represents image in (iv). (**iv**) Magnified image from (iii), showing EdU staining overlaid with PHH3+ counting markers. Red circles surround ectopic mitoses. In this section, the majority of ectopic mitoses are EdU+ (12/15), whereas most apical mitoses are EdU- (8/11). (**v**) Quantification of 1 h EdU pulse chase analysis of apical and ectopic mitoses. A significantly greater proportion of ectopic mitoses are EdU+ compared to apical mitoses, suggesting IKNM is disrupted in the basal-apical migration of nuclei. (**B**) 2 h EdU chase follow-up study using a single E11.5 non-macroscopically phenotypic mutant embryo. (**i**) Example section showing EdU staining after 2 h chase period, overlaid with PHH3+ markers from the same section (PHH3 channel image not shown). Rectangle area represents image in (ii). (**ii**) Magnified image showing EdU staining overlaid with PHH3+ counting markers. Red circles surround ectopic mitoses. In this section, the majority of apical mitoses (8/9), and all ectopic mitoses (5/5) are EdU+. (**iii**) Quantification of 2 h EdU pulse chase analysis of apical and ectopic mitoses. The proportions of apical mitoses and ectopic mitoses that are EdU+ do not differ significantly. Both apical and ectopic mitoses were >80% EdU+. **Statistical analysis**: % EdU+ cells / PHH3+ apical cells vs ectopic cells after 1 h EdU pulse chase analysis: *** $p \leq 0.001$; Student's t-test. No significant variation in % EdU+ cells / PHH3+ apical cells vs ectopic cells after 2 h EdU pulse chase analysis. Error bars: standard error. Mutant: non-macroscopically phenotypic for 1 h EdU chase: n = 3 embryos. Total no. apical mitoses counted: 968, ectopic mitoses: 907. Mutant: non-macroscopically phenotypic for 2 h EdU chase: n = 1 embryo. Total no. apical mitoses counted: 567, ectopic mitoses: 359.

A much higher proportion of ectopic mitoses (i.e. PHH3+ cells away from the apical border) were EdU+ (~47%), compared to apical mitoses after a 1 h EdU chase (~13%) (Figure 5-4, A). This infers that in relation to IKNM, the basal to apical movement of nuclei is impaired, rather than failure of nuclei to complete the 'return journey' from apical to basal surfaces in G1 (Figure 5-5). As a control experiment, a 2 h EdU pulse chase analysis was performed in a single non-macroscopically phenotypic mutant embryo. Here, the majority of both ectopic and apical mitoses were labelled (>80%), and the two populations did not differ significantly from each other (Figure 5-5, B). This shows that the initial conclusion was correct, and the low % EdU+ apical mitoses after 1 h is not due to failure of labelling or complete disruption of IKNM, but rather due to nuclei destined to divide apically having not yet reached the apical surface after only 1 h (Figure 5-5). This is consistent with the known cell cycle length of 10.5 h in neuroepithelial cells at E11.5, where S-phase length exceeds 5 h and G2 length exceeds 1 h (Kauffman, 1968).

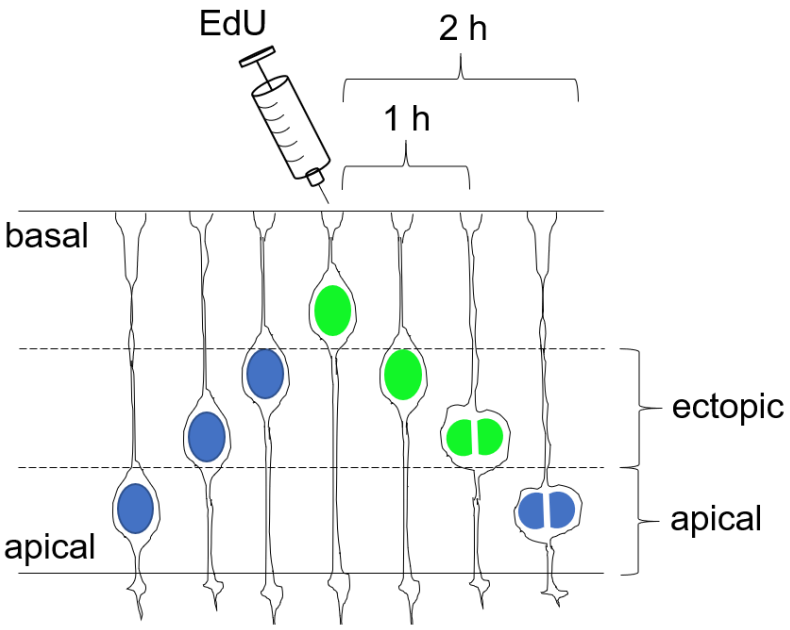

Figure 5-5: Diagrammatic summary showing EdU analysis of apical and ectopic mitoses

Nuclei move from the apical border to the basal border during G1 (blue represents EdU- nuclei). Cells at the basal border in S phase are labelled at the point of EdU injection (green represents EdU+ nuclei). Results showed that after 1 h, more cells going through mitosis were labelled away from the apical border compared to those at the apical border. This inferred that ectopic mitoses arise due to impaired nuclear migration in the basal to apical direction, usually restricted to cells in G2. To confirm this finding and to rule out the possibility of complete disruption of IKNM, a control experiment in which a 2 h chase was used, showed a high proportion of EdU+ cells going through mitosis, both apical and ectopic. This shows that IKNM is not completely disrupted, and that 2 h is sufficient for 'normal' cells to reach the apical surface to go through mitosis.

In summary, by the time *Trp53bp2*$^{\Delta 3/\Delta 3}$ embryos reach E11.5, new mitoses are arising in ectopic locations, and mitoses at the apical border are reducing. Following this finding, it was shown that interkinetic nuclear migration is being disrupted as cells move from the basal surface to the apical surface, however the process is not entirely dysfunctional, as some labelled cells are still able to travel the full distance to the apical border.

5.3 Discussion

5.3.1 Closing in on the role of apico-basal polarity in *Trp53bp2*$^{\Delta 3/\Delta 3}$ embryos

While neural tube lumenal circumference becomes progressively reduced in ASPP2 mutant embryos, this chapter found that apical markers continue to be localised to the remaining lumenal borders, as long as they are visible. This doesn't rule out an apico-basal polarity defect, as disruption was seen elsewhere in the neural tube, most notably in F-actin and PAR3 staining. In the non-macroscopically phenotypic mutants, F-actin distribution appeared to closely correspond with TUJ1 patterning, with apparent increased ventral apical expression, and increased mid and dorsal basal expression. It is known that actin filaments regulate growth cone motility and axon guidance in immature neurons (Compagnucci et al., 2016) which explains why F-actin is localised to developing motor neurons.

The open macroscopically phenotypic mutant example in Figure 5-1 is extremely interesting in terms of the mechanistic origin of multiple lumens. Two distinct rosettes could be seen in the neuroepithelium away from the midline, with a central lumen or puncta stained positive for both N-cadherin and F-actin. Supporting the idea that these rosettes are self-assembled, it has previously been found that N-cadherin interacts with nectin-2 through extracellular domains in the *Xenopus* neural tube, and they cooperatively enhance apical constriction by driving the accumulation of F-actin at the apical cell surface (Morita et al., 2010). The first stages of rosette formation have also been found to include accumulation of F-actin, myosin-II, PAR3 and N-cadherin in the apical domains of epithelial cells, resulting in apical constriction, rosette formation and possible opening of the acto-myosin-rich centre to form a central lumen (Harding et al., 2014). An alternative possibility is that rosettes are simply a by-product of the original lumen, reduced in size and misaligned due to severe neuroepithelial disruption. This could be investigated in a future study by introducing a label such as a fluorescently labelled lectin (e.g. wheat germ agglutinin) into the lumen at an early stage of

development, in order to label neuroepithelial cells bordering the original lumen.

PAR3 is a strong candidate for mediating an apico-basal defect in ASPP2 mutants. ASPP2 has previously been shown to interact and colocalise with PAR3 at apical junctions in polarised epithelial cells, while depletion of ASPP2 causes defects in PAR3 localisation (Cong et al., 2010, Sottocornola et al., 2010). As ASPP2 binds to PAR3 via its N-terminal, the part of the protein proven to be knocked down completely in *Trp53bp2*$^{\Delta 3/\Delta 3}$ embryos (Vives et al., 2006), this interaction must be disrupted. Even if the ΔN-ASPP2 variant protein is made in *Trp53bp2*$^{\Delta 3/\Delta 3}$ embryos (see Chapter 4), this would not be expected to interact with PAR3. Expression of PAR3 was found to be disorganised in the ventral neuroepithelium, in the form of clusters, or asymmetrically distributed either side of a recently closed midline lumen. It has been shown that when PAR3 is expressed ectopically in the chick neuroepithelium, it is able to coordinate the recruitment of other protein members of the PAR complex, as well as additional polarity complexes and junction-associated proteins such as N-cadherin, to the same region (Afonso and Henrique, 2006). PAR3 was even shown to be concentrated in the region close to the `luminal' surface of neuroepithelial rosettes, also occupied by N-Cadherin and β-Catenin (Afonso and Henrique, 2006), supporting the self-assembly theory of rosette formation in *Trp53bp2*$^{\Delta 3/\Delta 3}$ embryos. Therefore, changes in PAR3 localisation, a direct result of ASPP2 deletion, could be the driving force behind mislocalisation of apical proteins and subsequent neuroepithelial disruption in *Trp53bp2*$^{\Delta 3/\Delta 3}$ embryos.

At E9.5, there was no change in apical mitotic index, despite a significant increase in ectopic mitoses, in ASPP2 mutants. When cells ‘round up’ and enter mitosis at the apical surface, this contributes mechanically to expansion of the lumen (Hoijman et al., 2015). Hence, the normal apical mitotic index may be directly related to the unchanged lumen circumference present in ASPP2 mutants at E9.5 (see Chapter 4). It also follows that the ectopic mitoses which are already present at E9.5 are additional to apical mitoses, suggesting a defect in IKNM which is independent of lumenal circumference.

On the other hand, by E11.5 ectopic mitoses have started to replace apical mitoses, which become significantly reduced, and so this transition could be mechanistically related to the gradual disruption and loss of lumen in the mutant neural tube. The disturbance of apical marker localisation detected in ASPP2 mutants is consistent with an abnormality of IKNM as a cause of ectopic mitoses in the mutant embryos.

Previous studies that describe ectopic mitoses, have not assessed IKNM or simply state that it must be disrupted (Cui et al., 2007, Katayama et al., 2011, Kadowaki et al., 2007). Here, an EdU pulse-chase experiment was used to determine which aspect of IKNM is misregulated. Ectopic mitoses were shown to arise due to the impaired basal-apical movement of nuclei within the neuroepithelium, as a 1 h labelling period was sufficient to label ectopic mitoses, but not apical mitoses, which were only labelled 2 h after EdU pulse. The mechanisms which control this segment of nuclear migration, usually restricted to the G2 phase of the cell cycle, is contested. Tpx2, a protein involved in microtubule organisation, was found to localize to the apical processes during G2, and its depletion impaired the basal-to-apical migration of G2-phase nuclei, leading to increased mitosis in a subapical position (Kosodo et al., 2011). Regulation of dynein, the minus-end-directed microtubule motor protein, has also been implicated in the apical movement of nuclei (Tsai and Gleeson, 2005, Gambello et al., 2003, Cappello et al., 2006). Other than microtubule-driven mechanisms, actin and myosin have also been implicated in this phase of IKNM within the neuroepithelium, as cytochalasin B, an actin depolymerizing agent, and blebbistatin, a myosin inhibitor, both disrupt IKNM during apical migration of nuclei (Spear and Erickson, 2012a).

Further studies could involve assessing expression of each IKNM-related protein to determine which is disrupted in *Trp53bp2*$^{\Delta 3/\Delta 3}$ embryos. This might help solve the puzzle of IKNM regulation. However, perhaps the mislocalisation of PAR3 and subsequent recruitment of other apical proteins, is sufficient to ‘redefine’ the apical domain, and therefore ‘trick’ mechanical proteins that normally regulate IKNM into instructing cells to enter M phase

before reaching the lumenal border. Ectopic mitoses are an additional feature of the chick neuroepithelium following ectopic overexpression of PAR3. It was suggested that the higher adhesiveness of PAR3-overexpressing cells compared to their neighbouring cells causes IKNM to be arrested, and cells to divide at ectopic positions (Afonso and Henrique, 2006).

The results of this chapter allow the original model of phenotypic progression (Figure 4-14) to be expanded, providing a hypothesis for NTD development and progression in *Trp53bp2*$^{\Delta 3/\Delta 3}$ embryos.

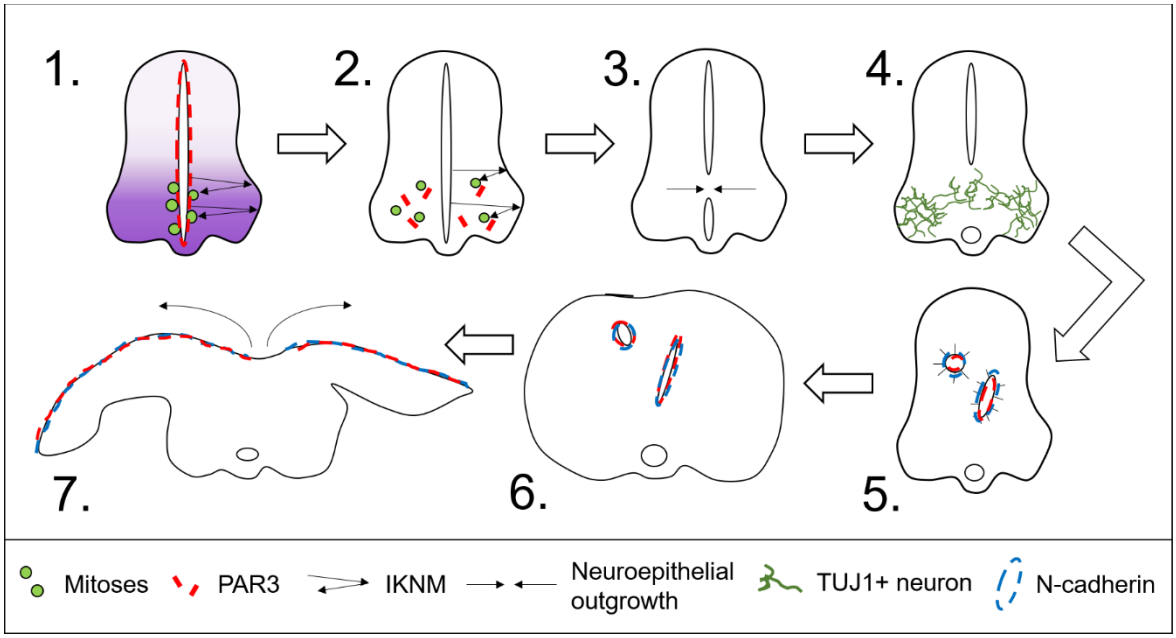

Figure 5-6: Final model of phenotypic progression in *Trp53bp2*$^{\Delta 3/\Delta 3}$ embryos

1. In the wild-type situation, ASPP2 (purple) is expressed throughout the neuroepithelium, most expressed in the ventral region. It binds to PAR3 and controls its localisation to the apical border, allowing IKNM to occur 'normally' and mitosis to occur at the lumenal border. **2.** Knockdown of ASPP2 results in the mislocalisation of PAR3, initially in the ventral neuroepithelium. This causes disruption of IKNM, where nuclei are prevented from migrating the full width of the neuroepithelium in a basal-apical direction, and instead enter mitosis away from the apical border. **3.** Mislocalised PAR3 expression causes other apical proteins and adheren junctional proteins, such as N-cadherin, to be recruited away from the lumenal surface. The loss of the apical border-related proteins, and mitoses occurring away from the lumen, and therefore no longer contributing to expansion of the lumen (Hoijman et al., 2015), allows neuroepithelial outgrowth across the midline, forming a bridge between 2 separate lumens. **4.** Newly formed neurons are now able to cross the midline via the neuroepithelial bridge. **5.** Disruption continues as the apical border is gradually degraded. Rosettes form where PAR3 is accumulated ectopically, recruiting other apical-related proteins, which then open to form new lumens. **6.** As development progresses, hydrostatic pressure within the diminished and abnormal lumens is increased, and accumulating TUJ1 neurons in the midline ventrally 'push' newly formed lumens towards the dorsal surface. **7.** Eventually, the lumenal pressure and close proximity of lumens to the roof-plate, causes neural tube

rupture, exposing the neuroepithelium to the dorsal exterior of the embryo which forms a plaque over a persistent small lumen retained above the floor-plate.

This model brings together the findings in this thesis so far, combined with the literature around apico-basal polarity (Costa et al., 2008, Cappello et al., 2006, Paridaen and Huttner, 2014), IKNM (Del Bene, 2011), neural tube patterning (Pfaff et al., 1996, Briscoe et al., 2000), cases of abnormality/multiple lumens within the neuroepithelium (Munson et al., 2008, Katayama et al., 2011), and neural tube reopening (Smith et al., 1993). Although PAR3 has been reported on numerus occasions to be a key regulator of apico-basal polarity and lumen formation (Cong et al., 2010, Sottocornola et al., 2010, Afonso and Henrique, 2006), the alternative reason for initial disruption of interkinetic nuclear migration is the role of the shorter isoform BBP, and its role in cell cycle regulation. As previously mentioned, BBP, when transiently transfected into cells, has been shown to result in the accumulation of transfected cells in the G2/M phase of the cell cycle (Naumovski and Cleary, 1996), suggesting that upon knockdown of BBP, cells in *Trp53bp2*$^{\Delta 3/\Delta 3}$ embryos could enter M phase earlier, bypassing this cell cycle arrest. Any disruption in the cell cycle would have drastic effects on neuroepithelial structure, and could lead to the phenotypes seen in these mice. However, the inconclusive findings regarding BBP (Naumovski and Cleary, 1996), compared to the sheer quantity of evidence regarding PAR3 disruption and its consequences (Afonso and Henrique, 2006), and the many mouse and zebrafish mutants which exhibit similar phenotypes following disruption of an apical protein (Katayama et al., 2011, Kadowaki et al., 2007, Cui et al., 2007, Munson et al., 2008), PAR3 remains a key player in this proposed model.

5.3.2 Questions remain to be answered

Although PAR3 appears to be a likely candidate leading to the apico-basal defect in *Trp53bp2*$^{\Delta 3/\Delta 3}$ embryos, ASPP2 has many other binding partners, as well as its best-known binding partner, p53. For example, it has been shown

that ASPP2 binds and activates YAP, a component of the Hippo pathway, which has been shown to regulate neural progenitor cell number (Royer et al., 2014, Cao et al., 2008). ASPP2 has also been shown to bind to APP-BP1, a component of the neddylation pathway, via its N-terminal, leading to a decrease in cell proliferation and neuronal apoptosis (Chen et al., 2003). As a final example, ASPP2 has been identified as a transcriptional target of STAT1 and regulator of neuroinflammation (Turnquist et al., 2014). This incredibly diverse role suggests many factors and pathways need to be considered to fully understand the variable phenotype seen in *Trp53bp2*$^{\Delta 3/\Delta 3}$ embryos.

Although the model depicted in Figure 5-6, provides a good basis to understand this unique NTD, it does not explain the significant increase in total mitotic index in *Trp53bp2*$^{\Delta 3/\Delta 3}$ embryos. Increased proliferation in neural progenitor cells has also been seen in mouse mutants with defective apical adherens junctions. For example, the loss of RhoA in neural progenitor cells was shown to cause the disruption of adherens junctions and hyperproliferation (Katayama et al., 2011). In this instance, it was proposed that hyperproliferation of neural progenitor cells was caused by hyperactivation of the hedgehog pathway, as they saw increased expression of downstream target genes of Shh signalling, and an expansion of the PAX6+ cell population (Katayama et al., 2011). This mechanism was also suggested as a reason for hyperplasia in mice lacking the essential adherens junction gene, αE-catenin, where Smoothened, a critical member of the Shh pathway, was seen to be up-regulated in mutant mouse cortices (Lien et al., 2006). Although downstream targets of Shh signalling were not assessed here, there was no significant change seen in the pattern of Shh-induced transcription factor expression throughout the neuroepithelium, and the only lumen retained, despite complete disruption of the neuroepithelium, was just superior to the floor-plate, an area directly influenced by Shh signalling.

The diversity of ASPP2 protein interactions, the contested regulators of IKNM, and the complex relationships between apical polarity proteins, adherens junctions and cell proliferation (Stepniak et al., 2009), make the

NTDs in *Trp53bp2*$^{\Delta 3/\Delta 3}$ embryos a difficult problem to solve. However, an increased mitotic index is a characteristic that is likely to significantly contribute to the lethal NTD phenotype in *Trp53bp2*$^{\Delta 3/\Delta 3}$ embryos, and provides an important and relatively easier phenotype to address.

Chapter 6 Targeting the phenotype in ASPP2$^{\Delta exon3/\Delta exon3}$ embryos through the use of DAPT in whole embryo culture

6.1 Introduction

In the uterus, rodent embryos of E10.5 or older increasingly rely on oxygen and nutrient transfer via the chorio-allantoic placenta (Cockroft, 1973). It has been shown previously that development of older embryos *in vitro* can be supported by increasing the oxygen supply to 95 % O2, 5 % CO2, however, further development of the embryo is prevented by the harmful effect of the high oxygen pressure on the yolk sac itself, which loses blood circulation and ceases to function (New and Coppola, 1970). It was later found that exteriorisation of the embryo from the yolk sac and removal of the amnion improved development of late-stage rodent embryos (Cockroft, 1973). It was assumed that by growing the embryo with the yolk sac open allowed the use of capillary circulation at the embryonic surface for oxygen transfer, in addition to any contribution from the opened yolk sac, which remains in vascular continuity with the embryo (Cockroft, 1973). The open yolk sac technique has since been used for a variety of methods such as pharmacological manipulation of blood and lymphatic vascularisation (Zeeb et al., 2012), testing serum-free media (Moore-Scott et al., 2003), and manipulating BMP4 signalling gradients via bead implantation (Behesti et al., 2006), yet it remains a rarely used model.

To study the effect of a chemical inhibitor or solution on the development of rodent embryos *in vitro*, dissolved reagents can be introduced directly to the culture medium. Using this method, as opposed to an *in vivo* approach, the maternal system is by-passed and therefore maternal metabolizing enzymes are removed from the experimental design. Here, due to the complexity of the mechanisms controlling apico-basal polarity and the controversy surrounding IKNM, it was decided to target the over-proliferation phenotype in ASPP2 mutant mice, using this method. It was hypothesised that the increase in mitotic index contributed to the final reopening of the neural tube in *Trp53bp2*$^{\Delta 3/\Delta 3}$ embryos (Figure 5-6), and therefore a reduction in

proliferation, using a chemical inhibitor or reagent, could partially rescue or slow down the phenotype.

Various inhibitors have previously been shown to reduce proliferation. For example, retinoic acid has been introduced into mouse whole embryo culture systems, and shown to reduce proliferation; however, this also results in limb deformities and median cleft lip (Goulding and Pratt, 1986, Watanabe and Pratt, 1991). Hydroxyurea (HU), a drug which selectively inhibits ribonucleoside diphosphate reductase (Wright et al., 1990), has been shown to reduce the number of mitotic cells in the ventricular zone of slice cultures when applied to the medium (Kosodo et al., 2011). Nocodozole, which acts through disrupting microtubule assembly, has been reported to inhibit mitosis in E5.5 embryo cultures (Stuckey et al., 2011). Finally, DAPT, a small molecule inhibitor that blocks Notch activity, has been shown on multiple occasions to decrease proliferation and increase differentiation in neural progenitors (Theocharatos et al., 2013, Nelson et al., 2007, Wang et al., 2009). Due to the multiple examples of the use of DAPT in whole embryo culture (Kitajima et al., 2013, Richard et al., 2013, Voelkel et al., 2014), this inhibitor was chosen for use in *Trp53bp2*$^{\Delta 3/\Delta 3}$ embryo cultures.

It is important to note that due to time limitations, the following results are from a pilot study only, designed to:

- Assess the possibility of culturing late stage embryos from E10.5 – E11.5

- Test various concentrations of DAPT for use in whole embryo culture

- Begin to assess whether this inhibitor would be a suitable reagent to reduce proliferation in *Trp53bp2*$^{\Delta 3/\Delta 3}$ embryos

6.2 Results

6.2.1 Macroscopic morphology of DAPT-treated embryos

DAPT is known to both decrease proliferation and increase differentiation in neural progenitors (Theocharatos et al., 2013). To target the overgrowth phenotype and increased mitotic index in *Trp53bp2*$^{\Delta 3/\Delta 3}$ embryos (Figure 4-6), embryos were cultured between E10.5 and E11.5 in the presence or absence of DAPT. This time point was chosen to precede abnormal TUJ1 patterning seen in E11.5 embryos (Figure 4-11), with the aim of inducing differentiation before the disruptive phenotype progressed further. Where DAPT has previously been used in mouse whole embryo culture, concentrations varied between 40/50 µM (Kitajima et al., 2013, Richard et al., 2013) and 200 µM (Voelkel et al., 2014). Therefore, 100 µM was chosen as the starting concentration. Figure 6-1 shows example images of wild-type embryos cultured via the open yolk sac technique in the presence of DAPT, and parallel controls with the addition of DMSO vehicle only.

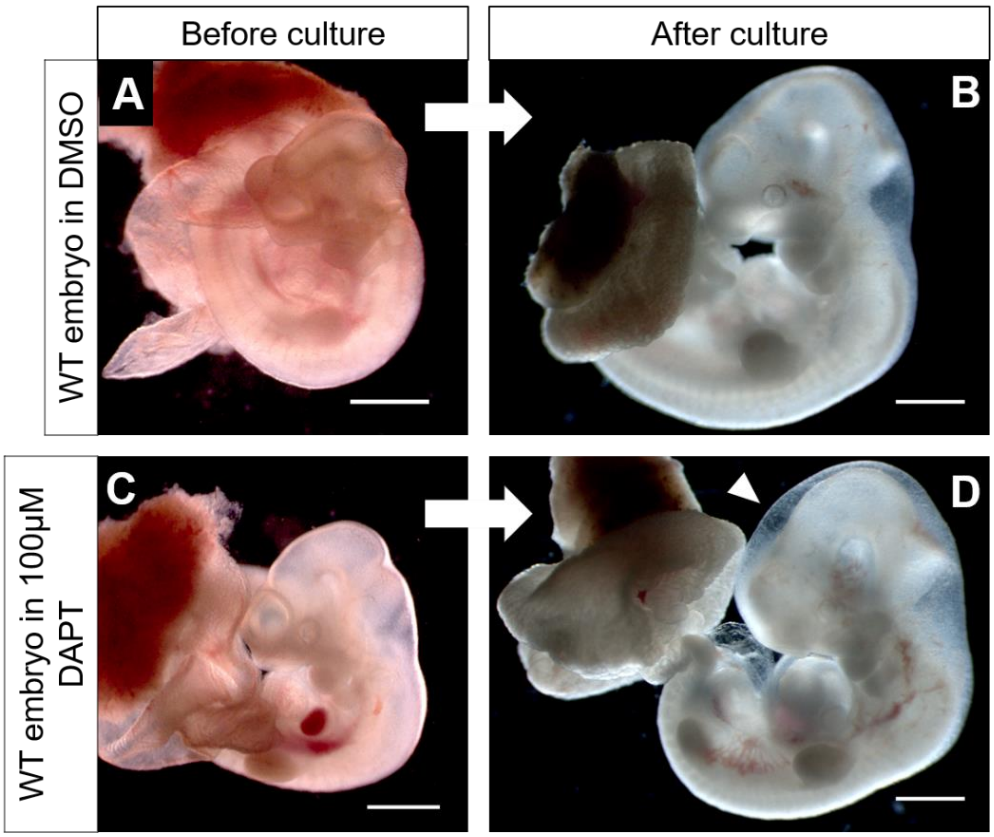

Figure 6-1: Example images of embryos pre- and post-culture in DMSO and DAPT

Two wild-type embryos cultured in DMSO (A-B) and 100 µM DAPT (C-D) for 24 h in 100% rat serum. (**A**) E10.5 WT embryo before culture, following dissection from the yolk sac and removal of the amnion. (**B**) Embryo (A), following 24 h culture in DMSO. Significant development is seen, including branchial arch development, brain enlargement and body axis elongation. (**C**) E10.5 WT embryo in the same experiment as (A,B). (**D**) Embryo (C), following 24 h culture in 100 µM DAPT. Significant development is seen including brain enlargement and body axis elongation. Oedema can be especially affecting the head region (see arrow head), and pigmentation around the developing eye is reduced, compared to (B). Scale bars 1 mm.

Substantial development was achieved when E10.5 ASPP2 embryos were cultured for 24 h in 100% rat serum + DMSO / + DAPT using the open yolk sac technique. In the majority of embryos, including mutants, enlargement of the head region and elongation of the body axis were evident following the culture period in both treatment groups (Figure 6-1, B, D). Branchial arches were often seen to develop further, and the developing eyes became pigmented (Figure 6-1, B). This showed that it is possible to culture *Trp53bp2*$^{\Delta 3/\Delta 3}$ embryos at this late stage in gestation. However, despite an

increase in size, embryos cultured in DAPT often exhibited severe oedema in the head region (arrow head Figure 6-1, D), a rarer occurrence in embryos cultured in DMSO. DAPT concentrations were reduced in the light of this high frequency of oedema, to assess whether lower concentrations could reduce toxicity.

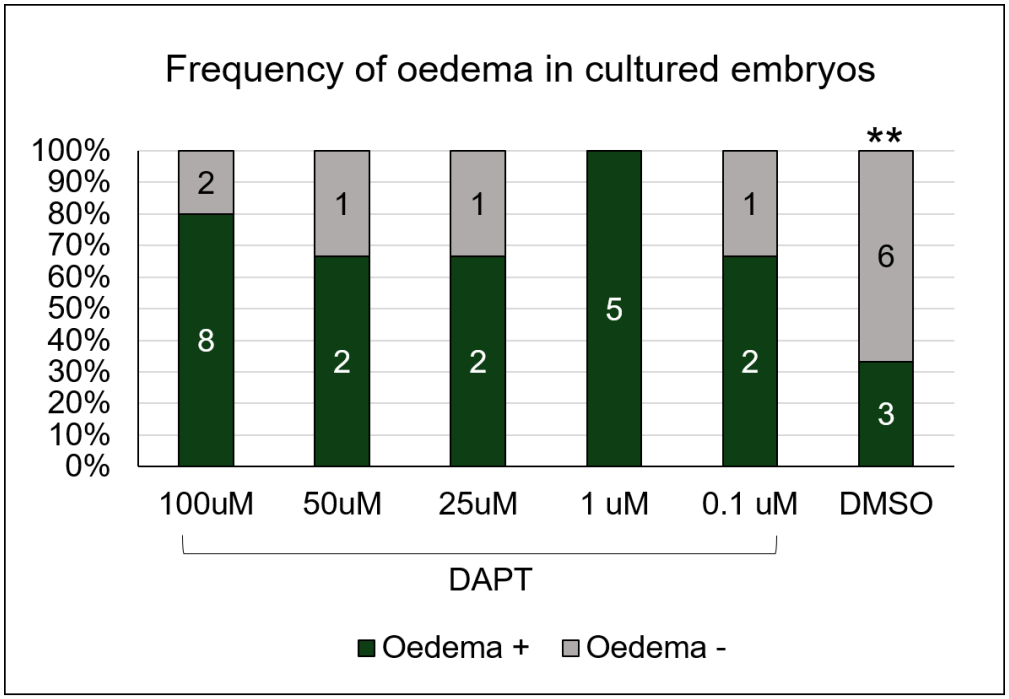

Figure 6-2: Frequency of oedema in WT/Het embryos cultured in defined concentrations of DAPT, and DMSO

Frequency of oedema in WT and Het embryos cultured in DAPT concentrations: 100, 50, 25, 1 and 0.1 µM, and DMSO. Oedema frequency in all DAPT cultures was 66.6% or higher. Oedema frequency in embryos cultured in DMSO was significantly lower than the combined frequency of embryos cultured in DAPT (all concentrations). **Statistical analysis:** Chi-square contingency table (5X2) showed no significant difference in oedema frequency between the separate DAPT concentrations. Chi-square test comparing DMSO and combined DAPT groups: ** $p \leq 0.01$. n = numbers shown on bars.

Graded dilutions of DAPT were tested at final concentrations of 100, 50, 25, 1 and 0.1 µM. Although mutant embryos were included in 25 and 100 µM DAPT cultures, only WT and Het embryos from ASPP2 litters were used to assess dose-response. Oedema was observed in >60% of WT and Het cultured embryos at all concentrations of DAPT (Figure 6-2), including 2/3

embryos cultured at the lowest tested concentration of DAPT: 0.1 µM. The highest incidence of oedema was at 1 µM DAPT, where 5/5 embryos exhibited oedema. Only 3/9 embryos cultured in DMSO exhibited oedema, which was significantly lower than the combined frequency of all DAPT cultures.

To get an overall picture of how DAPT was affecting the cultured embryos, a phenotypic assessment was made, including growth measurements: head and dorsal lengths. In the interests of evaluating the general effect of DAPT, all concentrations were grouped for macroscopic morphology comparisons. Figure 6-3 shows the macroscopic phenotype analysis in WT/Het and mutant groups.

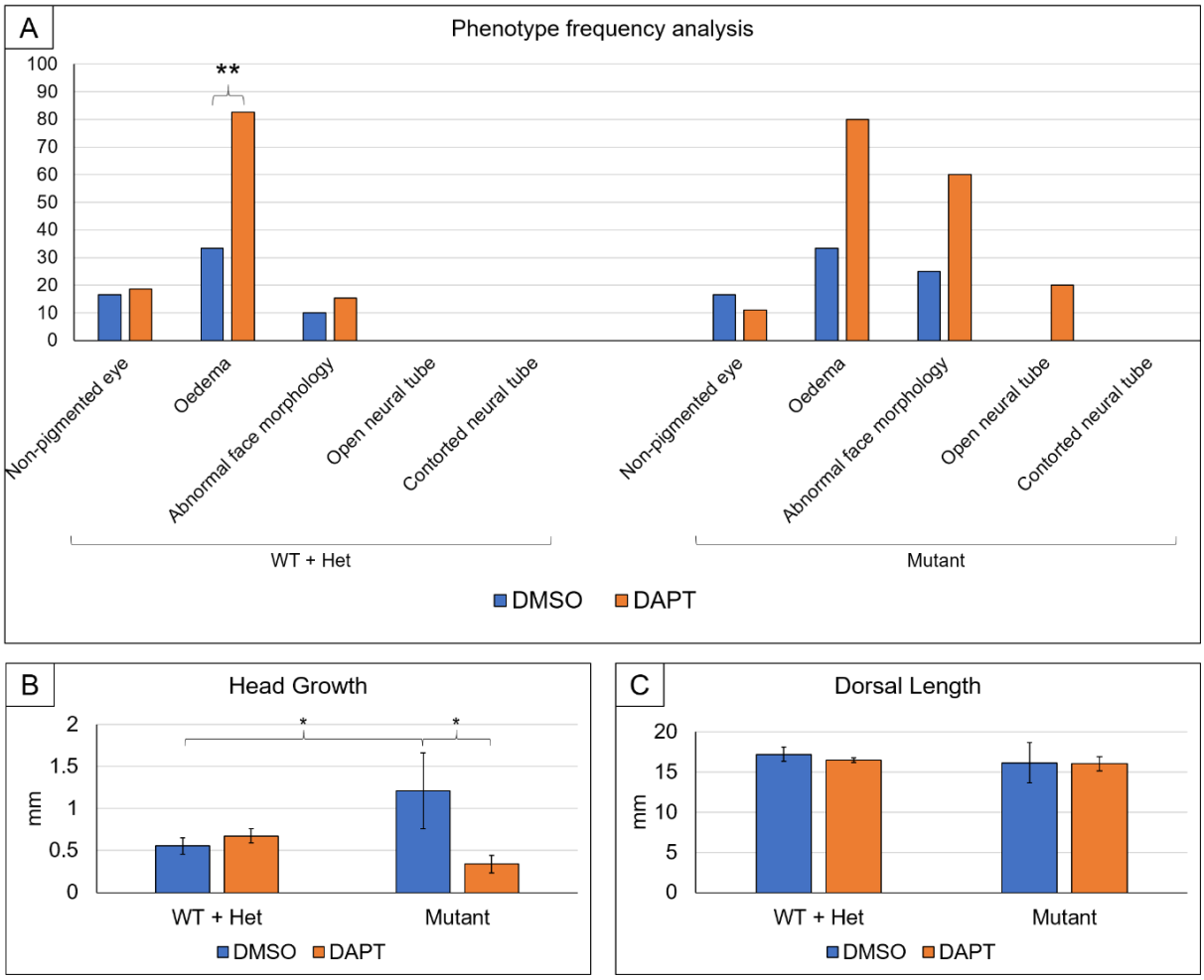

Figure 6-3: Macroscopic phenotype analysis of WT/Het and mutant embryos cultured in DMSO and DAPT

(**A**) Phenotypic frequency of: non-pigmented eyes, oedema, abnormal face morphology, open neural tube and contorted neural tube in WT/Het and mutant embryos cultured in DMSO or DAPT. Non-pigmented eyes and abnormal face morphology did not differ significantly between DAPT and DMSO in WT/Het embryos. Oedema was significantly increased in DAPT-cultured embryos compared to DMSO-cultured embryos. There were no embryos with an open or contorted neural tube. There was no significant difference in any of the phenotypes of mutant embryos between DAPT and DMSO cultures. There was no significant difference between WT/Het and mutant frequencies in each phenotype category. (**B**) Head growth analysis, calculated as the difference between head length pre- and post-culture. There was no significant difference in head growth between DMSO and DAPT WT/Het embryos. Head growth in mutant embryos cultured in DMSO was significantly greater than in those cultured in DAPT, and significantly greater than DMSO-cultured WT/Het embryos. (**C**) Dorsal length of embryos post-culture. Dorsal length did not differ significantly between DMSO or DAPT cultures in any embryo group, nor between WT/Het and mutant embryos. **Statistical analysis:** Chi-square tests performed between DMSO and combined DAPT groups in each category, and between WT/Het and mutant frequencies in DAPT / DMSO cultured embryos in each phenotype category. ** $p \leq 0.01$, * $p \leq 0.05$. Error bars: standard error. WT/Het DMSO n = 9; WT/Het DAPT n = 24; Mutant DMSO n = 3; Mutant DAPT n = 5.

Eye pigmentation, oedema, abnormal face morphology, open or contorted neural tubes (all characteristics of *Trp53bp2*$^{\Delta 3/\Delta 3}$ embryos) were assessed following culture in DMSO or DAPT. In WT/Het embryos, oedema was the only macroscopic phenotype affected by introducing DAPT into the culture medium (Figure 6-3, A). The low incidences of abnormal face morphology and no eye pigmentation in WT/Het embryos was due to the presence of oedema in the head region. In mutant embryos, DAPT had no significant effect on macroscopic morphology, and embryos did not differ in phenotype frequencies compared to WT/Het embryos (Figure 6-3, A). This is likely due to the low numbers of mutants, as these phenotypes have been shown previously in *Trp53bp2*$^{\Delta 3/\Delta 3}$ embryos (Figure 4-4).

Due to the previous finding of overgrowth in the head region (Figure 4-4, F, I), head growth and dorsal length were measured. No significant difference was found in dorsal length between DMSO- and DAPT-treated WT/Het, or mutant embryos (Figure 6-3, C). However, head growth in DMSO-treated mutant embryos was significantly increased compared to DMSO-treated WT/Het embryos (Figure 6-3, B). This suggests overgrowth of the head region in mutant embryos also occurs in culture, compared to normal enlargement of the brain in WT/Het embryos. Head growth in DMSO-treated mutant embryos was also significantly increased compared to DAPT-treated mutant embryos (Figure 6-3, B). This suggests DAPT may reduce or control overgrowth to a certain extent. However, the presence of oedema complicated the analysis of head growth. Further experiments and higher sample numbers would be required to fully understand the effect of DAPT on macroscopic phenotype.

The high frequency of oedema, even in wild-type embryos, suggested all tested concentrations of DAPT resulted in toxicity in whole embryo culture. To further examine the effect of DAPT, and to explore its potential in reducing proliferation and increasing differentiation in the neuroepithelium, the histological morphology of ASPP2 embryos was assessed post-culture.

6.2.2 Histological morphology of DAPT-treated embryos

To assess the potential of DAPT in reducing proliferation, PHH3 analysis was undertaken on WT and mutant embryo sections only. Histological morphology was deduced from embryo sections, and TUJ1 staining was performed on a selection of samples to assess the effect of DAPT on neural differentiation.

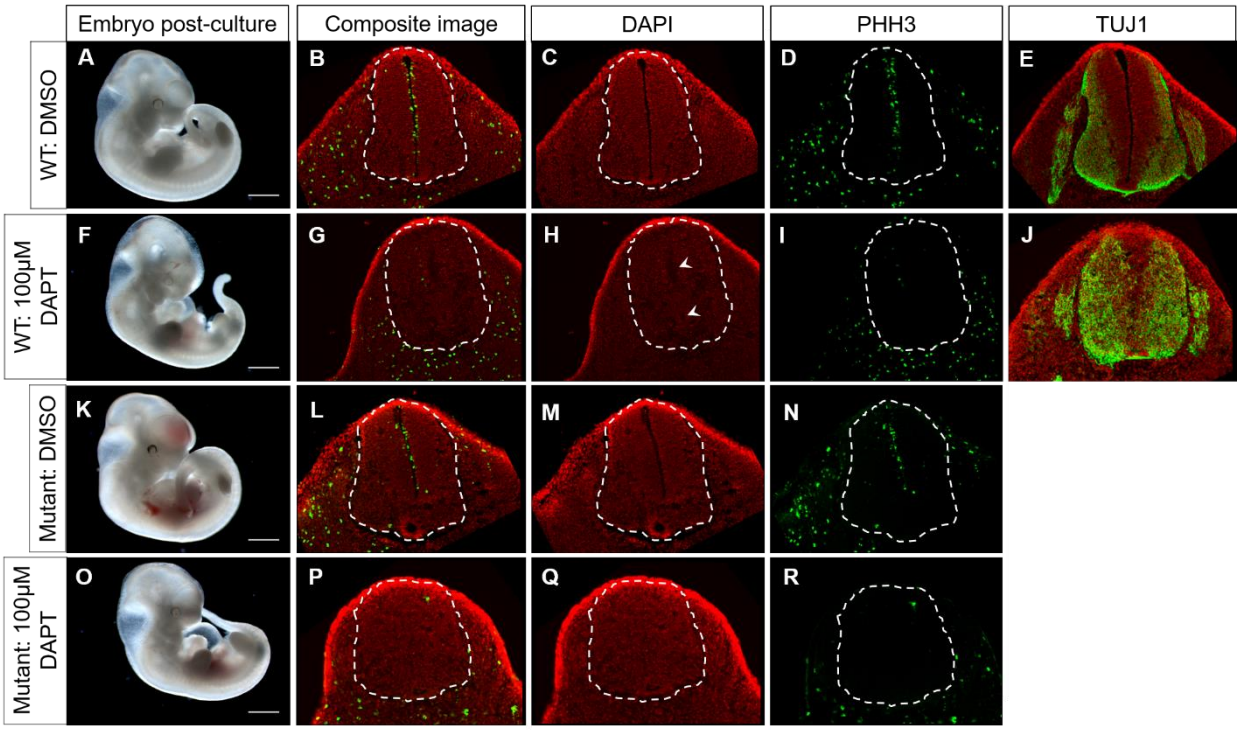

Figure 6-4: Histological morphology of WT and mutant embryos cultured in DAPT- or DMSO-treated medium

A/F/K/G: Whole embryo images, post-culture. B/G/L/P: composite images showing neural tube section with DAPI (red), PHH3 (green) processed from embryo in adjacent image. C/H/M/Q: DAPI staining only (red). D/I/N/R: PHH3 staining only (green). (**A**) WT embryo post-culture in DMSO. (**B**) Composite image of neural tube section from embryo in (A). (**C**) DAPI staining shows a midline lumen spanning the dorso-ventral axis of the neural tube. (**D**) PHH3 staining shows the majority of mitoses lie along the apical border of the neural tube, at the lumenal surface. (**E**) TUJ1 staining of a different section taken from WT embryo in (A). TUJ1 positive areas include the ventro-lateral and basal regions of the neural tube. (**F**) WT embryo cultured in 100 µM DAPT-supplemented medium. (**G**) Composite image of neural tube section from embryo in (F). (**H**) DAPI staining shows disruption of the neuroepithelium, with 2 separated, ill-defined lumens (see arrow heads). (**I**) Very few PHH3+ cells are seen within the neuroepithelium. (**J**) TUJ1 staining of a different section taken from WT embryo in (F). TUJ1 staining is seen in the majority of the neuroepithelium, with positive cells crossing the midline at multiple locations. (**K**) Mutant embryo cultured in DMSO-supplemented medium. (**L**) Composite image of neural tube section from embryo in (K). (**M**) DAPI staining shows a neural tube exhibiting 2 lumens, including one small circular lumen above the floor-plate. (**N**) The majority of PHH3+ mitoses lie along the apical border of the upper lumen, with a few mitoses in ectopic locations within the neuroepithelium. (**O**) Mutant embryo cultured in

100 μM DAPT-supplemented medium. (**P**) Composite image of neural tube section from embryo in (O). (**Q**) DAPI staining shows substantial cellular disruption in the neuroepithelium. A small singular lumen can be seen above the floor-plate. (**R**) Very few PHH3+ cells are seen within the neuroepithelium. Scale bars 1 mm.

The histological morphology and location of PHH3+ cells, in WT and mutant embryos cultured in DMSO, closely matched that of E11.5 embryos developed *in vivo*, described previously (Figure 4-5 and Figure 4-6). For example, the neural tube of WT embryos, cultured for 24 h in DMSO-supplemented medium, exhibited a single midline lumen that spanned the dorso-ventral axis. PHH3+ cells were numerous and were located adjacent to the lumenal surface, at the apical border of the neural tube. (Figure 6-4, C, D). Mutant embryos had a more varied appearance, as previously shown, yet often exhibited a small circular lumen above the floor-plate, and an incomplete lumen more dorsally. PHH3+ cells were located both along the lumen and in ectopic locations throughout the neuroepithelium (Figure 6-4, M, N).

The effect of DAPT was striking. Disruption of the neuroepithelium was evident in both WT and mutant embryo sections, with cells crossing the midline and loss of the lumen(s) or a reduction in lumen size (Figure 6-4, H, G). Similar to sections from *in vivo* mutant embryos, a small lumen was often present above the floor-plate, even in WT embryos (Figure 6-4, H). This disrupted histological morphology was present at all tested concentrations of DAPT. TUJ1 staining was present in a larger proportion of neuroepithelial cells in DAPT-treated WT embryos, compared with DMSO-cultured controls (Figure 6-4, J, E). Notably, TUJ1+ cells crossed the midline in these DAPT-treated WT embryos. PHH3+ cells appeared greatly reduced in DAPT-treated neural tubes, both WT and mutant, with only a few mitoses remaining in the neuroepithelium. These findings support the known role of DAPT in reducing proliferation and increasing neuronal differentiation in neuroepithelial progenitors (Theocharatos et al., 2013).

To explore the dose-response of DAPT in relation to reduced proliferation in the neural tube, PHH3+ cells were quantified as before (Figure 4-6), using the available WT and mutant embryo sections. Ectopic mitotic analysis and lumen circumference measurements were also included due to the loss of lumen seen in the 100 µM DAPT-cultured embryos (Figure 6-4, H, Q).

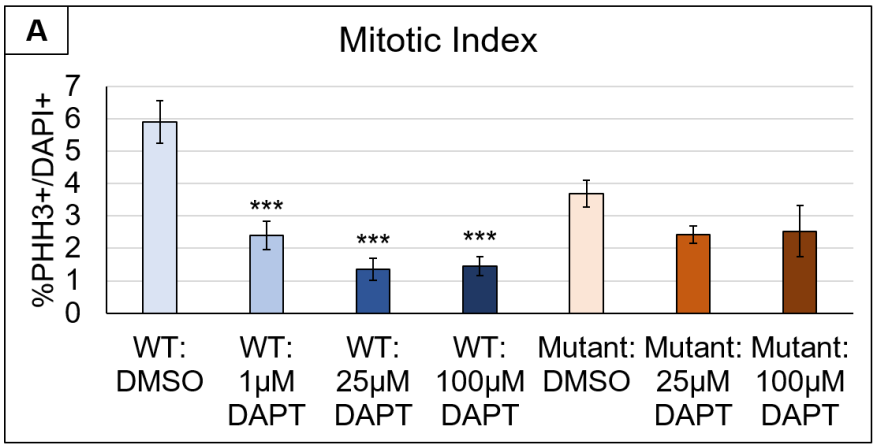

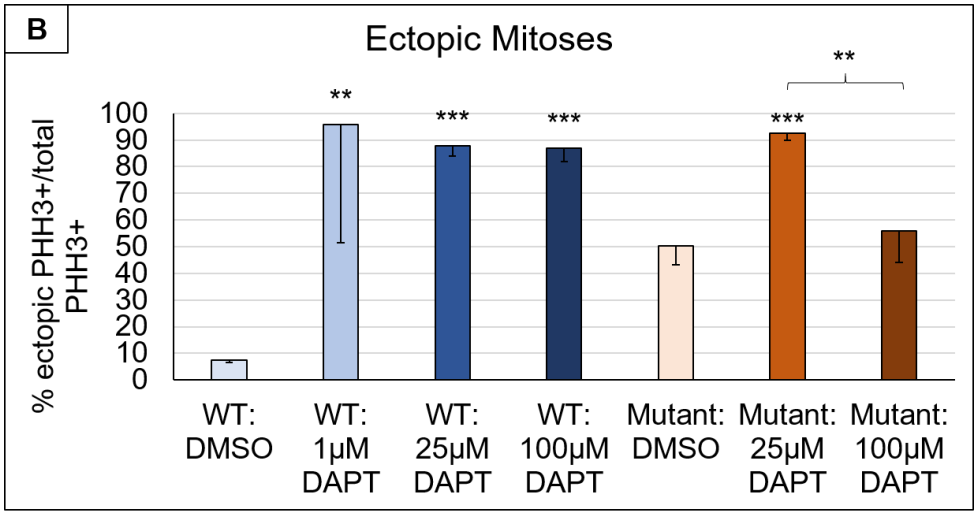

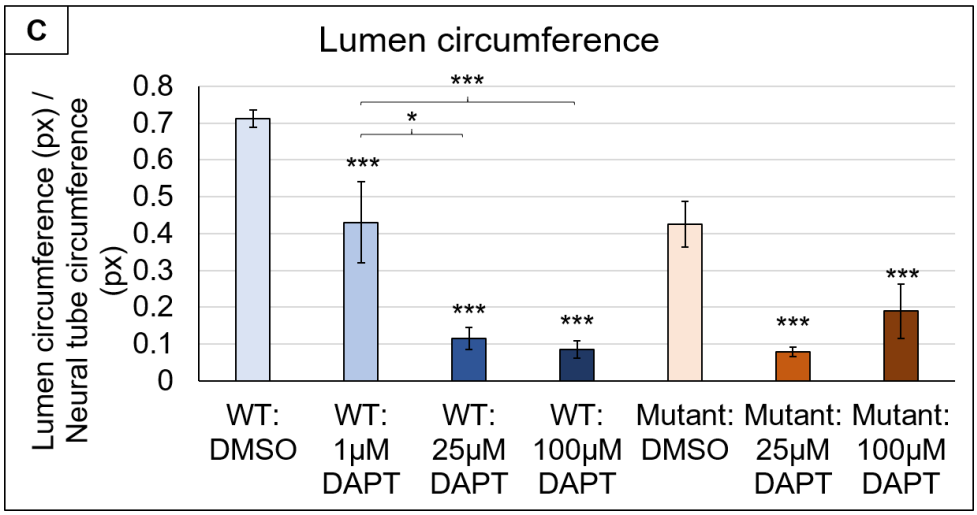

Figure 6-5: Mitotic index, % ectopic mitoses and lumen circumference of wild-type and mutant embryos treated with DMSO and DAPT

PHH3+ and lumen circumference analysis using embryo sections from WT: DMSO, WT: DAPT (1/25/100 μM), Mutant: DMSO and Mutant: DAPT (25/100 μM). (**A**) Mitotic index (%PHH3+/DAPI+ cells). DAPT-treated WT embryos had a significantly reduced mitotic index compared with DMSO-treated WT embryos. There was no significant difference between DAPT concentrations. The mitotic index of mutant embryos did not significantly differ when

DAPT was added, compared with DMSO. (**B**) Ectopic mitoses (% ectopic PHH3+/total PHH3+ cells). DAPT-treated WT embryos had a significantly higher % ectopic mitoses than DMSO-treated WT embryos. There was no significant difference between DAPT concentrations. 25 µM DAPT-treated mutant embryos had a significantly increased ectopic mitotic index compared to DMSO-treated and 100 µM DAPT-treated mutants, which did not differ from each other. (**C**) Lumen circumference (px), normalised to neural tube circumference (px). Lumen circumference was significantly reduced in DAPT-treated WT embryos compared to DMSO-treated WT embryos. There is some evidence of a dose-response effect, as 1 µM DAPT-treated WT embryos have a significantly larger lumen circumference than those treated with 25 and 100 µM DAPT. The latter differ significantly from DMSO-treated WT embryos. DAPT-treated mutant embryos have a significantly reduced lumen circumference compared with DMSO-treated mutants. **Statistical analysis:** One-way ANOVA between DMSO and all DAPT concentrations within WT and mutant embryo groups, showed significance in mitotic index, ectopic mitotic index and lumen circumference for all analyses ($p \leq 0.001$), with the exception of mitotic index in mutant embryos ($p > 0.05$). Post-hoc pair-wise tests of DMSO / DAPT-treated embryos: *** $p \leq 0.001$, ** $p \leq 0.01$, * $p \leq 0.05$; Student's t-tests. Error bars: standard error. WT DMSO: n = 3, WT: 1 µM DAPT: n = 2, WT: 25 µM DAPT: n = 1, WT: 100 µM DAPT n = 3. Mutant DMSO: n = 2, Mutant: 25 µM DAPT: n = 3, Mutant: 100 µM DAPT n = 2. 3-4 slides analysed per embryo, 4-5 sections per slide.

Preliminary quantitative results strongly suggest that mitotic index is reduced in WT embryos cultured in all concentrations of DAPT (100, 25 and 1 µM), compared with DMSO-treated control embryos. Interestingly, mitotic index in mutant embryos did not significantly differ between DAPT- and DMSO-treated cultures (Figure 6-5, A). A dramatic increase in % ectopic mitoses was seen in all DAPT concentrations in WT, and in mutant embryos treated with 25 µM DAPT, compared to DMSO embryos. As ectopic mitoses are scored as being away from the lumen border, this correlates with loss of the lumen following DAPT treatment (Figure 6-4, H, Q). Lumen circumference was found to be significantly reduced in all DAPT-treated embryos, compared with control DMSO-treated embryos. Dose-response of DAPT seemed insignificant, with the exception of lumen circumference in WT embryos, where 1 µM DAPT had a significantly larger lumen circumference than 25 µM and 100 µM DAPT-treated embryos.

6.3 Discussion

This chapter has demonstrated that mouse embryos can be cultured in the period E10.5-E11.5, using 100% rat serum and the open yolk sac method, with considerable developmental progression. Moreover, the DAPT inhibitor

was successfully used to probe the phenotypic development of wild-type and *Trp53bp2*$^{\Delta 3/\Delta 3}$ mutants. While DAPT was found to be toxic to embryos, even at concentrations far below those reported in the whole embryo culture literature, it nevertheless was shown to reduce proliferation and increase differentiation in the neuroepithelium, as expected from its known function of inhibiting Notch signalling.

The initial hypothesis was that the anti-proliferative properties of DAPT might counteract the increased mitotic activity observed in *Trp53bp2*$^{\Delta 3/\Delta 3}$ mutants, and hence reduce the severity of the neural tube 'overgrowth' defects. In fact, a quite different result was obtained, in which wild-type embryos were caused by DAPT to exhibit a phenotype with striking resemblance to that seen in *Trp53bp2*$^{\Delta 3/\Delta 3}$ mutants. This involved neuroepithelial disruption with differentiating cells crossing the midline and occluding the primary lumen, exactly as seen in mutant embryos *in vivo*. DAPT-treated wild-type embryos even replicated the small lumen retained just superior to the floor-plate. Mitoses were suppressed by DAPT (not increased as in *Trp53bp2*$^{\Delta 3/\Delta 3}$ mutants) but among those mitoses that still occurred, a high % were ectopic. Hence, DAPT treatment produces a partial 'phenocopy' of the *Trp53bp2*$^{\Delta 3/\Delta 3}$ mutant. Consistent with this finding, DAPT had relatively little effect on mutant embryos: there was certainly no 'rescue' observed, and instead the phenotype worsened in terms of a further increase in % ectopic mitoses (at 25 μM DAPT only) and with a further reduction in lumen circumference. This finding with DAPT may provide clues to the origin of the NT defect in *Trp53bp2*$^{\Delta 3/\Delta 3}$ mutants, as Notch signalling plays key roles in regulating both apico-basal polarity and the balance between cell proliferation and differentiation.

Considering apico-basal polarity, Notch1 was found to be distributed in an apically-biased manner in the mouse neuroepithelium, specifically around adherens junctions of the apical endfeet (Hatakeyama et al., 2014). In the zebrafish retina, anti-neurogenic Notch signals are enriched on the apical side of the neuroepithelium, as part of a Notch signalling gradient along the apico-basal axis (Del Bene et al., 2008). CSL$^{-/-}$ mutant mice, which are

devoid of canonical Notch signalling, demonstrate a neural tube phenotype consistent with apico-basal cell polarity, including deficiencies in the expression of apical polarity markers within the neuroepithelium (Main et al., 2013). Hence, the effect of DAPT in phenocopying the ASPP2 loss of function phenotype may support the hypothesis that impaired apico-basal polarity is a key factor leading to neuroepithelial disruption in *Trp53bp2*$^{\Delta 3/\Delta 3}$ mutants. This conclusion receives support from previous work that identified faulty apical adherens junction formation in *Trp53bp2*$^{\Delta 3/\Delta 3}$ mutant brains, and suggested a key role for a direct protein-protein interaction involving ASPP2 and PAR3 (Sottocornola et al., 2010). It remains to be determined whether Notch signalling may be involved in the apico-basal polarity disorder in *Trp53bp2*$^{\Delta 3/\Delta 3}$ mutants, or whether DAPT is able to phenocopy the defect by disturbing apico-basal polarity by a 'parallel' mechanism to that which depends on ASPP2.

In terms of the balance between cell proliferation and differentiation, DAPT caused wild-type embryos to show an increase in TUJ1-positive neurons that extended towards the midline, forming a tissue bridge that occluded the primary lumen in some cases. This was a striking recapitulation of the ASPP2 loss of function phenotype, and supports the idea that enhanced neuronal differentiation may play a key role leading to the disorganised, multi-lumen NT phenotype of *Trp53bp2*$^{\Delta 3/\Delta 3}$ mutants. Moreover, ectopic mitoses were more common in DAPT-treated embryos, as in *Trp53bp2*$^{\Delta 3/\Delta 3}$ mutants, although it is unclear whether this might be a direct effect of Notch inhibition, or secondary to reduction in lumen circumference.

DAPT usage has been informative, but the multiple cellular effects of Notch inhibition complicate the interpretation of its embryonic effects. Although there are other anti-proliferative reagents that could be assessed in embryo culture, considering the overlap between cell cycle, proliferation, and IKNM, which relies on apico-basal polarity, it may prove difficult to target over-proliferation in an isolated manner. For example, hydroxyurea, a drug that has been shown to reduce the number of mitotic cells in the neuroepithelium, does so by preventing entry into G2-phase and perturbing apical-to-basal

migration (Kosodo et al., 2011). Cyclopamine, which inhibits *Smoothened*, a Shh receptor, could provide an alternative as it is able to reduce total cell number and control hyperplasia. However, cyclopamine has no worsening effect on cortical disorganisation in αE-catenin$^{-/-}$ mouse mutants with faulty adherens junctions (Lien et al., 2006). Perhaps cyclopamine, combined with an IKNM-targeted reagent which specifically improves basal-apical migration, could potentially co-rescue both the defective apico-basal polarity and over-proliferation phenotype in *Trp53bp2*$^{\Delta 3/\Delta 3}$ embryos. However, this would depend on the status of Shh signalling in ASPP2 mutant embryos, which appears unaffected, based on Shh-gradient-determined transcription factor expression.

Oedema - swelling due to fluid trapped in the embryo's tissues - was found to be significantly increased in DAPT-treated embryos. Generalised subcutaneous oedema in the embryo has been associated with disruption of the lymphatic system (Qu et al., 2010), and cardiovascular defects (Schneider et al., 2004), as a result of damaged or congested cardio or lymphatic vasculature. Notch target genes *Hey1* and *Hey2* are known to be required for embryonic vasculature development (Fischer et al., 2004). Furthermore, knockdown of *Notch2* in the embryo has been shown to cause myocardial hypoplasia and oedema (McCright et al., 2001). This may explain the significant increase in oedema seen in DAPT-treated embryos.

In conclusion, the inhibition of Notch signalling by DAPT in these embryo culture experiments has provided support for a role for both apico-basal polarity and enhanced neuronal differentiation in ASPP2 loss of function mutant embryos. Future experiments could take these studies forward by perhaps targeting IKNM, and re-establishing polarity across the neuroepithelium, in order to attempt to rescue the complex phenotype seen in *Trp53bp2*$^{\Delta 3/\Delta 3}$ embryos.

Chapter 7 Concluding remarks

7.1 Overview of the research findings

It has been demonstrated here that whole embryo culture (WEC) is a valuable technique in studying the development of mammalian embryos. In reducing the use of rat serum in WEC, it will hopefully become a more accessible and attractive method for researchers. Recent advances in other *in vitro* techniques such as embryonic brain slice cultures (Eid et al., 2018, Iyer et al., 2018), and 'gastruloid' cultures derived from embryonic stem cells (Beccari et al., 2018), will develop the field further, hopefully with the consideration of the NC3Rs and its values. A recent study addressing researcher's attitudes to the 3R's demonstrated a reversal of the 'hierarchy' of the 3Rs, prioritizing Refinement over Reduction, and Reduction over Replacement (Franco et al., 2018). Here, by reducing rat serum in whole embryo culture, rat usage will ultimately be reduced. Furthermore, by decreasing costs and limiting the time taken to produce rat serum, the technique should also become feasible for more laboratories researching embryonic development. In turn, this will reduce manipulation of pregnant dams, and therefore *refine* developmental studies, through application of reagents into the culture medium (as in Chapter 6), rather than through injection or feed.

Although many mouse mutants exhibiting NTDs are studied at the time point at which whole embryo culture was optimised (E8.5-E9.5), it became of interest to study an NTD mouse mutant with a late-occurring phenotype. It has been suggested that the post-neurulation 'rupture' mechanism may be plausible for some cases of human NTDs, however this idea has been greatly contested (Gardner, 1968, Hook, 1992). The complex phenotype of ASPP2 mutant embryos may broaden views on the possibility of neural tube rupture and open minds to alternative mechanisms leading to NTDs, other than failure of primary neurulation (Greene and Copp, 2014). Through studying both macroscopically phenotypic and non-macroscopically phenotypic ASPP2 embryos, the principle of 'partial penetrance' has also

been examined. Here, it was found that mutants that appear 'normal' macroscopically simply have a less advanced phenotype, and tend to suggest that the *Trp53bp2*$^{\Delta 3/\Delta 3}$ phenotype is actually fully penetrant. This finding has greatly benefitted understanding of the ASPP2 phenotypic progression (Figure 5-6), and could perhaps be applied to other mouse mutants that exhibit incomplete penetrance (Asai-Coakwell et al., 2009, Pereira et al., 1994).

Disruption of apical/basal polarity appears to be a major factor leading to the phenotype in *Trp53bp2*$^{\Delta 3/\Delta 3}$ embryos (Chapter 4). Apico-basal polarity is essential for IKNM within the neuroepithelium, which, although is a complex mechanism, can be broken down into stages to better understand where the failure occurs. This was achieved here, through the use of EdU labelling, where it was found that ectopic mitoses arose due to impaired basal-apical movement of nuclei (Figure 5-4). The mechanistic control of IKNM, however, is highly contested, and therefore remains a difficult process to understand and manipulate experimentally. Reasons for this could include the variety of species in which IKNM has been reported, and the difference in epithelial thickness being assessed. It's possible that different mechanisms are required to move nuclei greater distances within the neuroepithelium (Spear and Erickson, 2012b). Perhaps on the scale of an individual *Trp53bp2*$^{\Delta 3/\Delta 3}$ embryo, this could also explain why IKNM disruption causes reopening in some areas and not in others.

When considering the growing number of apical polarity-related mouse mutants which exhibit NTDs (Katayama et al., 2011, Kadowaki et al., 2007, Cappello et al., 2006), there appears to be a necessity to expand our knowledge of polarity genes in human NTD cases. PCP-related genes have been extensively studied in mouse mutants for their role in NTDs, such as Vangl2 (Kibar et al., 2011), Scrb1 (Murdoch et al., 2003) and Celsr1 (Curtin et al., 2003), and missense variants of *VANGL1, SCRIB, CELSR1* have been linked to sporadic and familial cases of spinal dysraphism in humans (Kibar et al., 2009, Robinson et al., 2012). The association between the planar cell polarity pathway and apical polarity/IKNM has been documented in multiple

incidences (Ciruna et al., 2006, Williams et al., 2014), stressing the importance of considering apical polarity in the context of other processes and pathways acting within the neuroepithelium. Furthermore, PAR3, a significant player in the ASPP2 phenotype (Sottocornola et al., 2010), has been implicated in human NTDs. Genetic variants in PARD3 have been associated with susceptibility to NTDs in a Chinese Han population (Gao et al., 2012), and deleterious variants of PARD3 in the aPKC-binding region have been shown to contribute to human cranial NTDs (Chen et al., 2017).

7.2 Strengths and Weaknesses

The significant strengths of this project lay in the optimisation of an embryo culture technique, and the extensive characterisation of a mouse mutant with a complex NTD phenotype. The 3R's were considered throughout, including a significant reduction of serum-use in neurulation stage embryo culture, and demonstration of an inhibitor study *in vitro*, using late-stage ASPP2 embryos with the open yolk sac technique. Limitations in relation to the 3R's included the use of *in vivo* EdU injections. Pilot studies which evaluated introducing EdU into the culture medium resulted in insufficient staining, in comparison to *in vivo* results (data not shown).

ASPP2 mouse mutants have thus far been assessed based on macroscopic morphology, tumour incidence, or histological morphology of the head region only (Sottocornola et al., 2010, Vives et al., 2006, Zak et al., 2016). This report gave a detailed cellular assessment of the histological morphology of *Trp53bp2*$^{\Delta 3/\Delta 3}$ embryos, in the spinal region of the neural tube. This led to substantiation of the PAR3-mediated apico-basal polarity defect theory, first posed by *Sottocornola* (Sottocornola et al., 2010), which had not since been addressed. The detail to which this phenotype was analysed is a significant strength of this report. It has also been demonstrated that by including 'non-macroscopically phenotypic' embryos in the analysis, this can lead to a proposed mechanistic progression of the phenotype.

Hypothesis-led research such as the EdU/IKNM study, and the use of DAPT in culture, were important first steps towards fully understanding the neural tube reopening phenotype in ASPP2 mutant embryos. The inhibitor study, although resulting in unexpected outcomes, further highlighted the importance of apical polarity in *Trp53bp2*$^{\Delta 3/\Delta 3}$ embryos. A potential weakness of not being able to complete this initial inhibitor study, or achieve a rescue of the phenotype, came down to time limitations.

7.3 Future directions

The reduction of rat serum by 50%, in the culture of neurulation-stage mouse embryos, was a great success of this work. Further experimentation could advance the uses of the GMEM + defined supplements medium, beyond the E8.5-E9.5 period of organogenesis. For example, culture of alternative embryonic stages may be achievable in reduced serum. There is also a possibility that rat serum could be reduced further for less sensitive developmental time points or for shorter cultures. Finally, as detailed in Appendices, many embryo culture studies have used rat or hamster embryos instead of mouse embryos. Testing the use of reduced serum for alternative rodent species could further enhance the prospects of this technique.

PAR3 is the only reported binding partner of ASPP2 with a direct association to apical polarity, and has the ability to recruit other apical proteins to an ectopic position, resulting in disruption of apico-basal polarity (Sottocornola et al., 2010, Afonso and Henrique, 2006). For these reasons, and finding evident disruption of PAR3 in *Trp53bp2*$^{\Delta 3/\Delta 3}$ embryos (Figure 5-2), it was hypothesised that mislocalisation of PAR3 leads to the extensive subsequent neuroepithelial disruption (Figure 5-6). *In vitro* methods could be used to explore this idea further. For example, *Calegari et al* developed a technique whereby a plasmid with a constitutive GFP promoter is injected into the neural tube lumen of an E10.5 embryo, followed by electroporation and 24 h culture, to induce GFP expression in specific regions of the neuroepithelium (Calegari et al., 2002). This technique could be used to assess whether induced overexpression of PAR3 at the apical border of the neuroepithelium

could reduce disruption and potentially rescue the phenotype. If so, this would indicate the vital importance of PAR3 in the control of apico-basal polarity and bring into question the role of apical-polarity genes in human NTDs.

Other possible rescue experiments should target IKNM mechanisms and apico-basal polarity. Considering the finding that basal to apical movement of nuclei is impaired in *Trp53bp2*$^{\Delta 3/\Delta 3}$ embryos (Figure 5-4), focus should lie with proteins involved in this process. Depletion of Tpx2, a protein involved in microtubule organisation, has been shown to impair the basal-to-apical migration of G2-phase nuclei, leading to increased mitosis in a subapical position (Kosodo et al., 2011). Perhaps overexpression of Tpx2 at the apical border could contribute to microtubule regulation and improved basal to apical migration. Dynein, the minus-end-directed microtubule motor protein, has also been implicated in the apical movement of nuclei (Gambello et al., 2003, Tsai et al., 2010, Cappello et al., 2011). Also, human mutations in the *NDE1* gene, which is involved in the regulation of cytoplasmic dynein, have been shown to cause extreme microcephaly (Alkuraya et al., 2011). A recent study found that overexpression of NDEL1, the paralogue of NDE1, rescued apical nuclear migration in NDE1-deficient radial glial progenitors (Doobin et al., 2016). This method could be applied here to improve IKNM in the neuroepithelium of *Trp53bp2*$^{\Delta 3/\Delta 3}$ embryos.

Finally, it may also be relevant to investigate the association between ASPP2, cancer, and the phenotype seen in *Trp53bp2*$^{\Delta 3/\Delta 3}$ embryos. There are characteristics in ASPP2 mutant embryos described here that adhere to the hallmarks of cancer such as overgrowth, increased proliferation and disrupted tissue morphology. ASPP2 is most often reported in cancer-related articles (Liu et al., 2018, Wu et al., 2018, Li et al., 2018), due to its relation with p53, or indeed acting independently of p53. It has also been shown that heterozygous ASPP2 mice develop spontaneous tumours and double homozygous knockout of both p53 and ASPP2 results in embryonic lethality (Vives et al., 2006). However, this tells us little of the functional overlap, and the role of p53 in the development of NTDs. ΔN-ASPP2, if persisting in

Trp53bp2$^{\Delta 3/\Delta 3}$ embryos as expected, may provide an alternative explanation for the cancer-like characteristics, due to its role in enhancing cell proliferation and survival through the inhibition of p53 (Van Hook et al., 2017). Although western blots were attempted to assess ASPP2 isoform presence in embryos with and without exon 3, unfortunately poor antibody quality and time constraints prevented a conclusive outcome (data not shown). Optimisation of this method, perhaps through the generation of novel antibodies that target both the C-terminal and N-terminal of ASPP2, could explore whether ΔN-ASPP2 is retained in *Trp53bp2*$^{\Delta 3/\Delta 3}$ embryos, and if it plays a role in the emergence of NTDs.

In conclusion, this thesis has explored opportunities to improve scientific methods in relation to the 3Rs, which can be explored in a broader range of embryo studies. Detailed characterisation of *Trp53bp2*$^{\Delta 3/\Delta 3}$ embryos has highlighted a fascinating and diverse phenotype which gives credence to studying apico-basal polarity defects in relation to NTDs.

Bibliography

1991. Prevention of neural tube defects: results of the Medical Research Council Vitamin Study. MRC Vitamin Study Research Group. *Lancet,* 338**,** 131-7.

ABDOLLAHI, M. R., MORRISON, E., SIREY, T., MOLNAR, Z., HAYWARD, B. E., CARR, I. M., SPRINGELL, K., WOODS, C. G., AHMED, M., HATTINGH, L., CORRY, P., PILZ, D. T., STOODLEY, N., CROW, Y., TAYLOR, G. R., BONTHRON, D. T. & SHERIDAN, E. 2009. Mutation of the variant alpha-tubulin TUBA8 results in polymicrogyria with optic nerve hypoplasia. *Am J Hum Genet,* 85**,** 737-44.

AFONSO, C. & HENRIQUE, D. 2006. PAR3 acts as a molecular organizer to define the apical domain of chick neuroepithelial cells. *J Cell Sci,* 119**,** 4293-304.

AGNISH, N. D. & KOCHHAR, D. M. 1976. Direct exposure of postimplantation mouse embryos to 5-bromodeoxyuridine in vitro and its effect on subsequent chondrogenesis in the limbs. *J Embryol Exp Morphol,* 36**,** 623-38.

AHLGREN, S., VOGT, P. & BRONNER-FRASER, M. 2003. Excess FoxG1 causes overgrowth of the neural tube. *J Neurobiol,* 57**,** 337-49.

AHMAD, F. U., DWARAKANATH, S., SHARMA, B. S. & MAHAPATRA, A. K. 2008. Multiple neural tube defects: a clinical series of seven cases and their embryological basis. *Pediatr Neurosurg,* 44**,** 280-7.

AKAZAWA, M., AKAZAWA, S., HASHIMOTO, M., AKASHI, M., YAMAZAKI, H., TAHARA, D., YAMAMOTO, H., YAMAGUCHI, Y., NAKANISHI, T. & NAGATAKI, S. 1989. Effects of brief exposure to insulin-induced hypoglycemic serum during organogenesis in rat embryo culture. *Diabetes,* 38**,** 1573-8.

ALKURAYA, F. S., CAI, X., EMERY, C., MOCHIDA, G. H., AL-DOSARI, M. S., FELIE, J. M., HILL, R. S., BARRY, B. J., PARTLOW, J. N., GASCON, G. G., KENTAB, A., JAN, M., SHAHEEN, R., FENG, Y. & WALSH, C. A. 2011. Human mutations in NDE1 cause extreme microcephaly with lissencephaly [corrected]. *Am J Hum Genet,* 88**,** 536-47.

ALONSO, M. I., GATO, A., MORO, J. A., MARTIN, P. & BARBOSA, E. 1999. Involvement of sulfated proteoglycans in embryonic brain expansion at earliest stages of development in rat embryos. *Cells Tissues Organs,* 165**,** 1-9.

AMBROSO, J. L. & HARRIS, C. 1993. Chloroquine embryotoxicity in the postimplantation rat conceptus in vitro. *Teratology,* 48**,** 213-26.

ANDERSEN, H. S., GAMBLING, L., HOLTROP, G. & MCARDLE, H. J. 2006. Maternal iron deficiency identifies critical windows for growth and cardiovascular development in the rat postimplantation embryo. *J Nutr,* 136**,** 1171-7.

ASAI-COAKWELL, M., FRENCH, C. R., YE, M., GARCHA, K., BIGOT, K., PERERA, A. G., STAEHLING-HAMPTON, K., MEMA, S. C., CHANDA, B., MUSHEGIAN, A., BAMFORTH, S., DOSCHAK, M. R., LI, G., DOBBS, M. B., GIAMPIETRO, P. F., BROOKS, B. P., VIJAYALAKSHMI, P., SAUVE, Y., ABITBOL, M., SUNDARESAN, P., VAN HEYNINGEN, V., POURQUIE, O., UNDERHILL, T. M.,

WASKIEWICZ, A. J. & LEHMANN, O. J. 2009. Incomplete penetrance and phenotypic variability characterize Gdf6-attributable oculo-skeletal phenotypes. *Hum Mol Genet,* 18**,** 1110-21.

BAEK, C., FREEM, L., GOIAME, R., SANG, H., MORIN, X. & TOZER, S. 2018. Mib1 prevents Notch Cis-inhibition to defer differentiation and preserve neuroepithelial integrity during neural delamination. *PLoS Biol,* 16**,** e2004162.

BANTING, G. S., BARAK, O., AMES, T. M., BURNHAM, A. C., KARDEL, M. D., COOCH, N. S., DAVIDSON, C. E., GODBOUT, R., MCDERMID, H. E. & SHIEKHATTAR, R. 2005. CECR2, a protein involved in neurulation, forms a novel chromatin remodeling complex with SNF2L. *Hum Mol Genet,* 14**,** 513-24.

BASSUK, A. G. & KIBAR, Z. 2009. Genetic basis of neural tube defects. *Semin Pediatr Neurol,* 16**,** 101-10.

BAYE, L. M. & LINK, B. A. 2007. Interkinetic nuclear migration and the selection of neurogenic cell divisions during vertebrate retinogenesis. *J Neurosci,* 27**,** 10143-52.

BECCARI, L., MORIS, N., GIRGIN, M., TURNER, D. A., BAILLIE-JOHNSON, P., COSSY, A. C., LUTOLF, M. P., DUBOULE, D. & ARIAS, A. M. 2018. Multi-axial self-organization properties of mouse embryonic stem cells into gastruloids. *Nature,* 562**,** 272-276.

BEHESTI, H., HOLT, J. K. & SOWDEN, J. C. 2006. The level of BMP4 signaling is critical for the regulation of distinct T-box gene expression domains and growth along the dorso-ventral axis of the optic cup. *BMC Dev Biol,* 6**,** 62.

BERBERIAN, R. M., EURICH, G. E., RIOS, G. A. & HARRIS, C. 1996. Formation of glutathione adducts and 2-aminofluorene from 2-nitrosofluorene in postimplantation rat conceptuses in vitro. *Reprod Toxicol,* 10**,** 273-84.

BERGAMASCHI, D., SAMUELS, Y., JIN, B., DURAISINGHAM, S., CROOK, T. & LU, X. 2004. ASPP1 and ASPP2: common activators of p53 family members. *Mol Cell Biol,* 24**,** 1341-50.

BERUBE, N. G., JAGLA, M., SMEENK, C., DE REPENTIGNY, Y., KOTHARY, R. & PICKETTS, D. J. 2002. Neurodevelopmental defects resulting from ATRX overexpression in transgenic mice. *Hum Mol Genet,* 11**,** 253-61.

BRISCOE, J., PIERANI, A., JESSELL, T. M. & ERICSON, J. 2000. A homeodomain protein code specifies progenitor cell identity and neuronal fate in the ventral neural tube. *Cell,* 101**,** 435-45.

BRISCOE, J., SUSSEL, L., SERUP, P., HARTIGAN-O'CONNOR, D., JESSELL, T. M., RUBENSTEIN, J. L. & ERICSON, J. 1999. Homeobox gene Nkx2.2 and specification of neuronal identity by graded Sonic hedgehog signalling. *Nature,* 398**,** 622-7.

BROWN, N. A. & FABRO, S. 1981. Quantitation of rat embryonic development in vitro: a morphological scoring system. *Teratology,* 24**,** 65-78.

BUCKLEY, C. E., REN, X., WARD, L. C., GIRDLER, G. C., ARAYA, C., GREEN, M. J., CLARK, B. S., LINK, B. A. & CLARKE, J. D. 2013. Mirror-symmetric microtubule assembly and cell interactions drive lumen formation in the zebrafish neural rod. *Embo j,* 32**,** 30-44.

BUCKLEY, S. K., STEELE, C. E. & NEW, D. A. 1978. In vitro development of early postimplantation rat embryos. *Dev Biol,* 65**,** 396-403.

BULIC-JAKUS, F., STRAHINIC-BELOVARI, T., MARIC, S., JEZEK, D., JURIC-LEKIC, G., VLAHOVIC, M. & SERMAN, D. 2001. Chemically defined protein-free in vitro culture of mammalian embryo does not restrict its developmental potential for differentiation of skin appendages. *Cells Tissues Organs,* 169**,** 134-43.

BULTMAN, S., GEBUHR, T., YEE, D., LA MANTIA, C., NICHOLSON, J., GILLIAM, A., RANDAZZO, F., METZGER, D., CHAMBON, P., CRABTREE, G. & MAGNUSON, T. 2000. A Brg1 null mutation in the mouse reveals functional differences among mammalian SWI/SNF complexes. *Mol Cell,* 6**,** 1287-95.

BURDEN, N., CHAPMAN, K., SEWELL, F. & ROBINSON, V. 2015. Pioneering better science through the 3Rs: an introduction to the national centre for the replacement, refinement, and reduction of animals in research (NC3Rs). *J Am Assoc Lab Anim Sci,* 54**,** 198-208.

BURREN, K. A., SAVERY, D., MASSA, V., KOK, R. M., SCOTT, J. M., BLOM, H. J., COPP, A. J. & GREENE, N. D. 2008. Gene-environment interactions in the causation of neural tube defects: folate deficiency increases susceptibility conferred by loss of Pax3 function. *Hum Mol Genet,* 17**,** 3675-85.

CALEGARI, F., HAUBENSAK, W., YANG, D., HUTTNER, W. B. & BUCHHOLZ, F. 2002. Tissue-specific RNA interference in postimplantation mouse embryos with endoribonuclease-prepared short interfering RNA. *Proc Natl Acad Sci U S A,* 99**,** 14236-40.

CALEGARI, F., MARZESCO, A. M., KITTLER, R., BUCHHOLZ, F. & HUTTNER, W. B. 2004. Tissue-specific RNA interference in post-implantation mouse embryos using directional electroporation and whole embryo culture. *Differentiation,* 72**,** 92-102.

CALVARD, R. A. 1978. Picture thresholding using an iterative selection method. *IEEE Transactions on Systems, Man, and Cybernetics,* 8**,** 630-632.

CAMPBELL, L. R. & SOHAL, G. S. 1990. The pattern of neural tube defects created by secondary reopening of the neural tube. *J Child Neurol,* 5**,** 336-40.

CAO, X., PFAFF, S. L. & GAGE, F. H. 2008. YAP regulates neural progenitor cell number via the TEA domain transcription factor. *Genes Dev,* 22**,** 3320-34.

CAPPELLO, S., ATTARDO, A., WU, X., IWASATO, T., ITOHARA, S., WILSCH-BRAUNINGER, M., EILKEN, H. M., RIEGER, M. A., SCHROEDER, T. T., HUTTNER, W. B., BRAKEBUSCH, C. & GOTZ, M. 2006. The Rho-GTPase cdc42 regulates neural progenitor fate at the apical surface. *Nat Neurosci,* 9**,** 1099-107.

CAPPELLO, S., MONZO, P. & VALLEE, R. B. 2011. NudC is required for interkinetic nuclear migration and neuronal migration during neocortical development. *Dev Biol,* 357**,** 326-35.

CASTRANIO, T. & MISHINA, Y. 2009. Bmp2 is required for cephalic neural tube closure in the mouse. *Dev Dyn,* 238**,** 110-22.

CHAMBERLAIN, C. E., JEONG, J., GUO, C., ALLEN, B. L. & MCMAHON, A. P. 2008. Notochord-derived Shh concentrates in close association with the apically positioned basal body in neural target cells and forms a

dynamic gradient during neural patterning. *Development,* 135**,** 1097-106.
CHAMBERS, B. J., KLEIN, N. W., NOSEL, P. G., KHAIRALLAH, L. H. & ROMANOW, J. S. 1995. Methionine overcomes neural tube defects in rat embryos cultured on sera from laminin-immunized monkeys. *J Nutr,* 125**,** 1587-99.
CHANG, H., HUYLEBROECK, D., VERSCHUEREN, K., GUO, Q., MATZUK, M. M. & ZWIJSEN, A. 1999. Smad5 knockout mice die at mid-gestation due to multiple embryonic and extraembryonic defects. *Development,* 126**,** 1631-42.
CHAPMAN, D. L. & PAPAIOANNOU, V. E. 1998. Three neural tubes in mouse embryos with mutations in the T-box gene Tbx6. *Nature,* 391**,** 695-7.
CHATOT, C. L., KLEIN, N. W., PIATEK, J. & PIERRO, L. J. 1980. Successful culture of rat embryos on human serum: use in the detection of teratogens. *Science,* 207**,** 1471-3.
CHEN, X., AN, Y., GAO, Y., GUO, L., RUI, L., XIE, H., SUN, M., LAM HUNG, S., SHENG, X., ZOU, J., BAO, Y., GUAN, H., NIU, B., LI, Z., FINNELL, R. H., GUSELLA, J. F., WU, B. L. & ZHANG, T. 2017. Rare Deleterious PARD3 Variants in the aPKC-Binding Region are Implicated in the Pathogenesis of Human Cranial Neural Tube Defects Via Disrupting Apical Tight Junction Formation. *Hum Mutat,* 38**,** 378-389.
CHEN, Y., LIU, W., NAUMOVSKI, L. & NEVE, R. L. 2003. ASPP2 inhibits APP-BP1-mediated NEDD8 conjugation to cullin-1 and decreases APP-BP1-induced cell proliferation and neuronal apoptosis. *J Neurochem,* 85**,** 801-9.
CIRUNA, B., JENNY, A., LEE, D., MLODZIK, M. & SCHIER, A. F. 2006. Planar cell polarity signalling couples cell division and morphogenesis during neurulation. *Nature,* 439**,** 220-4.
CLARKSON, S. G., DOERING, J. V. & RUNNER, M. N. 1969. Growth of postimplantation mouse embryos cultured in a serum-supplemented, chemically defined medium. *Teratology,* 2**,** 181-5.
COCKROFT, D. L. 1973. Development in culture of rat foetuses explanted at 12.5 and 13.5 days of gestation. *J Embryol Exp Morphol,* 29**,** 473-83.
COCKROFT, D. L. 1979. Nutrient requirements of rat embryos undergoing organogenesis in vitro. *J Reprod Fertil,* 57**,** 505-10.
COCKROFT, D. L. 1987. Growth and proliferation in mouse parietal yolk sac during whole embryo culture. *J Reprod Fertil,* 81**,** 575-81.
COCKROFT, D. L. & COPPOLA, P. T. 1977. Teratogenic effects of excess glucose on head-fold rat embryos in culture. *Teratology,* 16**,** 141-6.
COCKROFT, D. L. & NEW, D. A. 1978. Abnormalities induced in cultured rat embryos by hyperthermia. *Teratology,* 17**,** 277-83.
COELHO, C. N., WEBER, J. A., KLEIN, N. W., DANIELS, W. G. & HOAGLAND, T. A. 1989. Whole rat embryos require methionine for neural tube closure when cultured on cow serum. *J Nutr,* 119**,** 1716-25.
COMPAGNUCCI, C., PIEMONTE, F., SFERRA, A., PIERMARINI, E. & BERTINI, E. 2016. The cytoskeletal arrangements necessary to neurogenesis. *Oncotarget,* 7**,** 19414-29.
CONG, W., HIROSE, T., HARITA, Y., YAMASHITA, A., MIZUNO, K., HIRANO, H. & OHNO, S. 2010. ASPP2 regulates epithelial cell polarity through the PAR complex. *Curr Biol,* 20**,** 1408-14.

COSTA, M. R., WEN, G., LEPIER, A., SCHROEDER, T. & GOTZ, M. 2008. Par-complex proteins promote proliferative progenitor divisions in the developing mouse cerebral cortex. *Development,* 135**,** 11-22.

CUI, S., OTTEN, C., ROHR, S., ABDELILAH-SEYFRIED, S. & LINK, B. A. 2007. Analysis of aPKClambda and aPKCzeta reveals multiple and redundant functions during vertebrate retinogenesis. *Mol Cell Neurosci,* 34**,** 431-44.

CURTIN, J. A., QUINT, E., TSIPOURI, V., ARKELL, R. M., CATTANACH, B., COPP, A. J., HENDERSON, D. J., SPURR, N., STANIER, P., FISHER, E. M., NOLAN, P. M., STEEL, K. P., BROWN, S. D., GRAY, I. C. & MURDOCH, J. N. 2003. Mutation of Celsr1 disrupts planar polarity of inner ear hair cells and causes severe neural tube defects in the mouse. *Curr Biol,* 13**,** 1129-33.

DAS, R. M. & STOREY, K. G. 2014. Apical abscission alters cell polarity and dismantles the primary cilium during neurogenesis. *Science,* 343**,** 200-4.

DAVIDSON, C. M., NORTHRUP, H., KING, T. M., FLETCHER, J. M., TOWNSEND, I., TYERMAN, G. H. & AU, K. S. 2008. Genes in glucose metabolism and association with spina bifida. *Reprod Sci,* 15**,** 51-8.

DEAK, K. L., DICKERSON, M. E., LINNEY, E., ENTERLINE, D. S., GEORGE, T. M., MELVIN, E. C., GRAHAM, F. L., SIEGEL, D. G., HAMMOCK, P., MEHLTRETTER, L., BASSUK, A. G., KESSLER, J. A., GILBERT, J. R. & SPEER, M. C. 2005. Analysis of ALDH1A2, CYP26A1, CYP26B1, CRABP1, and CRABP2 in human neural tube defects suggests a possible association with alleles in ALDH1A2. *Birth Defects Res A Clin Mol Teratol,* 73**,** 868-75.

DEL BENE, F. 2011. Interkinetic nuclear migration: cell cycle on the move. *Embo j,* 30**,** 1676-7.

DEL BENE, F., WEHMAN, A. M., LINK, B. A. & BAIER, H. 2008. Regulation of neurogenesis by interkinetic nuclear migration through an apical-basal notch gradient. *Cell,* 134**,** 1055-65.

DESMOND, M. E. & JACOBSON, A. G. 1977. Embryonic brain enlargement requires cerebrospinal fluid pressure. *Dev Biol,* 57**,** 188-98.

DETRAIT, E. R., GEORGE, T. M., ETCHEVERS, H. C., GILBERT, J. R., VEKEMANS, M. & SPEER, M. C. 2005. Human neural tube defects: developmental biology, epidemiology, and genetics. *Neurotoxicol Teratol,* 27**,** 515-24.

DIBBERN, D. A., JR., GLAZNER, G. W., GOZES, I., BRENNEMAN, D. E. & HILL, J. M. 1997. Inhibition of murine embryonic growth by human immunodeficiency virus envelope protein and its prevention by vasoactive intestinal peptide and activity-dependent neurotrophic factor. *J Clin Invest,* 99**,** 2837-41.

DING, X. F., ZHAO, Y. Q., HU, Z. Y., LIN, K., WANG, F., LIU, S. H., WU, Y., WU, L. Y., ZHAO, T., HUANG, X., WU, Y., ZHU, L. L., FAN, W. H. & FAN, M. 2012. Efficient gene transfer into neonatal mouse brain using electroporation. *Neurochem Res,* 37**,** 1392-8.

DOOBIN, D. J., KEMAL, S., DANTAS, T. J. & VALLEE, R. B. 2016. Severe NDE1-mediated microcephaly results from neural progenitor cell cycle arrests at multiple specific stages. *Nat Commun,* 7**,** 12551.

DOUDNEY, K., GRINHAM, J., WHITTAKER, J., LYNCH, S. A., THOMPSON, D., MOORE, G. E., COPP, A. J., GREENE, N. D. & STANIER, P. 2009. Evaluation of folate metabolism gene polymorphisms as risk factors for open and closed neural tube defects. *Am J Med Genet A,* 149a**,** 1585-9.

DRAKOU, K. & GEORGIADES, P. 2015. A serum-free and defined medium for the culture of mammalian postimplantation embryos. *Biochem Biophys Res Commun,* 468**,** 813-9.

DYER, L. A. & PATTERSON, C. 2013. A novel ex vivo culture method for the embryonic mouse heart. *J Vis Exp***,** e50359.

EBRON-MCCOY, M. T., BEYER, P. E., OGLESBY, L. A. & KAVLOCK, R. J. 1988. In vitro culture of postimplantation hamster embryos. *Reprod Toxicol,* 2**,** 31-6.

EID, L., LACHANCE, M., HICKSON, G. & ROSSIGNOL, E. 2018. Ex Utero Electroporation and Organotypic Slice Cultures of Embryonic Mouse Brains for Live-Imaging of Migrating GABAergic Interneurons. *J Vis Exp*.

ELLINGTON, S. K. 1987. In vitro analysis of glucose metabolism and embryonic growth in postimplantation rat embryos. *Development,* 100**,** 431-9.

ELLIS-HUTCHINGS, R. G. & CARNEY, E. W. 2010. Whole embryo culture: a "New" technique that enabled decades of mechanistic discoveries. *Birth Defects Res B Dev Reprod Toxicol,* 89**,** 304-12.

EOM, D. S., AMARNATH, S. & AGARWALA, S. 2013. Apicobasal polarity and neural tube closure. *Dev Growth Differ,* 55**,** 164-72.

EPSTEIN, D. J., VEKEMANS, M. & GROS, P. 1991. Splotch (Sp2H), a mutation affecting development of the mouse neural tube, shows a deletion within the paired homeodomain of Pax-3. *Cell,* 67**,** 767-74.

ERICSON, J., BRISCOE, J., RASHBASS, P., VAN HEYNINGEN, V. & JESSELL, T. M. 1997. Graded sonic hedgehog signaling and the specification of cell fate in the ventral neural tube. *Cold Spring Harb Symp Quant Biol,* 62**,** 451-66.

ESTIBEIRO, J. P., BROOK, F. A. & COPP, A. J. 1993. Interaction between splotch (Sp) and curly tail (ct) mouse mutants in the embryonic development of neural tube defects. *Development,* 119**,** 113-21.

FERLAND, R. J., BATIZ, L. F., NEAL, J., LIAN, G., BUNDOCK, E., LU, J., HSIAO, Y. C., DIAMOND, R., MEI, D., BANHAM, A. H., BROWN, P. J., VANDERBURG, C. R., JOSEPH, J., HECHT, J. L., FOLKERTH, R., GUERRINI, R., WALSH, C. A., RODRIGUEZ, E. M. & SHEEN, V. L. 2009. Disruption of neural progenitors along the ventricular and subventricular zones in periventricular heterotopia. *Hum Mol Genet,* 18**,** 497-516.

FINDLEY, T. O., TENPENNY, J. C., O'BYRNE, M. R., MORRISON, A. C., HIXSON, J. E., NORTHRUP, H. & AU, K. S. 2017. Mutations in folate transporter genes and risk for human myelomeningocele. *Am J Med Genet A,* 173**,** 2973-2984.

FISCHER, A., SCHUMACHER, N., MAIER, M., SENDTNER, M. & GESSLER, M. 2004. The Notch target genes Hey1 and Hey2 are required for embryonic vascular development. *Genes Dev,* 18**,** 901-11.

FISHER, D. L. & MARTINEZ DE VILLARREAL, L. 1982. Effects of hormones on postimplantation mouse embryos in vitro. II. Progesterone and estrogen. *J Exp Zool,* 224**,** 205-10.

FLEMING, A., GERRELLI, D., GREENE, N. D. & COPP, A. J. 1997. Mechanisms of normal and abnormal neurulation: evidence from embryo culture studies. *Int J Dev Biol,* 41**,** 199-212.

FLICK, B. & KLUG, S. 2006. Whole embryo culture: an important tool in developmental toxicology today. *Curr Pharm Des,* 12**,** 1467-88.

FLYNN, T. J., FRIEDMAN, L., BLACK, T. N. & KLEIN, N. W. 1987. Methionine and iron as growth factors for rat embryos cultured in canine serum. *J Exp Zool,* 244**,** 319-24.

FRANCO, N. H., SANDOE, P. & OLSSON, I. A. S. 2018. Researchers' attitudes to the 3Rs-An upturned hierarchy? *PLoS One,* 13**,** e0200895.

FRANKE, B., VERMEULEN, S. H., STEEGERS-THEUNISSEN, R. P., COENEN, M. J., SCHIJVENAARS, M. M., SCHEFFER, H., DEN HEIJER, M. & BLOM, H. J. 2009. An association study of 45 folate-related genes in spina bifida: Involvement of cubilin (CUBN) and tRNA aspartic acid methyltransferase 1 (TRDMT1). *Birth Defects Res A Clin Mol Teratol,* 85**,** 216-26.

FU, Y., WANG, L. L., YI, D., JIN, L., LIU, J., ZHANG, Y. & REN, A. 2015. Association between maternal single nucleotide polymorphisms in genes regulating glucose metabolism and risk for neural tube defects in offspring. *Birth Defects Res A Clin Mol Teratol,* 103**,** 471-8.

GALEA, G. L., MEAKIN, L. B., SUGIYAMA, T., ZEBDA, N., SUNTERS, A., TAIPALEENMAKI, H., STEIN, G. S., VAN WIJNEN, A. J., LANYON, L. E. & PRICE, J. S. 2013. Estrogen receptor alpha mediates proliferation of osteoblastic cells stimulated by estrogen and mechanical strain, but their acute down-regulation of the Wnt antagonist Sost is mediated by estrogen receptor beta. *J Biol Chem,* 288**,** 9035-48.

GALLOWAY, S. M., PERRY, P. E., MENESES, J., NEBERT, D. W. & PEDERSEN, R. A. 1980. Cultured mouse embryos metabolize benzo[a]pyrene during early gestation: genetic differences detectable by sister chromatid exchange. *Proc Natl Acad Sci U S A,* 77**,** 3524-8.

GAMBELLO, M. J., DARLING, D. L., YINGLING, J., TANAKA, T., GLEESON, J. G. & WYNSHAW-BORIS, A. 2003. Multiple dose-dependent effects of Lis1 on cerebral cortical development. *J Neurosci,* 23**,** 1719-29.

GAO, Y., CHEN, X., SHANGGUAN, S., BAO, Y., LU, X., ZOU, J., GUO, J., DAI, Y. & ZHANG, T. 2012. Association study of PARD3 gene polymorphisms with neural tube defects in a Chinese Han population. *Reprod Sci,* 19**,** 764-71.

GARDNER, W. J. 1968. Myelocele: rupture of the neural tube? *Clin Neurosurg,* 15**,** 57-79.

GARDNER, W. J. 1980. Hypothesis; overdistention of the neural tube may cause anomalies of non-neural organs. *Teratology,* 22**,** 229-38.

GEORGOPOULOU, N., HUREL, C., POLITIS, P. K., GAITANOU, M., MATSAS, R. & THOMAIDOU, D. 2006. BM88 is a dual function molecule inducing cell cycle exit and neuronal differentiation of neuroblastoma cells via cyclin D1 down-regulation and retinoblastoma protein hypophosphorylation. *J Biol Chem,* 281**,** 33606-20.

GORDON, J., MOORE, B. A., BLACKBURN, C. C. & MANLEY, N. R. 2014. Serum-free culture of mid-gestation mouse embryos: a tool for the study of endoderm-derived organs. *Methods Mol Biol,* 1092**,** 183-94.

GOTZ, M. & HUTTNER, W. B. 2005. The cell biology of neurogenesis. *Nat Rev Mol Cell Biol,* 6**,** 777-88.

GOULDING, E. H. & PRATT, R. M. 1986. Isotretinoin teratogenicity in mouse whole embryo culture. *J Craniofac Genet Dev Biol,* 6**,** 99-112.

GRAHAM, V., KHUDYAKOV, J., ELLIS, P. & PEVNY, L. 2003. SOX2 functions to maintain neural progenitor identity. *Neuron,* 39**,** 749-65.

GREENE, N. D. & COPP, A. J. 2009. Development of the vertebrate central nervous system: formation of the neural tube. *Prenat Diagn,* 29**,** 303-11.

GREENE, N. D. & COPP, A. J. 2014. Neural tube defects. *Annu Rev Neurosci,* 37**,** 221-42.

GREGGIO, C., DE FRANCESCHI, F., FIGUEIREDO-LARSEN, M., GOBAA, S., RANGA, A., SEMB, H., LUTOLF, M. & GRAPIN-BOTTON, A. 2013. Artificial three-dimensional niches deconstruct pancreas development in vitro. *Development,* 140**,** 4452-62.

GUNBERG, D. L. 1976. In vitro development of postimplantation rat embryos cultured on dialyzed rat serum. *Teratology,* 14**,** 65-9.

GURNIAK, C. B., PERLAS, E. & WITKE, W. 2005. The actin depolymerizing factor n-cofilin is essential for neural tube morphogenesis and neural crest cell migration. *Dev Biol,* 278**,** 231-41.

HARDING, M. J., MCGRAW, H. F. & NECHIPORUK, A. 2014. The roles and regulation of multicellular rosette structures during morphogenesis. *Development,* 141**,** 2549-58.

HARDWICK, L. J., ALI, F. R., AZZARELLI, R. & PHILPOTT, A. 2015. Cell cycle regulation of proliferation versus differentiation in the central nervous system. *Cell Tissue Res,* 359**,** 187-200.

HARDY, R. P. & NEW, D. A. 1991. Effects of the anti-progestin RU 38486 on rat embryos growing in culture. *Food Chem Toxicol,* 29**,** 361-2.

HARRIS, B. S., FRANZ, T., ULLRICH, S., COOK, S., BRONSON, R. T. & DAVISSON, M. T. 1997. Forebrain overgrowth (fog): a new mutation in the mouse affecting neural tube development. *Teratology,* 55**,** 231-40.

HARRIS, C. 1993. Glutathione biosynthesis in the postimplantation rat conceptus in vitro. *Toxicol Appl Pharmacol,* 120**,** 247-56.

HARRIS, M. J. & JURILOFF, D. M. 2007. Mouse mutants with neural tube closure defects and their role in understanding human neural tube defects. *Birth Defects Res A Clin Mol Teratol,* 79**,** 187-210.

HARRIS, M. J. & JURILOFF, D. M. 2010. An update to the list of mouse mutants with neural tube closure defects and advances toward a complete genetic perspective of neural tube closure. *Birth Defects Res A Clin Mol Teratol,* 88**,** 653-69.

HARRIS, T. J. & TEPASS, U. 2010. Adherens junctions: from molecules to morphogenesis. *Nat Rev Mol Cell Biol,* 11**,** 502-14.

HATAKEYAMA, J., WAKAMATSU, Y., NAGAFUCHI, A., KAGEYAMA, R., SHIGEMOTO, R. & SHIMAMURA, K. 2014. Cadherin-based adhesions in the apical endfoot are required for active Notch signaling to control neurogenesis in vertebrates. *Development,* 141**,** 1671-82.

HEIL, S. G., VAN DER PUT, N. M., TRIJBELS, F. J., GABREELS, F. J. & BLOM, H. J. 1999. Molecular genetic analysis of human folate receptors in neural tube defects. *Eur J Hum Genet,* 7**,** 393-6.

HERNANDEZ-DIAZ, S., WERLER, M. M., WALKER, A. M. & MITCHELL, A. A. 2001. Neural tube defects in relation to use of folic acid antagonists during pregnancy. *Am J Epidemiol,* 153**,** 961-8.

HILDEBRAND, J. D. & SORIANO, P. 1999. Shroom, a PDZ domain-containing actin-binding protein, is required for neural tube morphogenesis in mice. *Cell,* 99**,** 485-97.

HIRIART, E., VAN VLIET, P., DIRSCHINGER, R. J., EVANS, S. M. & PUCEAT, M. 2014. Cell labeling and injection in developing embryonic mouse hearts. *J Vis Exp*.

HIRSCH, E., SAOTOME, I. & HIRSH, D. 1995. A model of intrauterine infection and preterm delivery in mice. *Am J Obstet Gynecol,* 172**,** 1598-603.

HODGE, R. D., D'ERCOLE, A. J. & O'KUSKY, J. R. 2004. Insulin-like growth factor-I accelerates the cell cycle by decreasing G1 phase length and increases cell cycle reentry in the embryonic cerebral cortex. *J Neurosci,* 24**,** 10201-10.

HOIJMAN, E., RUBBINI, D., COLOMBELLI, J. & ALSINA, B. 2015. Mitotic cell rounding and epithelial thinning regulate lumen growth and shape. *Nat Commun,* 6**,** 7355.

HOLLYDAY, M. 2001. Neurogenesis in the vertebrate neural tube. *Int J Dev Neurosci,* 19**,** 161-73.

HOOK, E. B. 1992. Neural tube rupture as a cause of neural tube defects. *Lancet,* 339**,** 1000.

HUANG, Y., WILKIE, R. & WILSON, V. 2015. Methods for Precisely Localized Transfer of Cells or DNA into Early Postimplantation Mouse Embryos. *J Vis Exp***,** e53295.

HUTTON, S. R. & PEVNY, L. H. 2011. SOX2 expression levels distinguish between neural progenitor populations of the developing dorsal telencephalon. *Dev Biol,* 352**,** 40-7.

HUXHAM, I. M. & BECK, F. 1985. Maternal transferrin uptake by and transfer across the visceral yolk sac of the early postimplantation rat conceptus in vitro. *Dev Biol,* 110**,** 75-83.

ILLERA, M. J., CULLINAN, E., GUI, Y., YUAN, L., BEYLER, S. A. & LESSEY, B. A. 2000. Blockade of the alpha(v)beta(3) integrin adversely affects implantation in the mouse. *Biol Reprod,* 62**,** 1285-90.

IVANOV, A. I. 2008. Actin motors that drive formation and disassembly of epithelial apical junctions. *Front Biosci,* 13**,** 6662-81.

IYER, A., SUBRAMANIAN, L. & TOLE, S. 2018. Organotypic Explants of the Embryonic Rodent Hippocampus: An Accessible System for Transgenesis. *Bio Protoc,* 8.

JOHNSON, W. G., STENROOS, E. S., SPYCHALA, J. R., CHATKUPT, S., MING, S. X. & BUYSKE, S. 2004. New 19 bp deletion polymorphism in intron-1 of dihydrofolate reductase (DHFR): a risk factor for spina bifida acting in mothers during pregnancy? *Am J Med Genet A,* 124a**,** 339-45.

JONES, E. A., CROTTY, D., KULESA, P. M., WATERS, C. W., BARON, M. H., FRASER, S. E. & DICKINSON, M. E. 2002. Dynamic in vivo imaging of postimplantation mammalian embryos using whole embryo culture. *Genesis,* 34**,** 228-35.

JURILOFF, D. M. & HARRIS, M. J. 2012. A consideration of the evidence that genetic defects in planar cell polarity contribute to the etiology of human neural tube defects. *Birth Defects Res A Clin Mol Teratol,* 94**,** 824-40.

KACHILELE, S. G. & NEW, D. A. 1988. Effects of temporary cooling, and of different explantation and storage conditions, on the subsequent development of post-implantation rat embryos in vitro. *Teratology,* 38**,** 381-7.

KADOWAKI, M., NAKAMURA, S., MACHON, O., KRAUSS, S., RADICE, G. L. & TAKEICHI, M. 2007. N-cadherin mediates cortical organization in the mouse brain. *Dev Biol,* 304**,** 22-33.

KALASKAR, V. K. & LAUDERDALE, J. D. 2014. Mouse embryonic development in a serum-free whole embryo culture system. *J Vis Exp*.

KARABULUT, A. K., ULGER, H. & PRATTEN, M. K. 2000. Protection by free oxygen radical scavenging enzymes against salicylate-induced embryonic malformations in vitro. *Toxicol In Vitro,* 14**,** 297-307.

KATAYAMA, K., MELENDEZ, J., BAUMANN, J. M., LESLIE, J. R., CHAUHAN, B. K., NEMKUL, N., LANG, R. A., KUAN, C. Y., ZHENG, Y. & YOSHIDA, Y. 2011. Loss of RhoA in neural progenitor cells causes the disruption of adherens junctions and hyperproliferation. *Proc Natl Acad Sci U S A,* 108**,** 7607-12.

KAUFFMAN, S. L. 1968. Lengthening of the generation cycle during embryonic differentiation of the mouse neural tube. *Exp Cell Res,* 49**,** 420-4.

KESBY, G. J. 1992. In vitro development of rat embryos undergoing organogenesis in heparin-plasma. *Teratology,* 45**,** 293-301.

KESBY, G. J. 2000. Toxicity of heparin in postimplantation whole-embryo culture. *Toxicol Appl Pharmacol,* 163**,** 60-6.

KIBAR, Z., BOSOI, C. M., KOOISTRA, M., SALEM, S., FINNELL, R. H., DE MARCO, P., MERELLO, E., BASSUK, A. G., CAPRA, V. & GROS, P. 2009. Novel mutations in VANGL1 in neural tube defects. *Hum Mutat,* 30**,** E706-15.

KIBAR, Z., SALEM, S., BOSOI, C. M., PAUWELS, E., DE MARCO, P., MERELLO, E., BASSUK, A. G., CAPRA, V. & GROS, P. 2011. Contribution of VANGL2 mutations to isolated neural tube defects. *Clin Genet,* 80**,** 76-82.

KIBAR, Z., VOGAN, K. J., GROULX, N., JUSTICE, M. J., UNDERHILL, D. A. & GROS, P. 2001. Ltap, a mammalian homolog of Drosophila Strabismus/Van Gogh, is altered in the mouse neural tube mutant Loop-tail. *Nat Genet,* 28**,** 251-5.

KIM, T. H., GOODMAN, J., ANDERSON, K. V. & NISWANDER, L. 2007. Phactr4 regulates neural tube and optic fissure closure by controlling PP1-, Rb-, and E2F1-regulated cell-cycle progression. *Dev Cell,* 13**,** 87-102.

KITAJIMA, K., OKI, S., OHKAWA, Y., SUMI, T. & MENO, C. 2013. Wnt signaling regulates left-right axis formation in the node of mouse embryos. *Dev Biol,* 380**,** 222-32.

KLUG, S., LEWANDOWSKI, C. & NEUBERT, D. 1985. Modification and standardization of the culture of early postimplantation embryos for toxicological studies. *Arch Toxicol,* 58**,** 84-8.

KOSODO, Y., SUETSUGU, T., SUDA, M., MIMORI-KIYOSUE, Y., TOIDA, K., BABA, S. A., KIMURA, A. & MATSUZAKI, F. 2011. Regulation of interkinetic nuclear migration by cell cycle-coupled active and passive mechanisms in the developing brain. *Embo j,* 30**,** 1690-704.

KOSODO, Y., TOIDA, K., DUBREUIL, V., ALEXANDRE, P., SCHENK, J., KIYOKAGE, E., ATTARDO, A., MORA-BERMUDEZ, F., ARII, T., CLARKE, J. D. & HUTTNER, W. B. 2008. Cytokinesis of neuroepithelial cells can divide their basal process before anaphase. *Embo j,* 27**,** 3151-63.

KUWAHARA, A., HIRABAYASHI, Y., KNOEPFLER, P. S., TAKETO, M. M., SAKAI, J., KODAMA, T. & GOTOH, Y. 2010. Wnt signaling and its downstream target N-myc regulate basal progenitors in the developing neocortex. *Development,* 137**,** 1035-44.

LANE, M. & GARDNER, D. K. 1994. Increase in postimplantation development of cultured mouse embryos by amino acids and induction of fetal retardation and exencephaly by ammonium ions. *J Reprod Fertil,* 102**,** 305-12.

LANE, M. & GARDNER, D. K. 1997. Nonessential amino acids and glutamine decrease the time of the first three cleavage divisions and increase compaction of mouse zygotes in vitro. *J Assist Reprod Genet,* 14**,** 398-403.

LANGE, C., HUTTNER, W. B. & CALEGARI, F. 2009. Cdk4/cyclinD1 overexpression in neural stem cells shortens G1, delays neurogenesis, and promotes the generation and expansion of basal progenitors. *Cell Stem Cell,* 5**,** 320-31.

LEUNG, K. Y., PAI, Y. J., CHEN, Q., SANTOS, C., CALVANI, E., SUDIWALA, S., SAVERY, D., RALSER, M., GROSS, S. S., COPP, A. J. & GREENE, N. D. E. 2017. Partitioning of One-Carbon Units in Folate and Methionine Metabolism Is Essential for Neural Tube Closure. *Cell Rep,* 21**,** 1795-1808.

LEW, S. M. & KOTHBAUER, K. F. 2007. Tethered cord syndrome: an updated review. *Pediatr Neurosurg,* 43**,** 236-48.

LEWANDOWSKI, C., KLUG, S., NAU, H. & NEUBERT, D. 1986. Pharmacokinetic aspects of drug effects in vitro: effects of serum protein binding on concentration and teratogenicity of valproic acid and 2-en-valproic acid in whole embryos in culture. *Arch Toxicol,* 58**,** 239-42.

LI, H., WANG, X., ZHANG, C., CHENG, Y., YU, M., ZHAO, K., GE, W., CAI, A., ZHANG, Y., HAN, F. & HU, Y. 2018. HDAC1-induced epigenetic silencing of ASPP2 promotes cell motility, tumour growth and drug resistance in renal cell carcinoma. *Cancer Lett,* 432**,** 121-131.

LIEM, K. F., JR., TREMML, G. & JESSELL, T. M. 1997. A role for the roof plate and its resident TGFbeta-related proteins in neuronal patterning in the dorsal spinal cord. *Cell,* 91**,** 127-38.

LIEM, K. F., JR., TREMML, G., ROELINK, H. & JESSELL, T. M. 1995. Dorsal differentiation of neural plate cells induced by BMP-mediated signals from epidermal ectoderm. *Cell,* 82**,** 969-79.

LIEN, W. H., KLEZOVITCH, O., FERNANDEZ, T. E., DELROW, J. & VASIOUKHIN, V. 2006. alphaE-catenin controls cerebral cortical size by regulating the hedgehog signaling pathway. *Science,* 311**,** 1609-12.

LIU, B., YANG, L., LI, X. J., LI, R., SUN, W., CHEN, X. Y. & LIU, J. C. 2018. Expression and significance of ASPP2 in squamous carcinoma of esophagus. *Kaohsiung J Med Sci,* 34**,** 321-329.

LU, W., ZHU, H., WEN, S., LAURENT, C., SHAW, G. M., LAMMER, E. J. & FINNELL, R. H. 2007. Screening for novel PAX3 polymorphisms and risks of spina bifida. *Birth Defects Res A Clin Mol Teratol,* 79**,** 45-9.

LU, X., BORCHERS, A. G., JOLICOEUR, C., RAYBURN, H., BAKER, J. C. & TESSIER-LAVIGNE, M. 2004. PTK7/CCK-4 is a novel regulator of planar cell polarity in vertebrates. *Nature,* 430**,** 93-8.

LUIJTEN, M., VAN BEELEN, V. A., VERHOEF, A., RENKENS, M. F., VAN HERWIJNEN, M. H., WESTERMAN, A., VAN SCHOOTEN, F. J., PENNINGS, J. L. & PIERSMA, A. H. 2010. Transcriptomics analysis of retinoic acid embryotoxicity in rat postimplantation whole embryo culture. *Reprod Toxicol,* 30**,** 333-40.

LUKASZEWICZ, A., SAVATIER, P., CORTAY, V., GIROUD, P., HUISSOUD, C., BERLAND, M., KENNEDY, H. & DEHAY, C. 2005. G1 phase regulation, area-specific cell cycle control, and cytoarchitectonics in the primate cortex. *Neuron,* 47**,** 353-64.

LUO, H., LIU, X., WANG, F., HUANG, Q., SHEN, S., WANG, L., XU, G., SUN, X., KONG, H., GU, M., CHEN, S., CHEN, Z. & WANG, Z. 2005. Disruption of palladin results in neural tube closure defects in mice. *Mol Cell Neurosci,* 29**,** 507-15.

LUPO, P. J., CANFIELD, M. A., CHAPA, C., LU, W., AGOPIAN, A. J., MITCHELL, L. E., SHAW, G. M., WALLER, D. K., OLSHAN, A. F., FINNELL, R. H. & ZHU, H. 2012. Diabetes and obesity-related genes and the risk of neural tube defects in the national birth defects prevention study. *Am J Epidemiol,* 176**,** 1101-9.

MAHALIK, S. K., VAZE, D., KANOJIA, R. P., NARASIMHAN, K. L. & RAO, K. L. 2013. Multiple neural tube defects may not be very rare. *Childs Nerv Syst,* 29**,** 609-19.

MAIN, H., RADENKOVIC, J., JIN, S. B., LENDAHL, U. & ANDERSSON, E. R. 2013. Notch signaling maintains neural rosette polarity. *PLoS One,* 8**,** e62959.

MANSOURI, A. & GRUSS, P. 1998. Pax3 and Pax7 are expressed in commissural neurons and restrict ventral neuronal identity in the spinal cord. *Mech Dev,* 78**,** 171-8.

MARGOLIS, B. & BORG, J. P. 2005. Apicobasal polarity complexes. *J Cell Sci,* 118**,** 5157-9.

MARTIN, C., ALONSO, M. I., SANTIAGO, C., MORO, J. A., DE LA MANO, A., CARRETERO, R. & GATO, A. 2009. Early embryonic brain development in rats requires the trophic influence of cerebrospinal fluid. *Int J Dev Neurosci,* 27**,** 733-40.

MARTIN, P. & COCKROFT, D. L. 1999. Culture of postimplantation mouse embryos. *Methods Mol Biol,* 97**,** 7-22.

MASSARWA, R. & NISWANDER, L. 2013. In toto live imaging of mouse morphogenesis and new insights into neural tube closure. *Development,* 140**,** 226-36.

MATSUDA, M. & YASUTOMI, M. 1995. Axial rotation in rat embryos: involvement of changes in the shapes and arrangement of cells. *Cell Struct Funct,* 20**,** 1-12.

MCCRIGHT, B., GAO, X., SHEN, L., LOZIER, J., LAN, Y., MAGUIRE, M., HERZLINGER, D., WEINMASTER, G., JIANG, R. & GRIDLEY, T. 2001. Defects in development of the kidney, heart and eye vasculature in mice homozygous for a hypomorphic Notch2 mutation. *Development,* 128**,** 491-502.

MCSHANE, S. G., MOLE, M. A., SAVERY, D., GREENE, N. D., TAM, P. P. & COPP, A. J. 2015. Cellular basis of neuroepithelial bending during mouse spinal neural tube closure. *Dev Biol,* 404**,** 113-24.

MENEGOLA, E., BROCCIA, M. L., PRATI, M. & GIAVINI, E. 1999. Development of rat embryos cultured in serum from diabetic rats. *Biol Neonate,* 75**,** 65-72.

MERELLO, E., MASCELLI, S., RASO, A., PIATELLI, G., CONSALES, A., CAMA, A., KIBAR, Z., CAPRA, V. & MARCO, P. D. 2015. Expanding the mutational spectrum associated to neural tube defects: literature revision and description of novel VANGL1 mutations. *Birth Defects Res A Clin Mol Teratol,* 103**,** 51-61.

MINGUZZI, S., SELCUKLU, S. D., SPILLANE, C. & PARLE-MCDERMOTT, A. 2014. An NTD-associated polymorphism in the 3' UTR of MTHFD1L can affect disease risk by altering miRNA binding. *Hum Mutat,* 35**,** 96-104.

MISSMER, S. A., SUAREZ, L., FELKNER, M., WANG, E., MERRILL, A. H., JR., ROTHMAN, K. J. & HENDRICKS, K. A. 2006. Exposure to fumonisins and the occurrence of neural tube defects along the Texas-Mexico border. *Environ Health Perspect,* 114**,** 237-41.

MIYAMOTO, Y., SAKANE, F. & HASHIMOTO, K. 2015. N-cadherin-based adherens junction regulates the maintenance, proliferation, and differentiation of neural progenitor cells during development. *Cell Adh Migr,* 9**,** 183-92.

MOHD-ZIN, S. W., MARWAN, A. I., ABOU CHAAR, M. K., AHMAD-ANNUAR, A. & ABDUL-AZIZ, N. M. 2017. Spina Bifida: Pathogenesis, Mechanisms, and Genes in Mice and Humans. *Scientifica (Cairo),* 2017**,** 5364827.

MOORE-SCOTT, B. A., GORDON, J., BLACKBURN, C. C., CONDIE, B. G. & MANLEY, N. R. 2003. New serum-free in vitro culture technique for midgestation mouse embryos. *Genesis,* 35**,** 164-8.

MORGAGNI 1769. The Seats and Causes of Diseases investigated by Anatomy; in five books, containing a great variety of dissections, with remarks. *London,* 2.

MORITA, H., NANDADASA, S., YAMAMOTO, T. S., TERASAKA-IIOKA, C., WYLIE, C. & UENO, N. 2010. Nectin-2 and N-cadherin interact through extracellular domains and induce apical accumulation of F-actin in apical constriction of Xenopus neural tube morphogenesis. *Development,* 137**,** 1315-25.

MORRISON, K., PAPAPETROU, C., HOL, F. A., MARIMAN, E. C., LYNCH, S. A., BURN, J. & EDWARDS, Y. H. 1998. Susceptibility to spina bifida; an association study of five candidate genes. *Ann Hum Genet,* 62**,** 379-96.

MORRISS, G. M. & NEW, D. A. 1979. Effect of oxygen concentration on morphogenesis of cranial neural folds and neural crest in cultured rat embryos. *J Embryol Exp Morphol,* 54**,** 17-35.

MUNSON, C., HUISKEN, J., BIT-AVRAGIM, N., KUO, T., DONG, P. D., OBER, E. A., VERKADE, H., ABDELILAH-SEYFRIED, S. & STAINIER, D. Y. 2008. Regulation of neurocoel morphogenesis by Pard6 gamma b. *Dev Biol,* 324**,** 41-54.

MURCIANO, A., ZAMORA, J., LOPEZ-SANCHEZ, J. & FRADE, J. M. 2002. Interkinetic nuclear movement may provide spatial clues to the regulation of neurogenesis. *Mol Cell Neurosci,* 21**,** 285-300.

MURDOCH, J. N., DAMRAU, C., PAUDYAL, A., BOGANI, D., WELLS, S., GREENE, N. D., STANIER, P. & COPP, A. J. 2014. Genetic interactions between planar cell polarity genes cause diverse neural tube defects in mice. *Dis Model Mech,* 7**,** 1153-63.

MURDOCH, J. N., HENDERSON, D. J., DOUDNEY, K., GASTON-MASSUET, C., PHILLIPS, H. M., PATERNOTTE, C., ARKELL, R., STANIER, P. & COPP, A. J. 2003. Disruption of scribble (Scrb1) causes severe neural tube defects in the circletail mouse. *Hum Mol Genet,* 12**,** 87-98.

NAIT-OUMESMAR, B., STECCA, B., FATTERPEKAR, G., NAIDICH, T., CORBIN, J. & LAZZARINI, R. A. 2002. Ectopic expression of Gcm1 induces congenital spinal cord abnormalities. *Development,* 129**,** 3957-64.

NAKAJIMA, M., SASAKI, M., KOBAYASHI, Y., OHNO, Y. & USAMI, M. 1997. Rat embryo culture using rabbit serum as a medium for developmental toxicity studies. *J Appl Toxicol,* 17**,** 185-8.

NAKATSU, T., UWABE, C. & SHIOTA, K. 2000. Neural tube closure in humans initiates at multiple sites: evidence from human embryos and implications for the pathogenesis of neural tube defects. *Anat Embryol (Berl),* 201**,** 455-66.

NAUMOVSKI, L. & CLEARY, M. L. 1996. The p53-binding protein 53BP2 also interacts with Bc12 and impedes cell cycle progression at G2/M. *Mol Cell Biol,* 16**,** 3884-92.

NELSON, B. R., HARTMAN, B. H., GEORGI, S. A., LAN, M. S. & REH, T. A. 2007. Transient inactivation of Notch signaling synchronizes differentiation of neural progenitor cells. *Dev Biol,* 304**,** 479-98.

NEW, D. A. 1966. Development of rat embryos cultured in blood sera. *J Reprod Fertil,* 12**,** 509-24.

NEW, D. A. 1967. Development of explanted rat embryos in circulating medium. *J Embryol Exp Morphol,* 17**,** 513-25.

NEW, D. A. 1978. Whole-embryo culture and the study of mammalian embryos during organogenesis. *Biol Rev Camb Philos Soc,* 53**,** 81-122.

NEW, D. A. & BRENT, R. L. 1972. Effect of yolk-sac antibody on rat embryos grown in culture. *J Embryol Exp Morphol,* 27**,** 543-53.

NEW, D. A. & COPPOLA, P. T. 1970. Effects of different oxygen concentrations on the development of rat embryos in culture. *J Reprod Fertil,* 21**,** 109-18.

NEW, D. A. & COPPOLA, P. T. 1977. Development of a placental blood circulation in rat embryos in vitro. *J Embryol Exp Morphol,* 37**,** 227-35.

NEW, D. A., COPPOLA, P. T. & COCKROFT, D. L. 1976a. Comparison of growth in vitro and in vivo of post-implantation rat embryos. *J Embryol Exp Morphol,* 36**,** 133-44.

NEW, D. A., COPPOLA, P. T. & COCKROFT, D. L. 1976b. Improved developement of head-fold rat embryos in culture resulting from low

oxygen and modifications of the culture serum. *J Reprod Fertil,* 48**,** 219-22.
NEW, D. A., COPPOLA, P. T. & TERRY, S. 1973. Culture of explanted rat embryos in rotating tubes. *J Reprod Fertil,* 35**,** 135-8.
NEW, D. A. & DANIEL, J. C., JR. 1969. Cultivation of rat embryos explanted at 7.5 to 8.5 days of gestation. *Nature,* 223**,** 515-6.
NEW, D. A. & STEIN, K. F. 1964. CULTIVATION OF POST-IMPLANTATION MOUSE AND RAT EMBRYOS ON PLASMA CLOTS. *J Embryol Exp Morphol,* 12**,** 101-11.
NISHIMURA, Y. V., SHINODA, T., INAGUMA, Y., ITO, H. & NAGATA, K. 2012. Application of in utero electroporation and live imaging in the analyses of neuronal migration during mouse brain development. *Med Mol Morphol,* 45**,** 1-6.
O'RAHILLY, R. & MULLER, F. 2002. The two sites of fusion of the neural folds and the two neuropores in the human embryo. *Teratology,* 65**,** 162-70.
OKUDA, Y., OGURA, E., KONDOH, H. & KAMACHI, Y. 2010. B1 SOX coordinate cell specification with patterning and morphogenesis in the early zebrafish embryo. *PLoS Genet,* 6**,** e1000936.
PADMANABHAN, R. 1984. Experimental induction of cranioschisis aperta and exencephaly after neural tube closure. A rat model. *J Neurol Sci,* 66**,** 235-43.
PADMANABHAN, R. 1990. Scanning-electron-microscopic studies on the pathogenesis of exencephaly and cranioschisis induced in the rat after neural tube closure. *Acta Anat (Basel),* 138**,** 97-110.
PAI, Y. J., ABDULLAH, N. L., MOHD-ZIN, S. W., MOHAMMED, R. S., ROLO, A., GREENE, N. D., ABDUL-AZIZ, N. M. & COPP, A. J. 2012. Epithelial fusion during neural tube morphogenesis. *Birth Defects Res A Clin Mol Teratol,* 94**,** 817-23.
PANGILINAN, F., MOLLOY, A. M., MILLS, J. L., TROENDLE, J. F., PARLE-MCDERMOTT, A., SIGNORE, C., O'LEARY, V. B., CHINES, P., SEAY, J. M., GEILER-SAMEROTTE, K., MITCHELL, A., VANDERMEER, J. E., KREBS, K. M., SANCHEZ, A., CORNMAN-HOMONOFF, J., STONE, N., CONLEY, M., KIRKE, P. N., SHANE, B., SCOTT, J. M. & BRODY, L. C. 2012. Evaluation of common genetic variants in 82 candidate genes as risk factors for neural tube defects. *BMC Med Genet,* 13**,** 62.
PARIDAEN, J. T. & HUTTNER, W. B. 2014. Neurogenesis during development of the vertebrate central nervous system. *EMBO Rep,* 15**,** 351-64.
PENKOV, L. I., PLATONOV, E. S. & NEW, D. A. 1995. Prolonged development of normal and parthenogenetic postimplantation mouse embryos in vitro. *Int J Dev Biol,* 39**,** 985-91.
PEREIRA, R., HALFORD, K., SOKOLOV, B. P., KHILLAN, J. S. & PROCKOP, D. J. 1994. Phenotypic variability and incomplete penetrance of spontaneous fractures in an inbred strain of transgenic mice expressing a mutated collagen gene (COL1A1). *J Clin Invest,* 93**,** 1765-9.
PFAFF, S. L., MENDELSOHN, M., STEWART, C. L., EDLUND, T. & JESSELL, T. M. 1996. Requirement for LIM homeobox gene Isl1 in motor neuron generation reveals a motor neuron-dependent step in interneuron differentiation. *Cell,* 84**,** 309-20.

PIERSMA, A. H. 1993. Whole embryo culture and toxicity testing. *Toxicol In Vitro,* 7**,** 763-8.

PIERSMA, A. H., ATTENON, P., BECHTER, R., GOVERS, M. J., KRAFFT, N., SCHMID, B. P., STADLER, J., VERHOEF, A. & VERSEIL, C. 1995. Interlaboratory evaluation of embryotoxicity in the postimplantation rat embryo culture. *Reprod Toxicol,* 9**,** 275-80.

PIERSMA, A. H., VERHOEF, A., OPPERHUIZEN, A., KLAASSEN, R., VAN EIJKEREN, J. & OLLING, M. 1998. Embryotoxicity of carbamazepine in rat postimplantation embryo culture after in vitro exposure via three different routes. *Reprod Toxicol,* 12**,** 161-8.

PINTER, E., REECE, E. A., LERANTH, C. Z., SANYAL, M. K., HOBBINS, J. C., MAHONEY, M. J. & NAFTOLIN, F. 1986. Yolk sac failure in embryopathy due to hyperglycemia: ultrastructural analysis of yolk sac differentiation associated with embryopathy in rat conceptuses under hyperglycemic conditions. *Teratology,* 33**,** 73-84.

POIRIER, K., KEAYS, D. A., FRANCIS, F., SAILLOUR, Y., BAHI, N., MANOUVRIER, S., FALLET-BIANCO, C., PASQUIER, L., TOUTAIN, A., TUY, F. P., BIENVENU, T., JORIOT, S., ODENT, S., VILLE, D., DESGUERRE, I., GOLDENBERG, A., MOUTARD, M. L., FRYNS, J. P., VAN ESCH, H., HARVEY, R. J., SIEBOLD, C., FLINT, J., BELDJORD, C. & CHELLY, J. 2007. Large spectrum of lissencephaly and pachygyria phenotypes resulting from de novo missense mutations in tubulin alpha 1A (TUBA1A). *Hum Mutat,* 28**,** 1055-64.

POLITIS, P. K., MAKRI, G., THOMAIDOU, D., GEISSEN, M., ROHRER, H. & MATSAS, R. 2007. BM88/CEND1 coordinates cell cycle exit and differentiation of neuronal precursors. *Proc Natl Acad Sci U S A,* 104**,** 17861-6.

PRATTEN, M. K., BROOKE, A. M., BROOME, S. C. & BECK, F. 1988. The effect of epidermal growth factor, insulin and transferrin on the growth-promoting properties of serum depleted by repeated culture of postimplantation rat embryos. *Development,* 104**,** 137-45.

PRISCOTT, P. K. & FORD, J. R. 1985. An in vitro model of acetaldehyde metabolism by rodent conceptuses. *In Vitro Cell Dev Biol,* 21**,** 88-92.

QU, X., TOMPKINS, K., BATTS, L. E., PURI, M. & BALDWIN, H. S. 2010. Abnormal embryonic lymphatic vessel development in Tie1 hypomorphic mice. *Development,* 137**,** 1285-95.

REICHENBACH, A., SCHAAF, P. & SCHNEIDER, H. 1990. Primary neurulation in teleosts--evidence for epithelial genesis of central nervous tissue as in other vertebrates. *J Hirnforsch,* 31**,** 153-8.

RELTON, C. L., WILDING, C. S., PEARCE, M. S., LAFFLING, A. J., JONAS, P. A., LYNCH, S. A., TAWN, E. J. & BURN, J. 2004. Gene-gene interaction in folate-related genes and risk of neural tube defects in a UK population. *J Med Genet,* 41**,** 256-60.

RENNEBECK, G., KLEYMENOVA, E. V., ANDERSON, R., YEUNG, R. S., ARTZT, K. & WALKER, C. L. 1998. Loss of function of the tuberous sclerosis 2 tumor suppressor gene results in embryonic lethality characterized by disrupted neuroepithelial growth and development. *Proc Natl Acad Sci U S A,* 95**,** 15629-34.

RICHARD, C., DREVON, C., CANTO, P. Y., VILLAIN, G., BOLLEROT, K., LEMPEREUR, A., TEILLET, M. A., VINCENT, C., ROSSELLO

CASTILLO, C., TORRES, M., PIWARZYK, E., SPECK, N. A., SOUYRI, M. & JAFFREDO, T. 2013. Endothelio-mesenchymal interaction controls runx1 expression and modulates the notch pathway to initiate aortic hematopoiesis. *Dev Cell,* 24**,** 600-11.

RIVERA-PEREZ, J. A., JONES, V. & TAM, P. P. 2010. Culture of whole mouse embryos at early postimplantation to organogenesis stages: developmental staging and methods. *Methods Enzymol,* 476**,** 185-203.

ROBINSON, A., ESCUIN, S., DOUDNEY, K., VEKEMANS, M., STEVENSON, R. E., GREENE, N. D., COPP, A. J. & STANIER, P. 2012. Mutations in the planar cell polarity genes CELSR1 and SCRIB are associated with the severe neural tube defect craniorachischisis. *Hum Mutat,* 33**,** 440-7.

ROLO, A., SAVERY, D., ESCUIN, S., DE CASTRO, S. C., ARMER, H. E., MUNRO, P. M., MOLE, M. A., GREENE, N. D. & COPP, A. J. 2016. Regulation of cell protrusions by small GTPases during fusion of the neural folds. *Elife,* 5**,** e13273.

ROYER, C., KOCH, S., QIN, X., ZAK, J., BUTI, L., DUDZIEC, E., ZHONG, S., RATNAYAKA, I., SRINIVAS, S. & LU, X. 2014. ASPP2 links the apical lateral polarity complex to the regulation of YAP activity in epithelial cells. *PLoS One,* 9**,** e111384.

SABAPATHY, K., JOCHUM, W., HOCHEDLINGER, K., CHANG, L., KARIN, M. & WAGNER, E. F. 1999. Defective neural tube morphogenesis and altered apoptosis in the absence of both JNK1 and JNK2. *Mech Dev,* 89**,** 115-24.

SADLER, T. W. 1979. Culture of early somite mouse embryos during organogenesis. *J Embryol Exp Morphol,* 49**,** 17-25.

SADLER, T. W. & NEW, D. A. 1981. Culture of mouse embryos during neurulation. *J Embryol Exp Morphol,* 66**,** 109-16.

SALIH, M. A., MURSHID, W. R. & SEIDAHMED, M. Z. 2014. Classification, clinical features, and genetics of neural tube defects. *Saudi Med J,* 35 Suppl 1**,** S5-s14.

SAMUELS-LEV, Y., O'CONNOR, D. J., BERGAMASCHI, D., TRIGIANTE, G., HSIEH, J. K., ZHONG, S., CAMPARGUE, I., NAUMOVSKI, L., CROOK, T. & LU, X. 2001. ASPP proteins specifically stimulate the apoptotic function of p53. *Mol Cell,* 8**,** 781-94.

SANDER, M., PAYDAR, S., ERICSON, J., BRISCOE, J., BERBER, E., GERMAN, M., JESSELL, T. M. & RUBENSTEIN, J. L. 2000. Ventral neural patterning by Nkx homeobox genes: Nkx6.1 controls somatic motor neuron and ventral interneuron fates. *Genes Dev,* 14**,** 2134-9.

SANYAL, M. K. 1980. Development of the rat conceptus in vitro and associated changed in components of culture medium. *J Embryol Exp Morphol,* 58**,** 1-12.

SAUER 1935. Mitosis in the nerual tube. *The journal of comparative neurology,* 62**,** 377-405.

SAXTON, T. M. & PAWSON, T. 1999. Morphogenetic movements at gastrulation require the SH2 tyrosine phosphatase Shp2. *Proc Natl Acad Sci U S A,* 96**,** 3790-5.

SCHMID, B. P., KAO, J. & GOULDING, E. 1985. Evidence for reopening of the cranial neural tube in mouse embryos treated with cadmium chloride. *Experientia,* 41**,** 271-2.

SCHMIDT, R., STRAHLE, U. & SCHOLPP, S. 2013. Neurogenesis in zebrafish - from embryo to adult. *Neural Dev,* 8**,** 3.

SCHNEIDER, J. E., BOSE, J., BAMFORTH, S. D., GRUBER, A. D., BROADBENT, C., CLARKE, K., NEUBAUER, S., LENGELING, A. & BHATTACHARYA, S. 2004. Identification of cardiac malformations in mice lacking Ptdsr using a novel high-throughput magnetic resonance imaging technique. *BMC Dev Biol,* 4**,** 16.

SCHOENWOLF, G. C. 1984. Histological and ultrastructural studies of secondary neurulation in mouse embryos. *Am J Anat,* 169**,** 361-76.

SHANBHAG 1994. Utilization of information measure as a means of image thresholding. *Graph. Models Image Process.,* 56**,** 414-419.

SHANG, E., WANG, X., WEN, D., GREENBERG, D. A. & WOLGEMUTH, D. J. 2009. Double bromodomain-containing gene Brd2 is essential for embryonic development in mouse. *Dev Dyn,* 238**,** 908-17.

SHANG, Y., ZHAO, H., NIU, B., LI, W. I., ZHOU, R., ZHANG, T. & XIE, J. 2008. Correlation of polymorphism of MTHFRs and RFC-1 genes with neural tube defects in China. *Birth Defects Res A Clin Mol Teratol,* 82**,** 3-7.

SHAW, G. M., LU, W., ZHU, H., YANG, W., BRIGGS, F. B., CARMICHAEL, S. L., BARCELLOS, L. F., LAMMER, E. J. & FINNELL, R. H. 2009. 118 SNPs of folate-related genes and risks of spina bifida and conotruncal heart defects. *BMC Med Genet,* 10**,** 49.

SHI, O. Y., YANG, H. Y., SHEN, Y. M., SUN, W., CAI, C. Y. & CAI, C. Q. 2014. Polymorphisms in FZD3 and FZD6 genes and risk of neural tube defects in a northern Han Chinese population. *Neurol Sci,* 35**,** 1701-6.

SMITH, M. S., UPFOLD, J. B. & SHIOTA, K. 1993. Neural tube defects in the parietal region of human embryos: failure to close or closure-reopening? *Neuropathol Appl Neurobiol,* 19**,** 66-73.

SMITH, P. K., KROHN, R. I., HERMANSON, G. T., MALLIA, A. K., GARTNER, F. H., PROVENZANO, M. D., FUJIMOTO, E. K., GOEKE, N. M., OLSON, B. J. & KLENK, D. C. 1985. Measurement of protein using bicinchoninic acid. *Anal Biochem,* 150**,** 76-85.

SOLDANO, K. L., GARRETT, M. E., COPE, H. L., RUSNAK, J. M., ELLIS, N. J., DUNLAP, K. L., SPEER, M. C., GREGORY, S. G. & ASHLEY-KOCH, A. E. 2013. Genetic association analyses of nitric oxide synthase genes and neural tube defects vary by phenotype. *Birth Defects Res B Dev Reprod Toxicol,* 98**,** 365-73.

SOLEMAN, D., CORNEL, L., LITTLE, S. A. & MIRKES, P. E. 2003. Teratogen-induced activation of the mitochondrial apoptotic pathway in the yolk sac of day 9 mouse embryos. *Birth Defects Res A Clin Mol Teratol,* 67**,** 98-107.

SONG, B., BIAN, Q., ZHANG, Y. J., SHAO, C. H., LI, G., LIU, A. A., JING, W., LIU, R., ZHOU, Y. Q., JIN, G. & HU, X. G. 2015. Downregulation of ASPP2 in pancreatic cancer cells contributes to increased resistance to gemcitabine through autophagy activation. *Mol Cancer,* 14**,** 177.

SOTTOCORNOLA, R., ROYER, C., VIVES, V., TORDELLA, L., ZHONG, S., WANG, Y., RATNAYAKA, I., SHIPMAN, M., CHEUNG, A., GASTON-MASSUET, C., FERRETTI, P., MOLNAR, Z. & LU, X. 2010. ASPP2 binds Par-3 and controls the polarity and proliferation of neural progenitors during CNS development. *Dev Cell,* 19**,** 126-37.

SOZEN, B., AMADEI, G., COX, A., WANG, R., NA, E., CZUKIEWSKA, S., CHAPPELL, L., VOET, T., MICHEL, G., JING, N., GLOVER, D. M. & ZERNICKA-GOETZ, M. 2018. Self-assembly of embryonic and two extra-embryonic stem cell types into gastrulating embryo-like structures. *Nat Cell Biol,* 20**,** 979-989.

SPEAR, P. C. & ERICKSON, C. A. 2012a. Apical movement during interkinetic nuclear migration is a two-step process. *Dev Biol,* 370**,** 33-41.

SPEAR, P. C. & ERICKSON, C. A. 2012b. Interkinetic nuclear migration: a mysterious process in search of a function. *Dev Growth Differ,* 54**,** 306-16.

SPENCE, J. R., MAYHEW, C. N., RANKIN, S. A., KUHAR, M. F., VALLANCE, J. E., TOLLE, K., HOSKINS, E. E., KALINICHENKO, V. V., WELLS, S. I., ZORN, A. M., SHROYER, N. F. & WELLS, J. M. 2011. Directed differentiation of human pluripotent stem cells into intestinal tissue in vitro. *Nature,* 470**,** 105-9.

STEELE, C. E. & NEW, D. A. 1974. Serum variants causing the formation of double hearts and other abnormalities in explanted rat embryos. *J Embryol Exp Morphol,* 31**,** 707-19.

STEELE, C. E., NEW, D. A., ASHFORD, A. & COPPING, G. P. 1983a. Teratogenic action of hypolipidemic agents: an in vitro study with postimplantation rat embryos. *Teratology,* 28**,** 229-36.

STEELE, C. E., TRASLER, D. G. & NEW, D. A. 1983b. An in vivo/in vitro evaluation of the teratogenic action of excess vitamin A. *Teratology,* 28**,** 209-14.

STEPHENS, R., LIM, K., PORTELA, M., KVANSAKUL, M., HUMBERT, P. O. & RICHARDSON, H. E. 2018. The Scribble Cell Polarity Module in the Regulation of Cell Signaling in Tissue Development and Tumorigenesis. *J Mol Biol,* 430**,** 3585-3612.

STEPNIAK, E., RADICE, G. L. & VASIOUKHIN, V. 2009. Adhesive and signaling functions of cadherins and catenins in vertebrate development. *Cold Spring Harb Perspect Biol,* 1**,** a002949.

STOCKER, A. M. & CHENN, A. 2015. The role of adherens junctions in the developing neocortex. *Cell Adh Migr,* 9**,** 167-74.

STOTTMANN, R. W., BERRONG, M., MATTA, K., CHOI, M. & KLINGENSMITH, J. 2006. The BMP antagonist Noggin promotes cranial and spinal neurulation by distinct mechanisms. *Dev Biol,* 295**,** 647-63.

STRIELEMAN, P. J. & METZGER, B. E. 1993. Glucose and scyllo-inositol impair phosphoinositide hydrolysis in the 10.5-day cultured rat conceptus: a role in dysmorphogenesis? *Teratology,* 48**,** 267-78.

STUCKEY, D. W., CLEMENTS, M., DI-GREGORIO, A., SENNER, C. E., LE TISSIER, P., SRINIVAS, S. & RODRIGUEZ, T. A. 2011. Coordination of cell proliferation and anterior-posterior axis establishment in the mouse embryo. *Development,* 138**,** 1521-30.

SULLIVAN, A. & LU, X. 2007. ASPP: a new family of oncogenes and tumour suppressor genes. *Br J Cancer,* 96**,** 196-200.

TAKAHASHI, M., MAKINO, S., KIKKAWA, T. & OSUMI, N. 2014. Preparation of rat serum suitable for mammalian whole embryo culture. *J Vis Exp***,** e51969.

TAKAHASHI, N., KOBAYASHI, S., JIANG, X., KITAGORI, K., IMAI, K., HIBI, Y. & OKAMOTO, T. 2004. Expression of 53BP2 and ASPP2 proteins from TP53BP2 gene by alternative splicing. *Biochem Biophys Res Commun,* 315**,** 434-8.

TAKASATO, M., ER, P. X., CHIU, H. S., MAIER, B., BAILLIE, G. J., FERGUSON, C., PARTON, R. G., WOLVETANG, E. J., ROOST, M. S., CHUVA DE SOUSA LOPES, S. M. & LITTLE, M. H. 2015. Kidney organoids from human iPS cells contain multiple lineages and model human nephrogenesis. *Nature,* 526**,** 564-8.

TARLATZIS, B. C., SANYAL, M. K., BIGGERS, W. J. & NAFTOLIN, F. 1984. Continuous culture of the postimplantation rat conceptus. *Biol Reprod,* 31**,** 415-26.

TAWK, M., ARAYA, C., LYONS, D. A., REUGELS, A. M., GIRDLER, G. C., BAYLEY, P. R., HYDE, D. R., TADA, M. & CLARKE, J. D. 2007. A mirror-symmetric cell division that orchestrates neuroepithelial morphogenesis. *Nature,* 446**,** 797-800.

THEOCHARATOS, S., WILKINSON, D. J., DARLING, S., WILM, B., KENNY, S. E. & EDGAR, D. 2013. Regulation of progenitor cell proliferation and neuronal differentiation in enteric nervous system neurospheres. *PLoS One,* 8**,** e54809.

TIMMER, J. R., WANG, C. & NISWANDER, L. 2002. BMP signaling patterns the dorsal and intermediate neural tube via regulation of homeobox and helix-loop-helix transcription factors. *Development,* 129**,** 2459-72.

TORCHINSKY, A., BROKHMAN, I., SHEPSHELOVICH, J., ORENSTEIN, H., SAVION, S., ZASLAVSKY, Z., KOIFMAN, M., DIERENFELD, H., FEIN, A. & TODER, V. 2003. Increased TNF-alpha expression in cultured mouse embryos exposed to teratogenic concentrations of glucose. *Reproduction,* 125**,** 527-34.

TSAI, J. W., LIAN, W. N., KEMAL, S., KRIEGSTEIN, A. R. & VALLEE, R. B. 2010. Kinesin 3 and cytoplasmic dynein mediate interkinetic nuclear migration in neural stem cells. *Nat Neurosci,* 13**,** 1463-71.

TSAI, L. H. & GLEESON, J. G. 2005. Nucleokinesis in neuronal migration. *Neuron,* 46**,** 383-8.

TSAI, W. 1985. Moment-preserving thresholding: a new approach. *Computer Vision, Graphics, and Image Processing,* 29**,** 377-393.

TSUNEKAWA, Y., BRITTO, J. M., TAKAHASHI, M., POLLEUX, F., TAN, S. S. & OSUMI, N. 2012. Cyclin D2 in the basal process of neural progenitors is linked to non-equivalent cell fates. *Embo j,* 31**,** 1879-92.

TUNG, E. W. & WINN, L. M. 2011. Valproic acid increases formation of reactive oxygen species and induces apoptosis in postimplantation embryos: a role for oxidative stress in valproic acid-induced neural tube defects. *Mol Pharmacol,* 80**,** 979-87.

TURNQUIST, C., WANG, Y., SEVERSON, D. T., ZHONG, S., SUN, B., MA, J., CONSTANINESCU, S. N., ANSORGE, O., STOLP, H. B., MOLNAR, Z., SZELE, F. G. & LU, X. 2014. STAT1-induced ASPP2 transcription identifies a link between neuroinflammation, cell polarity, and tumor suppression. *Proc Natl Acad Sci U S A,* 111**,** 9834-9.

ULGER, H., KARABULUT, A. K. & PRATTEN, M. K. 2000. The growth promoting effects of bFGF, PD-ECGF and VEGF on cultured

postimplantation rat embryos deprived of serum fractions. *J Anat,* 197 (Pt 2)**,** 207-19.
USAMI, M., MITSUNAGA, K., MIYAJIMA, A., SUNOUCHI, M. & DOI, O. 2010. Complement component C3 functions as an embryotrophic factor in early postimplantation rat embryos. *Int J Dev Biol,* 54**,** 1277-85.
USAMI, M., NAKAJIMA, M., MITSUNAGA, K., MIYAJIMA, A., SUNOUCHI, M. & DOI, O. 2009. Proteomic analysis of indium embryotoxicity in cultured postimplantation rat embryos. *Reprod Toxicol,* 28**,** 477-88.
USAMI, M. & OHNO, Y. 1996. Partial purification and characterization of serum embryotrophic factor required for early postimplantation growth of rat embryos in culture. *J Exp Zool,* 276**,** 403-14.
VAN HOOK, K., WANG, Z., CHEN, D., NOLD, C., ZHU, Z., ANUR, P., LEE, H. J., YU, Z., SHEPPARD, B., DAI, M. S., SEARS, R., SPELLMAN, P. & LOPEZ, C. D. 2017. DeltaN-ASPP2, a novel isoform of the ASPP2 tumor suppressor, promotes cellular survival. *Biochem Biophys Res Commun,* 482**,** 1271-1277.
VAN MAELE-FABRY, G., DELHAISE, F. & PICARD, J. J. 1992. Evolution of the developmental scores of sixteen morphological features in mouse embryos displaying 0 to 30 somites. *Int J Dev Biol,* 36**,** 161-7.
VAN MAELE-FABRY, G., PICARD, J. J., ATTENON, P., BERTHET, P., DELHAISE, F., GOVERS, M. J., PETERS, P. W., PIERSMA, A. H., SCHMID, B. P., STADLER, J. & ET AL. 1991. Interlaboratory evaluation of three culture media for postimplantation rodent embryos. *Reprod Toxicol,* 5**,** 417-26.
VAN WINKLE, L. J. 2001. Amino acid transport regulation and early embryo development. *Biol Reprod,* 64**,** 1-12.
VIVES, V., SU, J., ZHONG, S., RATNAYAKA, I., SLEE, E., GOLDIN, R. & LU, X. 2006. ASPP2 is a haploinsufficient tumor suppressor that cooperates with p53 to suppress tumor growth. *Genes Dev,* 20**,** 1262-7.
VOELKEL, J. E., HARVEY, J. A., ADAMS, J. S., LASSITER, R. N. & STARK, M. R. 2014. FGF and Notch signaling in sensory neuron formation: a multifactorial approach to understanding signaling pathway hierarchy. *Mech Dev,* 134**,** 55-66.
VOLCIK, K. A., SHAW, G. M., ZHU, H., LAMMER, E. J., LAURENT, C. & FINNELL, R. H. 2003. Associations between polymorphisms within the thymidylate synthase gene and spina bifida. *Birth Defects Res A Clin Mol Teratol,* 67**,** 924-8.
WANG, L., JIN, L., LIU, J., ZHANG, Y., YUAN, Y., YI, D. & REN, A. 2014. Maternal genetic polymorphisms of phase II metabolic enzymes and the risk of fetal neural tube defects. *Birth Defects Res A Clin Mol Teratol,* 100**,** 13-21.
WANG, Y., TU, W., LOU, Y., XIE, A., LAI, X., GUO, F. & DENG, Z. 2009. Mesenchymal stem cells regulate the proliferation and differentiation of neural stem cells through Notch signaling. *Cell Biol Int,* 33**,** 1173-9.
WATANABE, T. & PRATT, R. M. 1991. Effects of retinoic acid on embryonic development of mice in culture. *Experientia,* 47**,** 493-7.
WEBSTER, W. S., BROWN-WOODMAN, P. D. & RITCHIE, H. E. 1997. A review of the contribution of whole embryo culture to the determination of hazard and risk in teratogenicity testing. *Int J Dev Biol,* 41**,** 329-35.

WILLIAMS, M., YEN, W., LU, X. & SUTHERLAND, A. 2014. Distinct apical and basolateral mechanisms drive planar cell polarity-dependent convergent extension of the mouse neural plate. *Dev Cell,* 29**,** 34-46.

WILSON, V. & BEDDINGTON, R. S. 1996. Cell fate and morphogenetic movement in the late mouse primitive streak. *Mech Dev,* 55**,** 79-89.

WLODARCZYK, B., BIERNACKI, B., MINTA, M. & ZMUDZKI, J. 2001. Postimplantation whole embryo culture assay for hamsters: an alternative to rat and mouse. *ScientificWorldJournal,* 1**,** 227-34.

WOODHEAD, G. J., MUTCH, C. A., OLSON, E. C. & CHENN, A. 2006. Cell-autonomous beta-catenin signaling regulates cortical precursor proliferation. *J Neurosci,* 26**,** 12620-30.

WRIGHT, J. A., CHAN, A. K., CHOY, B. K., HURTA, R. A., MCCLARTY, G. A. & TAGGER, A. Y. 1990. Regulation and drug resistance mechanisms of mammalian ribonucleotide reductase, and the significance to DNA synthesis. *Biochem Cell Biol,* 68**,** 1364-71.

WU, J. I., RAJENDRA, R., BARSI, J. C., DURFEE, L., BENITO, E., GAO, G., KURUVILLA, M., HRDLICKOVA, R., LISS, A. S. & ARTZT, K. 2007. Targeted disruption of Mib2 causes exencephaly with a variable penetrance. *Genesis,* 45**,** 722-7.

WU, J. T. & GU, Z. 1981. The effect of intrauterine injection of concanavalin A on implantation in mice and rats. *Contraception,* 23**,** 667-75.

WU, T., SONG, H., XIE, D., ZHAO, B., XU, H., WU, C., HUA, K., DENG, Y., JI, C., HU, J. & FANG, L. 2018. Silencing of ASPP2 promotes the proliferation, migration and invasion of triple-negative breast cancer cells via the PI3K/AKT pathway. *Int J Oncol,* 52**,** 2001-2010.

XU, W., BARIBAULT, H. & ADAMSON, E. D. 1998. Vinculin knockout results in heart and brain defects during embryonic development. *Development,* 125**,** 327-37.

YAMADA, T., PFAFF, S. L., EDLUND, T. & JESSELL, T. M. 1993. Control of cell pattern in the neural tube: motor neuron induction by diffusible factors from notochord and floor plate. *Cell,* 73**,** 673-86.

YANG, S. L., YANG, M., HERRLINGER, S., LIANG, C., LAI, F. & CHEN, J. F. 2015. MiR-302/367 regulate neural progenitor proliferation, differentiation timing, and survival in neurulation. *Dev Biol,* 408**,** 140-50.

YBOT-GONZALEZ, P., COGRAM, P., GERRELLI, D. & COPP, A. J. 2002. Sonic hedgehog and the molecular regulation of mouse neural tube closure. *Development,* 129**,** 2507-17.

YBOT-GONZALEZ, P., SAVERY, D., GERRELLI, D., SIGNORE, M., MITCHELL, C. E., FAUX, C. H., GREENE, N. D. & COPP, A. J. 2007. Convergent extension, planar-cell-polarity signalling and initiation of mouse neural tube closure. *Development,* 134**,** 789-99.

YEN, J. C., CHANG, F. J. & CHANG, S. 1995. A new criterion for automatic multilevel thresholding. *IEEE Trans Image Process,* 4**,** 370-8.

YIN, L., LIN, Y., WANG, X., SU, Y., HU, H., LI, C., WANG, L. & JIANG, Y. 2018. The family of apoptosis-stimulating proteins of p53 is dysregulated in colorectal cancer patients. *Oncol Lett,* 15**,** 6409-6417.

ZAGANJOR, I., SEKKARIE, A., TSANG, B. L., WILLIAMS, J., RAZZAGHI, H., MULINARE, J., SNIEZEK, J. E., CANNON, M. J. & ROSENTHAL, J. 2016. Describing the Prevalence of Neural Tube Defects Worldwide: A Systematic Literature Review. *PLoS One,* 11**,** e0151586.

ZAK, J., VIVES, V., SZUMSKA, D., VERNET, A., SCHNEIDER, J. E., MILLER, P., SLEE, E. A., JOSS, S., LACASSIE, Y., CHEN, E., ESCOBAR, L. F., TUCKER, M., AYLSWORTH, A. S., DUBBS, H. A., COLLINS, A. T., ANDRIEUX, J., DIEUX-COESLIER, A., HABERLANDT, E., KOTZOT, D., SCOTT, D. A., PARKER, M. J., ZAKARIA, Z., CHOY, Y. S., WIECZOREK, D., INNES, A. M., JUN, K. R., ZINNER, S., PRIN, F., LYGATE, C. A., PRETORIUS, P., ROSENFELD, J. A., MOHUN, T. J. & LU, X. 2016. ASPP2 deficiency causes features of 1q41q42 microdeletion syndrome. *Cell Death Differ,* 23**,** 1973-1984.

ZEEB, M., AXNICK, J., PLANAS-PAZ, L., HARTMANN, T., STRILIC, B. & LAMMERT, E. 2012. Pharmacological manipulation of blood and lymphatic vascularization in ex vivo-cultured mouse embryos. *Nat Protoc,* 7**,** 1970-82.

ZHONG, W., JIANG, M. M., SCHONEMANN, M. D., MENESES, J. J., PEDERSEN, R. A., JAN, L. Y. & JAN, Y. N. 2000. Mouse numb is an essential gene involved in cortical neurogenesis. *Proc Natl Acad Sci U S A,* 97**,** 6844-9.

ZHU, H., ENAW, J. O., MA, C., SHAW, G. M., LAMMER, E. J. & FINNELL, R. H. 2007. Association between CFL1 gene polymorphisms and spina bifida risk in a California population. *BMC Med Genet,* 8**,** 12.

ZHU, M., TAO, J., VASIEVICH, M. P., WEI, W., ZHU, G., KHORIATY, R. N. & ZHANG, B. 2015. Neural tube opening and abnormal extraembryonic membrane development in SEC23A deficient mice. *Sci Rep,* 5**,** 15471.

ZIGMAN, M., TRINH LE, A., FRASER, S. E. & MOENS, C. B. 2011. Zebrafish neural tube morphogenesis requires Scribble-dependent oriented cell divisions. *Curr Biol,* 21**,** 79-86.

ZOHN, I. E., ANDERSON, K. V. & NISWANDER, L. 2007. The Hectd1 ubiquitin ligase is required for development of the head mesenchyme and neural tube closure. *Dev Biol,* 306**,** 208-21.

ZOHN, I. E., CHESNUTT, C. R. & NISWANDER, L. 2003. Cell polarity pathways converge and extend to regulate neural tube closure. *Trends Cell Biol,* 13**,** 451-4.

ZOHN, I. E. & SARKAR, A. A. 2008. Modeling neural tube defects in the mouse. *Curr Top Dev Biol,* 84**,** 1-35.

Appendices

Literature review: ‘Postimplantation rodent embryo culture medium’ (PubMed), and relevant Denis New publications.

Reference	Species	Gestational age	Media components used	Development assessed?
(Drakou and Georgiades, 2015)	Mouse	E5.5-E7.5	N2B27 (serum-free medium containing N2 and B27 supplements)	Yes - comparisons with embryo staging system.
(Huang et al., 2015)	Mouse	E7.5-E9.5	1:1 or 3:1 rat serum:GMEM with defined supplements	No.
(Gordon et al., 2014)	Mouse	E10.5-E11.5	Knockout serum free medium	No.
(Kalaskar and Lauderdale, 2014)	Mouse	E10.5-E11.5	Knockout serum free medium	Yes - comparisons with *in vivo* grown embryos.
(Tung and Winn, 2011)	Mouse	E9-E10	9:1 rat serum: Hanks' balanced salt solution (HBSS)	Yes - comparisons with *in vitro* cultured embryos in rat serum + HBSS.
(Usami et al., 2010)	Rat	E9.5-E11.5	Rabbit and rat sera, complement component C3 and HBSS.	No.
(Luijten et al., 2010)	Rat	E10-E11	Rat serum and pregnant bovine serum, supplemented with D-glucose and L-methionine	No - gene expression analysis only.
(Usami et al., 2009)	Rat	E10.5-E11.5	Rat serum	Yes - comparisons with *in vitro* cultured embryos in normal rat serum.
(Andersen et al., 2006)	Rat	E10.5-E12.5	95:1 rat serum:Tyrode's solution	Yes - comparisons with *in vitro* cultured embryos in control rat serum/Tyrode's.
(Torchinsky et al., 2003)	Mouse	E8-E10	3:1 FBS:DMEM and penicillin streptomycin.	Partially - heart beat and open neural tube assessed. Comparisons with *in vivo* and normal glucose level *in vitro* controls.
(Soleman et al., 2003)	Mouse	E8.5-E9.5	4:1 rat serum:HBSS	No.
(Jones et al., 2002)	Mouse	E8.5-E10.5	1:1 rat serum:DMEM supplemented with HEPES and penicillin streptomycin.	Yes - comparisons with *in vivo* grown embryo staging system.
(Wlodarczyk et al., 2001)	Hamster	E7.5-E8.5	2:1 McCoy 5A medium:hamster serum	Yes - comparisons with *in vitro* cultured embryos in control McCoy medium and hamster serum.
(Bulic-Jakus et al., 2001)	Rat	E9.5-embryo explants	Protein and serum-free MEM, supplemented with transferrin and insulin, or serum.	No, only epidermal differentiation.
(Karabulut et al., 2000)	Rat	E9.5-E11.5	Rat serum	Yes - comparisons with *in vitro* cultured embryos in normal rat serum.
(Ulger et al., 2000)	Rat	E9.5-E11.5	Fractionated rat serum with growth factors.	Yes - comparisons with *in vitro* cultured embryos in normal rat serum.
(Kesby, 2000)	Rat	E9.5-E11.5	1:1 rat serum:DMEM supplemented with penicillin streptomycin.	Yes - comparisons with *in vitro* cultured embryos in 1:1 rat serum:DMEM.

Reference	Species	Gestational age	Media components used	Development assessed?
(Menegola et al., 1999)	Rat	E9.5-E11.5	Rat serum from diabetic/control rats.	Yes - comparisons with *in vitro* cultured embryos in normal rat serum.
(Piersma et al., 1998)	Rat	E10-E11	Rat serum.	Yes - comparisons with *in vitro* cultured embryos in normal rat serum.
(Dibbern et al., 1997)	Mouse	E9-6h culture	Rat serum supplied by Harlan Sprague Dawley Inc.	Yes - growth and somite number comparisons with *in vitro* cultured embryos in normal rat serum.
(Nakajima et al., 1997)	Rat	E9.5-E11.5	Rat and rabbit serum supplemented with glucose.	Yes - comparisons with *in vitro* cultured embryos in normal rat serum.
(Berberian et al., 1996)	Rat	E10-E11	2:1 HBSS:rat serum	Yes - comparisons with *in vitro* cultured embryos in normal rat serum.
(Usami and Ohno, 1996)	Rat	E9.5-E11.5	Rat and rabbit serum.	Partially - only total protein content assessed. Comparisons with *in vitro* cultured embryos in rabbit serum.
(Penkov et al., 1995)	Mouse	E9.5-E11.5	3:1 DMEM:rat serum supplemented with penicillin streptomycin.	Yes - comparisons with non-parthenogenetic embryos in 3:1 DMEM:rat serum.
(Piersma et al., 1995)	Rat	E8.5-E10.5	Rat serum	Yes - comparisons with *in vitro* cultured embryos in normal rat serum with added solvent only.
(Harris, 1993)	Rat	E10-E10.5	2:1 HBSS:rat serum	No.
(Strieleman and Metzger, 1993)	Rat	E9.5-E10.5	3:1 rat serum:isotonic saline with supplemental D-glucose and scyllo-inositol.	No.
(Ambroso and Harris, 1993)	Rat	E10-E11	1:2 rat serum:HBSS supplemented with penicilillin streptomycin.	Yes - comparisons with *in vitro* cultured embryos in 1:2 rat serum:HBSS supplemented with penicilillin streptomycin.
(Kesby, 1992)	Rat	E10-E12	1:1 rat serum or heparin-plasma:DMEM.	Yes - comparisons with *in vitro* cultured embryos in 1:1 rat serum:DMEM.
(Hardy and New, 1991)	Rat	E9.5-E11.5	1:1 rat serum:DMEM supplemented with L-glutamine	Yes - comparisons with *in vitro* cultured embryos in normal rat serum.
(Van Maele-Fabry et al., 1991)	Mouse	E8.5-E11.5	Rat serum and human serum supplemented with d-glucose.	Yes- comparisons between the three types of culture media: rat serum, human serum and a mixture of 80% human serum and 20% rat serum.
(Akazawa et al., 1989)	Rat	E9.5-E11.5	3:1 rat serum:isotonic saline supplemented with glucose and penicillin streptomycin. Hypoglycemic serum.	Yes - comparisons with *in vitro* cultured embryos in 3:1 rat serum: isotonic saline supplemented with penicillin streptomycin.
(Kachilele and New, 1988)	Rat	E9.5-E11.5	Rat serum	Yes - comparisons with *in vitro* cultured embryos in normal rat serum cultured immediately after explantation.
(Pratten et al., 1988)	Rat	E9.5-E11.5	Rat serum, 'exhausted' rat serum and dialysed serum.	Yes - comparisons with *in vitro* cultured embryos in normal (non-'exhausted') rat serum or rat serum after dialysis.
(Ebron-McCoy et al., 1988)	Hamster	E8-E10	70:30 McCoy's 5A medium:rat serum and 100% rat serum.	Yes - comparisons with *in vivo* grown embryos.

Reference	Species	Gestational age	Media components used	Development assessed?
(Cockroft, 1987)	Mouse	E9-E11	Rat serum	Yes - comparisons with *in vivo* embryos.
(Ellington, 1987)	Rat	E9.5-E12.5	Rat serum supplemented with penicillin streptomycin	Yes - comparisons with *in vitro* cultured embryos in non-glucose-supplemented rat serum.
(Lewandowski et al., 1986)	Rat	E9.5-E11.5	Bovine Serum	Yes - comparisons with *in vitro* cultured embryos in normal bovine serum.
(Huxham and Beck, 1985)	Rat	E9.5-E11.5	Rat serum, 1:1 rat serum:HBSS, and human serum	Yes – comparisons between pure rat serum and diluted rat serum cultured embryos.
(Klug et al., 1985)	Rat	E9.5-E11.5	Bovine serum supplemented with Tyrode-phosphate buffer	Yes - comparisons with *in vivo* embryos.
(Priscott and Ford, 1985)	Rat and Mouse	E10-E13	3:1 DMEM:rat serum supplemented with penicillin streptomycin.	No.
(Tarlatzis et al., 1984)	Rat	E10-E14	Rat serum	Yes - comparisons with earlier stages, development progression described.
(Steele et al., 1983a)	Rat	E9.5-E11.5	Rat serum	Yes - comparisons with *in vitro* cultured embryos in normal rat serum.
(Steele et al., 1983b)	Rat	E9.5-E11.5	Rat serum	Yes - comparisons with embryos cultured or grown from non - injected dams.
(Fisher and Martinez de Villarreal, 1982)	Mouse	E9-E11	1:1 FBS:Waymouth's medium containing insulin	Yes - comparisons with progesterone-free controls.
(Sadler and New, 1981)	Mouse	E8.5-E10.5	Rat serum or 1:1 rat serum:DMEM/Waymouth's medium	Yes - comparisons with *in vivo* embryos.
(Galloway et al., 1980)	Mouse	E7.5-E10	Eagle's basal medium, amino acids and FBS	No.
(Morriss and New, 1979)	Rat	E9.5-E11.5	Rat serum	No - only neural folds assessed.
(Buckley et al., 1978)	Rat	E7.5-E12.5	Rat serum	Yes - comparisons between different conditions (roller bottle/watchglass, maternal/male rat serum).
(Cockroft and New, 1978)	Rat	E9.5-E11.5	Rat serum	Yes - comparisons with embryos cultured at 38 degrees celcius.
(New and Coppola, 1977)	Rat	E9.5-E12.5	Rat serum	No - placental growth and circulation only.
(Agnish and Kochhar, 1976)	Mouse	E11-E13	1:1 FBS:Waymouth's medium	No.
(Gunberg, 1976)	Rat	E10-E11	Rat serum, dialysed serum and buffered salt solution	Yes - comparisons with *in vitro* cultured embryos in normal rat serum.
(New et al., 1976a)	Rat	E9.5-E11.5	Rat serum	Yes - comparisons with *in vivo* littermates
(New et al., 1976b)	Rat	E9.5-E11.5	Rat serum	Yes - comparisons between serum preparation and gassing techniques.
(Steele and New, 1974)	Rat	E8.5-E9.5	Rat serum	Yes - comparisons between various rat sera conditions.
(New et al., 1973)	Rat	E10.5-E13.5	Rat serum	Yes - comparisons between roller bottle and circulator culture methods.

Reference	Species	Gestational age	Media components used	Development assessed?
(New and Brent, 1972)	Rat	E9.5-E11.5	Rat serum	Yes - comparisons with *in vitro* cultured embryos in normal rat serum.
(New and Coppola, 1970)	Rat	E9.5-E13.5	Rat serum	Yes - comparisons with earlier stages and between different O2 concentrations, developmental progression described.
(New and Daniel, 1969)	Rat	E7.5-E11.5	Rat serum	Yes - descriptive analysis of development.
(Clarkson et al., 1969)	Mouse	E8.5-E9.5	Commercial rat serum and Waymouth's MB 752/1 medium	Yes - comparisons with *in vitro* cultured embryos in normal rat serum. Witschi staging and DNA/RNA/protein analysis.
(New, 1967)	Rat	E10.5-E12.5	Rat serum	Yes - comparisons between various rat sera, in various conditions.
(New, 1966)	Rat	E9.5-E11.5	Rat serum	Yes - comparisons between various rat sera.
(New and Stein, 1964)	Rat and Mouse	E7-E11	Fowl plasma and embryo extract from chick/mouse	Yes - comparisons against earlier stages, development progression described.